Doctoral Programme in Mechanical, Fluids and Aerospace Engineering

Universitat Politècnica de Catalunya (UPC)

Departament de Ciència dels Materials i Enginyeria Metal·lúrgica (CMEM)

Escola Superior d'Enginyeries Industrial, Aeroespacial i Audiovisual de Terrassa (ESEIAAT)

Development of the *In Situ* Forming of a Liquid Infused Preform (ISFLIP) process

A new manufacturing technique for high performance Fibre Reinforced Polymer (FRP) components

Appendices (Vol. 2 of 2 Vol.)

by

Jaime Juan Muñoz

Supervisor: Dr. Núria Salán Ballesteros

Thesis submitted to the Universitat Politècnica de Catalunya (UPC)

for the degree of Doctor of Philosophy, May 2017

This page intentionally left blank

Summary

List of figures

List of tables

List of abbreviations

ANCOVA	Analysis of Covariance	HPDM	High Permeability Distribution Medium
ANOVA	Analysis of Variance	ILNS	Inter-Laminar Normal Strength
CBS	Curved Beam Strength	ISFLIP	*In Situ* forming of a Liquid
CTWF	Carbon Twill Weave Fabric		Infused Preform
DOE	Design Of Experiments	PAT	Porous Area Type
FRP	Fibre Reinforced Polymers	RBD	Randomized Block Design
GLM	General Lineal Model	RGB	Red, Green, Blue
GTWF	Glass Twill Weave Fabric	VI	VI

List of symbols

v	Volume fraction	P	Pressure
m	Mass fraction	P_{diaph}	Pressure between diaphragms
M	Mass*	P_{mould}	Pressure into the mould cavity
ρ	Density	T	Temperature
n	Number of units of a set of elements*	$T_{0\rightarrow fill_0}$	Temperature profile until filling from resin mixing
h	Thickness	$T_{0\rightarrow pfill_0}$	Temperature profile until post-filling from resin mixing
l	Length*		
w	Width		

* Symbol repeated to refer to more than one concept in different contexts throughout the dissertation.

t	Time
$t_{0\rightarrow fill_0}$	Time until filling from resin mixing
$t_{0\rightarrow fill_{end}}$	Time until filling end from resin mixing
$t_{0\rightarrow pfill_0}$	Time until post-filling from resin mixing
RH	Relative humidity
Ca^*	Modified capillary number
γ	Surface tension
θ	Contact angle between solid and fluid*
u	Volume-averaged velocity
μ	Dynamic viscosity*
$\boldsymbol{K}$	Second order tensor of permeability
L	Filling length
α	Relative position*
x	Absolute position*
x_f	Flow front position
u_f	Macroscopic resin velocity at the flow front
α	Degree of cure*
C_{air}	Air solubility at a fixed temperature
H	Henry's law solubility constant
P_{air}	Partial pressure of air
γ	Surface energy
s_0	Porous area fraction
S_0	Porous area
$\bar{V}_0^{surf}$	Average surface void volume
σ	Stress
τ	Shear stress
ε	Strain
E	Modulus of elasticity
F	Load
s	Deflection at the mid-point
l'	Span between supports
v	Crosshead speed
$\dot{\varepsilon}$	Strain rate
M	Bending moment*
δ	Crosshead displacement
r	Coordinate in the radial direction
θ	Coordinate in the tangential direction*
a_0	Void area fraction
A_0	Void area
$\emptyset_{Feret}$	Feret's diameter
φ_{Feret}	Feret's angle
AR	Aspect ratio
y	Response variable
x	Regressor variable*
n	Number of observations, replicates*
k	Number of treatments, order of the factorial design
R^2	Coefficient of determination
R^2_{adj}	Adjusted coefficient of determination
R^2_{pred}	Predicted coefficient of determination
SS	Sum of squares
MS	Mean of squares
df	Degrees of freedom
β	Coefficient of regression*
l	Effect of a factor or interaction*
S^2	Sample variance
α	Significance level*
α	Probability of type I error*

* Symbol repeated to refer to more than one concept in different contexts throughout the dissertation.

β	Probability of type II error*	χ_u^2	Chi-square distribution
H_0	Null hypothesis		with u degrees of freedom
H_A	Alternative hypothesis	ε	Error
F_0	F-statistic of the null hypothesis	e	Residual
p	Statistic used in hypothesis testing	μ	Mean*
$N(\mu, \sigma^2)$	Normal distribution	σ^2	Variance
	with mean μ and variance σ^2	τ	Effect of a treatment*
t_n	Student's t-distribution		
	with n degrees of freedom		

Superscripts

$intra$	Intra-tow	$\bar{}$	Average
$inter$	Inter-tow	$\hat{}$	Estimated
$inlet$	Inlet	$'$	Adjusted
$vent$	Vent		

Subscripts

f	Fibre*	$pfill$	Post-filling
r	Resin*	$cure$	Curing
0	Void*	$form$	Forming
0	Initial*	amb	Ambient
i	Inner	atm	Atmospheric
o	Outer	vac	Vacuum
m	Mean	f	Flexural*
α	Degree of cure	r	Radial direction*
deg	Degassing	θ	Tangential direction
deb	Debulking	M	Maximum stress (strength)*
$fill$	Filling	M	Model*

* Symbol or subscript repeated to refer to more than one concept in different contexts throughout the dissertation.

T Total

. Total

E Error

This page intentionally left blank

Appendix A

Cause and effect diagrams

Two cause and effect diagrams are shown in Figure A.1 and Figure A.2 that include the major causes in Vacuum Infusion (VI) manufacturing affecting final fibre volume fraction, v_f, and void volume fraction, v_0, contents, respectively. Both cause and effect diagrams were built from the extensive literature review presented in Chapter 2, and served as the basis for the rigorous analyses of VI manufacturing conducted throughout the thesis in order to find an effective processing methodology for the *In Situ* Forming of a Liquid Infused Preform (ISFLIP) process.

A similar approach to air outgassing could have been followed with volatile components evaporation such as styrene in Figure A.2; however, since its implications in epoxy resin systems are not of major concern, it was eluded the expansion of this cause for clarity reasons.

In VI manufacturing, resins remained in a low-viscosity state along the degassing, filling and post-filling steps until final gelation at the curing step. Resin viscosity variations in the low-viscosity state range were not considered a key factor neither in degassing performance nor in later bubble nucleation into the laminate; hence, it was not included in the Outgassing branch of the diagram. Obviously, the high viscosity increment which occurs after gelation inhibits any bubble nucleation.

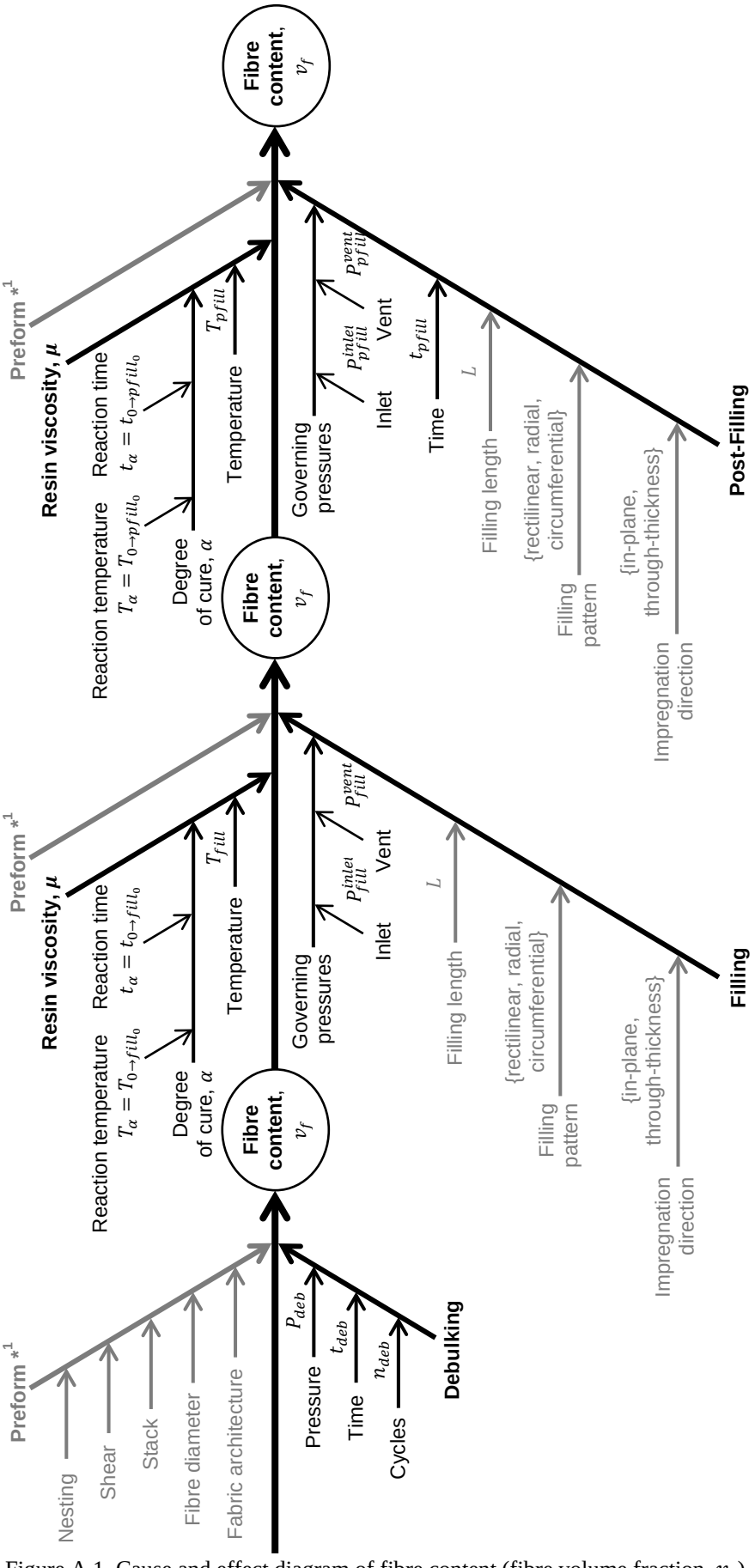

Figure A.1. Cause and effect diagram of fibre content (fibre volume fraction, v_f) in VI manufacturing (in black, causes directly associated with processing).

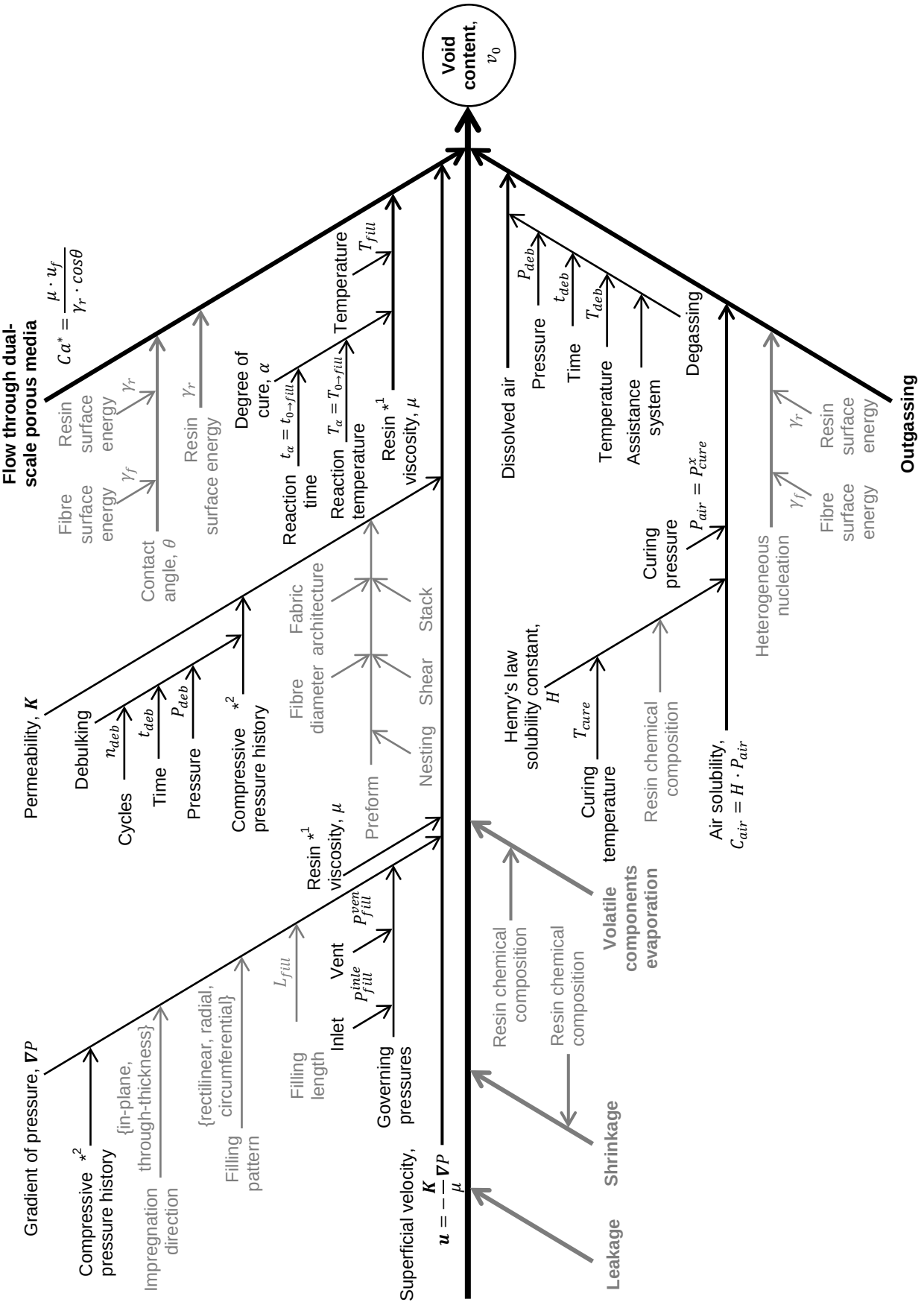

Figure A.2. Cause and effect diagram of void content (void volume fraction, v_0) in VI manufacturing (in black, causes directly associated with processing).

This page intentionally left blank

Appendix B

Workbenches and equipment

B.1. Vacuum Infusion (VI)

The workbench and the equipment used in the VI manufacturing experiments are shown in Figure B.1.

All different degassing procedures were conducted in an air-tight chamber of volume capacity 26 l. The pressure in the degassing chamber was measured with a differential pressure transducer Gems 2200HG1A0. This chamber was equipped with an air-tight electric power point to feed electronic devices into the chamber while resin was being degassed.

Preform assemblies were connected to a vacuum pump Becker U 4.20 through an air-tight reservoir of 10 l, in which vacuum level was manually controlled by a throttle valve and measured by a differential pressure vacuum gauge of accuracy $\pm 3\%$ of the full span, 100 kPa.

Resin flow through the preform was recorded through a high-definition webcam Logitech C920. Besides, thickness evolution during post-filling was monitored through a laser displacement meter system which consisted on three laser micrometres Keyence LC-2100 with sensor heads LC-2320. In Chapter 4, the two sensor heads were placed to measure preform thickness variation at approx. 30 mm from the inlet and venting channels; while, in Chapter 5, the two sensors heads were placed to take repeated measures of the preform thickness variation at approx. 30 mm from the inlet channel, which is the configuration shown in Figure B.1.

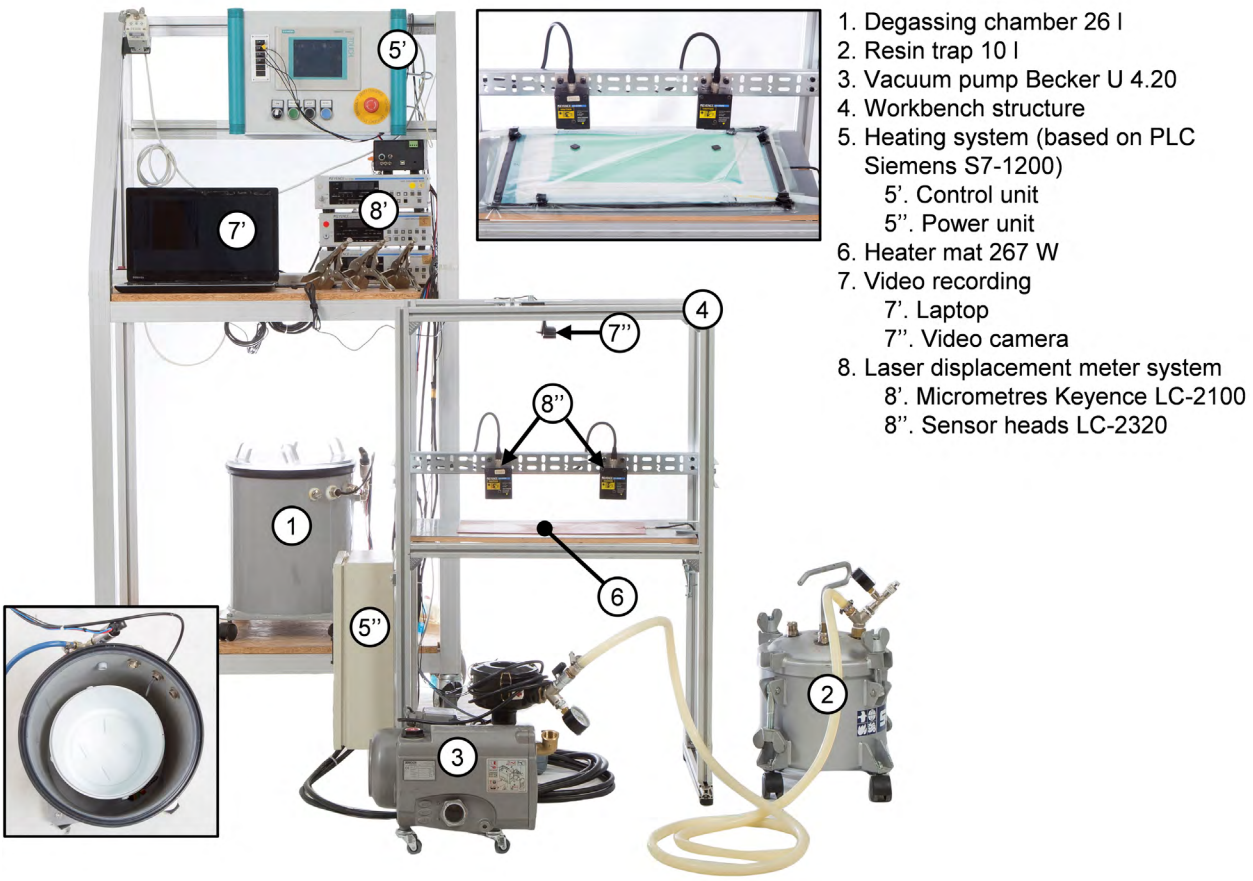

Figure B.1. Workbench for VI manufacturing.

The heating source was a heating blanket placed under the mould. Assemblies were covered with a non-woven polyester fabric of thickness 20 mm to guarantee a homogeneous temperature distribution along specimen thickness. Heating power was governed through closed-loop PID controllers that monitored blanket temperature through 'J' type thermocouples.

Throughout the thesis, different magnetic stirring systems were used to combine vacuum degassing with high speed stirring. In Chapter 4, in the screening of different degassing procedures, a single-point commercial magnetic stirrer was used (Figure B.2.a). Stirring was conducted with a single rod of length 40 mm and diameter 8 mm at ≈ 300 rpm.

In the second set of VI experiments, in Chapter 5, degassing was assisted by a multi-position magnetic stirrer (four magnetic rods of diameter 8 mm and length 40 mm) at 700 ± 25 rpm (Figure B.2.b). This new stirring system was constructed from 80x80 mm PC four-wire fans, which allowed speed regulation and measuring. The control system was based on Arduino board MEGA 2560. Resin degassing for manufacturing of ISFLIP specimens was also assisted by this magnetic stirring device.

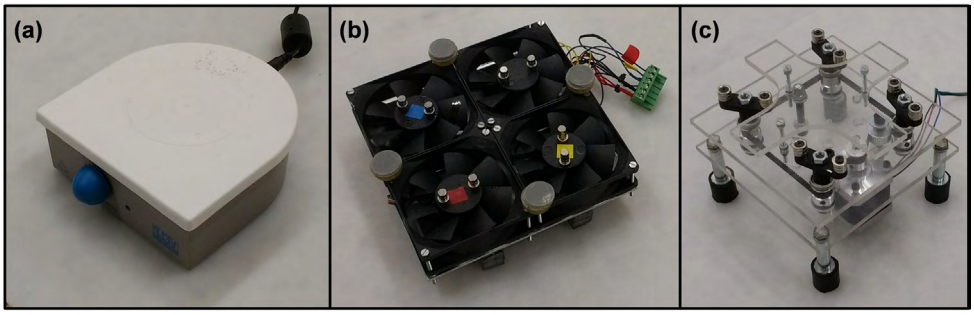

Figure B.2. Magnetic stirrers used along the research project: (a) screening of degassing procedures (Chapter 4), (b) screening of filling and post-filling conditions (Chapter 5 and Chapter 6), and (c) new model for future experimentation.

After proving the concept of the four-points magnetic stirrer, a new device, also thought to be controlled through Arduino, has been built for future experimentation (Figure B.2.c).

B.2. *In Situ* Forming of a Liquid Infused Preform (ISFLIP)

ISFLIP specimens were manufactured with the prototype described in detail in Chapter 3 (Figure B.3). The same resin trap and vacuum pump mentioned in the previous section were used to carry out the VI-related steps in ISFLIP manufacturing. Besides, another vacuum pump Becker U 4.20 was used to evacuate air between diaphragms and from the mould cavity; hence, two vacuum pumps were working in parallel.

The same heating system used in the VI experiments controlled temperature during the curing step, but the heating source was the grid of infrared panels instead of the heater mat. Heating power was governed through closed-loop PID controllers that monitored upper diaphragm temperature through 'J' type thermocouples. It was experimentally checked that under constant target temperatures, temperature difference with respect to between diaphragms fell under 3℃ in less than 10 min.

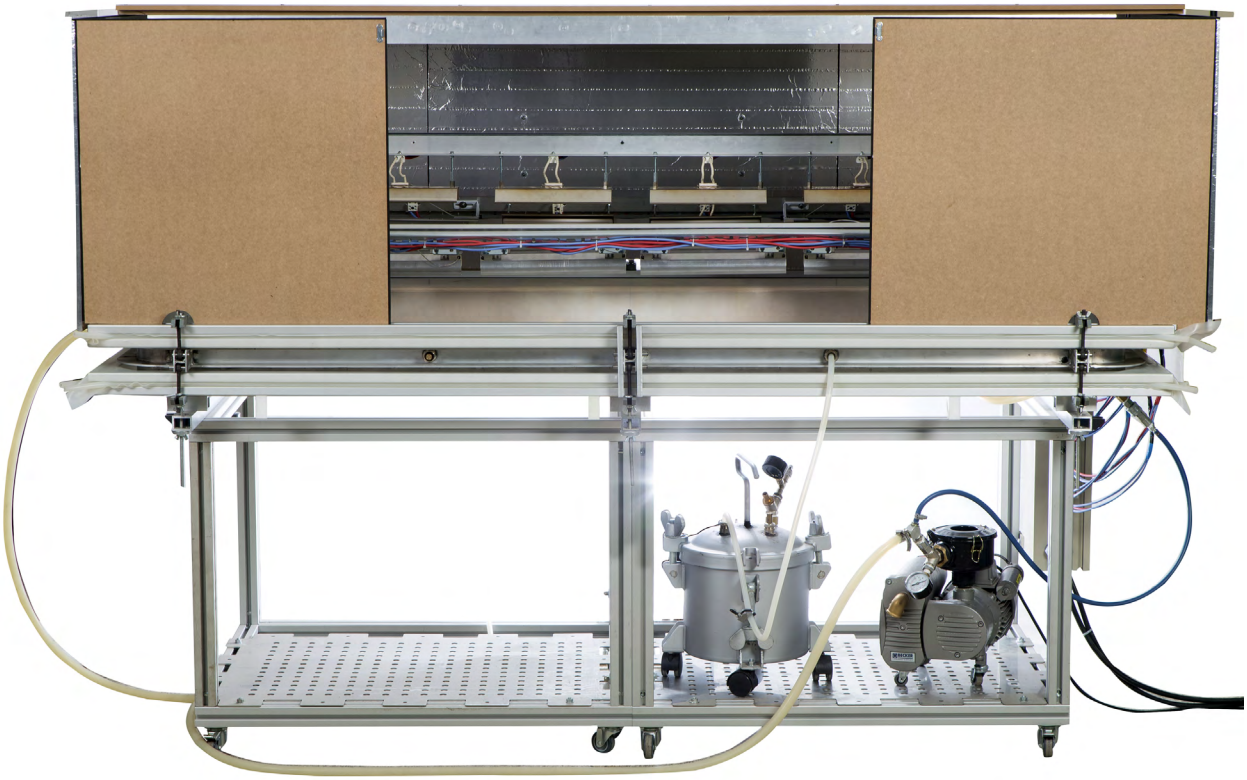

Figure B.3. ISFLIP prototype.

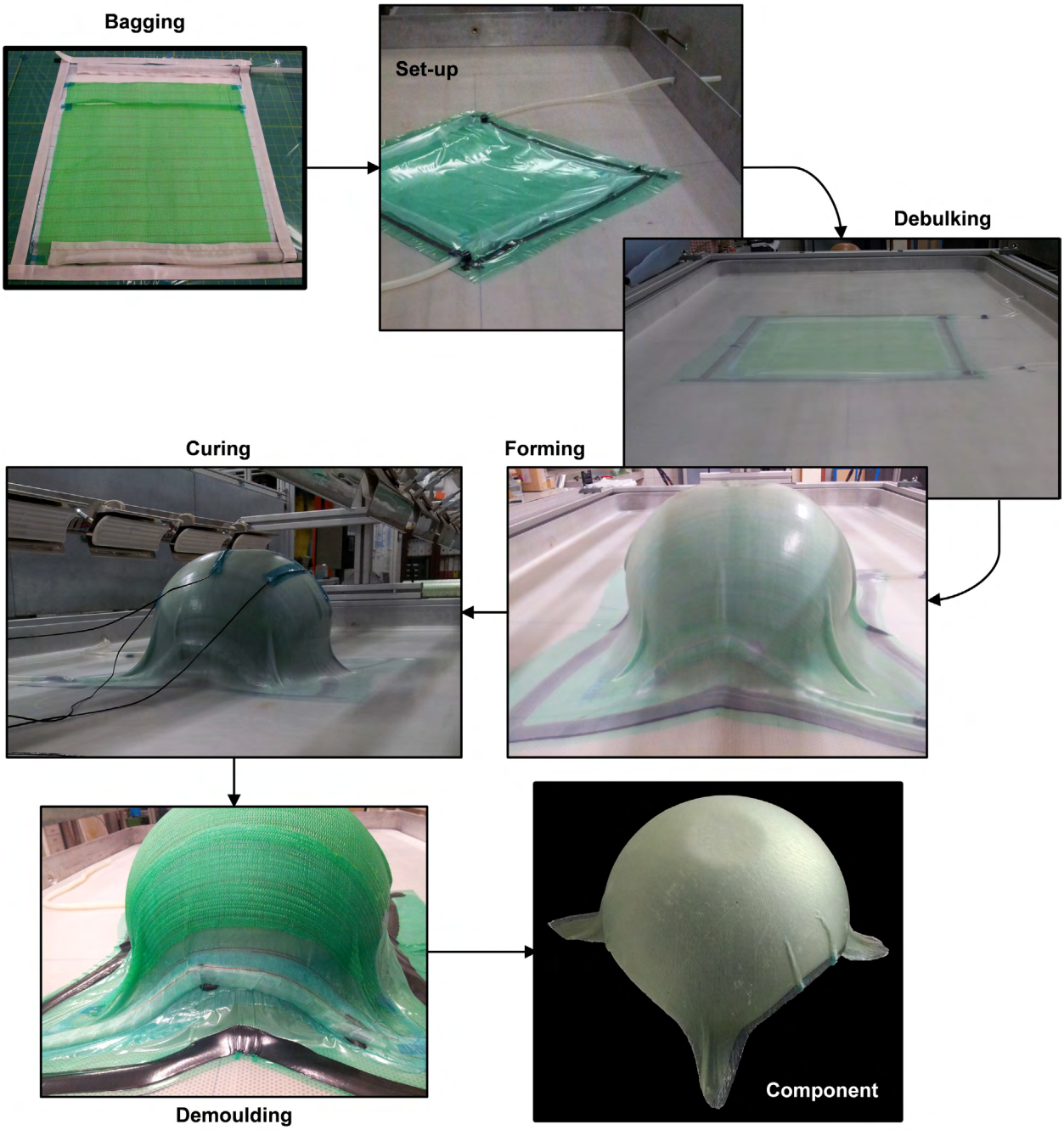

Figure B.4. Illustration of some of the main processing steps carried out to manufacture hemisphere shape specimens through ISFLIP.

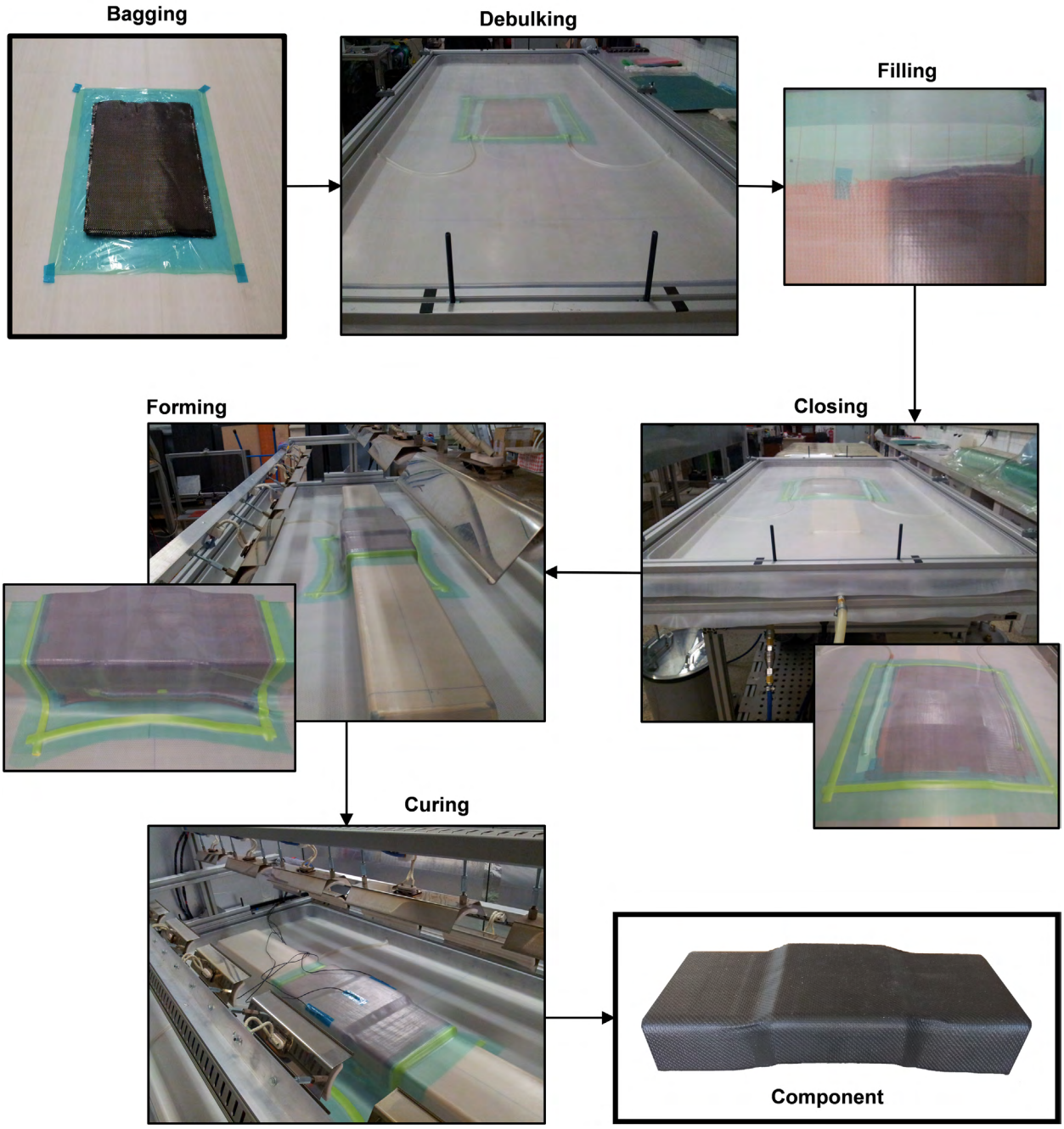

Figure B.5. Illustration of some of the main processing steps carried out to manufacture ‘C’ cross-section profiles through ISFLIP.

Appendix C

Process monitoring

C.1. Report

Apart from recording degassing steps and, in case of VI specimens presented in Chapters 4 and 5, also filling steps, data of environmental and manufacturing conditions was gathered trough forms shown in Figure C.1 to conduct later statistical analyses and check that nuisance factors were not affecting the quality of the manufactured specimens. Besides, preform thickness evolution of VI specimens during post-filling steps, which was measured through a laser displacement system, was also gathered through forms shown in Figure C.2.

Manufacturing template

Date:

Laminate id.

Debulking		
Interval [min]		
Check for leaks. Apply full vacuum for 5 min. Then disconnect the vacuum pump (air-tight assembly). Wait the specified debulking interval.		
Time	Pressure start [kPa]	Pressure end [kPa]
Mixing		
Time	Humidity [%]	Temperature [°C]
Stirring		
Start stirring within 1min after mixing. Aid the stirring with a rod for 1min.		
Time		
Degassing		
Description		
Start degassing within 5min after stirring. If degassing is combined with any stirring task, stop stirring 5min before degassing end.		
Time	Pressure [kPa]	
Filling		
Vent pressure [kPa]		
Turn camera on, place thermocouples and set micrometers to zero. Apply full-vacuum for 2min. Then adjust vacuum level to the specified vent pressure. When resin reaches the vent, clamp the inlet and wait until homogeneous thickness.		
Time	Humidity [%]	Temperature [°C]
Post-filling		
Vent pressure [kPa]		
Description		
Time		

Cure		
Vent pressure [kPa]		
Description		
Adjust vacuum level to the specified vent pressure.		
Time	Humidity [%]	Temperature [°C]
End		
Time	Humidity [%]	Temperature [°C]
Observations		

Figure C.1. Forms to gather environmental and manufacturing conditions.

Micrometer data

Date: Laminate id.:

Time [min]	Micr. 1 [mm]	Micr. 2 [mm]	Micr. 3 [mm]	Time (min)	Micr. 1 [mm]	Micr. 2 [mm]	Micr. 3 [mm]
1				31			
2				32			
3				33			
4				34			
5				35			
6				36			
7				37			
8				38			
9				39			
10				40			
11				41			
12				42			
13				43			
14				44			
15				45			
16				46			
17				47			
18				48			
19				49			
20				50			
21				51			
22				52			
23				53			
24				54			
25				55			
26				56			
27				57			
28				58			
29				59			
30				60			

Figure C.2. Form to gather preform thickness evolution during post-filling.

C.2. Video recording

By way of example, Figure C.3 and Figure C.4 show the corresponding time lapse of degassing and filling steps, respectively, carried out for manufacturing of specimen B3 (Chapter 5), that was the last VI specimen manufactured and presented in this thesis. It must be mentioned that time required to pass from a similar state to that shown in Figure C.3 for 4 min to a similar state to that shown for 8 min was in general almost twice; however, in resin degassing for specimen B3, it happened faster.

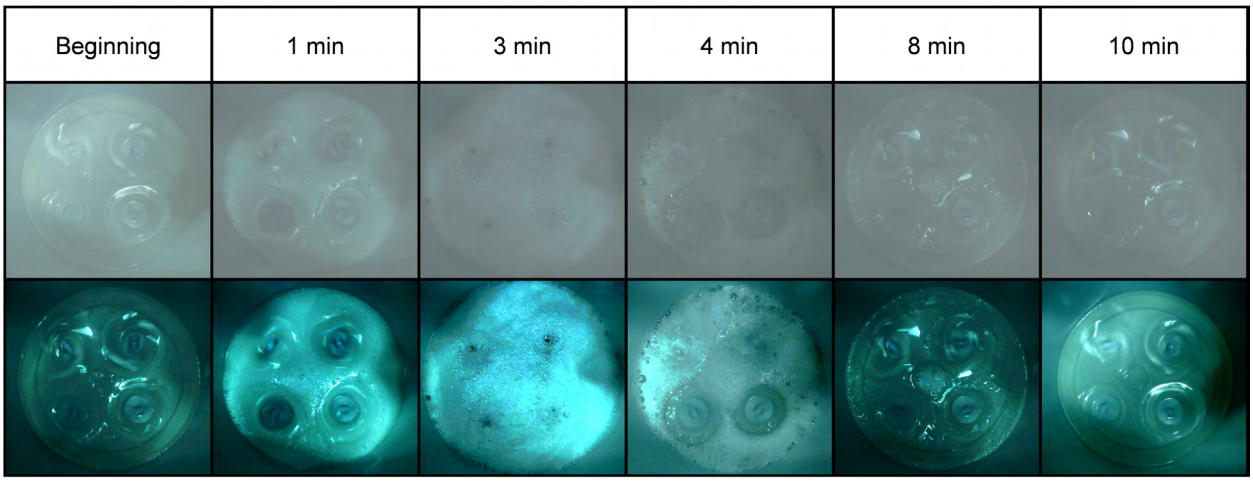

Figure C.3. Time lapse of the degassing step (original and enhanced contrast pictures) carried out for manufacturing of specimen B3 (Chapter 5).

C.3. Environmental conditions

Environmental conditions are nuisance factors that can affect manufactured parts. Relative humidity, RH, and ambient temperature, T_{amb}, were written down in forms like that shown in Figure C.1 at different points of the experiment. Environmental conditions during manufacturing of specimens presented in Chapter 4 are provided in Table C.1, of specimens presented in Chapter 5 in Table C.2, and of specimens presented in Chapter 6 in Table C.3.

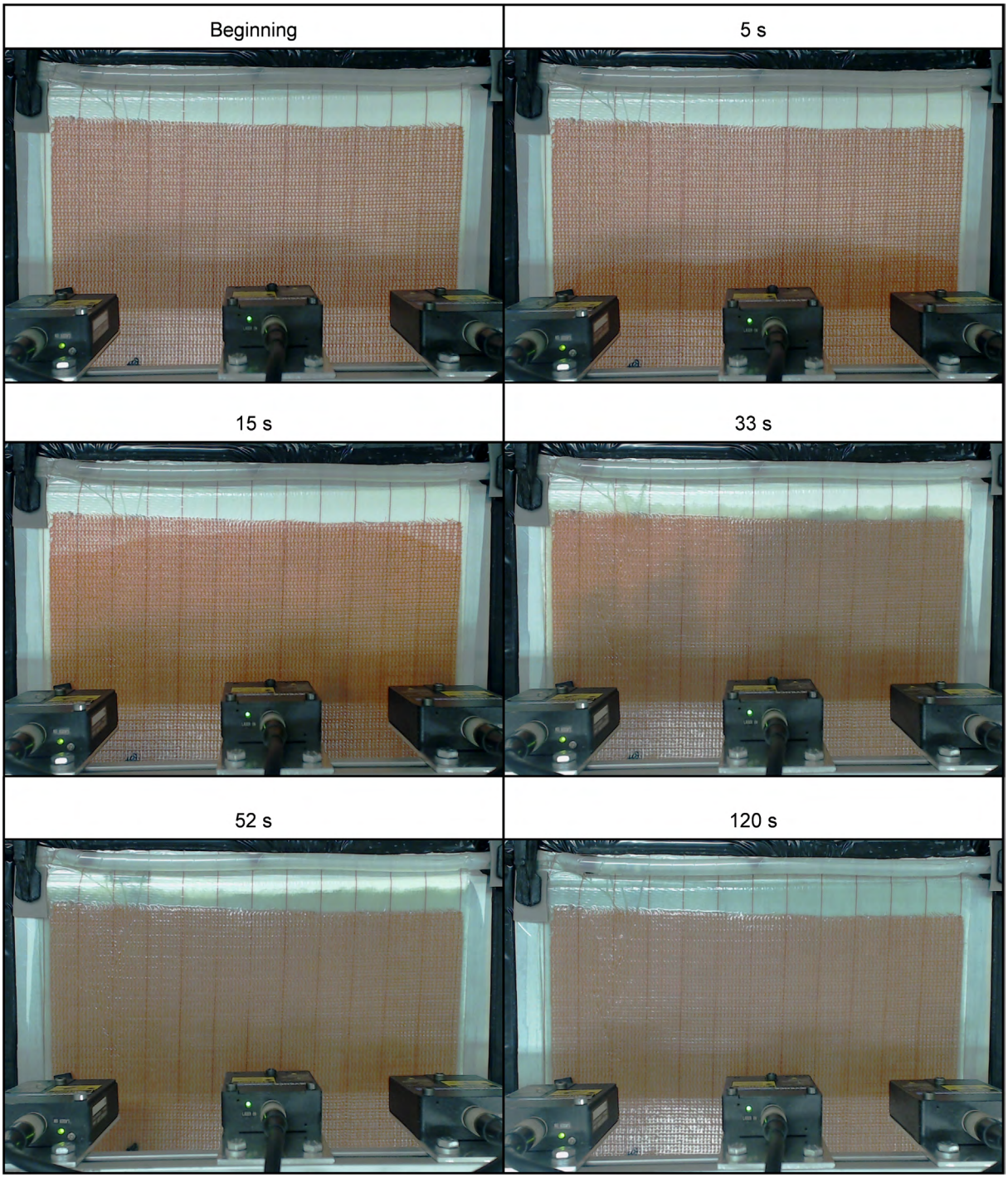

Figure C.4. Time lapse of the filling step carried out for manufacturing of specimen B3 (Chapter 5).

Table C.1. Environmental conditions during manufacturing of VI specimens presented in Chapter 4.

Factor	**Specimen**							
	1	**2**	**3**	**4**	**5**	**6**	**7**	**8**
Mean humidity, $\overline{RH}$ [%]	65	60	61	63	61	62	61	60
Mean temperature, $\bar{T}$ [°C]	23,5	23,8	23,6	23,3	23,5	22,5	24,4	23,5
Degassing temperature, T_{deg} [°C]	22	23,5	23	22	22	22	24	23
Filling temperature, T_{fill} [°C]	24	24	24	23	24	22	24	23
Post-filling temperature, T_{pfill} [°C]	24	24	24	24	24	23	25	24

Table C.2. Environmental conditions during manufacturing of VI specimens presented in Chapter 5.

Factor	Specimen							
	A1	**A2**	**A3**	**A4**	**B1**	**B1'**	**B2**	**B3**
Mean humidity, $\overline{RH}$ [%]	66	63	65	66	66	69	62	64
Mean temperature, $\bar{T}$ [°C]	22,8	24,0	23,0	24,6	21,9	22,5	24,8	22,5
Degassing temperature, T_{deg} [°C]	22	23	22	22	22	22	26	23
Filling temperature, T_{fill} [°C]	22	23	22	25	21	23	24	22
Post-filling temperature, T_{pfill} [°C]	24	25	24	26	21	23	24	23

Table C.3. Environmental conditions during manufacturing of ISFLIP specimens presented in Chapter 6.

Factor	Specimen							
	A1	**A2**	**A3**	**A4**	**B1**	**B2**	**B3**	**B4**
Mean humidity, $\overline{RH}$ [%]	57	59	63	59	61	63	65	67
Mean temperature, $\bar{T}$ [°C]	25,0	24,4	25,0	25,4	24,1	22,9	24,0	24,0
Degassing temperature, T_{deg} [°C]	24	27	24	25	24	22	26	26
Filling temperature, T_{fill} [°C]	25	24	24	26	24	22	22	22
Post-filling temperature, T_{pfill} [°C]	25	22	26	24	23	21	24	24

C.4. Manufacturing conditions

Parameters (design factors and held-constant factors) governing processing of VI and ISFLIP specimens manufactured along the research are shown in Table C.4, Table C.5 and Table C.6.

Debulking pressure, P_{deb}, of VI specimens analysed in Chapter 4; degassing pressure, P_{deg}; and inlet pressures along filling, P_{fill}^{inlet}, post-filling, P_{pfill}^{inlet}, and cure, P_{cure}^{inlet}, were monitored with a differential pressure transducer Gems 2200HG1A0; while the rest of monitored pressures were read through a differential pressure vacuum gauge of accuracy $\pm 3\%$ of the full span, 100 kPa.

Accuracy of measured times provided in Table C.4, Table C.5 and Table C.6. was of the order of minutes, not being enough in case of filling times, t_{fill}, of VI specimens in which preform impregnation was carried out through the thickness (Table C.5). Therefore, more accurate partial and total t_{fill} were measured from recorded videos (Table C.7).

Table C.4. Manufacturing conditions of VI specimens presented in Chapter 4.

Factor	Specimen							
	1	**2**	**3**	**4**	**5**	**6**	**7**	**8**
Debulking pressure, P_{deb} [kPa]	-94,6	-95,2	-95	-95,9	-97,8	-97,1	-96,1	-96,4
Debulking pressure drop, ΔP_{deb} [kPa]*1	-0,2	-1,9	-2,1	-0,3	-0,6	-1,9	-0,3	-0,1
Degassing pressure, P_{deg} [kPa]	-97,1	-97,1	-97	-98,1	-98,2	-98,6	-97,5	-98,1
Degassing assistance system*2	N&P	N,S&P	S	P	N	-	NS	NP
Filling inlet pressure, P_{fill}^{inlet} [kPa]	0	0	0	0	0	0	0	0
Filling vent pressure, P_{fill}^{vent} [kPa]	-90	-90	-90	-90	-90	-90	-90	-90
Post-filling inlet pressure, P_{pfill}^{inlet} [kPa]	Clamp	Clamp	Clamp	Clamp	Clamp	Clamp	Clamp	Clamp
Post-filling vent pressure, P_{pfill}^{vent} [kPa]	-90	-90	-90	-90	-90	-90	-90	-90
Curing inlet pressure, P_{cure}^{inlet} [kPa]	Clamp	Clamp	Clamp	Clamp	Clamp	Clamp	Clamp	Clamp
Curing vent pressure, P_{cure}^{vent} [kPa]	-90	-90	-90	-90	-90	-90	-90	-90
Debulking time, t_{deb} [min]	87	104	101	106	97	77	119	91
Degassing time, t_{deg} [min]	20	40	40	40	40	20	20	20
Time until filling, $t_{0\rightarrow fill_0}$ [min]	57	78	70	79	61	48	45	50
Time until post-filling, $t_{0\rightarrow pfill_0}$ [min]	116	140	146	156	123	106	95	109
Filling time, t_{fill} [min]	59	62	76	77	62	58	50	59
Post-filling time, t_{pfill} [min]	35	34	32	31	32	42	30	29
Time until curing, $t_{0\rightarrow cure_0}$ [min]	151	174	178	187	155	148	125	138
Cure profile	3°C/min / 80°C / 180 min							

*1 Pressure drop during the air-tightness checking after 30 min.
*2 Degassing assistance systems: adding a nucleation medium (N), high-speed stirring (S) and later pressurization (P).

Table C.5. Manufacturing conditions of VI specimens presented in Chapter 5.

Factor	Specimen							
	A1	**A2**	**A3**	**A4**	**B1**	**B1'**	**B2**	**B3**
Debulking pressure, P_{deb} [kPa]	-92,5	-95,5	-95,5	-94,0	-96,0	-94,5	-96,0	-95,5
Debulking pressure drop, ΔP_{deb} [kPa]*1	-0,5	-0,5	-1,0	-1,0	0,0	-1,5	-2,0	-1,5
Degassing pressure, P_{deg} [kPa]	-98,3	-98,1	-98,0	-98,3	-98,1	-98,4	-98,4	-98,0
Degassing assistance system*2	MS	MS	MS	MS	MS	MS	MS	MS
Filling inlet pressure, P_{fill}^{inlet} [kPa]	-40,3	-40,3	0	0	0	0	0	0
Filling vent pressure, P_{fill}^{vent} [kPa]	-90	-95	-90	-95	-90	-90	-90	-94
Post-filling inlet pressure, P_{pfill}^{inlet} [kPa]	-90,1	-90,0	-89,8	-90,0	Clamp	Clamp	Clamp	-90,0
Post-filling vent pressure, P_{pfill}^{vent} [kPa]	-90	-90	-90	-90	-90	-90	-90	-90
Curing inlet pressure, P_{cure}^{inlet} [kPa]	-90,1	89,8	-90,0	-90,1	Clamp	Clamp	Clamp	-90,0
Curing vent pressure, P_{cure}^{vent} [kPa]	-90	-90	-90	-90	-90	-90	-90	-90
Debulking time, t_{deb} [min]	87	73	109	81	75	102	77	89
Degassing time, t_{deg} [min]	30	30	30	30	30	30	30	30
Time until filling, $t_{0\rightarrow fill_0}$ [min]	61	51	42	54	54	43	44	52
Time until post-filling, $t_{0\rightarrow pfill_0}$ [min]	67	55	47	57	57	45	51	56
Filling time, t_{fill} [min]	6	4	5	3	3	2	7	4
Post-filling time, t_{pfill} [min]	25	36	40	32	32	39	29	33
Time until curing, $t_{0\rightarrow cure_0}$ [min]	92	91	87	89	89	84	80	89
Cure profile	3°C/min / 60°C / 60 min / 3°C/min / 80°C / 120 min							

*1 Pressure drop during the air-tightness checking after 30 min.
*2 Degassing assistance systems: multi-point high-speed stirring (MS).

Table C.6. Manufacturing conditions of ISFLIP specimens presented in Chapter 6.

Factor	Specimen							
	A1	**A2**	**A3**	**A4**	**B1**	**B2**	**B3**	**B4**
Debulking pressure, P_{deb} [kPa]	-95,0	-96,0	-96,0	-95,5	-94,0	-95,5	-95,5	-94,5
Debulking pressure drop, ΔP_{deb} [kPa]*1	-1,5	0,0	-1,0	-1,0	-2,0	-1,0	-1,0	-2,0
Degassing pressure, P_{deg} [kPa]	-98,3	-98,4	-98,2	-98,1	-98,4	-98,4	98,4	-98,2
Degassing assistance system*2	MS	MS	MS	MS	MS	MS	MS	MS
Filling inlet pressure, P_{fill}^{inlet} [kPa]	0	0	0	0	0	0	0	0
Filling vent pressure, P_{fill}^{vent} [kPa]	-95	-96	-95	-95	-95	-95	-96	-95
Post-filling inlet pressure, P_{pfill}^{inlet} [kPa]	-91	-89,2	-88,6	-89,5	-90,0	-89,8	-89,8	-89,9
Post-filling vent pressure, P_{pfill}^{vent} [kPa]	-90	-90	-90	-90	-90	-90	-90	-90
Curing inlet pressure, P_{cure}^{inlet} [kPa]	-90,1	-89,2	-88,9	-89,3	-90,0	-89,8	-89,8	-89,7
Curing vent pressure, P_{cure}^{vent} [kPa]	-90	-90	-90	-90	-90	-90	-90	-90
Debulking time, t_{deb} [min]	104	95	144	103	100	94	105	121
Degassing time, t_{deg} [min]	30	30	30	30	30	30	30	30
Time until filling, $t_{0\rightarrow fill_0}$ [min]	54	45	46	49	60	53	52	48
Time until post-filling, $t_{0\rightarrow pfill_0}$ [min]	68	59	57	62	72	66	62	60
Filling time, t_{fill} [min]	14	14	11	13	12	13	10	12
Post-filling time, t_{pfill} [min]	31	41	42	23	36	48	29	41
Pressure between diaphragms, P_{diaph} [kPa]	-90	-90	-90	-90	-90	-90	-90	-90
Pressure into mould cavity, P_{mould} [kPa]	-90	-90	-90	-90	-90	-90	-90	-90
Forming time, t_{form} [min]	<1	<1	<1	<1	<1	<1	<1	<1
Time until curing, $t_{0\rightarrow cure_0}$ [min]	99	100	99	85	108	114	91	101
Cure profile	3°C/min / 60°C / 60 min / 3°C/min / 80°C / 120 min							

*1 Pressure drop during the air-tightness checking after 30 min.
*2 Degassing assistance systems: multi-point high-speed stirring (MS).

Table C.7. Partial and total filling times, t_{fill}, of VI specimens presented in Chapter 5.

Factor	Specimen							
	A1	**A2**	**A3**	**A4**	**B1**	**B1'**	**B2**	**B3**
Time to cover HPDM [s]	30-35	31-38	12-15	15-17	14-19	15-21	19-22	16-20
Time to recover lead-lag [s]	107-132	92-154	33-45	54-69	42-50	58-80	29-45	36-40
Time to fill preform [s]	178-223	174-210	64-69	85-103	77-94	51-68	99-119	78-88
Time to reach venting channel [s]	203-258	194-232	70-83	90-115	77-94	51-68	80-96	78-88

C.5. Preform thickness evolution during post-filling

While preform filling can be visually assessed, the post-filling step, when preform is completely impregnated, should be monitored through the preform thickness or resin pressure evolution. During post-filling, excess of resin accumulated into the preform is evacuated to equalize fibre volume fraction, v_f. Since the required set-up to measure resin pressure into the preform cavity is complex due to the polymerization reaction of the resin, it was preferred to measure preform thickness evolution from the onset of the post-filling step with two laser displacement sensors Keyence LC-2320.

In the first set of eight specimens manufactured for the screening of degassing procedures (Chapter 4), the two laser sensors were placed at approx. 30 mm of the inlet and venting channels. Preform thickness variations for each specimen are shown in Figure C.5.

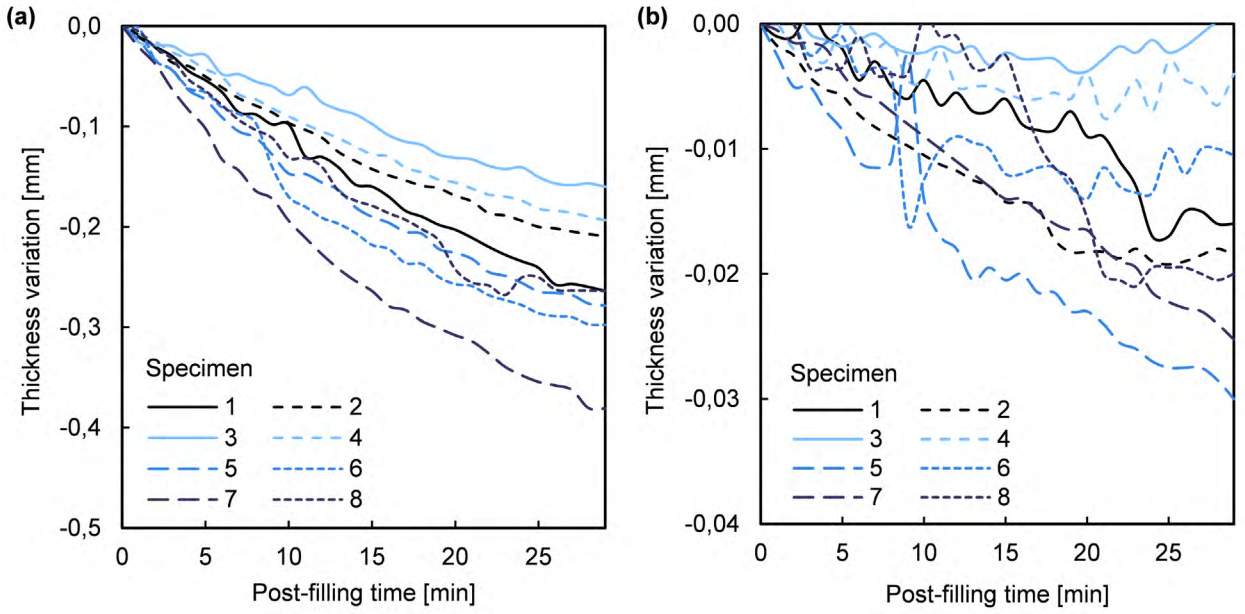

Figure C.5. Preform thickness variation during post-filling of specimens presented in Chapter 4: (a) sensor head placed at approx.30 mm of the inlet channel and (b) sensor head placed at approx. 30 mm of the venting channel.

In the second set of eight specimens manufactured for the screening of filling and post-filling conditions (Chapter 5), the two laser sensors were placed at approx. 30 mm of the inlet channels. In Figure C.6, it is shown preform thickness variation for different preform assembly configurations, and filling and post-filling conditions.

Curves shown in Figure C.6 were fitted through non-linear regression of data of both sensors and for various specimens. The regression equation of preform thickness variation, Δh, was

$$\Delta h = c_1 + c_2 \cdot e^{-\tau \cdot t_{pfill}} \quad (1)$$

where c_1, c_2 and τ are the fitting parameters, which are shown in Table C.8.

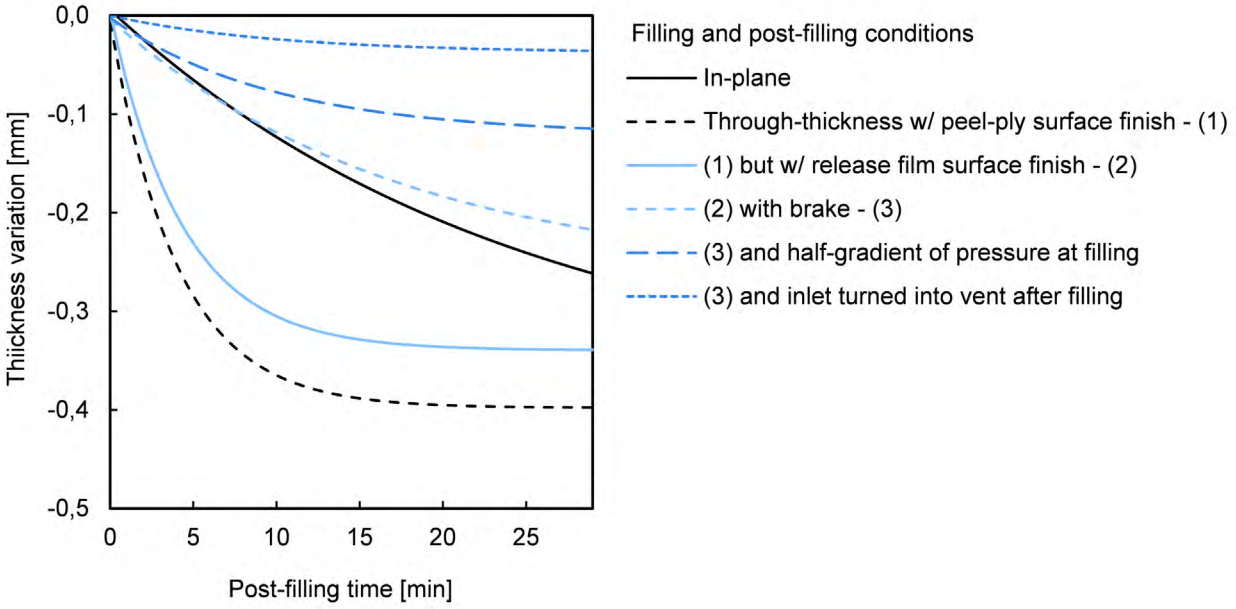

Figure C.6. Preform thickness variation during post-filling for different preform assembly configurations, and filling and post-filling conditions analysed in Chapter 5 (sensors placed at approx.30 mm of the inlet channel).

Table C.8. Environmental conditions during manufacturing of ISFLIP specimens presented in Chapter 6.

Filling and post-filling conditions	**Parameters**		
	c_1 [mm]	**c_2 [mm]**	**τ [1/min]**
In-plane flow with peel-ply upper release layer, full-gradient of pressure during filling, and without brake	-0,380	0,386	0,041
Through-thickness flow with peel-ply upper release layer, full-gradient of pressure during filling, and without brake	-0,398	0,391	0,247
Through-thickness flow with release film upper release layer, full-gradient of pressure during filling, and without brake	-0,340	0,343	0,229
Through-thickness flow with release film upper release layer, full-gradient of pressure during filling, and brake	-0,267	0,264	0,057
Through-thickness flow with release film upper release layer, half-gradient of pressure during filling, and brake	-0,121	0,119	0,101
Through-thickness flow with release film upper release layer, brake, and inlet turned into vent after filling	-0,038	0,038	0,101

Appendix D

Specimen characterization

This appendix serves as a complement of specimen characterization methods conducted throughout the research project and introduced in the main volume of the thesis dissertation. More extensive descriptions of the test methods are presented hereafter, as well as tests results which supplement in some way those shown in the main volume.

D.1. Specimens

D.1.1. Vacuum Infusion (VI)

VI specimens consisted on flat laminates formed by 9 layers of Glass Twill-Weave Fabrics (GTWF) of 320x220 mm and epoxy resin. Material details and stack configurations are available in the corresponding chapter: in-plane impregnated specimens in Chapter 4 and through-thickness impregnated specimens in Chapter 5. After being trimmed, a useful area of 300x200 mm per specimen was obtained.

In order to capture manufacturing parameter effects on final component quality, three different types of testing samples were regularly distributed over the useful area:

- Flexural properties were measured via three-point flexure samples coded as FYZ (60x15 mm), which were arranged in rows perpendicular to the main flow direction (direction x).

- Fibre, resin and void content fractions were calculated on samples CYZ (25x25 mm) distributed in a row parallel to the main flow direction via a loss on ignition method.
- Void content and morphology was studied through a row of samples MYZ (25x25 mm), also parallel to the main flow direction, via light microscopy. Micrographs were taken from cross-sections mark by the thicker line.

Specimens were identified by specimen labels (Y) assigned in the corresponding thesis chapter.

In case of in-plane impregnated specimens, three rows of flexural samples were placed near inlet and venting channels, and in an intermediated position to capture effects of gradient of pressure on outgassing behaviour of the epoxy resin. The generic pattern of samples used in this case is shown in Figure D.1.

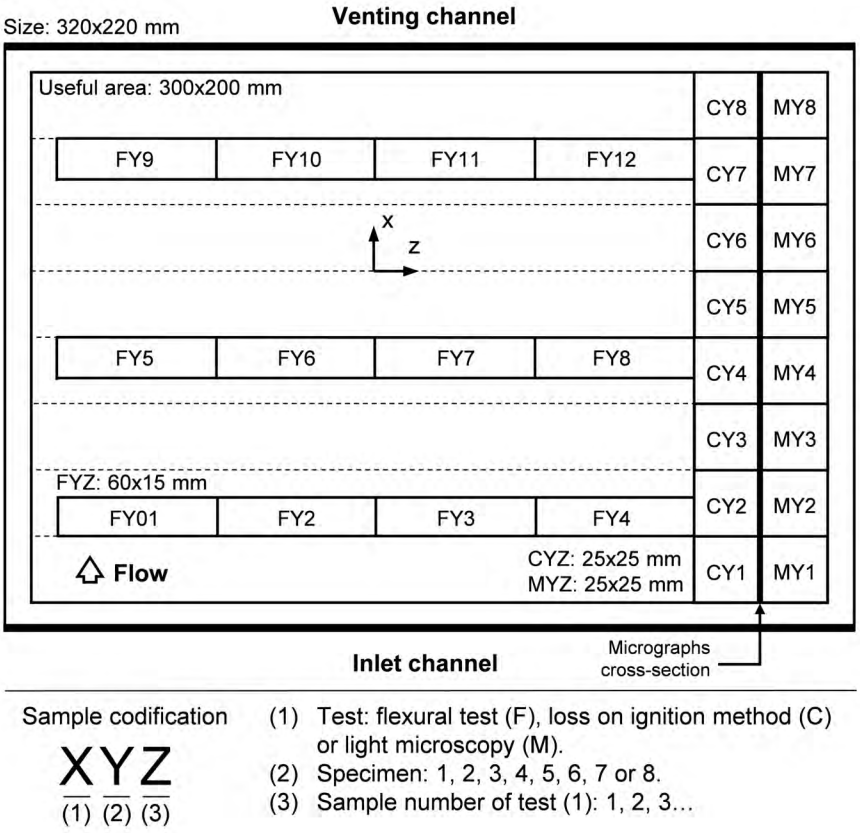

Figure D.1. Generic pattern of samples corresponding to specimens presented in Chapter 4 for screening of degassing procedures: size, distribution and codification rules.

In case of through-thickness impregnated specimens, due to the random distribution of porous areas, flexural samples were arranged according to each specimen needs. In Figure D.2, it is shown a possible pattern of samples including two rows of four flexural samples and one row of three flexural samples, which allow the lateral movement of samples to frame particular pore clusters. Besides, some samples MYZ had to be also placed in the region initially allocated to samples FYZ

to capture all different porosity distributions. Each samples MYZ with sample number (Z) higher than 08 was allocated in the region of samples FYZ.

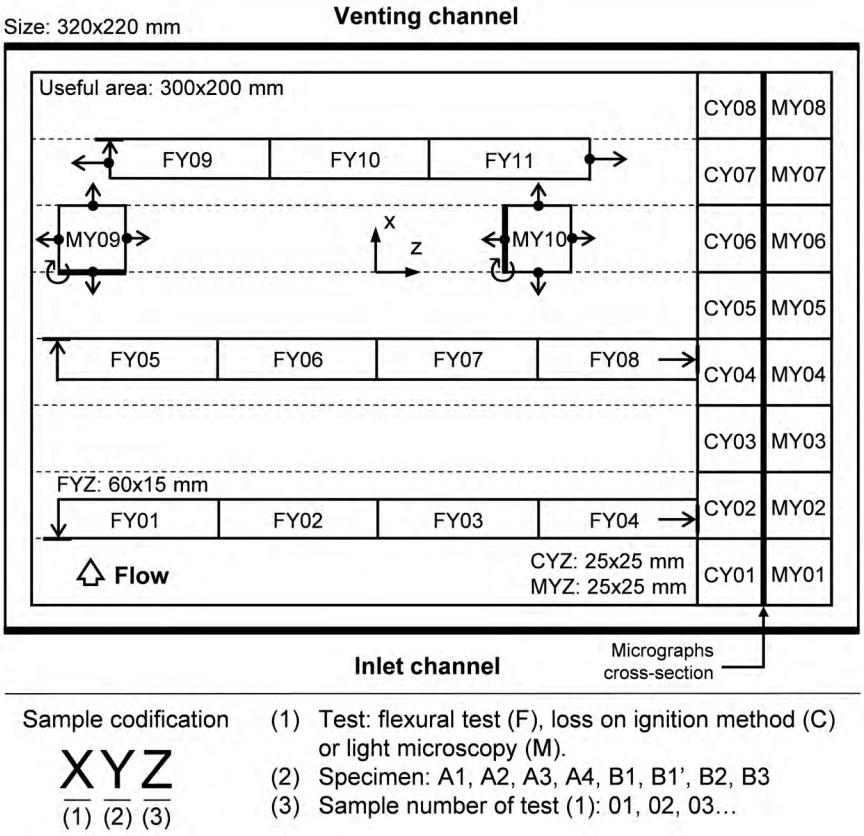

Figure D.2. Generic pattern of samples corresponding to specimens presented in Chapter 5 for screening of filling and post-filling conditions: size, distribution and codification rules.

D.1.2. *In Situ* Forming of a Liquid Infused Preform (ISFLIP)

A series of 'L' shape samples, obtained from specimens manufactured through ISFLIP, were tested in compression to measure the Inter-Laminar Normal Strength (ILNS) in the curved region (Figure D.3). ISFLIP specimens consisted on 'C' cross-section profiles formed by 9 layers of GTWF or Carbon Twill-Weave Fabrics (CTWF) and epoxy resin. Material details and stack configurations are available in Chapter 6.

D.2. Visual inspection

The translucent nature of the GTWF-epoxy specimens allowed to identify the specimen areas in which porosity was present. The open-source image processing package Fiji, based on ImageJ, was used to scan the top view pictures of the manufactured specimens.

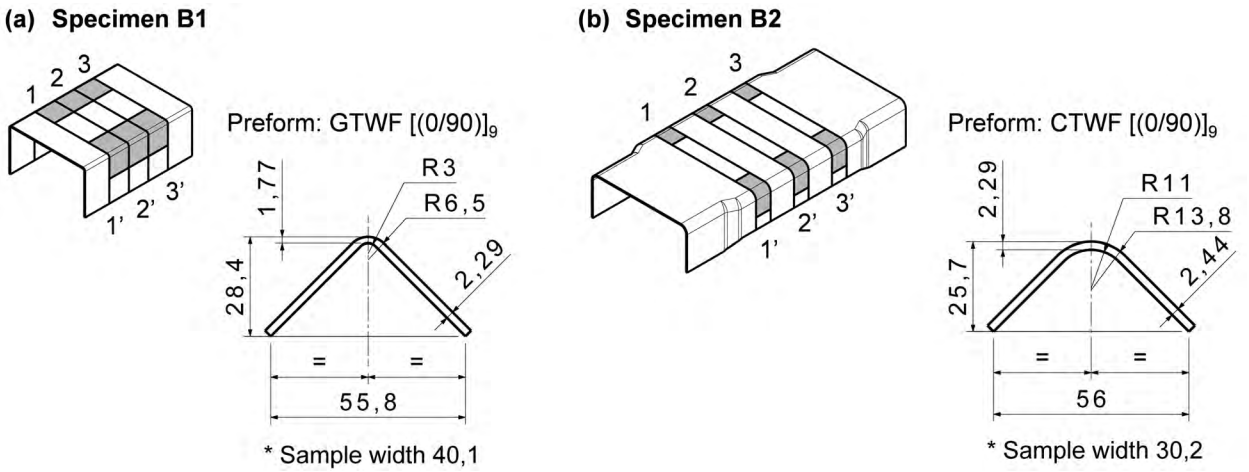

Figure D.3. Schematic drawing of 'L' shape samples location into each specimen and average dimensions.

D.2.1. In-plane impregnated specimens

For each specimen presented in Chapter 4, porous area fraction, s_0, was computed as the ratio of porous area, S_0, and specimen useful area, S_{useful}:

$$s_0 = \frac{S_0}{S_{useful}} \tag{2}$$

From the top view pictures of manufactured specimens, the following procedure was followed in Fiji to compute S_0 in pixels for each specimen, being S_{useful} the total number of pixels of the picture.

The macro Visual_Inspection1.ijm was run for each PAT present into each specimen. This macro combined a series of commands to be carried out by the user and a series of actions automatically conducted.

Commands

1. Open the top view picture of the specimen.
2. Select Brush tool (colour: black, width: 5) to mark the boundary between porous and non-porous areas.
3. Save processed picture using the specimen label (Y) in order to present the results of the processed pictures.

Actions

4. Convert RGB picture to grey scale.
5. Convert grey scale image to binary (threshold range: 0-0).

Commands

6. Select Flood filler tool (colour: black) and apply to the porous area.

Actions

7. Set the data to be gathered in the analysis of the porous area (parameters: area, centroid, perimeter, bounding rectangle, fit ellipse, shape descriptors, Feret's diameter, median, skewness, kurtosis, area fraction; invert Y coordinates: yes; decimal places: 3).
8. Analyse the porous area region (size:10-∞, circullarity:0,00-1,00, pixel units: yes, show masks: yes, display results: yes, clear results: yes).
9. List coordinates of all pixels belonging to the porous area (background value: 0, suppress log output: yes).

Commands

10. Save processed picture using the specimen label (Y).
11. Save coordinates of all pixels belonging to the porous area using the specimen label (Y).
12. Select the window containing the data gathered from the porous area region and save it using specimen label (Y).

Due to the in-plane preform impregnation and the decreasing gradient of pressure trapped into the preform when resin gelation occurred, a continuous porous area was formed in the proximity of the venting channel. S_0 was determined from the area (in pixels) of the single region of porosity.

D.2.2. Through-thickness impregnated specimens

Porosity of specimens presented in Chapter 5 was classified according to its macroscopic aspect of pore distribution, discerning between three different Porous Area Types (PAT): scattered porosity (PAT I), isolated pore clusters (PAT II) and large pore clusters (PAT III). Fractions of each PAT, s_0^i, were calculated as the ratio between the porous area corresponding to each type, S_0^i, and the specimen useful area, S_{useful}, such that

$$s_0^i = \frac{S_0^i}{S_{useful}}, \qquad i = I, II, III \tag{3}$$

From the top view pictures of manufactured specimens, the following procedure was followed in Fiji to compute S_0^i in pixels for each specimen, being S_{useful} the total number of pixels of the picture.

The macro Visual_Inspection2.ijm was run for each PAT present into each specimen. This macro combined a series of commands to be carried out by the user and a series of actions automatically conducted.

Commands

1. Open the top view picture of the specimen.

Actions

2. Convert RGB picture to grey scale.

Commands

3. Subtract background to highlight the difference between each PAT and non-porous areas: Process > Subtract background (Rolling ball radius: 10).

Actions

4. Enhance contrast (saturated pixels: 0,4%).
5. Convert grey scale image to binary (criterion: IsoData, Background:Dark).

Commands

6. Select the adequate threshold level to capture the corresponding PAT.

Actions

7. Overlay initial pictures over processed picture to assist artefacts removal (opacity: 75%).

Commands

8. Select Brush tool (colour: black) to paint over undesired artefacts present in the picture.
9. Select Brush tool (colour: red) to mark the boundary of the corresponding PAT regions.
10. Select Flood filler tool (colour: red) and apply to the corresponding PAT regions.

Actions

11. Set the data to be gathered in the analysis of regions of the corresponding PAT (parameters: area, centroid, perimeter, bounding rectangle, fit ellipse, shape descriptors, Feret's diameter, median, skewness, kurtosis, area fraction; invert Y coordinates: yes; decimal places: 3).
12. Analyse regions of the corresponding PAT (size:10-∞, circullarity:0,00-1,00, pixel units: yes, show masks: yes, display results: yes, clear results: yes).
13. List coordinates of all pixels belonging to the corresponding PAT (background value: 0, suppress log output: yes).

Commands

14. Save processed picture using the specimen label (Y).
15. Save coordinates of all pixels belonging to the corresponding PAT using the specimen label (Y).
16. Select the window containing the data gathered from the regions of the corresponding PAT and save it using the specimen label (Y).

Due to the through-thickness preform impregnation and an equalized pressure distribution into the preform when resin gelation occurred, each PAT occupied apparently random regions of the specimen. S_0^i was computed as the sum of areas (in pixels) of all individual PAT regions.

In order the present the results of the processed pictures, the macro Colour_Overlay.ijm was successively run adding a PAT each time to the original picture.

Commands

1. Open the original top view picture of the specimen.
2. Open the binary top view picture of the specimen.
3. Open in the lookup table editor the file with the colour codes for the corresponding PAT (PAT I.lut, PAT II.lut or PAT III.lut).

Actions

4. Overlap the binary picture after being coloured over the original picture.

Commands

5. Save processed picture using the specimen label (Y).

Original and binary top view pictures of all processed specimens, as well as all cited macros and lookup table files, are provided in electronic form.

D.3. Thickness measurement

The final thickness of VI specimens was checked by measuring thickness of samples MYZ, obtaining a continuous thickness distribution along specimens in the main flow direction (direction x) and, consequently, allowing the identification of possible thickness trends into specimens. Since thickness was measured in a wide area, it was also possible to compare thickness results with thickness tolerances of a potential competitor of Fibre Reinforced Polymer (FRP) components such as cold-rolled aluminium plates, UNE-EN 485-4:1994.

D.3.1. Method

Thickness was measured with a calibrated micrometre of resolution $0{,}01$ mm. For each specimen, three thickness measures h_{YZi} $(i = 1{,}2{,}3)$ were taken into each MYZ sample to obtain a mean value per sample

$$\bar{h}_{YZ.} = \frac{1}{3}\sum_{i=1}^{3} h_{YZi} \tag{4}$$

where Y referred to the specimen, and Z to the sample number (MYZ) into each specimen.

Then, thickness per sample of all specimens was averaged such that

$$\bar{h}_{.Z.} = \frac{1}{n_Y}\sum_{Y=1}^{n_Y} \bar{h}_{YZ.} \tag{5}$$

where n_Y was the number of specimens included in the considered set.

Finally, a mean thickness value was calculated for all $n_Z = 8$, MYZ samples per specimen as

$$\bar{h}_{\cdots} = \frac{1}{n_Z}\sum_{Z=1}^{n_Z} \bar{h}_{\cdot Z \cdot} \tag{6}$$

Equivalent tolerances according to UNE-EN 485-4:1994 were determined from to $\bar{h}_{\cdots}$.

D.3.2. Results

Measured thickness of in-plane impregnated specimens (Chapter 4) is depicted in Figure D.4.

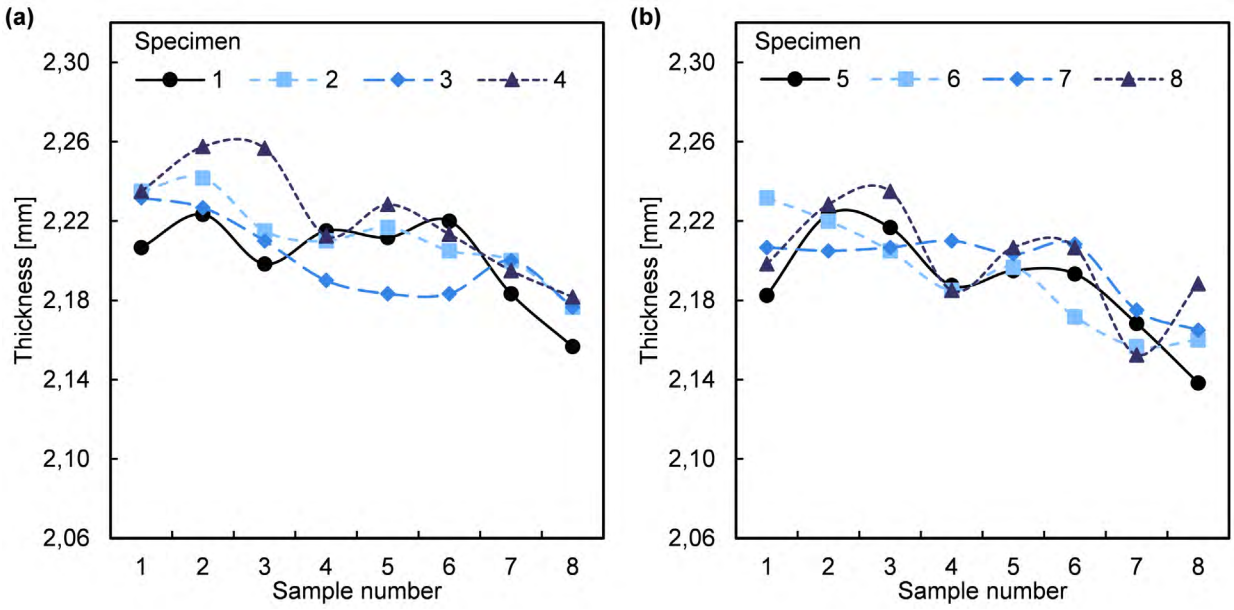

Figure D.4. Mean thickness per sample, $\bar{h}_{YZ\cdot}$, of VI specimens presented in Chapter 4.

Besides, Figure D.5 shows the mean thickness per sample for all specimens $\bar{h}_{\cdot Z \cdot}$ and its 95% confidence interval, maximum and minimum h_{YZi} and the equivalent tolerance determined from $\bar{h}_{\cdots} = 2{,}20$ mm according to UNE-EN 485-4:1994.

Measured thickness of through-thickness impregnated specimens (Chapter 5) is depicted in Figure D.6. Figure D.6.a contains thickness measures of specimens with release film surface finish, while Figure D.6.b contains thickness measures of specimens with peel-ply surface finish.

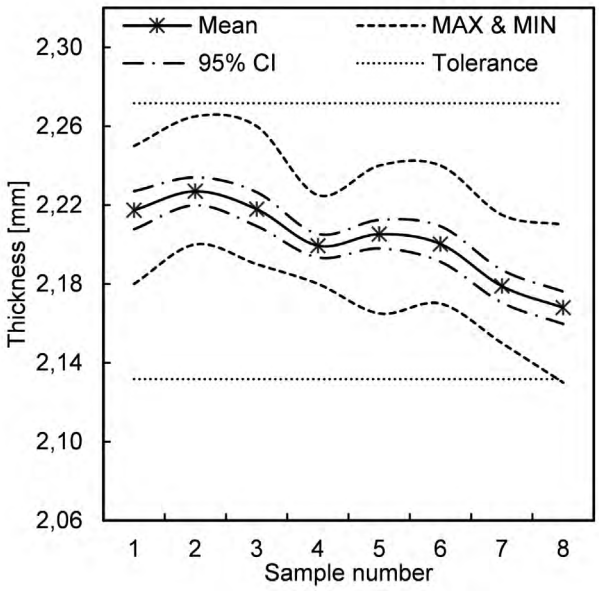

Figure D.5. Thickness descriptors of VI specimens presented in Chapter 4.

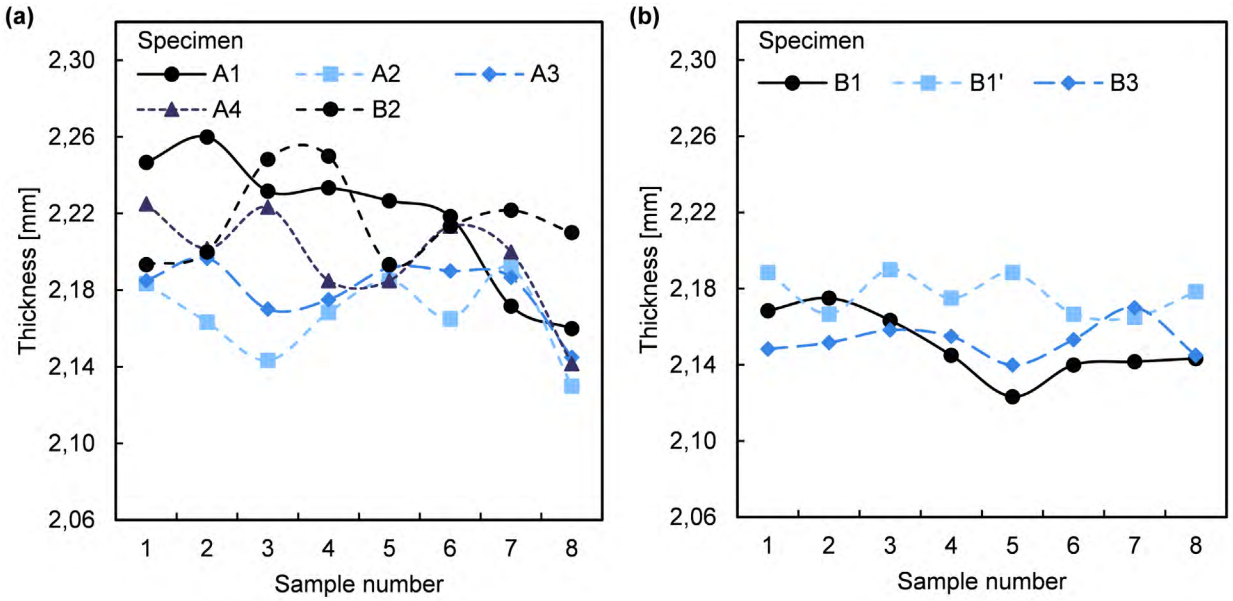

Figure D.6. Mean thickness per sample, $\bar{h}_{YZ.}$, of VI specimens presented in Chapter 5:
(a) specimens with release film surface finish and (b) specimens with peel-ply surface finish.

Additionally, Figure D.7 shows the mean thickness per sample for all specimens $\bar{h}_{.Z.}$ and its 95% confidence interval, maximum and minimum h_{YZi}, and the equivalent tolerance determined from $\bar{h}_{...} = 2{,}19$ mm and $\bar{h}_{...} = 2{,}16$ mm for release film and peel-ply surface finishes respectively, according to UNE-EN 485-4:1994. Figure D.7.a contains thickness descriptors of specimens with release film surface finish, while Figure D.7.b contains thickness descriptors of specimens with peel-ply surface finish.

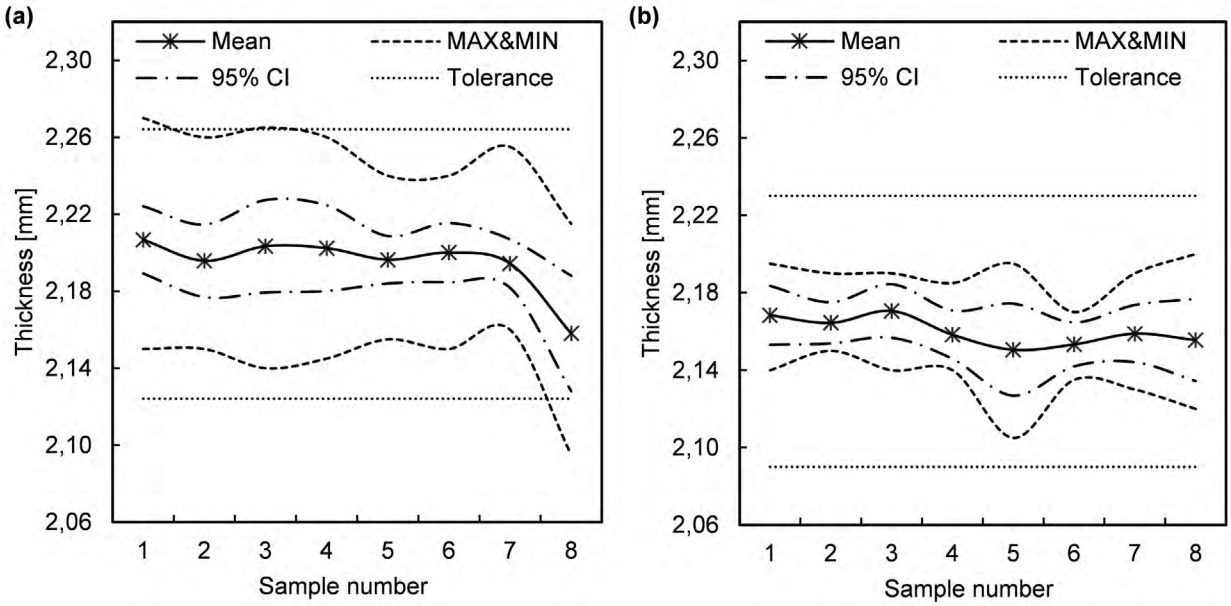

Figure D.7. Thickness descriptors of VI specimens presented in Chapter 5:
(a) specimens with release film surface finish and (b) specimens with peel-ply surface finish.

D.4. Loss on ignition method

Samples coded as CYZ in Figure D.1 and Figure D.2 were tested via the loss on ignition, also referred as “calcination”, method according to the procedure stated in the standards UNE-EN ISO 1172:1999 and UNE-EN ISO 7822:2001, in order to determine E-glass, epoxy resin and void contents. Both cited standards are addressed to textile glass reinforced polymers.

Calcinations were carried out in the facilities of the Departament de Ciència dels Materials i Enginyeria Metal·lúrgica (CMEM) of the Universitat Politècnica de Catalunya (UPC) in Terrassa. The special equipment employed to conduct the loss on ignition method was a set of porcelain crucibles, a desiccator with silica gel, an analytical balance Mettler Toledo H10W, a drying oven JP Selecta 2000201, and a muffle furnace Carbolite AAF1100.

D.4.1. Method

CYZ samples (nominal size 25x25 mm) resulted in a total weight between 2,20 g and 2,60 g, depending on the manufacturing conditions and the sample position into the specimen. Sample weights met the requirement stated in standard UNE-EN ISO 1172:1999 of sample weight for laminates between 2 g and 10 g; however, resulting volumes were smaller than 2 cm^3 recommended in standard UNE-EN ISO 7822:2001. Besides, all specimens had at least one

texturized surface, hence it was not possible to mechanically measure the real volume of the samples. Sample dimensions were measured with a calibrated micrometre of resolution 0,01 mm.

Before carrying out the loss on ignition method, crucibles into which samples were placed were checked through the following procedure:

1. Weigh a clean and dry crucible in the balance.
2. Place the crucible into the muffle furnace (pre-heated to 625 ℃) for 10 min.
3. Cool the crucible into the desiccator to environmental temperature.
4. Weight the crucible in the balance to check that no change in mass occurs.

Since no fillers were present into the specimens, Method A defined in the standards was adopted to determine component contents. The procedure followed to proceed with the calcination of each sample consisted on:

1. Measure sample volume (three measures per side and five thickness measures), V_{sample}.
2. Weight a clean and dry crucible on the balance, M_1.
3. Dry the sample placed in the crucible into the drying oven at 105 ℃ for 60 min.
4. Cool the crucible and the sample into the desiccator to environmental temperature.
5. Weight the crucible and the sample on the balance, M_2.
6. Place the crucible and the sample into the muffle furnace (pre-heated to 625 ℃) for 60 min.
7. Cooling the crucible and the residue into the desiccator to environmental temperature.
8. Weight the crucible and the residue on the balance, M_3.

Once M_1, M_2 and M_3 were determined, the glass mass fraction, m_f, and the resin mass fraction, m_r, were calculated as

$$m_f = \frac{M_3 - M_1}{\mathrm{M}_2 - M_1}\,, \qquad m_r = \frac{M_3 - M_2}{\mathrm{M}_2 - M_1} \tag{7}$$

Furthermore, from the nominal densities of E-glass fibre and epoxy resin, $\rho_f = 2544\ \mathrm{kg/m^3}$ and $\rho_r = 1095\ \mathrm{kg/m^3}$ [1], component volume fractions can be computed such that

$$v_f = \frac{m_f/\rho_f}{V_{sample}}\,, \qquad v_r = \frac{m_r/\rho_r}{V_{sample}} \tag{8}$$

and, finally, void volume fraction, v_0, was estimated for each sample by applying the balance of component fractions:

$$v_0 = 1 - v_f - v_r \tag{9}$$

The determination of v_0 presented two limitations: 25x25 mm samples resulted in a range of volumes ~1,4 cm^3 lower than the minimum 2 cm^3 recommended in the standards; and the texturized surfaces caused an over-estimation of sample volumes and, thus, $v_0 > 0\%$ were obtained even in samples with no porosity expectation.

Since translucent specimens allowed to identify which samples contained trapped pores, those n samples into each set with expectation of no porosity were used to compute an average surface void volume, $\bar{V}_0^{surf}$, as

$$\bar{V}_0^{surf} = \frac{1}{n}\sum\left(v_0 \cdot V_{sample}\right) \tag{10}$$

Then, updated fibre and resin volume fractions, v_f' and v_r' respectively, were calculated considering an adjusted volume according to $\bar{V}_0^{surf}$ such that

$$v_f' = \frac{m_f/\rho_f}{V_{sample} - \bar{V}_0^{surf}}, \qquad v_r' = \frac{m_r/\rho_r}{V_{sample} - \bar{V}_0^{surf}} \tag{11}$$

Finally, v_0' was estimated for each sample by applying the balance of component fractions:

$$v_0' = 1 - v_f' - v_r' \tag{12}$$

D.4.2. Results

In the set of VI specimens presented in Chapter 4 to screen between different degassing procedures, m_f, v_f and v_o of those calcined samples are shown in Figure D.8. Computed v_f' and v_0' are provided in Chapter 4, and corresponding resin contents can be determined through the balance of component fractions.

In case of the set of VI specimens presented in Chapter 5 to screen between different filling and post-filling conditions, m_f, v_f and v_o of those calcined samples are shown in Figure D.9. Computed v_f' are provided in Chapter 5, v_0' did not show significant enough levels and corresponding resin contents can be determined through the balance of component fractions.

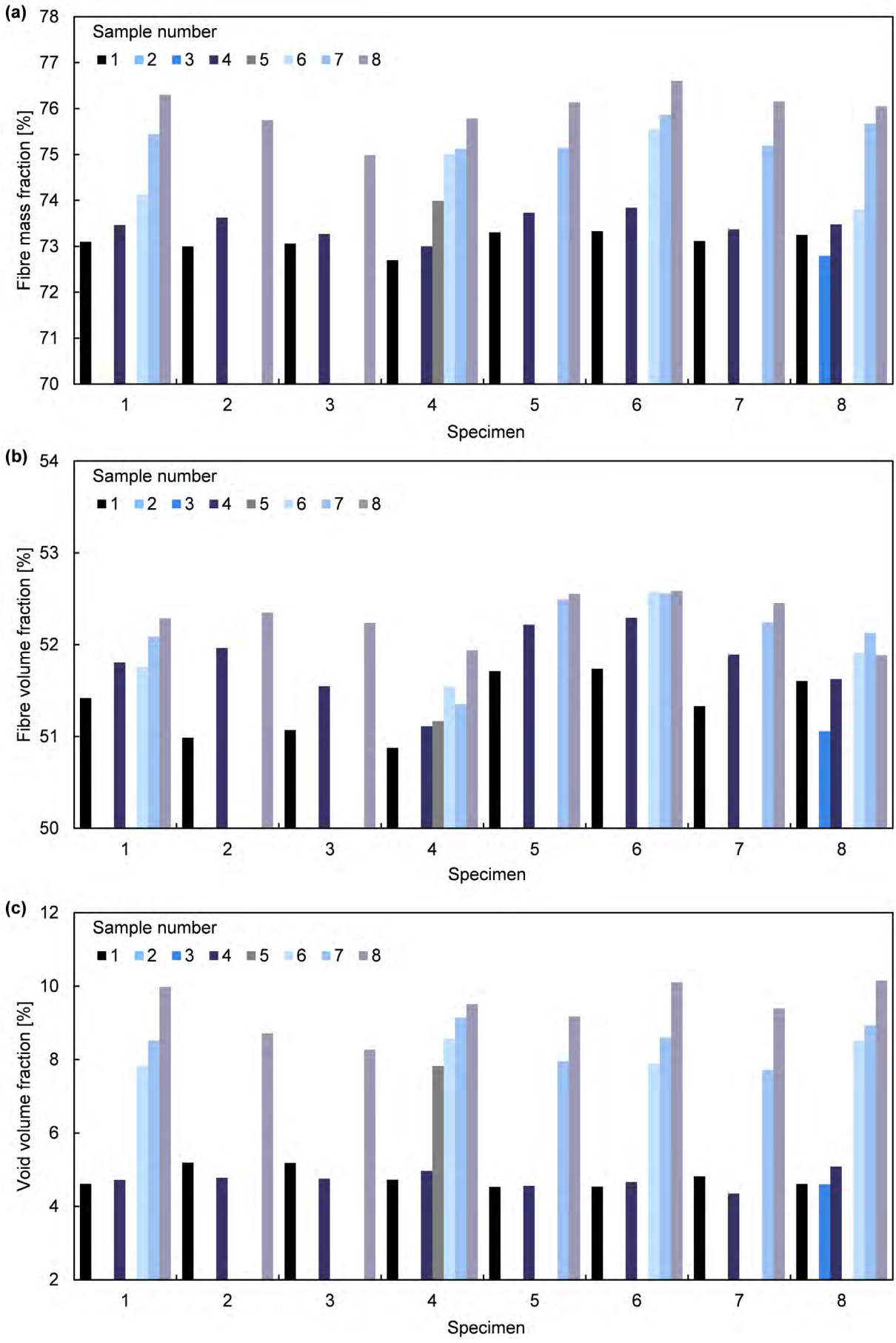

Figure D.8. Results of the loss on ignition method in the set of specimens presented in Chapter 4: (a) Mass fibre fraction, m_f, (b) fibre volume fraction, v_f, and (c) void volume fraction, v_0.

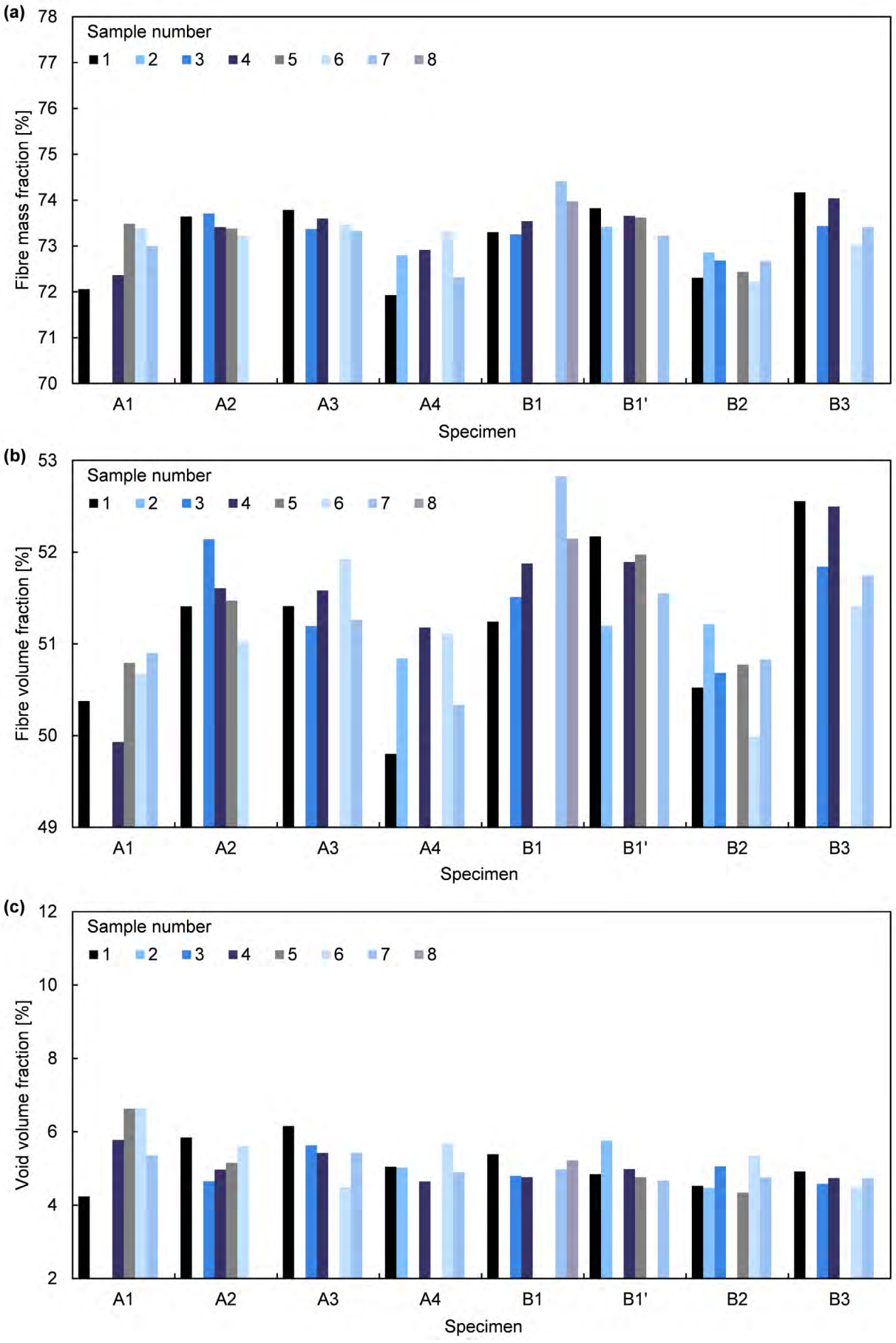

Figure D.9. Results of the loss on ignition method in the set of specimens presented in Chapter 5: (a) Mass fibre fraction, m_f, (b) fibre volume fraction, v_f, and (c) void volume fraction, v_0.

D.5. Three-point flexure test

Flexural properties of samples coded as FYZ in Figure D.1 and Figure D.2 were obtained through a three-point flexure test according to the procedure stated in the standard UNE-EN ISO 14125:1999.

Tests were carried out in the facilities of the Departament de Ciència dels Materials i Enginyeria Metal·lúrgica (CMEM) of the Universitat Politècnica de Catalunya (UPC) in Terrassa, with a MTS Universal testing machine equipped with a load cell of 10 kN.

D.5.1. Method

Information included below refers to the material type "Class III" defined in the standard, which corresponds to the GTWF reinforcement used in VI specimens. The three-point loading arrangement is shown in Figure D.10.

Nominal sample dimensions defined in the standard are length $l = 60$ mm, width $w = 15$ mm and thickness $h = 2$ mm. However, real sample thickness ranged from 2,1 mm to 2,3 mm depending on the manufacturing conditions and the sample position into the specimen. Sample cross-sections were measured with a calibrated micrometre of resolution 0,01 mm.

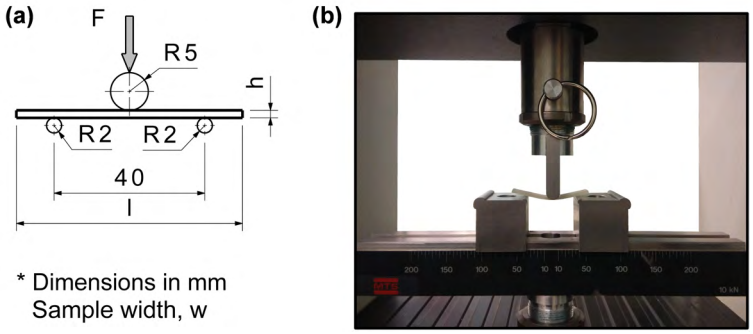

Figure D.10. Experimental set-up of the three-point flexure test: (a) schematic drawing and (b) test execution.

Samples were tested at 1 mm/min to keep strain rate $\dot{\varepsilon}$ as close as possible to 0,01. Speed v can be calculated from the following expression:

$$v = \frac{\dot{\varepsilon} l'^2}{6h} \tag{13}$$

where $l' = 40$ mm is the span between supports. For $h = 2{,}2$ mm, it resulted a testing speed $v = 1{,}21$ mm/min.

A thin polyethylene shim of thickness 0,5 mm was placed between the upper loading cylinder and the sample to avoid undesired failure of the compression face of the samples. Tests were not conducted to the complete failure of the material, but until a performance drop of at least 10% to allow later identification of the failure mode (Figure D.11).

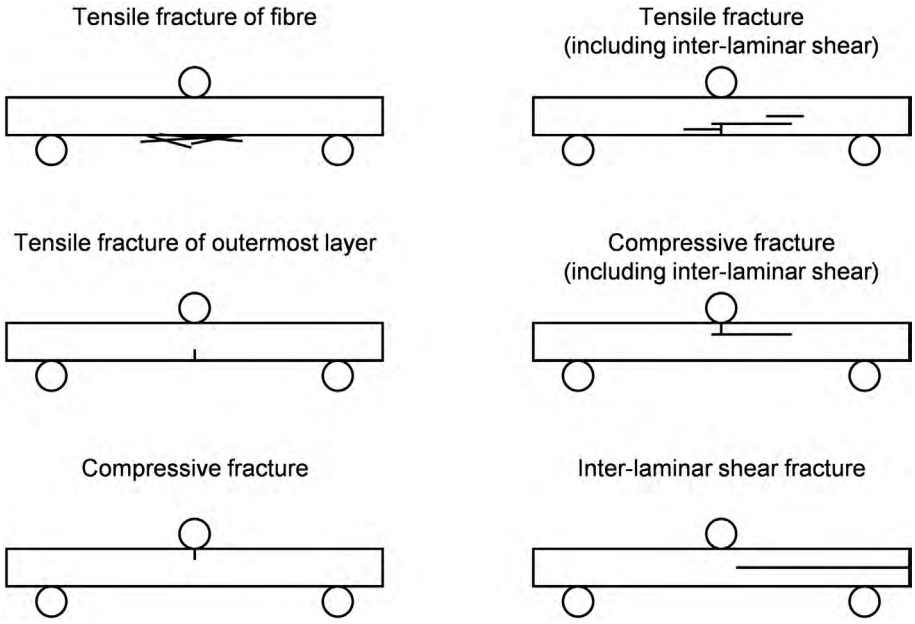

Figure D.11. Schematic drawings of possible failure models in three-point flexure tests.

Only tensile-initiated and compressive-initiated, remote from loading points, are acceptable failure modes. Failure initiated by inter-laminar shear are not acceptable too.

Flexure stress, σ_f, vs. strain, ε_f, response was calculated from the crosshead load, F, and deflection at the mid-point, s, by applying corrections due to large deflections; since the final deflection was larger than $0{,}1l'$:

$$\sigma_f = \frac{3Fl'}{2wh^2}\left\{1 + \left(\frac{s}{l'}\right)^2 - 3\left(\frac{sh}{l'^2}\right)\right\} \tag{14}$$

$$\varepsilon_f = \frac{h}{l'}\left\{6{,}00\frac{s}{l'} - 24{,}37\left(\frac{s}{l'}\right)^3 + 62{,}17\left(\frac{s}{l'}\right)^5\right\} \tag{15}$$

Flexural strength, σ_{fM}, is determined as the flexural stress sustained by the specimen at the maximum load. Flexural modulus, E_f, was estimated by applying a linear regression procedure to the curve σ_f vs. ε_f between $\varepsilon_f = 0{,}010$ and $\varepsilon_f = 0{,}014$, a section of the response curve in which slope kept stable after an initial instability that might have been caused by backslash in the spindles of the testing machine or by initial settling of the samples between the round supports.

D.5.2. Results

Flexural response curves σ_f vs. ε_f of samples from in-plane impregnated VI specimens (Chapter 4) are depicted in Figure D.12 and Figure D.13. Besides, σ_{fM} and E_f data is gathered in Table D.1.

Flexural response curves σ_f vs. ε_f of samples from through-thickness impregnated VI specimens (Chapter 5) are depicted in Figure D.14, Figure D.15, Figure D.16 and Figure D.17. Besides, σ_{fM} and E_f data is gathered in Table D.2. Samples are also classified according to testing orientation (upwards or downwards) and the PAT to which they belonged in Table D.3.

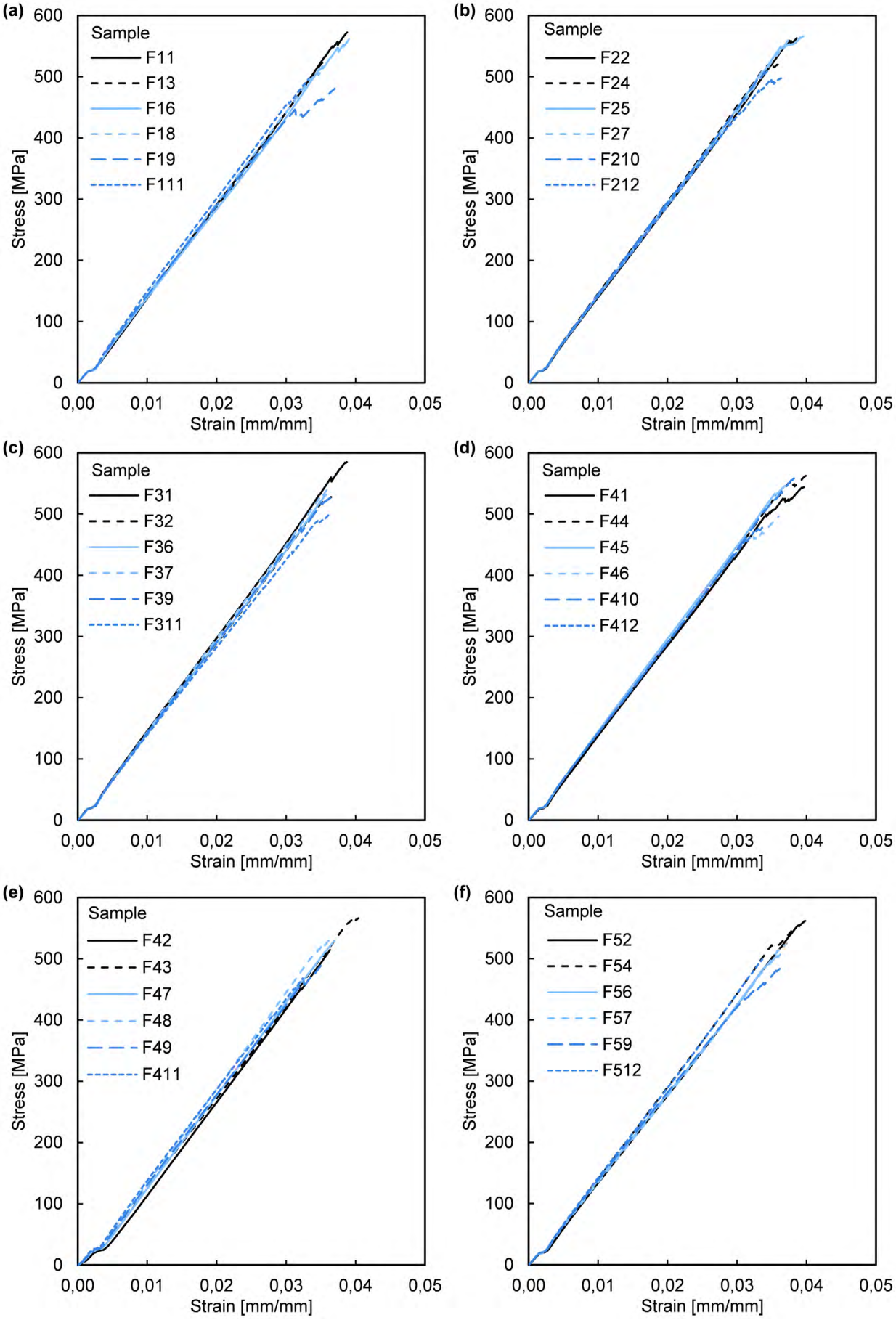

Figure D.12. Flexure response of samples belonging to specimens presented in Chapter 4 (1/2)

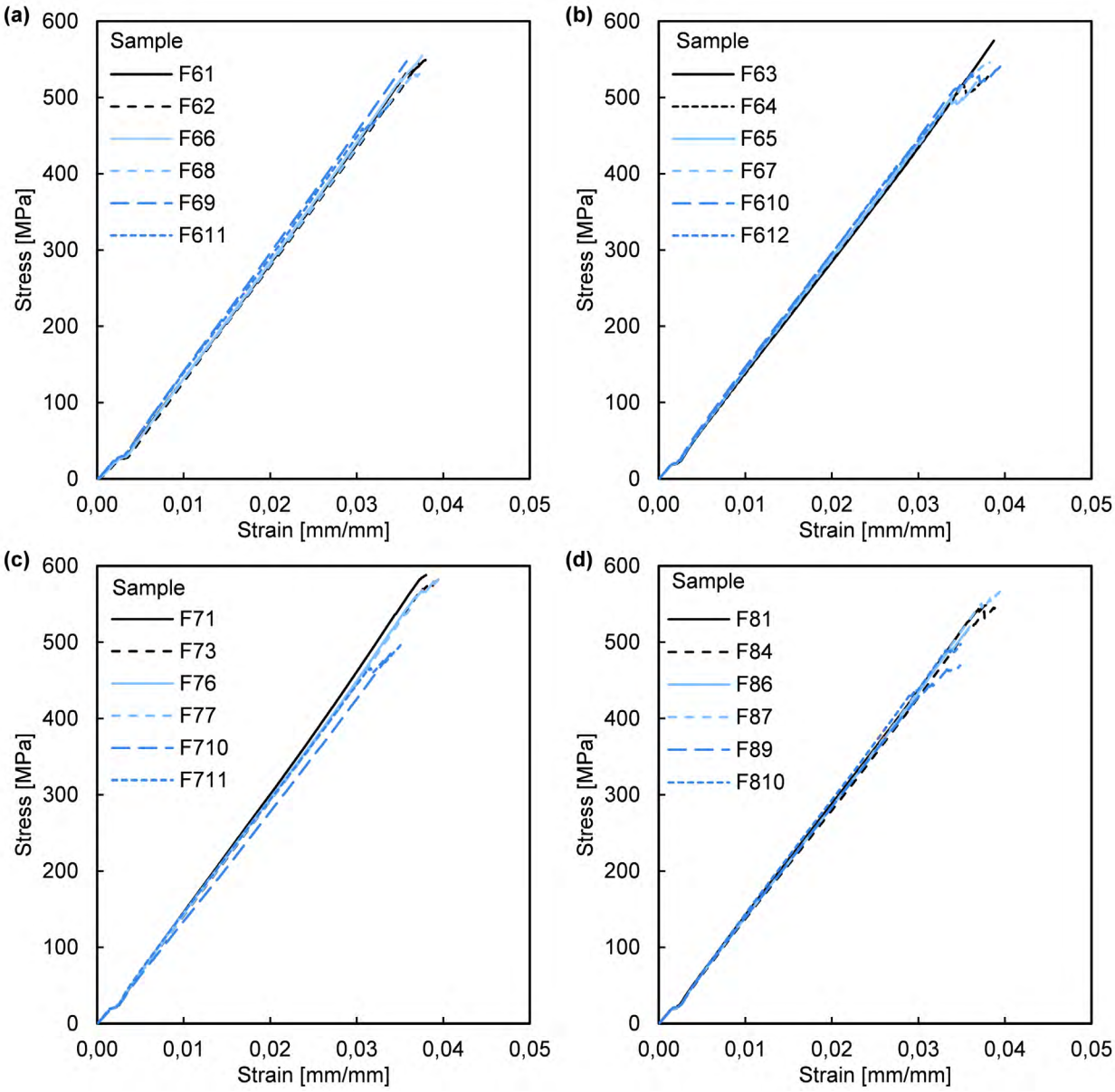

Figure D.13. Flexure response of samples belonging to specimens presented in Chapter 4 (2/2).

Table D.1. Flexural properties of samples belonging to specimens presented in Chapter 4.

Sample	σ_{fM} [MPa]	E_f [GPa]	Sample	σ_{fM} [MPa]	E_f [GPa]	Sample	σ_{fM} [MPa]	E_f [GPa]
F11	562	15,1	F16	551	14,3	*F19*	*471*	*14,3*
F13	517	14,4	F18	502	14,7	*F111*	*488*	*14,9*
F22	553	14,4	F25	556	14,6	*F210*	*500*	*14,7*
F24	518	14,6	F27	549	14,4	*F212*	*490*	*14,5*
F31	574	14,7	F36	522	14,4	F39	518	14,5
F32	518	14,4	F37	537	14,9	*F311*	*492*	*14,0*
F41	534	14,5	*F45*	*536*	*14,8*	*F49*	*488*	*14,8*
F42	515	15,4	*F46*	*487*	*14,6*	*F410*	*548*	*14,3*
F43	566	14,9	*F47*	*530*	*15,1*	*F411*	*468*	*14,9*
F44	553	14,5	*F48*	*538*	*15,3*	*F412*	*471*	*14,1*
F52	562	14,3	F56	507	14,1	*F59*	*483*	*14,4*
F54	545	15,0	F57	525	14,1	*F512*	*499*	*14,6*
F61	549	14,9	F65	520	14,9	*F69*	*547*	*15,3*
F62	545	15,3	F66	555	15,2	*F610*	*540*	*15,0*
F63	574	14,4	F67	546	14,7	*F611*	*493*	*14,9*
F64	532	14,8	F68	538	15,0	*F612*	*479*	*15,2*
F71	588	15,5	F76	582	15,0	*F710*	*493*	*14,1*
F73	583	15,0	F77	545	15,0	*F711*	*500*	*14,8*
F81	548	14,6	F86	520	14,5	*F89*	*469*	*14,4*
F84	546	14,3	F87	570	14,3	*F810*	*497*	*15,0*

* In italics those samples belonging to the porous area.

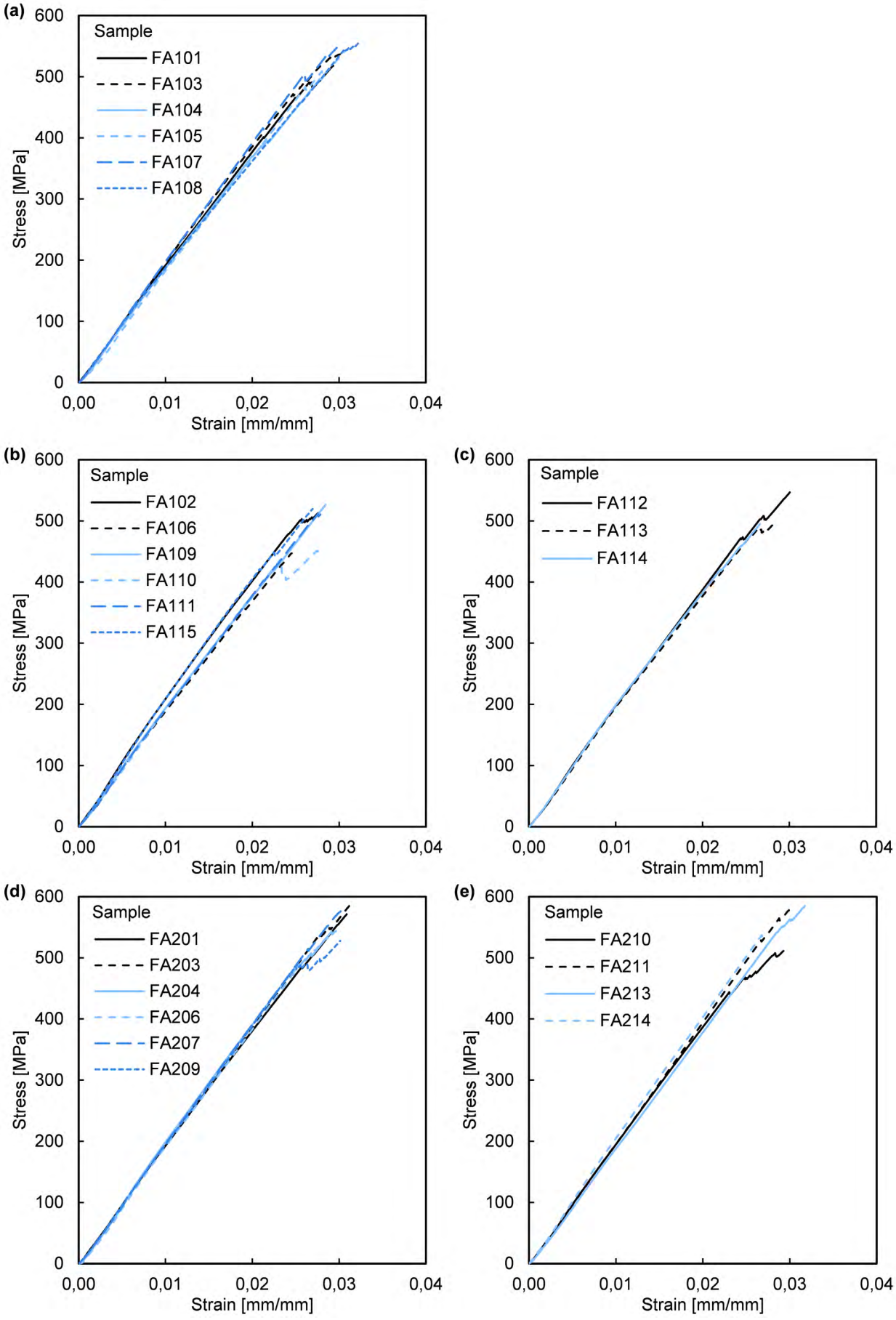

Figure D.14. Flexure response of samples belonging to specimens presented in Chapter 5 (1/4).

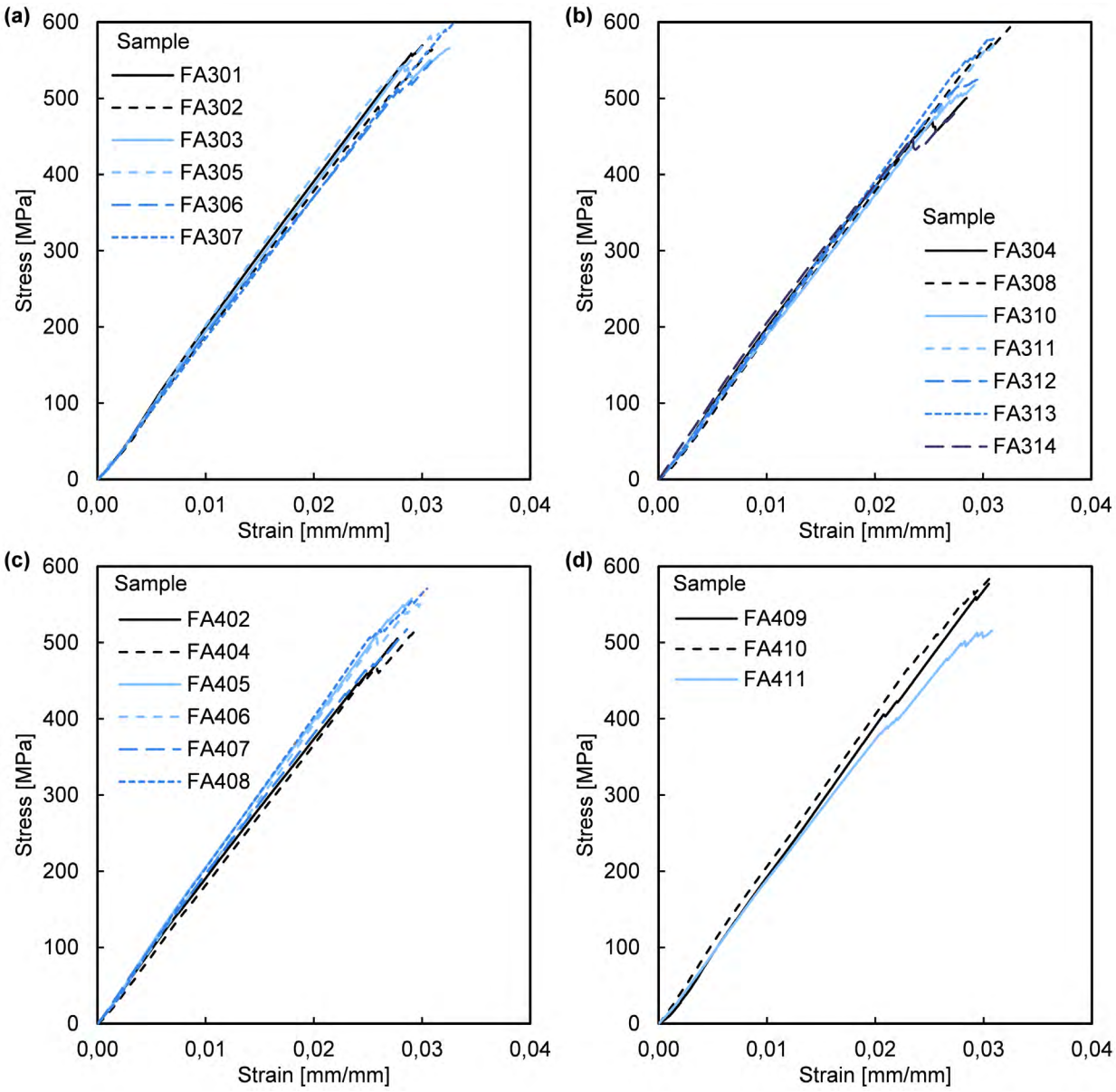

Figure D.15. Flexure response of samples belonging to specimens presented in Chapter 5 (2/4).

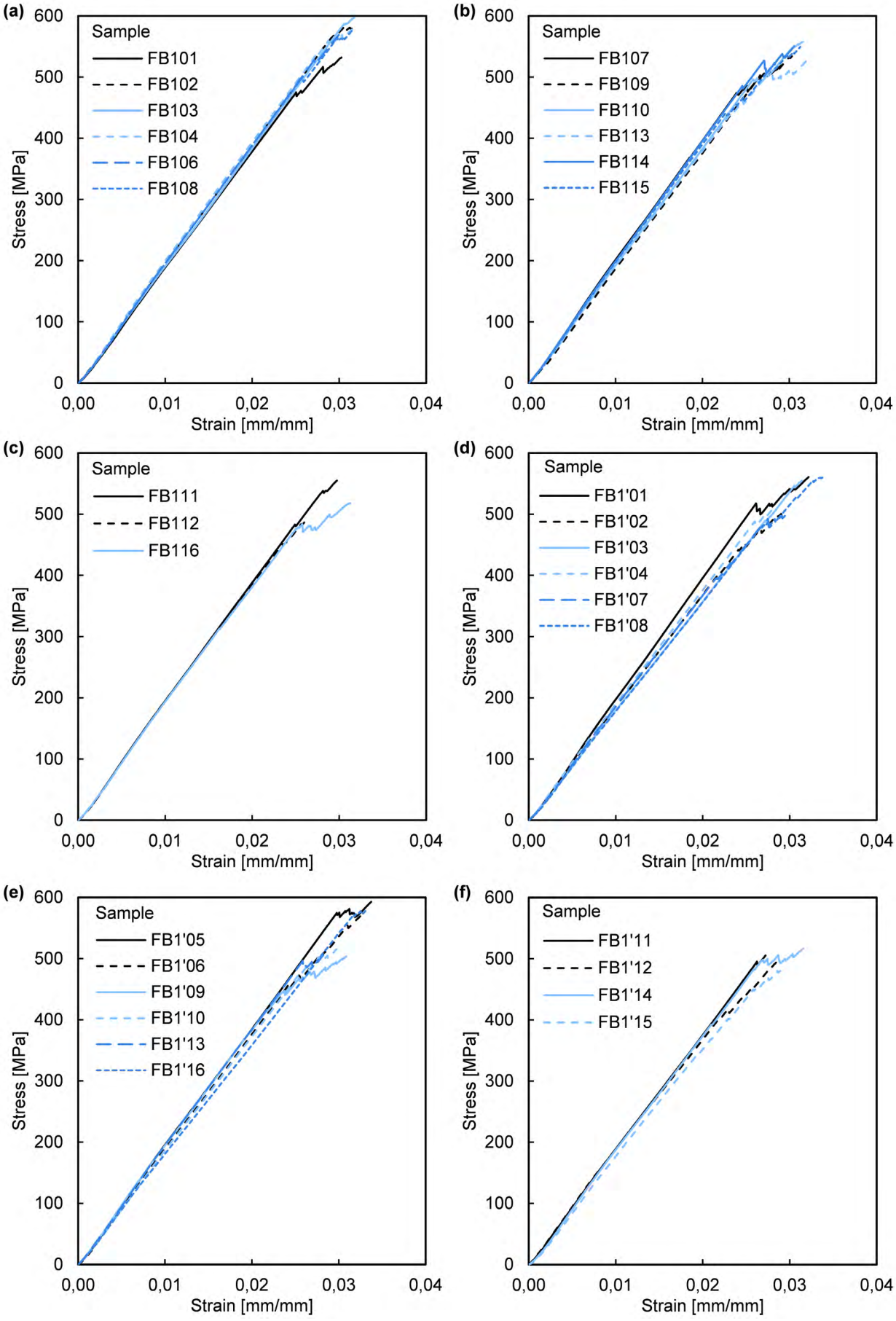

Figure D.16. Flexure response of samples belonging to specimens presented in Chapter 5 (3/4).

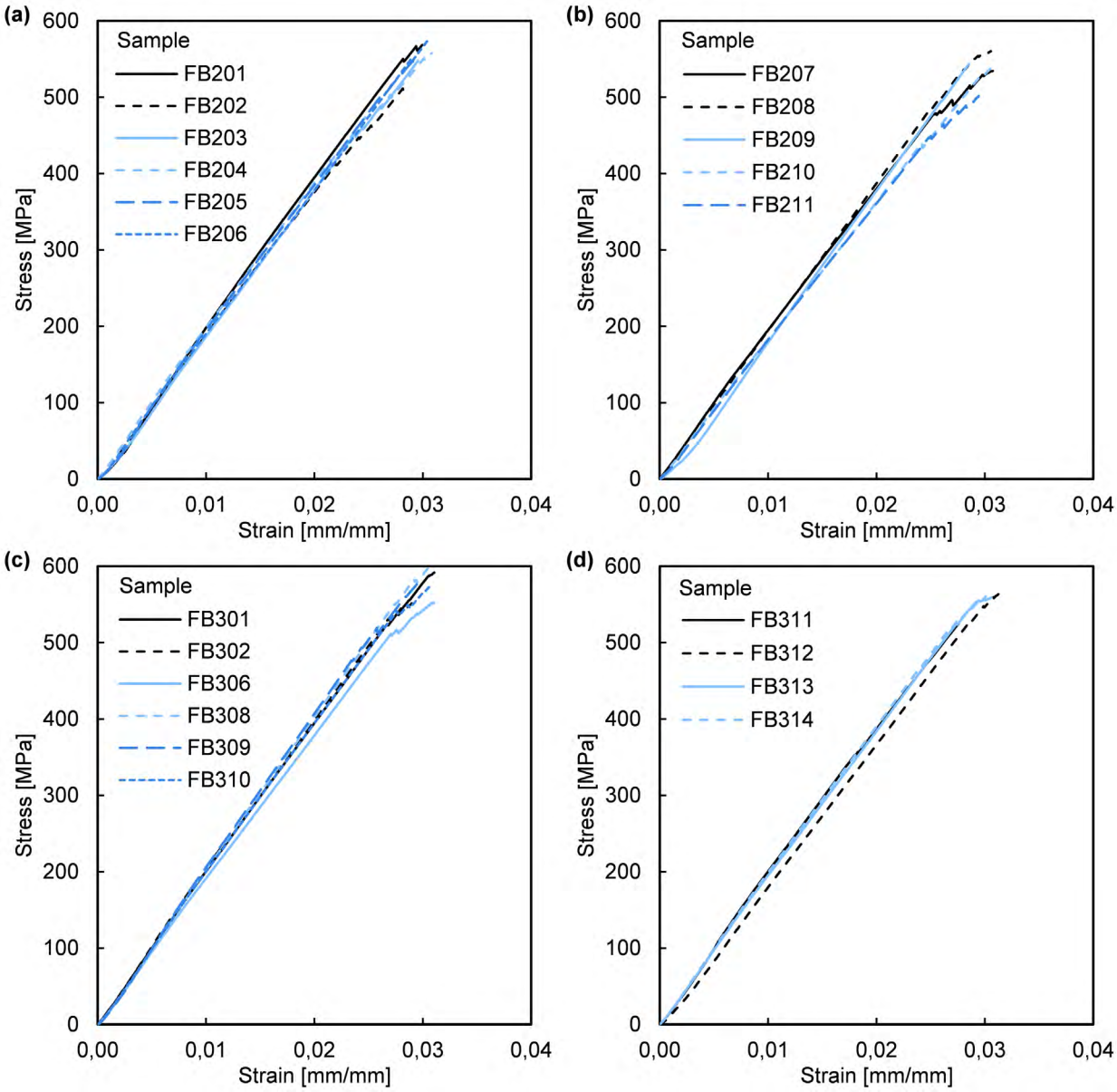

Figure D.17. Flexure response of samples belonging to specimens presented in Chapter 5 (4/4).

Table D.2. Flexural properties of samples belonging to specimens presented in Chapter 5.

Sample	σ_{fM} [MPa]	E_f [GPa]	Sample	σ_{fM} [MPa]	E_f [GPa]	Sample	σ_{fM} [MPa]	E_f [GPa]
FA101	518	18,2	FA106	447	18,1	FA111	515	18,3
FA102	513	19,8	FA107	547	19,2	FA112	547	18,6
FA103	537	19,2	FA108	556	17,7	FA113	499	18,2
FA104	500	18,6	FA109	526	18,3	FA114	495	18,5
FA105	544	18,2	FA110	453	18,8	FA115	519	19,9
FA201	571	18,9	FA207	576	19,5	FA213	585	18,7
FA203	591	19,1	FA209	528	19,2	FA214	537	19,9
FA204	544	19,4	FA210	511	19,5			
FA206	533	19,0	FA211	578	19,8			
FA301	569	19,2	FA306	548	18,1	FA312	524	19,5
FA302	566	18,7	FA307	597	18,5	FA313	578	19,4
FA303	566	18,9	FA308	593	19,0	FA314	485	18,9
FA304	500	18,8	FA310	517	18,1			
FA305	585	20,1	FA311	577	18,3			
FA402	505	18,5	FA406	556	19,4	FA409	577	19,3
FA404	514	18,4	FA407	517	18,7	FA410	584	19,6
FA405	558	19,4	FA408	571	19,8	FA411	516	18,5
FB101	532	18,7	FB107	519	19,2	FB112	493	19,0
FB102	585	19,2	FB108	579	19,2	FB113	531	18,6
FB103	597	18,6	FB109	537	18,7	FB114	550	19,4
FB104	578	19,4	FB110	558	18,9	FB115	549	19,2
FB106	569	19,1	FB111	555	19,2	FB116	518	19,0
FB1’01	561	19,4	FB1’07	503	18,3	FB1’12	503	17,9
FB1’02	504	18,1	FB1’08	561	17,7	FB1’13	505	18,9
FB1’03	555	17,6	FB1’09	504	18,7	FB1’14	517	18,3
FB1’04	510	18,7	FB1’10	515	18,4	FB1’15	484	18,0
FB1’05	593	18,7	FB1’11	505	18,5	FB1’16	581	17,7
FB1’06	574	18,4						
FB201	569	20,0	FB205	549	19,0	FB209	544	20,1
FB202	516	19,0	FB206	576	18,7	FB210	545	17,8
FB203	548	19,1	FB207	534	18,7	FB211	501	18,0
FB204	558	18,9	FB208	560	19,0			
FB301	592	19,5	FB309	577	20,0	FB312	565	18,6
FB302	552	19,6	FB310	576	19,6	FB313	559	18,7
FB306	553	18,6	FB311	525	19,1	FB314	560	19,1
FB308	608	20,2						

Table D.3. Classification of samples for three-point flexure belonging to specimens presented in Chapter 5 according to testing orientation and Porous Area Type (PAT).

Testing orientation	Porous Area Type (PAT)					
	Non-porous			PAT I	PAT II	PAT III
Upwards	FA203	FA406	FB203	FA101	FA115	FA112
	FA206	FA408	FB204	FA104	FA213	FA310
	FA209	FA409	FB206	FA105	FA311	FA313
	FA211	FB103	FB208	FA111	FA410	FB111
	FA302	FB104	FB306	FB1’03	FB110	FB116
	FA303	FB108	FB309	FB1’08	FB1’05	FB1’11
	FA307	FB115	FB312	FB1’09	FB1’06	
	FA308	FB1’02	FB313	FB1’16	FB210	
	FA404				FB314	
Downwards	FA201	FA405	FB201	FA103	FA210	FA106
	FA204	FA407	FB202	FA107	FA304	FA113
	FA207	FA411	FB205	FA108	FB102	FA114
	FA214	FB101	FB207	FA109	FB110	FA314
	FA301	FB102	FB301	FB1’04	FB107	FB112
	FA305	FB106	FB302	FB1’07	FB109	FB1’12
	FA306	FB113	FB308	FB1’13	FB114	FB1’15
	FA312	FB1’01	FB310		FB1’10	FB311
	FA402				FB1’14	
					FB209	
					FB211	

D.6. Compression test of ‘L’ shape samples

‘L’ shape samples depicted in Figure D.3 were tested in compression in order to determine their through-the-thickness tensile behaviour.

Tests were carried out in the facilities of the Division of Mechanics, Materials and Design of the Department of Engineering of the University of Cambridge, with a universal testing machine equipped with a load cell of 100 kN.

When a force is applied in a curved sample, a through-the-thickness tensile stress is produced. In layered materials such as FRPs, this tensile stress may cause failure at load levels much lower than predicted by in-plane strength properties due to their anisotropic nature. The thorough-the-thickness tensile stress at failure is referred as “Inter-Laminar Normal Strength” (ILNS). The development of ILNS promotes mode-I type of delamination propagation in curved regions. ILNS is quite sensitive to manufacturing quality and defects such as voids and ply folds [2–4].

D.6.1. Classical elasticity theory

Most of analytical analysis of Inter-Laminar Normal Stresses (ILNS) [5–7] are based on the classical elasticity theory equations addressed by Lekhnitskii for stresses in a cylindrically anisotropic homogeneous curved beam [8]. Lekhnitskii developed a series of expressions to determine the trough-the-thickness distribution of radial stress, σ_r, tangential stress, σ_θ, and shear stress, $\tau_{r\theta}$, according to specific loading cases, such as pure bending, an end load applied to at the centre of a particular cross-section and a load uninformedly along the curvilinear edge.

Above-mentioned analyses use the superposition principle to split real loading cases into a combination of the three loading cases addressed by Lekhnitskii, usually pure bending (Figure D.18.a) and end load application (Figure D.18.b). Total σ_r, σ_θ and $\tau_{r\theta}$ are computed as the sum of the individual stresses.

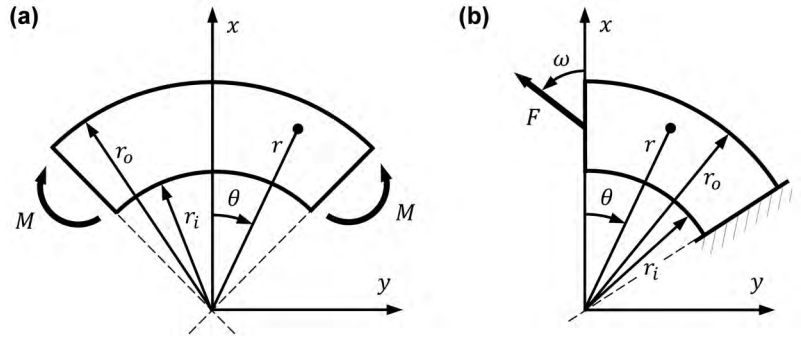

Figure D.18. Free-body diagrams of Lekhnitskii's studied loading cases: (a) pure bending and (b) end load.

The classical elasticity theory equations for plane stresses in a cylindrically anisotropic homogeneous curved beam under pure bending given by Lekhnitskii are

$$\sigma_r = -\frac{M}{r_o^2 wg}\left[1 - \frac{1-c^{k+1}}{1-c^{2k}}\left(\frac{r}{r_o}\right)^{k-1} - \frac{1-c^{k-1}}{1-c^{2k}}\cdot c^{k+1}\left(\frac{r_o}{r}\right)^{k+1}\right] \tag{16}$$

$$\sigma_\theta = -\frac{M}{r_o^2 wg}\left[1 - \frac{1-c^{k+1}}{1-c^{2k}}k\left(\frac{r}{r_o}\right)^{k-1} + \frac{1-c^{k-1}}{1-c^{2k}}kc^{k-1}\left(\frac{r_o}{r}\right)^{k+1}\right] \tag{17}$$

$$\tau_{r\theta} = 0 \tag{18}$$

where r is the radial coordinate ($r_i \le r \le r_o$), θ is the tangential coordinate, r_i is the inner radius of the curved beam, r_o is the outer radius of the curved bar, w is the width of the bar and

$$k = \sqrt{\frac{E_\theta}{E_r}} \tag{19}$$

$$c = \frac{r_o}{r_i} \tag{20}$$

$$g = \frac{1-c^2}{2} - \frac{k}{k+1} \cdot \frac{(1-c^{k+1})^2}{1-c^{2k}} + \frac{kc^2}{k-1} \cdot \frac{(1-c^{k-1})^2}{1-c^{2k}} \tag{21}$$

where E_r is the modulus of elasticity in direction r, E_θ is the modulus of elasticity in direction θ.

The radial location where maximum radial stress occurs is given by:

$$r(\sigma_{rM}) = \left[\frac{(k+1)(1-c^{k-1})c(r_i r_o)^k}{(k-1)(1-c^{k+1})}\right]^{1/2k} \tag{22}$$

Lekhnitskii also gives the equation for plane stresses in a curved beam due to an end load:

$$\sigma_r = -\frac{F}{r_o w g_1} \cdot \frac{r_o}{r}\left[\left(\frac{r}{r_o}\right)^\beta + c^\beta \left(\frac{r_o}{r}\right)^\beta - 1 - c^\beta\right] \sin(\theta+\omega) \tag{23}$$

$$\sigma_\theta = -\frac{F}{r_o w g_1} \cdot \frac{r_o}{r}\left[(1+\beta)\left(\frac{r}{r_o}\right)^\beta + (1-\beta)\left(\frac{r_o}{r}\right)^\beta c^\beta - 1 - c^\beta\right] \sin(\theta+\omega) \tag{24}$$

$$\tau_{r\theta} = -\frac{F}{r_o w g_1} \cdot \frac{r_o}{r}\left[\left(\frac{r}{r_o}\right)^\beta + c^\beta \left(\frac{r_o}{r}\right)^\beta - 1 - c^\beta\right] \cos(\theta+\omega) \tag{25}$$

where ω is the angle between the end load and direction θ in the cross-section in which the end load is applied, and

$$\beta = \sqrt{1 + \frac{E_\theta}{E_r}(1-2\nu_r) + \frac{E_\theta}{G_{r\theta}}} \tag{26}$$

$$g_1 = \frac{2}{\beta}\left(1-c^\beta\right) + \left(1+c^\beta\right)\ln c \tag{27}$$

where $G_{r\theta}$ is the shear modulus and ν_r is the Poisson's ratio.

The radial location where maximum radial stress occurs is given by:

$$r(\sigma_{rM}) = \left[\frac{r_o^\beta}{2(\beta-1)}\left[\sqrt{(1+c^\beta)^2 + 4c^\beta(\beta^2-1)} - \left(1+c^\beta\right)\right]\right]^{1/\beta} \tag{28}$$

These equations present an accurate distribution of stresses through the thickness of the specimen (coordinate r) and along the curved beam (coordinate θ), as has been checked at comparing analytical results with finite element analyses [6,7].

For FRP curved samples under certain conditions ($E_\theta/E_r \leq 6$ and r_m/h, where r_m is the mean radius and h is thickness) in which large deflections do not happen, it has been shown that the following expression gives consistent results for the maximum radial stress with an error lower than 2% with respect to Lekhnitskii's solution [9]:

$$\sigma_{rM} = \frac{3M}{2wh\sqrt{r_i r_o}} \tag{29}$$

where M is the resultant bending moment at a specific cross-section. σ_{rM} is given at $r = \sqrt{r_i r_o}$. The imposed condition on material properties, $E_\theta/E_r \leq 6$, is fulfilled by most of laminates based on stacks of woven fabrics.

D.6.2. Method

In the literature, it can be found a number of different experimental set-ups to measure ILNS of single curved FRP samples [6,10,11]. The standard ASTM D6415/D6415M proposes a four-point bending configuration to measure ILNS of 'L' shape samples. In the present work, it was adopted a compression set-up to measure ILNS of samples trimmed from 'C' cross-section profiles manufactured through ISFLIP (Figure D.19).

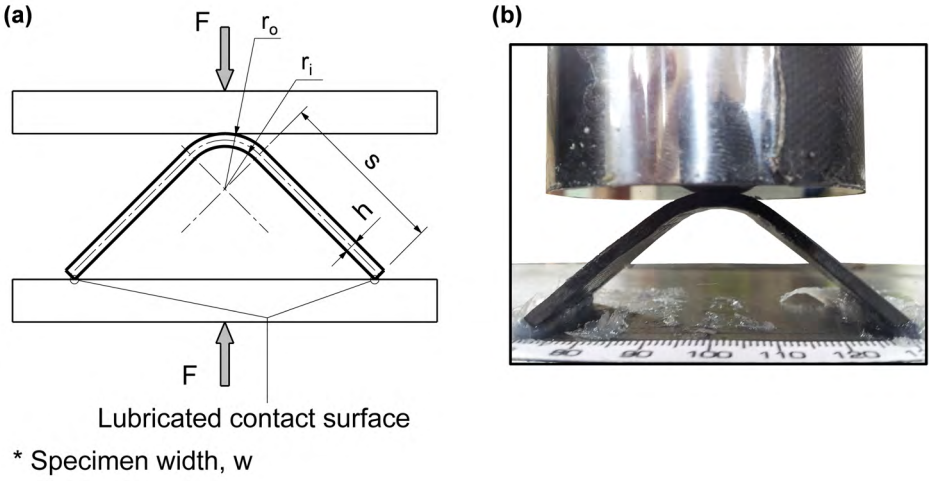

Figure D.19. Experimental set-up of the test for measuring the Inter-Laminar Normal Strength (ILNS) test: (a) schematic drawing and (b) test execution (deformed sample at failure).

The compression fixture consisted on a steel cylinder mounted on a universal testing machine and pushed against a large rigid steel plate. Wax was applied along the contact edges between the sample and the lower plate to facilitate edges sliding during the compression test.

Under loading, it is originated the complex stress state described by Lekhnitskii in the curved region: tangential, σ_θ; radial tensile, σ_r; and shear stresses, $\tau_{r\theta}$. Tangential stresses, σ_θ, are produced along fabric direction, being located tensile $\sigma_{\theta M}$ at the inner surface and the compressive $\sigma_{\theta M}$ at the outer surface. The magnitude of both stress levels depends on material properties and sample dimensions in the curved region.

Furthermore, the radial tensile stress, σ_r, ranges from zero at the inner and outer surfaces to a peak around the mean radius. An adequate sample failure produces delamination across the width instead of failure of inner and outer surface as in typical three-point flexure testing. The ILNS is given by the maximum radial tensile stress, σ_{rM}, measured during the test, which is given by Equation (29).

Although shear stresses, $\tau_{r\theta}$, are also originated, in the curved region, where failure occurs, inter-laminar normal stresses (σ_r) prevail over inter-laminar shear stresses.

In Figure D.20, it is depicted a free-body diagram with forces and moments acting on one of the symmetric halves of the tested sample.

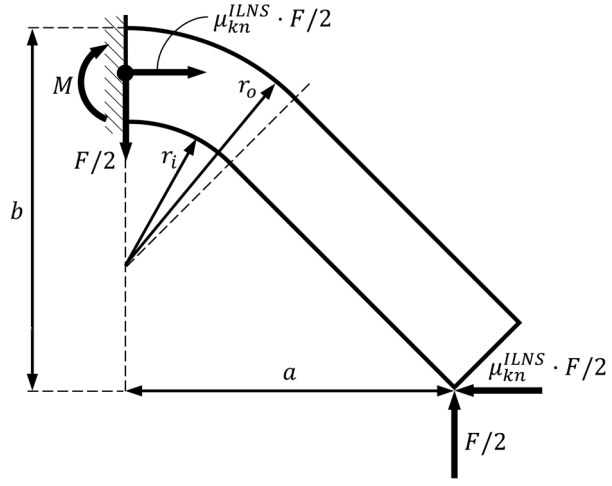

Figure D.20. Free-body diagram of a compressed ‘L’ shape sample.

From the balances of forces and moments, M acting on the middle cross-section of the sample was computed such that

$$M = \frac{F}{2}a - \mu_{kn}^{ILNS}\frac{F}{2}\left(b - \frac{r_o - r_i}{2}\right) = \frac{F}{2}a - \mu_{kn}^{ILNS}\frac{F}{2}\left(b_0 - \delta - \frac{r_o - r_i}{2}\right) \quad (30)$$

where the final height of the sample before failure, b, could be calculated from the initial height, b_0, and the displacement of the crosshead, δ; the final distance between contact edges, a, was visually assessed through a ruler attached to the supporting plate (Figure D.19.b); and the estimation of a kinematic coefficient of friction between the contact edges and the supporting plate, μ_{kn}^{ILNS}.

In order to estimate μ_{kn}^{ILNS}, a loading-unloading hysteresis loop cycle was conducted before reaching load levels close to failure (Figure D.21). Under the assumptions that μ_{kn}^{ILNS} remained independent on the applied load, F, and energy loss associated to the closed loop corresponded to friction between the sample edges and the supporting plate, μ_{kn}^{ILNS} was computed from an energy balance including the work done by F and the work done by the friction force, $2 \cdot \mu_{kn}^{ILNS} F/2$ such that

$$\frac{F_3 + F_2}{2}(\delta_3 - \delta_2) + \frac{F_1 + F_4}{2}(\delta_1 - \delta_4) + 2 \cdot \mu_{kn}^{ILNS} \frac{F_3 + F_2}{4}\left(\frac{a_3 - a_0}{2} - \frac{a_2 - a_0}{2}\right)$$
$$-2 \cdot \mu_{kn}^{ILNS} \frac{F_1 + F_4}{4}\left(\frac{a_1 - a_0}{2} - \frac{a_4 - a_0}{2}\right) = 0$$

$$\frac{F_3 + F_2}{2}(\delta_3 - \delta_2) + \frac{F_1 + F_4}{2}(\delta_1 - \delta_4) + \mu_{kn}^{ILNS} \frac{F_3 + F_2}{4}(a_3 - a_2)$$
$$- \mu_{kn}^{ILNS} \frac{F_1 + F_4}{4}(a_1 - a_4) = 0$$

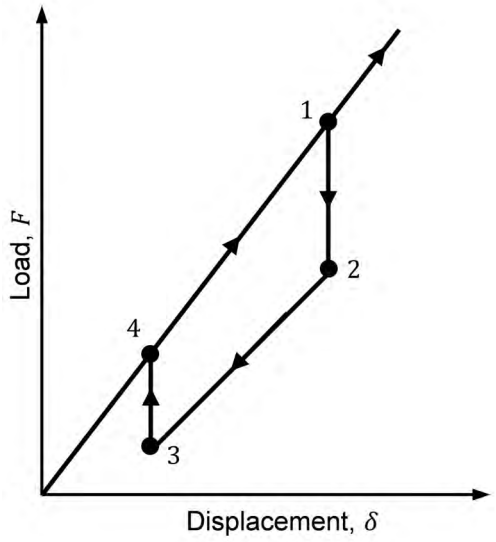

Figure D.21. Ideal unloading-loading hysteresis loop during the compression test of 'L' shape samples.

$$\mu_{kn}^{ILNS} = \frac{\frac{F_3 + F_2}{2}(\delta_3 - \delta_2) + \frac{F_1 + F_4}{2}(\delta_1 - \delta_4)}{\frac{F_1 + F_4}{4}(a_1 - a_4) - \frac{F_3 + F_2}{4}(a_3 - a_2)} \tag{31}$$

From the bending moment acting on the middle cross-section of the samples, the Curved Beam Strength (CBS), another characteristic parameter defined for curved layered specimens, can also be computed such that

$$CBS = M/w \tag{32}$$

Samples were tested at $1\ \mathrm{mm/s}$. Average sample dimensions are given in Figure D.3.

D.6.3. Results

Response curves curve F vs. δ of 'L' shape samples tested in compression from which ILNS were estimated are depicted in Figure D.22 and Figure D.23. Computed ILNS for each sample were provided in Chapter 6.

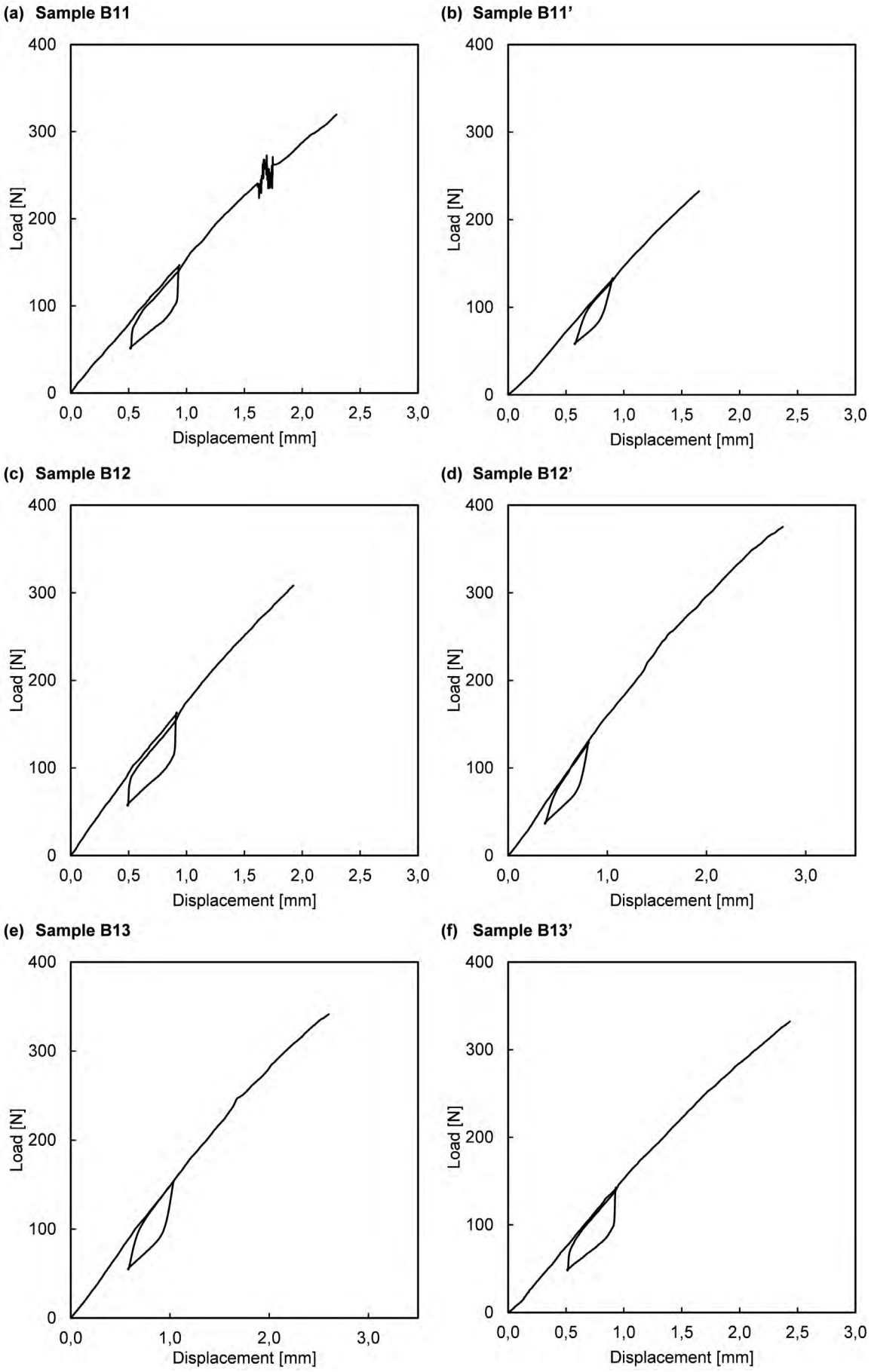

Figure D.22. Response curve load, F, vs. crosshead displacement, δ, of 'L' shape samples corresponding to specimen B1.

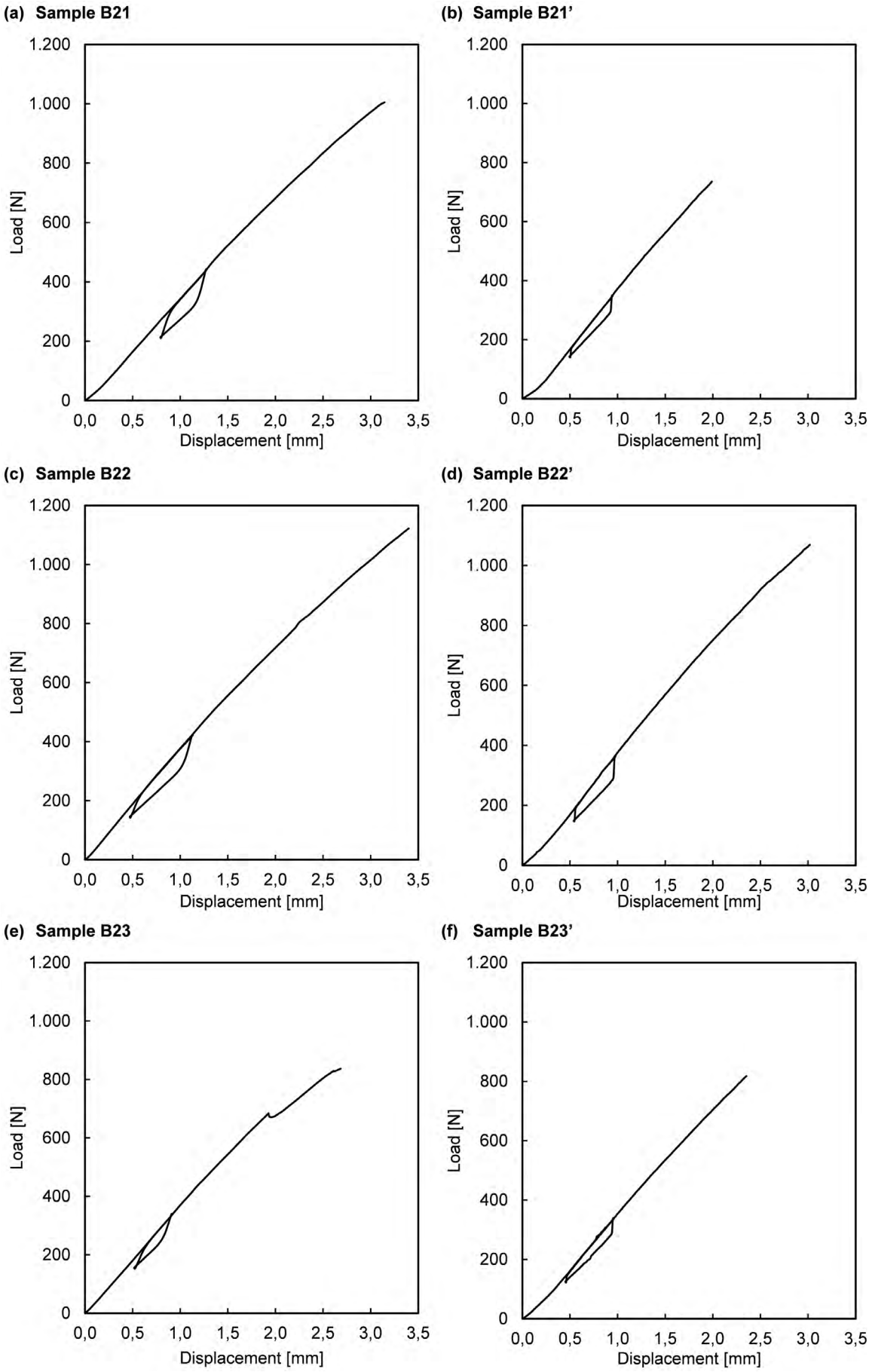

Figure D.23. Response curve load, F, vs. crosshead displacement, δ, of 'L' shape samples corresponding to specimen B2.

Appendix E

Light microscopy

During the course of the research project, it was necessary to conduct different analyses of porosity contained in specimens manufactured via VI, and a study of ILNS fracture of ‘L’ shape samples tested in compression and manufactured through ISFLIP. In this appendix, procedures to prepare samples, acquire micrographs and process digital images are presented, as well as resulting micrographic pictures.

Both micrographic sample preparation and digital image acquisition were carried out in the facilities of the Departament de Ciència dels Materials i Enginyeria Metal·lúrgica (CMEM) of the Universitat Politècnica de Catalunya (UPC) in Barcelona.

E.1. Sample preparation

The main challenge at preparing micrographic specimens of FRP composites resides in hardness difference between of the fibres and the matrix. Unique and comprehensive guidelines to understand specimen mechanics and preparation procedures are provided by the main suppliers of grinding and polishing products, Struers [12,13] and Buehler [14].

Samples MYZ (25x25 mm) shown in Figure D.1 and Figure D.2 were casted in round micrographic specimens of diameter 30 mm. Polyester resin was used as mounting medium. Six or seven samples were stacked in each micrographic specimen without any backup sample. Correspondence between orientation of samples in micrographic specimens and manufactured specimens is shown in Figure E.1.a and Figure E.1.b. Keeping an ordered arrangement of the

samples into each specimen was important to not confuse the lower surface (mould side) and the upper surface (HPDM side) of the samples.

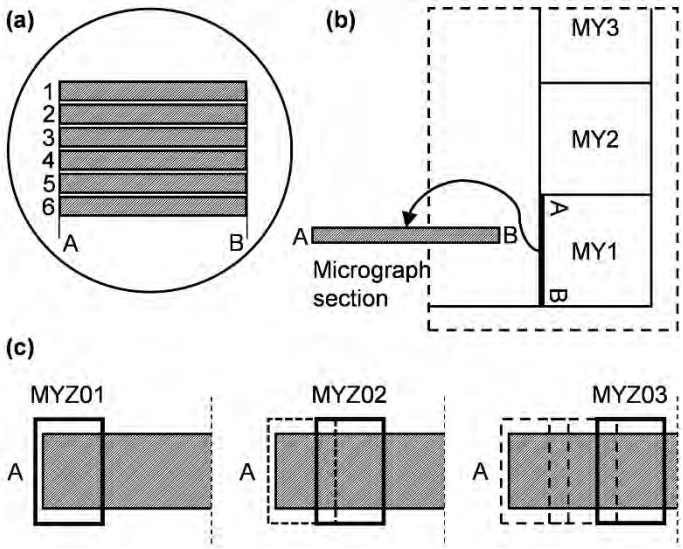

Figure E.1. Distribution of micrographic samples (a) in micrographic specimens and (b) in manufactured specimens, and (c) procedure of picture capture according to sample orientation.

In Figure E.1.a, it can be seen how samples were numbered into each micrographic specimen according to their order into the stack of samples.

A total of eight micrographic specimens were prepared with samples belonging to VI specimens (four micrographic specimens with samples of in-plane impregnated VI specimens, Chapter 4, and four micrographic specimens with samples of through-thickness VI specimens, Chapter 5):

1. M11, M14, M18, M21, M 24, M28.
2. M31, M34, M38, M41, M 44, M45, M48.
3. M51, M54, M58, M61, M 64, M66, M68.
4. M71, M74, M78, M81, M 84, M88.
5. MB201, MA401, MA101, MA102, MA103, MA109.
6. MX09 (90° ↷), MX10 (90° ↷), MY09, MY10, MB1’09, MB1’10.
7. MA110 (90° ↶), MA309 (180° ↶), MA310 (180° ↶), MA311 (90° ↶), MA313 (90° ↷), MA314, MA312 (90° ↷).
8. MB109 (90° ↶), MB110 (180° ↶), MB111 (90° ↶), MB112 (90° ↷), MB113 (180° ↶), MB114, MB1’11 (90° ↶).

In through-thickness VI specimens, some MYZ samples (sample number ≥ 9) were placed in the area initially allocated to flexural samples to covered random appearance of porous regions; therefore, cross-section from which micrographs were taken could be rotated with respect to the orientation shown in Figure E.1.b. In case being rotated, in the above list of samples per micrographic specimen, it has been pointed out between parenthesis.

The micrographic specimen number 6 also included some samples belonging to VI specimens that were not finally included in the presented work.

All samples included in any micrographic specimen are classified in Table E.1 and Table E.2 according to the non-porous or porous area to which they belonged.

Table E.1. Classification of samples for microscopy analysis belonging to specimens presented in Chapter 4 according to porosity content.

Non-porous area				Porous area		
M11	M31	M51	M71	M18	M48	M78
M14	M34	M54	M74	M28	M58	M88
M21	M41	M61	M81	M38	M66	
M24	M44	M64	M84	M45	M68	

Table E.2. Classification of samples for microscopy analysis belonging to specimens presented in Chapter 5 according to Porous Area Type (PAT).

Porous Area Type (PAT)				
Non-porous	**PAT I**	**PAT II**	**PAT III**	
MB201	MA101	MA110	MA109	MA314
MA401	MA102	MA311	MA309	MB110
	MA103	MB109	MA310	MB111
	MB1'09	MB112	MA312	MB114
	MB1'10	MB113	MA313	MB1'11

Two more micrographic specimens were prepared with the curved regions of 'L' shape samples belonging to specimens manufactured via ISFLIP (Figure D.3). After being tested in compression, samples had to be trimmed to fit into micrographic specimens of diameter 30 mm. Polyester resin was also used as mounting medium. Each micrographic specimen contained four samples:

9. B11', B12, B12', B13.
10. B21', B22', B23, B23'.

Micrographic specimens were grinded and polished automatically with a base Struers RotoPol-31 and a specimen mover Struers RotoForce-4. Rotation speed and normal load was kept constant during all specimen preparation, 300 rpm and 10 N respectively. Rotation in both base

and specimen mover was set in the same direction. The detailed preparation procedure is summarized in Table E.3.

Table E.3. Grinding and polishing procedure conducted with a base Struers RotoPol-31 and a specimen mover RotoForce-4 (all listed materials supplied by Struers).

Disc	Abrasive	Lubricant	Speed [rpm]	Load [N]	Rotation*	Time [min]
Grinding						
MD-Piano 220		Water	300	10	< <	10
MD-Piano 500		Water	300	10	< <	25
MD-Piano 1200		Water	300	10	< <	60
Polishing						
MD-Dac	Two-in-one suspension of 6 µm diamond and lubricant		300	10	< <	120
MD-Nap	Colloidal silica suspension		300	10	< <	20

* Base and specimen mover can adjust rotation in the same direction (< <) or in opposite directions (> <).

After flattening top and bottom round micrographic specimen faces, specimens were grinded with diamond discs MD-Piano 220 for 10 min; MD-Piano 500 for 20 min; MD-Piano 1200 for 60 min. Then, specimen was polished for 100 min with a cloth MD-Dac and a two-in-one suspension of 6 μm diamond and lubricant. Final polishing was performed for 50 min with a cloth MD-Nap and a colloidal silica suspension. Although a napless cloth in the last step had been preferred to avoid rounding of the fibre-resin interface, what would have been critical in fibre-resin content estimation; in void content estimation, this effect had minimal influence.

Some examples of micrographic specimens prepared are shown in Figure E.2.

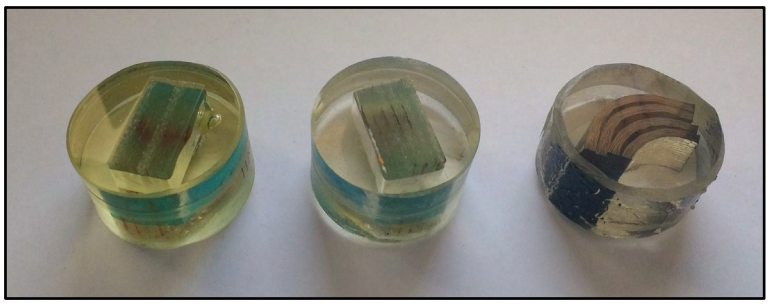

Figure E.2. Micrographic specimens.

E.2. Observations

Since no etching was carried out, after the final polishing step with colloidal silica, fibre and samples contour could be observed because of the uneven surface of the sample. Material erosion is more effective in soft than in hard materials. E-glass and carbon fibres are harder than the epoxy

resin used as matrix, which in turn is harder than the polyester resin used as mounting medium. Therefore, the observed black contours corresponded to regions which were not perpendicular to the observation plane and did not reflect the incident light (Figure E.3.a).

The quantitative evaluation of porosity content and porous morphology carried out in VI samples required a rigorous assessment of defects present on the surface of observation, which arose during the preparation of micrographic specimens. Figure E.3.b to Figure E.3.f show the defects that could be observed during the inspection of the micrographic specimens.

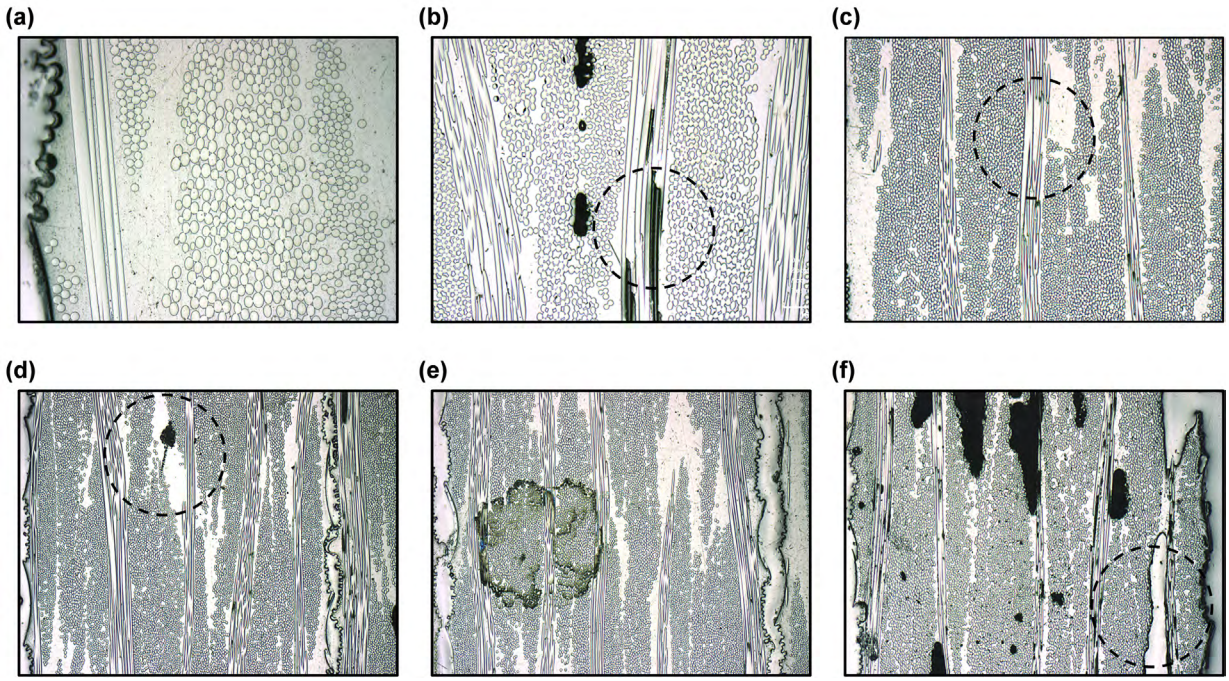

Figure E.3. Detail pictures of taken micrographs: (a) dark fibre and specimen contours, (b) detachment of fibres parallel to observed cross-section, (c) blurred fibre interfaces, (d) traces of polishing nap, (e) spots caused by improper specimen drying and (f) filling of pores with polyester resin (different scale among pictures).

E.3. Micrograph acquisition

Micrographs were taken with a microscope Olympus LEXT OLS3100 and processed with the corresponding Olympus analysis software. A number of fourteen to sixteen micrographs per sample were normally taken at 50X magnification and stitched to get a macro-picture covering the full sample length in case of VI specimens (Figure E.1.c). The number of micrographs to cover the full length of ISFLIP samples varied between thirty and forty according to each specimen. An overlap between micrographs of approx. $10-20\%$ was required to carry out the mentioned stitching process. Micrograph resolution was 1024x768, resulting in a scale of 130 pixels / 320 μm, and they were coded as "{micrographic sample id.}ii" (e.g. M1101).

In order to calibrate microscope lighting, in each micrographic specimen five extra pictures were taken of an area covering only the mounting medium. Each picture was named “Background {list of micrographic samples}_ii” (e.g. Background M11M14M18M21M24M28_01).

E.4. Digital image processing

The open source image processing package Fiji, based on ImageJ, was used to process micrographs. Porosity measurement was reduced to the central length of samples (2,3 mm) to not include edge imperfections caused during sample cutting. Void area fraction, a_0, was calculated in each macro-picture as the ratio of area occupied by voids A_0 and area occupied by the whole sample A_{sample}:

$$a_0 = \frac{\sum A_0}{A_{sample}} \tag{33}$$

In the following sub-sections, it is detailed the digital image processing procedure followed to carry out sample porosity computations.

E.4.1. Background lighting correction

The background illumination intensity provided by microscope light source optics is often not homogeneous throughout the view field, being common to have a bright spot in the middle. In order to correct illumination, a brightfield image was created by averaging a total of five pictures which were taken from the mounting medium region of each micrographic specimen.

The macro Brightfield.ijm (previous installation of plugin Gray_Morphology was necessary) was run for each micrographic specimen. All background pictures were processed at once. This macro combined a series of commands to be carried out by the user and a series of actions automatically conducted.

Commands

1. Select the input folder containing background pictures.
2. Select the output folder in which processed background pictures will be saved.

Actions

3. Convert RGB picture to grey scale.
4. Remove small black spots through a closing operation (circle mask size: 10,0).
5. Homogenize lighting profile through an opening operation (circle mask size: 50,0).
6. Save processed pictures in the selected folder.

The macro Average_Images.ijm was run, after opening all background pictures in Fiji, to average all five background pictures and obtain only one brightfield image per specimen. Brigthfield pictures were coded as “Brightfield {list of micrographic samples}” (e.g. Brightfield M11M14M18M21M24M28).

Actions

7. Average images in intensity.

Commands

8. Save processed picture.

Lighting was corrected by calculating the transmittance of the micrographs with respect to the brightfield and re-scaling the resulting image to 0-255.

$$Image_{corrected} = 255 \cdot \frac{Image_{original}}{Brightfield} \tag{34}$$

The macro Lighting_Correction.ijm (previous installation of plugin Calculator_Plus was necessary) was run for each micrographic specimen. All micrographs were processed at once.

Commands

9. Select the input folder containing micrographs.
10. Open the brightfield picture corresponding to the micrographic specimen to which micrographs belong.
11. Select the output folder in which processed micrographs will be saved.

Actions

12. Convert RGB pictures to grey scale.
13. Calculate transmittance of all micrographs.
14. Re-scale processed micrographs.
15. Save re-scaled processed micrographs in the selected folder.

E.4.2. Stitching

Once lighting was corrected in all micrographs, all pictures corresponding to one sample were stitched to create a macro-picture of the whole sample. As above mentioned, micrographs were taken with an approx. overlap of 20% with the previous and the following micrographs to allow stitching.

The macro Stitch_Images.ijm (previous installation of plugin Stitching [15] was necessary) was run for each sample. The resulting macro picture was saved as “{micrographic sample id.}” (e.g. M11).

Commands

1. Select the input folder containing micrographs.
2. Stitch micrographs with a regression threshold of 0,9 to guarantee picture overlapping.
3. Save processed macro-picture.

E.4.3. Preparation

Having an accurate surface profile is important to calculate a_0, since it is necessary to measure A_{sample}. Due to different hardness between epoxy resin of specimens and polyester resin used as mounting medium, an irregular shadow was present in specimen surface at taking micrographs; therefore, surface profile had to be outlined manually. Irregularity of the shadow avoided to perform this task automatically via any edge detection procedure.

Furthermore, polyester resin used as mounting medium filled some pores; hence, making also difficult the automation of pore identification to compute A_0. Some pore boundaries had to be outlined manually too.

Commands

1. Open the macro-picture of a sample.
2. Select Brush tool (colour: black, size: 6) to mark the surface profile.
3. Select Brush tool (colour: black, size: 6) to mark inner contour of voids that have been filled by the mounting medium.
4. Save processed macro-picture keeping its codification.

Once surface profile was accurately defined, each sample was aligned, framed to the central region of the macro-picture and trimmed to cover only the central length, 23 mm. The macro Align_Images.ijm was run for each sample.

Commands

5. Open the macro-picture with surface profile and voids already marked.
6. Select Multi-point tool to mark a series of guide points to frame the sample into the macro-picture.

Actions

7. Align image.

Commands

8. Save processed macro-picture keeping its codification.

The macro Trim_Images.ijm was run for each sample.

Commands

9. Open the aligned macro-picture.
10. Select Multi-point tool to mark a series of guide points to frame the sample into the macro-picture.

Actions

11. Discard area out of the bounds defined by the points.
12. Trim the macro-picture to the central length of 23 mm.

Commands

13. Save processed macro-picture keeping its codification.

E.4.4. Measurement

As pointed out in Equation (33), a_0 was calculated as the ratio of $\sum A_0$ and A_{sample}; however A_{sample} was computed from the area the whole macro-picture $A_{picture}$, and the area defined between the top and bottom surface profiles, and the top and bottom edges of the macro-picture $A_{external}$.

$$A_{sample} = A_{picture} - A_{external} \tag{35}$$

$A_{picture}$ was directly found from macro-picture size once macro-pictures had been trimmed to the central length ($height \cdot width$), while $A_{external}$ was measured after isolating top and bottom regions between surface profiles and macro-picture edges. The macro Surface_Profile.ijm was run for each sample.

Commands

1. Open the trimmed macro-picture.

Actions

2. Convert grey scale image to binary (threshold range: 0-0).
3. Overlay initial macro-picture over processed macro-picture to assist surface voids outline (opacity: 75%).
4. Select Straight line tool (colour: white, line width: 3) to outline surface voids connecting two points of the surface boundary.
5. Fill holes.
6. Set the data to be gathered in the analysis of outlined regions (parameters: area, centroid, perimeter, bounding rectangle, fit ellipse, shape descriptors, Feret's diameter, median, skewness, kurtosis, area fraction; invert Y coordinates: yes; decimal places: 3).
7. Analyse regions (size:100000-∞, circullarity:0,00-1,00, pixel units: yes, show masks: yes, display results: yes, clear results: yes).
8. List coordinates of all pixels belonging to out-of-sample regions (background value: 0, suppress log output: yes).

Commands

9. Save processed macro-picture keeping its codification.
10. Save coordinates of all pixels belonging to out-of-sample regions as "{micrographic sample id.}_surface profile_xy" (e.g. M11_surface profile_xy).

11. Select the window containing the data gathered from the regions as "{micrographic sample id.}_surface profile" (e.g. M11_surface profile).

$A_{external}$ was computed as the sum of areas of both top and bottom out-of-sample regions, A_{top} and A_{bottom} respectively.

A similar procedure was followed to measure A_0. The macro Voids.ijm was run for each sample.

Commands

12. Open the trimmed macro-picture.
13. Open the macro-picture with the surface profile.

Actions

14. Convert grey scale image (trimmed macro-picture) to binary (threshold range: 0-50).
15. Subtract the surface profile macro-picture from the trimmed macro picture.
16. Fill holes.
17. Overlay trimmed macro-picture over processed macro-picture to assist removal of external artefacts (opacity: 75%).
18. Select Brush tool (colour: white) to remove from the binary picture those artefacts that do not correspond to pores.
19. Set the data to be gathered in the analysis of pores (parameters: area, centroid, perimeter, bounding rectangle, fit ellipse, shape descriptors, Feret's diameter, median, skewness, kurtosis, area fraction; invert Y coordinates: yes; decimal places: 3).
20. Analyse pore regions (size:10-∞, circullarity:0,00-1,00, pixel units: yes, show masks: yes, display results: yes, clear results: yes).
21. List coordinates of all pixels belonging to pore regions (background value: 0, suppress log output: yes).

Commands

22. Save processed macro-picture keeping its codification.
23. Save coordinates of all pixels belonging to pore regions as "{micrographic sample id.}_voids_xy" (e.g. M11_voids_xy).
24. Select the window containing the data gathered from the regions as "{micrographic sample id.}_voids" (e.g. M11_voids).

Finally, a_0 was calculated through the following expression:

$$a_0 = \frac{\sum A_0}{height \cdot width - (A_{top} + A_{bottom})} \tag{36}$$

Additionally, Feret's diameter, $\emptyset_{Feret}$ (maximum distance between any two points belonging to a pore), Feret's angle, φ_{Feret} (angle formed by the Feret's diameter and the horizontal axis), and aspect ratio, AR, were also computed for all the voids belonging to each sample. AR was defined

as the ratio of the two second moments of area of a pore around its principal axes, i_1 and i_2 (AR of a circle and a square is 1) such that

$$AR = \frac{i_1}{i_2} \leq 1 \tag{37}$$

E.4.5. Report

A macro-picture was composed with the macro-pictures processed in the previous sub-sections to highlight porosity into each sample. The macro Micrograph_Picture.ijm was run for each sample.

Commands

1. Open the trimmed macro-picture.
2. Open the macro-picture with the surface profile.
3. Open the macro-picture with pores.

Actions

4. Overlap the surface profile macro-picture coloured in black (out-of-sample regions) and white over the trimmed macro-picture.
5. Overlap the pore macro-picture coloured in red (pores) and white over the previous macro-picture.

Commands

6. Save processed macro-picture keeping its codification.

E.5. Results

Original and processed macro-pictures, as well as all cited macros, are provided in electronic form. Table E.4 and Table E.5 summarize relevant parameters describing pore content and morphology.

Table E.4. Descriptors of pore content and morphology of intra-tow voids.

Sample	Number of voids [1/cm²]	Void area			Feret's diameter	
		Average [µm²]	Maximum [10³·µm²]	Fraction [%]	Average [µm]	Maximum [µm]
M18	272,9	757	2,75	0,21	37	93
M28	280,7	741	2,94	0,21	37	121
M38	58,6	533	2,80	0,03	32	73
M48	311,8	646	2,85	0,20	36	88
M58	137,7	847	2,95	0,12	36	95
M68	440,7	675	2,99	0,30	40	100
M78	468,0	704	2,93	0,33	35	80
M88	95,4	655	2,78	0,06	35	99
M45	147,3	691	2,94	0,10	39	158
M66	353,9	645	2,73	0,23	34	87
M391	402,8	518	2,85	0,21	33	140
M393	198,9	667	2,62	0,13	37	124
M429	226,1	363	2,48	0,08	27	165
M4210	293,6	264	1,47	0,08	25	85
M3910	76,7	136	0,34	0,01	19	41
M4111	126,4	281	1,25	0,04	25	49
M4012	80,2	687	2,88	0,06	49	242
M4013	148,5	481	2,84	0,07	40	255
M4110	9,4	173	0,33	0,00	18	25
M4113	18,8	801	1,34	0,02	40	142
M4010	73,9	504	1,47	0,04	40	187
M4014	145,6	449	1,87	0,07	37	184

Table E.5. Descriptors of pore content and morphology of inter-tow voids.

Sample	Number of voids [1/cm²]	Void area			Feret's diameter	
		Average [10³·µm²]	Maximum [10³·µm²]	Fraction [%]	Average [µm]	Maximum [µm]
M18	126,8	34,9	405,8	4,43	374	2930
M28	130,5	27,2	144,2	3,55	326	1043
M38	102,6	55,6	350,2	5,71	535	2613
M48	174,7	51,6	344,1	9,01	413	971
M58	98,3	38,5	307,2	3,79	520	3094
M68	177,6	35,0	146,7	6,22	385	2243
M78	206,6	31,0	262,0	6,41	336	1359
M88	156,1	43,4	166,0	6,77	378	1270
M45	88,9	39,5	133,5	3,51	334	1805
M66	135,5	31,9	145,6	4,32	451	1141
M391	22,8	29,9	55,1	0,68	310	503
M393	17,5	19,3	40,4	0,34	241	431
M429	14,7	55,7	98,3	0,82	427	611
M4210	4,3	6,1	7,2	0,03	178	231
M3910	31,4	41,3	92,4	1,29	443	987
M4111	26,0	40,5	76,6	1,05	395	709
M4012	39,0	32,2	114,5	1,25	428	1276
M4013	57,7	28,6	112,5	1,65	362	1050
M4110	72,7	55,3	166,0	4,02	597	1479
M4113	65,9	88,9	724,8	5,86	794	4901
M4010	83,1	46,9	208,8	3,90	479	1460
M4014	72,8	49,9	279,0	3,63	589	2233

This page intentionally left blank

Appendix F

Experimental design and data analysis

The need of analysing some experimental data to discern between significant factors governing VI and ISFLIP required the adoption of suitable experimental strategies and well-thought-out Design Of Experiments (DOE). In this appendix, some experimental design methods based on the Analysis of Variance (ANOVA) are firstly described and then specific methods applied throughout the research project are presented with their corresponding results. Statistical analyses were performed with the statistical software suite Minitab. As a general rule throughout the case studies, significance level at hypothesis testing was fixed at $\alpha = 0{,}05$.

F.1. Glossary

Block: A block is a categorical variable which explains variation in a response variable that is not caused by factors. Blocks are used in design of experiments and analysis to minimize bias and variance of the error because of nuisance factors which are known and controllable. Both fixed-effect and random-effect blocks are possible.

Contrast: It is usually called the total effect of a factor or interaction and it is computed as

$$\text{Contrast}_A = n \cdot 2^{k-1}(\bar{y}_{A^+} - \bar{y}_{A^-})$$

where k is the order of the factorial design and n the quantity of replicates.

Coefficient of determination (R^2): This number indicates how well data fit a statistical model. It measures the proportion of the total variability SS_T explained by the model SS_M. A potential problem with this statistic is that it always increases as factors are added to a model, even if these factors are not significant.

$$R^2 = \frac{SS_M}{SS_T}$$

Coefficient of determination, adjusted (R^2_{Adj}): It is a statistic that measures the proportion of the total variability SS_T explained by the model SS_M, and besides, it is adjusted for the size of the model. R^2_{Adj} can actually decrease if non-significant terms are added to a model.

$$R^2_{Adj} = 1 - \frac{SS_E/df_E}{SS_T/df_T}$$

Coefficient of determination, prediction (R^2_{Pred}): It is a measure of how well the model will predict new data.

$$R^2_{Pred} = 1 - \frac{PRESS}{SS_T}$$

where $PRESS$ is the predicted sum of squares and SS_T is the total sum of squares.

Coefficient of regression ($\hat{\beta}$): A regression coefficient gives the predicted increase in the response variable for a unit increase in the predictor variable controlling for all other variables in the model.

In case of two-level factorial designs, in which factor levels are usually coded ± 1, the coefficient of regression predicts an increase for two units in the factor.

$$\hat{\beta}_A = \frac{\bar{y}_{A^+} - \bar{y}_{A^-}}{2}$$

where $\bar{y}_{A^+}$ and $\bar{y}_{A^-}$ are the computed response variable averages at high $(+)$ and low levels $(-)$ of factor A respectively.

Covariate: A covariate is a continuous predictor variable.

Degree of Freedom (df): The number of degrees of freedom is the number of values in the final calculation of a statistic that are free to vary, for example:

- In a population of n observations $df = n - 1$.
- A factor A with a levels has $df_A = a - 1$.

- The interaction of two factors, A with a levels and B with b levels, shows $df_{AB} = (a-1)(b-1)$.
- If a factor B with b levels is nested on a factor A with a levels, $df_{B|A} = \mathrm{a}(b-1)$.
- In a statistical design with degrees of freedom df and model degrees of freedom df_M, the degrees of freedom for error equals to $df_E = df - df_M$.

Design, balanced: In design of experiments, a balanced design has an equal number of observations for all possible combinations of factor levels.

Design, saturated: Saturated designs are those designs which do not have any degree of freedom to compute error variance.

Design, unbalanced: In design of experiments, an unbalanced design does not have an equal number of observations for all possible combinations of factor levels.

Design, unsaturated: Unsaturated designs are those designs which still have some degrees of freedom to compute error variance without making additional assumptions.

Effect: In the design of experiments and analysis of variance, an effect of an independent variable (main factor) or a cross-product of independent variables (multiple-factor interaction) measures the variation of a dependent variable averaging across the levels of any other independent variables.

In case of two-level fractional designs, the effect is the difference between the average of the response variable $\bar{y}_{A^+}$ at which the factor (or interaction) is at high level $(+)$, and the average of the response variable $\bar{y}_{A^-}$ at which the factor (or interaction) is at low level $(-)$.

$$l_A = \bar{y}_{A^+} - \bar{y}_{A^-}$$

Error variance (S_E^2): The variance of the errors indicates how much observations deviate from the fitted surface. Suppose that $y_1, y_2 \cdots, y_n$ represents a sample which can be estimated by a model including $\beta_0, \beta_1, \cdots, \beta_k$ parameters, and that $\hat{y}_1, \hat{y}_2 \cdots, \hat{y}_n$ are the corresponding fitted values by the model, then

$$S_E^2 = \frac{\sum_{i=1}^{n}(y_i - \hat{y}_i)^2}{n - (k+1)}$$

Error, type I: In hypothesis testing, when the null hypothesis is true and you reject it, you make a type I error. The probability of making a type I error is α, which is the level of significance you set for your hypothesis test.

Error, type II: In hypothesis testing, when the null hypothesis is false and you fail to reject it, you make a type II error. The probability of making a type II error is β, which depends on the power of the test. The risk of committing a type II error is decreased by ensuring the test has enough power. It can be done by ensuring the sample size is large enough to detect a practical difference when one truly exists.

Factor: A factor is a categorical predictor variable (independent variable).

Factor, allowed-to-vary: Potential design factor that may exert some effect on the response, but for purposes of the present experiment these factors are not of interest; however, they cannot be held at a specific level and it is expected that randomization will balance possible effects.

Factor, controllable: Nuisance factor whose levels may be set by the experimenter. Blocking is often useful in dealing with nuisance controllable factors.

Factor, design: Factor selected to be studied in the experiment.

Factor, fixed-effect: Only the levels of interest of the factor are included in the study. Reached conclusions only apply to the levels considered and cannot be extended to other levels that were not in the study.

Factor, held-constant: Potential design factor that may exert some effect on the response, but for purposes of the present experiment these factors are not of interest; hence, they are held at a specific level.

Factor, noise: Nuisance factor which varies naturally and uncontrollably in the process. The experimenter must fund the settings of the controllable design factors that minimize the variability transmitted from the noise factors.

Factor, nuisance: Factor that may influence the experimental response but in which the interest of the experiment does not lie.

Factor, potential design: Factor that the experimenter may wish to vary in the experiment.

Factor, random-effect: From all possible levels of the factor, only a random sample of levels is included in a study; although interest is in all possible levels. Reached conclusions extend to all levels in the population.

Factor, uncontrollable: Nuisance factor which cannot be controlled by the experiment, but can be measured. Analysis of covariance can often be used for compensating its effect.

F-test: It is a statistical test in which the test statistic has an F-distribution under the null hypothesis, H_0. The test statistic is computed as

$$F_{u,v} = \frac{\chi_u^2/u}{\chi_v^2/v}$$

where χ_u^2 and χ_v^2 are two independent chi-square random variables with u and v degrees of freedom, respectively. It follows a F-distribution with u numerator degrees of freedom and v denominator degrees of freedom.

As an example of a statistic which follows a F-distribution, let $y_{11}, y_{12}\cdots, y_{1n_1}$ and $y_{21}, y_{22}\cdots, y_{2n_2}$ be random samples from two independent normal populations with common variance σ^2, and n_1 and n_2 degrees of freedom, respectively,

$$\frac{S_1^2}{S_2^2} \sim F_{n_1-1,n_2-1}$$

where S_1^2 and S_2^2 are the two sample variances.

Hypothesis, null (H_0): A statistical hypothesis is a statement about the population under study or about the distribution of a quantity under consideration. The null hypothesis is the hypothesis to be tested. It is a statement about a theory that is believed to be true but has not been proven. If the null hypothesis is rejected when it is true, a type I error occurs. If the null hypothesis is not rejected when it is false, a type II error occurs.

Hypothesis, alternative (H_A): A statistical hypothesis is a statement about the population under study or about the distribution of a quantity under consideration. The alternative hypothesis is the hypothesis which becomes true if null hypothesis H_0 is rejected.

Lack-of-fit: It accounts for the residual error which does not correspond to pure error or curvature (in case of including centre points).

Mean of Squares (MS): The mean of squares represent an estimate of population variance. It is calculated by dividing the corresponding sum of squares SS by the degrees of freedom df.

$$MS = \frac{SS}{df}$$

Model, restricted: At dealing with random-effects models, the restricted model basically incorporates the assumption that a random effect by fixed effect interaction sums to zero over the levels of the fixed effect.

Model, unrestricted: A model in which no additional restriction is applied to random effect by fixed effect interactions.

Observation: It is a set of data derived from an experimental unit.

Predicted Residual Sum of Squares ($PRESS$): It is a measure of how well the model will predict new data. A model with a small value of $PRESS$ indicates that the model is likely to be a good predictor. A fitted model having been produced, each observation in turn is removed and the model is refitted using the remaining observations. The out-of-sample predicted value is calculated for the omitted observation in each case, and the $PRESS$ statistic is calculated as the sum of the squares of all the resulting prediction errors:

$$PRESS = \sum_{i=1}^{n} \left(y_i - \hat{y}_{i,-i}\right)^2$$

where n is the quantity of observations.

Pseudo Standard Error (PSE**)**: The pseudo standard error proposed by Lenth's is an objective method for deciding which effects are active in the analysis of un-replicated experiments, when the model is saturated, and hence there are no degrees of freedom for estimating the error variance.

Population: It is any complete set of items or events, with at least one characteristic in common, which is of interest in an experiment.

Population mean (μ): Expected value of a population.

Population variance (σ^2): It is the mean of the squares of the deviations from the mean of a population. It is mean of the deviation of the statistical data.

Pure error: It accounts for the error caused by treatment replications.

p **value**: In statistics, the p value is a function of the observed sample results (a statistic) that is used for testing a statistical hypothesis. Before the test is performed, a threshold value is chosen, called the significance level of the test, traditionally 5% or 1% and denoted as α.

If the p value is equal to or smaller than α, it suggests that the observed data is inconsistent with the assumption that the null hypothesis is true and the hypothesis must be rejected.

Repeated measurements: Repeated measurements are multiple response measurements taken at the same combination of factor settings (levels). Repeated measurements are taken during the same experimental run or consecutive runs; while, replicate measurements are taken during identical but different experimental runs, which are often randomized.

Replication: Replicates are multiple experimental runs with the same factor settings (levels). Replicates are subject to the same sources of variability, independently of each other. You can replicate combinations of factor levels, groups of factor level combinations, or entire designs.

Residual (e): A residual is the difference between an observed value y_i and its corresponding fitted value $\hat{y}_i$.

$$e_i = y_i - \hat{y}_i$$

Run: In design of experiments, a run is each individual execution of a treatment.

Sample: It is a set of observations from a population.

Sample average ($\bar{y}$): It is a measure of the central tendency the sample. The sample average is an estimator of the population mean μ.

Suppose that $y_1, y_2 \cdots, y_n$ represents a sample, then

$$\bar{y} = \frac{\sum_{i=1}^{n} y_i}{n}$$

Sample standard deviation (S): It is a measure of dispersion the sample. It corresponds to the square root of the sample variance S^2.

Sample variance (S^2): It is a measure of the dispersion of the sample. A small variance indicates that data points tend to be very close to the mean, while a large variance indicates that data points are very spread out around the mean. Sample variance is an estimator of population variance σ^2.

Suppose that $y_1, y_2 \cdots, y_n$ represents a sample with sample average $\bar{y}$, then

$$S^2 = \frac{\sum_{i=1}^{n} (y_i - \bar{y})^2}{n-1}$$

Significance level (α): The significance level is the probability of rejecting the null hypothesis in hypothesis testing when it is true.

Standard error of the coefficient (se): The standard error of the estimate of a regression coefficient measures how precisely the model estimates the coefficient's unknown value. The standard error of the coefficient is always positive.

$$se_{coefficient} = \frac{S}{\sqrt{n}}$$

where S is the sample standard deviation and n the number of observations into the sample.

Standard error of the mean (se): It estimates the variability between sample means that you would obtain if you took multiple samples from the same population.

$$se_{mean} = \frac{S}{\sqrt{n}}$$

where S is the sample standard deviation and n the number of observations into the sample.

Sum of squares (SS): The sum of squares represents a measure of variation or deviation of the data. It is calculated as a summation of the squares of the differences from the average $\bar{y}$. The calculation of the total sum of squares SS_T considers both the sum of squares from factors and from randomness or error such as

$$SS_T = \sum_{i=1}^{n} (y_i - \bar{y})^2$$

Treatment: In design of experiments, combinations of factor levels are called treatments.

t-test: It is a statistical test in which the test statistic follows a Student's t-distribution under the null hypothesis H_0. The test statistic is computed as

$$t_k = \frac{z}{\sqrt{\chi_k^2/k}}$$

where z and χ_k^2 are independent standard normal and chi-square random variables respectively, and k quantifies the degrees of freedom.

As an example of a statistic which is distributed as Student's t-distribution, let $y_1, y_2 \cdots, y_n$ be a random sample from the distribution $N(\mu, \sigma^2)$, then

$$\frac{\bar{y} - \mu}{S/\sqrt{n}} \sim t_{n-1}$$

where $\bar{y}$ is the sample average and S is the sample variance.

F.2. Statistical methods

The statistical procedure analyses followed in this work are treated in depth by Montgomery [16], and Quinn and Keough [17].

F.2.1. General Lineal Models (GLM)

The General Linear Model (GLM) is an analysis of variance procedure in which the calculations are performed using a least squares regression approach to describe the statistical relationship between one or more predictors and a continuous response variable.

The main advantage of the GLM is its flexibility:

- Predictors can be factors and covariates.
- Factors may be crossed, factors A and B are crossed if every level of A can occur in every level of B, or nested, factor B is nested in factor A if levels of B only have meaning within specific levels of A.
- Effects of factors may be fixed or random.
- Covariates may be crossed with each other or with factors, or nested within factors.
- The design may be balanced, the number of observations is equal for all combinations of factor levels, or, conversely, unbalanced.

The GLM incorporates a number of different statistical models: ANOVA, Analysis of Covariance (ANCOVA), ordinary linear regression, t-test, F-test, etc.

In the subsequent sections, it is presented how the GLM is applied to different unbalanced design configurations which are of interest for the conducted experiments, from single-factor designs to multiple-factor designs including fixed-effect factors and random-effect blocks.

F.2.1.1. Single-factor models

In an experiment in which it is compared k treatments of a single factor with a total of observations, $n = \sum_{i=1}^{k} n_i$, observations shall be described using the linear statistical model

$$y_{ij} = \mu + \tau_i + \varepsilon_{ij} \begin{cases} i = 1,\cdots,k \\ j = 1,\cdots,n_i \end{cases} \tag{38}$$

where y_{ij} is the jth observation of the treatment i, μ is the overall mean, τ_i is the ith treatment effect, ε_{ij} is the random error term associated with the ijth observation, k is the quantity of

different treatments and n_i is the quantity of observations of the treatment i. Random errors are assumed to be normally and independently distributed with mean zero and constant for all treatments but unknown variance σ^2, $\varepsilon_{ij} \sim N(0, \sigma^2)$.

This model can describe two different situations:

– Fixed-effects model. The k treatments could have been specifically chosen by the experimenter. Conclusions reached here only apply to the treatments considered and cannot be extended to other treatments that were not in the study.
– Random-effects model. The k treatments could be a random sample from a larger population of treatments. Conclusions here extend to all the treatments in the population.

Before going in depth, some concepts must be introduced. The following expressions are even valid for unbalanced data, in which the number of observations taken into the same treatment is different. It is worth noting that balanced designs show two main advantages: the statistic test is relatively insensitive to small departures from the assumption of equal variances, and the power of the test is maximized.

Let $y_{i.}$ and $\bar{y}_{i.}$ represent the total and the average of observations under ith treatment

$$y_{i.} = \sum_{j=1}^{n_i} y_{ij}\,, \qquad \bar{y}_{i.} = \frac{1}{n_i}\sum_{j=1}^{n_i} y_{ij}\,, \qquad i = 1,\cdots,k$$

Likewise, let $y_{..}$ and $\bar{y}_{..}$ represent the grand total and grand average of all observations

$$y_{..} = \sum_{i=1}^{k}\sum_{j=1}^{n_i} y_{ij}\,, \qquad \bar{y}_{..} = \frac{1}{n}\sum_{i=1}^{k}\sum_{j=1}^{n_i} y_{ij}$$

Alternatively, previous totals and averages can be expressed in function of the effects model of Equation (38) such as

$$\bar{y}_{i.} = \mu + \tau_i + \bar{\varepsilon}_{i.}\,, \qquad i = 1,\cdots,k \tag{39}$$

$$\bar{y}_{..} = \mu + \frac{1}{n}\sum_{i=1}^{k} n_i\tau_i + \bar{\varepsilon}_{..} \tag{40}$$

The analysis of variance (ANOVA) is derived from a partition of the total variability into its components. Variability is measured via the total sum of squares as

$$SS_T = \sum_{i=1}^{k}\sum_{j=1}^{n_i}\left(y_{ij} - \bar{y}_{..}\right)^2 \tag{41}$$

since the sample variance, S^2, results at dividing SS_T by the appropriate degrees of freedom, df, such that

$$S^2 = \frac{\sum_{i=1}^{k}\sum_{j=1}^{n_i}\left(y_{ij} - \bar{y}_{..}\right)^2}{n-1} = \frac{SS_T}{n-1} \tag{42}$$

It can be rewritten SS_T as

$$\sum_{i=1}^{k}\sum_{j=1}^{n_i}\left(y_{ij} - \bar{y}_{..}\right)^2 = \sum_{i=1}^{k}\sum_{j=1}^{n_i}\left[(\bar{y}_{i.} - \bar{y}_{..}) + (y_{ij} - \bar{y}_{i.})\right]^2$$

$$= \sum_{i=1}^{k} n_i(\bar{y}_{i.} - \bar{y}_{..})^2 + \sum_{i=1}^{k}\sum_{j=1}^{n_i}\left(y_{ij} - \bar{y}_{i.}\right)^2 + 2\sum_{i=1}^{k}\sum_{j=1}^{n_i}(\bar{y}_{i.} - \bar{y}_{..})(y_{ij} - \bar{y}_{i.})$$

However, the cross-product term in the previous expression is zero, since

$$\sum_{j=1}^{n_i}(y_{ij} - \bar{y}_{i.}) = y_{i.} - n_i\left(\frac{y_{i.}}{n_i}\right) = 0$$

Thus, the total variability can be partitioned into two components, which describe differences between treatments and within treatments, represented by the model sum of squares, SS_M, and the error sum of squares, SS_E, such that

$$SS_T = \sum_{i=1}^{k} n_i(\bar{y}_{i.} - \bar{y}_{..})^2 + \sum_{i=1}^{k}\sum_{j=1}^{n_i}\left(y_{ij} - \bar{y}_{i.}\right)^2 = SS_M + SS_E \tag{43}$$

and

$$SS_M = \sum_{i=1}^{k} n_i(\bar{y}_{i.} - \bar{y}_{..})^2 \tag{44}$$

$$SS_E = \sum_{i=1}^{k}\sum_{j=1}^{n_i}\left(y_{ij} - \bar{y}_{i.}\right)^2 \tag{45}$$

Equivalent expressions can be developed to simplify computations of SS_T and SS_M,

$$SS_T = \sum_{i=1}^{k}\sum_{j=1}^{n_i} y_{ij}^2 - \frac{y_{..}^2}{n}$$

$$SS_M = \sum_{i=1}^{k} \frac{y_{i.}^2}{n_i} - \frac{y_{..}^2}{n}$$

whereas, SS_E can be just computed from the sum of squares balance, Equation (43), as

$$SS_E = SS_T - SS_M$$

Fixed-effects model

Denoted by μ_i the mean of the ith treatment, $\mu_i = \mu + \tau_i$ for $i = 1,\cdots, k$. In the fixed-effects model defined in Equation (38), it can be tested the equality of the k treatment means through the set of hypotheses

$$\begin{aligned} &H_0: \mu_1 = \mu_2 = \cdots = \mu_k \\ &H_A: \mu_i \neq \mu_j \text{ for at least one } i, j \end{aligned} \tag{46}$$

At thinking in μ as the overall mean so that

$$\mu = \frac{\sum_{i=1}^{k} \mu_i}{k} = \frac{k\mu + \sum_{i=1}^{k} \tau_i}{k} = \mu + \frac{1}{k}\sum_{i=1}^{k} \tau_i$$

Treatment effects, τ_i, can be thought of as deviations from μ which should meet the requirement

$$\sum_{i=1}^{k} \tau_i = 0 \tag{47}$$

Consequently, an equivalent set of hypotheses could be proposed via τ_i from the definition of μ_i as

$$\begin{aligned} &H_0: \tau_1 = \tau_2 = \cdots = \tau_k = 0 \\ &H_A: \tau_i \neq 0 \text{ for at least one } i \end{aligned} \tag{48}$$

Let MS_M and MS_E be called the model and error mean squares, respectively,

$$MS_M = \frac{SS_M}{k-1} \tag{49}$$

$$MS_E = \frac{SS_E}{n-k} \tag{50}$$

which are computed from the corresponding sum of squares and degrees of freedom. At examining the expected value of MS_E,

$$\begin{aligned} E(MS_E) = E\left(\frac{SS_E}{n-k}\right) &= \frac{1}{n-k} E\left[\sum_{i=1}^{k}\sum_{j=1}^{n_i}\left(y_{ij} - \bar{y}_{i.}\right)^2\right] \\ &= \frac{1}{n-k} E\left[\sum_{i=1}^{k}\sum_{j=1}^{n_i}\left(y_{ij}^2 - 2y_{ij}\bar{y}_{i.} + \bar{y}_{i.}^2\right)\right] \\ &= \frac{1}{n-k} E\left[\sum_{i=1}^{k}\sum_{j=1}^{n_i} y_{ij}^2 - 2\sum_{i=1}^{k} n_i\bar{y}_{i.}^2 + \sum_{i=1}^{k} n_i\bar{y}_{i.}^2\right] \\ &= \frac{1}{n-k} E\left[\sum_{i=1}^{k}\sum_{j=1}^{n_i} y_{ij}^2 - \sum_{i=1}^{k}\frac{y_{i.}^2}{n_i}\right] \end{aligned}$$

Substituting the effects model of Equation (38) and the corresponding expression of the set of relations shown in Equations (39) and (40) into the previous equation, it is obtained

$$\begin{aligned} E(MS_E) &= \frac{1}{n-k} E\left[\sum_{i=1}^{k}\sum_{j=1}^{n_i}\left(\mu + \tau_i + \varepsilon_{ij}\right)^2 - \sum_{i=1}^{k}\frac{(n_i\mu + n_i\tau_i + \varepsilon_{i.})^2}{n_i}\right] \\ &= \frac{1}{n-k} E\left[\left(n\mu^2 + 2\mu\sum_{i=1}^{k} n_i\tau_i + 2\mu\varepsilon_{..} + \sum_{i=1}^{k} n_i\tau_i^2 + 2\sum_{i=1}^{k}\tau_i\varepsilon_{i.} + \sum_{i=1}^{k}\sum_{j=1}^{n_i}\varepsilon_{ij}^2\right)\right. \\ &\quad \left. - \left(n\mu^2 + 2\mu\sum_{i=1}^{k} n_i\tau_i + 2\mu\varepsilon_{..} + \sum_{i=1}^{k} n_i\tau_i^2 + 2\sum_{i=1}^{k}\tau_i\varepsilon_{i.} + \sum_{i=1}^{k}\frac{\varepsilon_{i.}^2}{n_i}\right)\right] \\ &= \frac{1}{n-k} E\left[\sum_{i=1}^{k}\sum_{j=1}^{n_i}\varepsilon_{ij}^2 - \sum_{i=1}^{k}\frac{\varepsilon_{i.}^2}{n_i}\right] \end{aligned}$$

Assuming that the random error, ε_{ij}, follow a normal distribution with mean zero and common variance σ^2, $\varepsilon_{ij} \sim N(0, \sigma^2)$, terms involving ε_{ij}^2 and $\varepsilon_{i.}^2$ are replaced by σ^2 and $n_i\sigma^2$, respectively. Therefore,

$$E(MS_E) = \frac{1}{n-k} E[n\sigma^2 - k\sigma^2] = \sigma^2 \tag{51}$$

By conducting a similar approach in case of MS_M,

$$\begin{aligned} E(MS_M) &= E\left(\frac{SS_M}{k-1}\right) = \frac{1}{k-1} E\left[\sum_{i=1}^{k} n_i(\bar{y}_{i.} - \bar{y}_{..})^2\right] = \frac{1}{k-1} E\left[\sum_{i=1}^{k} n_i(\bar{y}_{i.}^2 - 2\bar{y}_{i.}\bar{y}_{..} + \bar{y}_{..}^2)\right] \\ &= \frac{1}{k-1} E\left[\sum_{i=1}^{k} n_i\bar{y}_{i.}^2 - 2\bar{y}_{..}\sum_{i=1}^{k} n_i\bar{y}_{i.} + n\bar{y}_{..}^2\right] \\ &= \frac{1}{k-1} E\left[\sum_{i=1}^{k} \frac{y_{i.}^2}{n_i} - \frac{2y_{..}}{n}\sum_{i=1}^{k} y_{i.} + \frac{y_{..}^2}{n}\right] = \frac{1}{k-1} E\left[\sum_{i=1}^{k} \frac{y_{i.}^2}{n_i} - \frac{y_{..}^2}{n}\right] \end{aligned}$$

Substituting the corresponding expressions of the set of relations shown in Equations (39) and (40) into the previous equation, it is obtained

$$\begin{aligned} E(MS_M) &= \frac{1}{k-1} E\left[\sum_{i=1}^{k} \frac{(n_i\mu + n_i\tau_i + \varepsilon_{i.})^2}{n_i} - \frac{\left(n\mu + \sum_{i=1}^{k} n_i\tau_i + \varepsilon_{..}\right)^2}{n}\right] \\ &= \frac{1}{k-1} E\left[\left(n\mu^2 + 2\mu\sum_{i=1}^{k} n_i\tau_i + 2\mu\varepsilon_{..} + \sum_{i=1}^{k} n_i\tau_i^2 + 2\sum_{i=1}^{k} \tau_i\varepsilon_{i.} \right.\right. \\ &\quad \left. + \sum_{i=1}^{k} \frac{\varepsilon_{i.}^2}{n_i}\right) \\ &\quad \left. - \left(n\mu^2 + 2\mu\sum_{i=1}^{k} n_i\tau_i + 2\mu\varepsilon_{..} + \frac{1}{n}\left(\sum_{i=1}^{k} n_i\tau_i\right)^2 + 2\frac{\varepsilon_{..}}{n}\sum_{i=1}^{k} n_i\tau_i + \frac{\varepsilon_{..}^2}{n}\right)\right] \\ &= \frac{1}{k-1} E\left[\sum_{i=1}^{k} n_i\tau_i^2 + 2\sum_{i=1}^{k} \tau_i\varepsilon_{i.} + \sum_{i=1}^{k} \frac{\varepsilon_{i.}^2}{n_i} - \frac{1}{n}\left(\sum_{i=1}^{k} n_i\tau_i\right)^2 \right. \\ &\quad \left. - 2\frac{\varepsilon_{..}}{n}\sum_{i=1}^{k} n_i\tau_i - \frac{\varepsilon_{..}^2}{n}\right] \end{aligned} \tag{52}$$

Since random error follow a normal distribution $\varepsilon_{ij} \sim N(0, \sigma^2)$; $E(\varepsilon_{ij}) = 0$ and terms involving $\varepsilon_{i.}^2$ and $\varepsilon_{..}^2$ are replaced by $n_i\sigma^2$ and $n\sigma^2$, respectively. Besides, all cross-products involving ε_{ij} have zero expectation due to ε_{ij} independence on τ_i. Finally, considering the effects restriction presented in Equation (47),

$$E(MS_M) = \frac{1}{k-1} E\left[\sum_{i=1}^{k} n_i\tau_i^2 + k\sigma^2 - \sigma^2\right] = \sigma^2 + \frac{\sum_{i=1}^{k} n_i\tau_i^2}{k-1} \tag{53}$$

If MS_E estimates σ^2 and there is no difference in μ_i (which implies $\tau_i = 0$), MS_M also estimates σ^2. If treatment means μ_i do differ, $E(MS_M) > \sigma^2$. Thus, a test of the hypothesis of no difference in μ_i can be performed by comparing MS_M and MS_E according to the developed relations for $E(MS_E)$ and $E(MS_M)$. This hypothesis is usually tested through an ANOVA as previously mentioned (Table F.1).

Table F.1 ANOVA table for the fixed-effects model for a single factor.

Source	df	SS	MS	**Expected** MS	F_0
Model	$k-1$	SS_M	MS_M	$\sigma^2 + \frac{\sum_{i=1}^{k} n_i\tau_i^2}{k-1}$	$\frac{MS_M}{MS_E}$
Error	$n-k$	SS_E	MS_E	σ^2	
Total	$n-1$	SS_T			

Assuming that the random errors are independent normal random variables, it follows by Cochran's Theorem that if the null hypothesis, H_0, is true, the ratio F_0 follows an F-distribution with $k-1$ numerator and $n-k$ denominator degrees of freedom.

$$F_0 = \frac{MS_M}{MS_E} \tag{54}$$

Thus an α level hypothesis testing rejects H_0 if $F_0 > F_{k-1,n-k}(\alpha)$. Alternatively, a p value approach could be also used for decision making. p value is computed from the reference distribution $F_{k-1,n-k}$ according to calculated F_0. H_0 would be rejected if $p < \alpha$.

From the set of expression of Equations (39) and (40) and accounting for the effects restriction fixed in Equation (47), model parameters introduced in Equation (38) are estimated by

$$\hat{\mu} = \bar{y}_{..}$$

$$\hat{\tau}_i = \bar{y}_{i.} - \bar{y}_{..}, \qquad i = 1, \cdots, k$$

Random-effects model

In a random-effects model, an additional assumption is made underlying the effects model presented in Equation (38): treatment effects, τ_i, are a random sample of independent variables from a population that is normally distributed with mean zero and variance σ_τ^2, $\tau_i \sim N(0, \sigma_\tau^2)$.

If τ_i are independent of ε_{ij}, the variance of an observation should be

$$Var(y_{ij}) = \sigma^2 + \sigma_\tau^2 \tag{55}$$

Since the treatments in the experiment should be a random sample from a larger population of treatments, the hypotheses of interest are

$$\begin{aligned} H_0&: \sigma_\tau^2 = 0 \\ H_A&: \sigma_\tau^2 > 0 \end{aligned} \tag{56}$$

If H_0 is true, all treatments are identical; whereas, if H_0 is false, it means that it exists variability between treatments.

In the random-effects model, no difference arises at computing the expected MS_E, hence MS_E is an estimator of σ^2 as shown in Equation (51). However, since effects restriction introduced in Equation (47) does not apply in the random-effects model anymore and $\tau_i \sim N(0, \sigma_\tau^2)$, τ_i^2 are replaced by σ_τ^2 in Equation (52).

Besides, due to $E(\tau_i) = 0$ and the independence of τ_i,

$$\left(\sum_{i=1}^{k} n_i \tau_i\right)^2 = \sum_{i=1}^{k} n_i^2 \tau_i^2$$

Therefore, Equation (52) evolves such as

$$E(MS_M) = \frac{1}{k-1} E\left[n\sigma_\tau^2 + k\sigma^2 - \frac{1}{n}\sum_{i=1}^{k} n_i^2 \tau_i^2 - \sigma^2\right] = \sigma^2 + n_0 \sigma_\tau^2 \tag{57}$$

where

$$n_0 = \frac{n^2 - \sum_{i=1}^{k} n_i^2}{(k-1)n} \tag{58}$$

Testing of hypothesis H_0 could be addressed again by comparing MS_M and MS_E, as in case of fixed-effects model; since, if there is no variability between treatments $\sigma_\tau^2 = 0$, MS_M also estimates σ^2. If variability exists between treatments $\sigma_\tau^2 > 0$, then $E(MS_M) > \sigma^2$. The ANOVA applied to the random-effects model is shown in Table F.2.

Table F.2. ANOVA table for the random-effects models for a single factor.

Source	df	SS	MS	**Expected** MS	F_0
Model	$k-1$	SS_M	MS_M	$\sigma^2 + \frac{n^2 - \sum_{i=1}^{k} n_i^2}{(k-1)n}\sigma_\tau^2$	$\frac{MS_M}{MS_E}$
Error	$n-k$	SS_E	MS_E	σ^2	
Total	$n-1$	SS_T			

The hypothesis testing ratio is formed as in Equation (54). Therefore, an α level hypothesis testing rejects H_0 if $F_0 > F_{k-1,n-k}(\alpha)$. Hypothesis testing can also be addressed from the computation of p as in fixed-effects models.

By inverting Equation (51) and (57), both variance components, σ^2 and σ_τ^2, can be estimated such as

$$\hat{\sigma}^2 = MS_E$$

$$\hat{\sigma}_\tau^2 = \frac{MS_M - MS_E}{n_0}$$

Occasionally, the ANOVA produces a negative variance component, which is nonnegative by definition. Three course of actions can be followed according to the experimenter criterion: using the estimate as evidence that the variance component is zero, estimating the variance component again by a different method which always yields to a non-negative value or reformulating the problem.

F.2.1.2. Multiple-factor models

A two-factor crossed design with a total of $n = \sum_{i=1}^{a}\sum_{j=1}^{b} n_{ij}$ observations shall be described using the linear statistical model

$$y_{ijk} = \mu + \tau_i + \beta_j + (\tau\beta)_{ij} + \varepsilon_{ijk} \begin{cases} i = 1,\cdots,a \\ j = 1,\cdots,b \\ k = 1,\cdots,n_{ij} \end{cases} \quad (59)$$

where y_{ijk} is the kth observation of the treatment with factor A at level i and factor B at level j, μ is the overall mean, τ_i is the ith effect level of factor A, β_j is the jth effect level of factor B, $(\tau\beta)_{ij}$ is the effect of the interaction between τ_i and β_j, and ε_{ijk} is the random error term associated with the ijkth observation, a is the quantity of different effect levels of factor A, b is the quantity of effect levels of factor B and n_{ij} is the number of observations of the ijth treatment. Random errors are assumed to be normally and independently distributed with mean zero and constant for all treatments but unknown variance σ^2, $\varepsilon_{ij} \sim N(0, \sigma^2)$.

Let $y_{i..}$, $y_{.j.}$, $y_{ij.}$ and $\bar{y}_{i..}$, $\bar{y}_{.j.}$, $\bar{y}_{ij.}$ represent the total and the average of observations under the ith effect level of factor A, the jth effect level of factor B and the ijth treatment such as

$$
\begin{aligned}
y_{i..} &= \sum_{j=1}^{b}\sum_{k=1}^{n_{ij}} y_{ijk}\,, \qquad \bar{y}_{i..} = \frac{1}{n_{i.}}\sum_{j=1}^{b}\sum_{k=1}^{n_{ij}} y_{ijk}\,, \qquad i = 1,\cdots,a \\
y_{.j.} &= \sum_{i=1}^{a}\sum_{k=1}^{n_{ij}} y_{ijk}\,, \qquad \bar{y}_{.j.} = \frac{1}{n_{.j}}\sum_{i=1}^{a}\sum_{k=1}^{n_{ij}} y_{ijk}\,, \qquad j = 1,\cdots,b \\
y_{ij.} &= \sum_{k=1}^{n_{ij}} y_{ijk}\,, \qquad \bar{y}_{ij.} = \frac{1}{n_{ij}}\sum_{k=1}^{n_{ij}} y_{ijk}\,, \qquad \begin{cases} i = 1,\cdots,a \\ j = 1,\cdots,b \end{cases}
\end{aligned}
\tag{60}
$$

Likewise, let $y_{..}$ and $\bar{y}_{..}$ represent the grand total and grand average of all observations

$$
y_{...} = \sum_{i=1}^{a}\sum_{j=1}^{b}\sum_{k=1}^{n_{ij}} y_{ijk}\,, \qquad \bar{y}_{...} = \frac{1}{n}\sum_{i=1}^{a}\sum_{j=1}^{b}\sum_{k=1}^{n_{ij}} y_{ijk} \tag{61}
$$

and $n_{i.}$ and $n_{.j}$ the partial totals of observations

$$
n_{i.} = \sum_{j=1}^{b} n_{ij}\,, \qquad n_{.j} = \sum_{i=1}^{a} n_{ij}
$$

SS_T can be split into SS_M and SS_E as in single-factor models. Besides, in order to partition SS_M into the corresponding sum of squares of the main factors and their interaction, SS_M can be rewritten as

$$SS_M = \sum_{i=1}^{a}\sum_{j=1}^{b} n_{ij}\left(\bar{y}_{ij.} - \bar{y}_{...}\right)^2$$

$$= \sum_{i=1}^{a}\sum_{j=1}^{b} n_{ij}\left[\left(\bar{y}_{i..} - \bar{y}_{...}\right) + \left(\bar{y}_{.j.} - \bar{y}_{...}\right) + \left(y_{ij.} - \bar{y}_{i..} - \bar{y}_{.j.} + \bar{y}_{...}\right)\right]^2$$

$$= \sum_{i=1}^{a} n_{i.}\left(\bar{y}_{i..} - \bar{y}_{...}\right)^2 + \sum_{j=1}^{b} n_{.j}\left(\bar{y}_{.j.} - \bar{y}_{...}\right)^2 + \sum_{i=1}^{a}\sum_{j=1}^{b} n_{ij}\left(y_{ij.} - \bar{y}_{i..} - \bar{y}_{.j.} + \bar{y}_{...}\right)^2$$

$$+ 2\sum_{i=1}^{a}\sum_{j=1}^{b} n_{ij}\left(\bar{y}_{i..} - \bar{y}_{...}\right)\left(\bar{y}_{.j.} - \bar{y}_{...}\right)$$

$$+ 2\sum_{i=1}^{a}\sum_{j=1}^{b} n_{ij}\left(\bar{y}_{i..} - \bar{y}_{...}\right)\left(y_{ij.} - \bar{y}_{i..} - \bar{y}_{.j.} + \bar{y}_{...}\right)$$

$$+ 2\sum_{i=1}^{a}\sum_{j=1}^{b} n_{ij}\left(\bar{y}_{.j.} - \bar{y}_{...}\right)\left(y_{ij.} - \bar{y}_{i..} - \bar{y}_{.j.} + \bar{y}_{...}\right)$$

In general, cross-product terms in the previous expression do not vanish in case of unbalanced designs; hence, it is not possible to find the variability associated to each main factor or interaction from directly partitioning SS_M.

In a balanced design, such as conventional factorial designs, in which $n_{ij} = n$ for $i = 1,\cdots,a$ and $j = 1,\cdots,b$, cross-product terms are zero. Therefore, the corresponding sum of squares result in

$$SS_T = SS_A + SS_B + SS_{AB} + SS_E = \sum_{i=1}^{a}\sum_{j=1}^{b}\sum_{k=1}^{n}\left(y_{ijk} - \bar{y}_{...}\right)^2$$

$$SS_M = S_A + SS_B + SS_{AB} = n\sum_{i=1}^{a}\sum_{j=1}^{b}\left(\bar{y}_{ij.} - \bar{y}_{...}\right)^2$$

$$\begin{aligned} SS_A &= bn\sum_{i=1}^{a}(\bar{y}_{i..} - \bar{y}_{...})^2 \\ SS_B &= an\sum_{j=1}^{b}\left(\bar{y}_{.j.} - \bar{y}_{...}\right)^2 \\ SS_{AB} &= n\sum_{i=1}^{a}\sum_{j=1}^{b}\left(y_{ij.} - \bar{y}_{.j.} - \bar{y}_{i..} + \bar{y}_{...}\right)^2 \\ SS_E &= \sum_{i=1}^{a}\sum_{j=1}^{b}\sum_{k=1}^{n}\left(y_{ijk} - \bar{y}_{ij.}\right)^2 \end{aligned} \tag{62}$$

In case of unbalanced designs, a new approach is required to measure variability, the adjusted sum of squares. The adjusted sum of squares of a factor is the unique portion of SS_T explained by this factor, regardless the order in which it was entered in the model. In the literature, it is also referred as type III sum of squares. It is widely accepted that the adjusted sum of squares is the preferred procedure to perform ANOVA for unbalanced designs [18–20].

In the two-factor crossed design introduced in Equation (59), the adjusted sum of squares of factor A is defined as the subtraction from the full model sum of squares, $SS_M(A,B,AB)$, of the sum of squares of the reduced model without factor A, $SS_M(B,AB)$,

$$\text{Adjusted } SS_A = SS_M(A,B,AB) - SS_M(B,AB)$$

Alternatively, the Adjusted SS_A can be also defined by the corresponding SS_E due to the equality of the total the sum of squares, $SS_T = SS_M + SS_E$, such that

$$\text{Adjusted } SS_A = SS_E(B,AB) - SS_E(A,B,AB)$$

Adjusted SS_B and Adjusted SS_{AB} are computed in the same way,

$$\text{Adjusted } SS_B = SS_E(A, AB) - SS_E(A, B, AB)$$

$$\text{Adjusted } SS_{AB} = SS_E(A, B) - SS_E(A, B, AB)$$

Definitions of SS_M and SS_E need to be redefined to account for the possibility of referring to models which do not include all factor combinations,

$$SS_M = \sum_{i=1}^{a}\sum_{j=1}^{b}\sum_{k=1}^{n_{ij}}\left(\hat{y}_{ijk} - \bar{y}_{...}\right)^2 \tag{63}$$

$$SS_E = \sum_{i=1}^{a}\sum_{j=1}^{b}\sum_{k=1}^{n_{ij}}\left(y_{ijk} - \hat{y}_{ijk}\right)^2 \tag{64}$$

where $\hat{y}_{ijk}$ is the fitted value of y_{ijk}.

If all the parameters introduced in the effects model presented in Equation (59) are considered, it results

$$\hat{y}_{ijk} = \hat{\mu} + \hat{\tau}_i + \hat{\beta}_j + \widehat{(\tau\beta)}_{ij}$$

However, if any factor or interaction is excluded from the model, different expressions are obtained:

- Including factors A and B,

$$\hat{y}_{ijk} = \hat{\mu} + \hat{\tau}_i + \hat{\beta}_j$$

- Including factor A and interaction AB,

$$\hat{y}_{ijk} = \hat{\mu} + \hat{\tau}_i + \widehat{(\tau\beta)}_{ij}$$

- Including factor B and interaction AB,

$$\hat{y}_{ijk} = \hat{\mu} + \hat{\beta}_j + \widehat{(\tau\beta)}_{ij}$$

It is worth noting that the last two expressions refer to unrealistic models; since the models include interactions, but not all corresponding main effects.

Parameters $\hat{\mu}$, $\hat{\tau}_i$, $\hat{\beta}_j$ and $(\widehat{\tau\beta})_{ij}$ for $i = 1,\cdots,a$ and $j = 1,\cdots,b$ are estimated by applying the least squares method to the corresponding effects model considering all observations. Parameters must be independently estimated for the full model and for each reduced model. In order to estimate the parameters, all factors must be considered as fixed-effect factors; although they were random.

Furthermore, it is also necessary to account for the conventional effect constrains applied to fixed-effect factors:

$$\sum_{i=1}^{a}\tau_i = 0, \qquad \sum_{j=1}^{b}\beta_j = 0, \qquad \sum_{i=1}^{a}(\alpha\beta)_{ij} = \sum_{j=1}^{b}(\alpha\beta)_{ij} = 0, \qquad \begin{cases} i = 1,\cdots,a \\ j = 1,\cdots,b \end{cases}$$

This procedure allows to deal with unbalanced designs, even when empty cells are present.

In case of balanced designs, the adjusted sums of squares coincide with the sums of squares obtained by the conventional formulation, and the model parameters can be estimated by means of the observation averages introduced in Equations (60) and (61),

$$\hat{\mu} = \bar{y}_{\cdots}$$

$$\hat{\tau}_i = \bar{y}_{i\cdot\cdot} - \bar{y}_{\cdots}, \qquad i = 1,\cdots,a$$

$$\hat{\beta}_j = \bar{y}_{\cdot j\cdot} - \bar{y}_{\cdots}, \qquad j = 1,\cdots,b$$

$$\left(\widehat{\tau\beta}\right)_{ij} = \bar{y}_{ij\cdot} - \bar{y}_{i\cdot\cdot} - \bar{y}_{\cdot j\cdot} + \bar{y}_{\cdots}, \qquad \begin{cases} i = 1,\cdots,a \\ j = 1,\cdots,b \end{cases}$$

Consequently,

$$\hat{y}_{ijk} = \hat{\mu} + \hat{\tau}_i + \hat{\beta}_j + \left(\widehat{\tau\beta}\right)_{ij} = \bar{y}_{\cdots} + (\bar{y}_{i\cdot\cdot} - \bar{y}_{\cdots}) + \left(\bar{y}_{\cdot j\cdot} - \bar{y}_{\cdots}\right) + \left(\bar{y}_{ij\cdot} - \bar{y}_{i\cdot\cdot} - \bar{y}_{\cdot j\cdot} + \bar{y}_{\cdots}\right) = \bar{y}_{ij\cdot}$$

Finally, it is worth partitioning SS_E into two components: pure error SS_{PE}, which accounts for variability corresponding to treatment replication, and lack-of-fit SS_{LOF}, which is a measure of the appropriateness of the fitted response and the necessity to increase the order of the model. Both error components are computed as

$$SS_{PE} = \sum_{i=1}^{k}\sum_{j=1}^{n_i}\left(y_{ijk} - \bar{y}_{ij\cdot}\right)^2 \tag{65}$$

$$SS_{LOF} = SS_E - SS_{PE} \tag{66}$$

As in single-factor models, sum of squares computations are not affected by the type of factor included, either fixed- or random-effect factors. Besides, hypothesis testing is also performed through ANOVA based on expected mean of squares; although in multiple-factor designs, the development of expected mean of squares expressions is much more complex.

The general idea is that each mean square arising from the model has an expected value of the form $F_1 + F_2$, where F_1 corresponds to the expected mean square of another term in the model and F_2 is zero if the associated null hypothesis, H_0, is true. Then, it is possible to construct a ratio of the form

$$F_0 = \frac{F_1 + F_2}{F_1} \tag{67}$$

that follows a F-distribution with $df_1 + df_2$ numerator degrees of freedom and df_1 denominator degrees of freedom. Thus an α level hypothesis testing rejects H_0 if $F_0 > F_{df_1+df_2,df_1}(\alpha)$. Nevertheless, it is not always possible to find a combination of terms which allows the construction of F-ratios of the form presented in Equation (67); specially when random effect factors are involved in interactions or nested in other factors. Hypothesis testing can also be addressed from the computation of p values from F_0 ratios.

It is worth noting that, in case of unbalanced designs, F_0 ratios are not constructed anymore with traditional mean of squares, but with adjusted mean of squares computed from adjusted sum of squares as

$$\text{Adjusted } MS_A = \frac{\text{Adjusted } SS_A}{df_A} \tag{68}$$

Fixed-effects model for two crossed factors

In the model introduced in Equation (59), if both factors A and B are considered fixed-effect factors; the following set of constrains is applied:

$$\sum_{i=1}^{a} \tau_i = 0, \qquad \sum_{j=1}^{b} \beta_j = 0, \qquad \sum_{i=1}^{a} (\alpha\beta)_{ij} = \sum_{j=1}^{b} (\alpha\beta)_{ij} = 0, \qquad \begin{cases} i = 1,\cdots,a \\ j = 1,\cdots,b \end{cases}$$

Three set of hypotheses, corresponding to each effect, are tested:

- Factor A,

$$H_0: \tau_i = 0, \qquad i = 1,\cdots,a$$
$$H_A: \tau_i \neq 0 \text{ for at least one } i \tag{69}$$

- Factor B,

$$H_0: \beta_j = 0, \qquad j = 1,\cdots,b$$
$$H_A: \beta_j \neq 0 \text{ for at least one } j \tag{70}$$

- Interaction AB,

$$H_0: (\alpha\beta)_{ij} = 0, \qquad \begin{cases} i = 1,\cdots,a \\ j = 1,\cdots,b \end{cases}$$
$$H_A: (\alpha\beta)_{ij} \neq 0 \text{ for at least one pair } i, j \tag{71}$$

Conducted ANOVA is summarized in Table F.3. Instead of detailed formulas of expected mean of squares, expressions including functions of the corresponding effect terms, Q_m for $m = 1,2,3$, are presented.

Table F.3 ANOVA table for the fixed-effects model for two crossed factors.

Source	df	**Adjusted** SS	**Adjusted** MS	**Expected** MS	F_0
A	$a-1$	SS_A	MS_A	$\sigma^2 + Q_1(\tau_i)$	$\frac{MS_A}{MS_E}$
B	$b-1$	SS_B	MS_B	$\sigma^2 + Q_2(\beta_j)$	$\frac{MS_B}{MS_E}$
AB	$(a-1)(b-1)$	SS_{AB}	MS_{AB}	$\sigma^2 + Q_3((\tau\beta)_{ij})$	$\frac{MS_{AB}}{MS_E}$
Error	$n-ab$	SS_E	MS_E	σ^2	
Total	$n-1$	SS_T			

As in single-factor designs, each set of hypotheses is tested through the corresponding ratio F_0.

Mixed-effects model for two factors

In Equation (72), it is introduced a mixed-effects model in which two factors, a fixed-effect factor A (treatments) and a random-effect factor B (blocks) are considered; but their interaction is not included. This kind of model without interaction between treatments and blocks is common in Randomized Block Designs (RBD).

$$y_{ijk} = \mu + \tau_i + \beta_j + \varepsilon_{ijk} \begin{cases} i = 1,\cdots,a \\ j = 1,\cdots,b \\ k = 1,\cdots,n_{ij} \end{cases} \tag{72}$$

where y_{ijk} is the kth observation of the treatment i and block j, μ is the overall mean, τ_i is the ith treatment effect, β_j is the jth block effect, ε_{ijk} is the random error term associated with the ijkth observation, a is the quantity of different treatments, b is the quantity of different blocks and n_{ij} is the quantity of observations of treatment i and block j. Random errors are assumed again to be normally and independently distributed with mean zero and constant for all treatments but unknown variance σ^2, $\varepsilon_{ijk} \sim N(0, \sigma^2)$.

The basic principle of blocking in experimental design is to group experimental units together into blocks and, then, each treatment is applied to one experimental unit into each block. Such designs are used when it is suspected that the background environment is patchy enough to increase the variation in the response variable substantially. Grouping experimental units in blocks may help to explain some of the total variation in the response variable and, thus, allowing more precise estimation of treatment effects.

The following constraint applies to treatments effects, τ_i, as in the fixed-effects model for a single factor:

$$\sum_{i=1}^{a} n_i \tau_i = 0$$

Whereas, block effects, β_j, are a random sample of independent variables, even of ε_{ijk}, from a population that is normally distributed with mean zero and variance σ_τ^2, $\tau_i \sim N(0, \sigma_\tau^2)$.

Two set of hypotheses, corresponding to each effect, are tested:

- Factor A (treatments),

$$\begin{aligned} &H_0: \tau_i = 0, \qquad i = 1,\cdots,a \\ &H_A: \tau_i \neq 0 \text{ for at least one pair } i \end{aligned} \tag{73}$$

- Factor B (blocks),

$$\begin{aligned} &H_0: \sigma_\beta^2 = 0 \\ &H_A: \sigma_\beta^2 > 0 \end{aligned} \tag{74}$$

The ANOVA table of the corresponding analysis is shown in Table F.4. Expected mean of squares are expressed in terms of a function of treatment effects τ_i, Q, and a function of the quantity of observations per treatment-block combination n_{ijk}, P.

Table F.4 ANOVA table for the mixed-effects model for two factors.

Source	df	Adjusted SS	Adjusted MS	Expected MS	F_0
Treat.	$a-1$	$SS_{Treat.}$	$MS_{Treat.}$	$\sigma^2 + Q(\tau_i)$	$\frac{MS_{Treat.}}{MS_E}$
Blocks	$b-1$	SS_{Blocks}	MS_{Blocks}	$\sigma^2 + P(n_{ijk})\sigma_\beta^2$	
Error	$n-a-b+1$	SS_E	MS_E	σ^2	
Total	$n-1$	SS_T			

The set of hypotheses for factor A are tested through the ratio $F_0 = MS_{Treat.}/MS_E$. However, blocks represent a restriction in randomization and the normality assumption is often questionable, to view $F_0 = MS_{Blocks}/MS_E$ as an exact F test on the existence of block variance is not a good general practice. However, as an approximate procedure to investigate the effect of the blocking variable, examining the ratio of MS_{Blocks} to MS_E is certainly reasonable. If this ratio is large, it implies that blocks have a large effect and that the noise reduction obtained by blocking was probably helpful in improving the precision of the comparison of treatment means.

Mixed-effects model for three factors

A new mixed-effects model is introduced in Equation (75) in which two crossed fixed-effect factors A and B (treatments) and a random-effect factor C (blocks) are considered.

$$y_{ijkl} = \mu + \tau_i + \beta_j + (\tau\beta)_{ij} + \delta_k + \varepsilon_{ijkl} \begin{cases} i = 1,\cdots,a \\ j = 1,\cdots,b \\ k = 1,\cdots,c \\ l = 1,\cdots,n_{ijk} \end{cases} \tag{75}$$

where y_{ijkl} is the lth observation of the treatment combination i and j, and block k; μ is the overall mean; τ_i is the ith effect level of factor A; β_j is the jth effect level of factor B; δ_k is the kth block effect; ε_{ijkl} is the random error term associated with the $ijkl$th observation; a is the quantity of different effect levels of factor A; b is the quantity of different effect levels of factor B; c is the quantity of different blocks; and n_{ijk} is the quantity of observations of the ijth treatment and the block k. Random errors are assumed again to be normally and independently distributed with mean zero and constant for all treatments but unknown variance σ^2, $\varepsilon_{ijkl} \sim N(0, \sigma^2)$.

The same set of constrains which apply to the fixed-effects model for two crossed factors are applicable to the fixed effects of the present design:

$$\sum_{i=1}^{a}\tau_i = 0, \qquad \sum_{j=1}^{b}\beta_j = 0, \qquad \sum_{i=1}^{a}(\alpha\beta)_{ij} = \sum_{j=1}^{b}(\alpha\beta)_{ij} = 0, \qquad \begin{cases} i = 1,\cdots,a \\ j = 1,\cdots,b \end{cases}$$

Block effects, δ_k, are a random sample of independent variables, even of ε_{ijkl}, from a population that is normally distributed with mean zero and variance σ_δ^2, $\delta_k \sim N(0, \sigma_\delta^2)$.

Four set of hypotheses, corresponding to each effect, are tested:

- Factor A,

$$\begin{aligned} &H_0: \tau_i = 0, \qquad i = 1,\cdots,a \\ &H_A: \tau_i \neq 0 \text{ for at least one } i \end{aligned} \tag{76}$$

- Factor B,

$$\begin{aligned} &H_0: \beta_j = 0, \qquad j = 1,\cdots,b \\ &H_A: \beta_j \neq 0 \ \textit{for at least one } j \end{aligned} \tag{77}$$

- Interaction AB,

$$\begin{aligned} &H_0: (\alpha\beta)_{ij} = 0, \qquad \begin{cases} i = 1,\cdots,a \\ j = 1,\cdots,b \end{cases} \\ &H_A: (\alpha\beta)_{ij} \neq 0 \text{ for at least one pair } i,j \end{aligned} \tag{78}$$

- Factor C,

$$\begin{aligned} &H_0: \sigma_\delta^2 = 0 \\ &H_A: \sigma_\delta^2 > 0 \end{aligned} \tag{79}$$

Each set of hypotheses is tested through the corresponding F_0 ratio computed in the ANOVA table depicted in Table F.5. Expected mean of squares are expressed in terms of functions of treatment effects, Q_m for $m = 1,2,3$, and a function of the quantity of observations per treatment-block combination n_{ijkl}, P.

Table F.5. ANOVA table for the mixed-effects model for three factors.

Source	df	Adjusted SS	Adjusted MS	Expected MS	F_0
A	$a-1$	SS_A	MS_A	$\sigma^2+Q_1(\tau_i)$	$\frac{MS_A}{MS_E}$
B	$b-1$	SS_B	MS_B	$\sigma^2+Q_2(\beta_j)$	$\frac{MS_B}{MS_E}$
AB	$(a-1)(b-1)$	SS_{AB}	MS_{AB}	$\sigma^2+Q_3((\tau\beta)_{ij})$	$\frac{MS_{AB}}{MS_E}$
Blocks	$c-1$	SS_{Blocks}	MS_{Blocks}	$\sigma^2+P(n_{ijkl})\sigma_\delta^2$	$\frac{MS_{Blocks}}{MS_E}$
Error	$n-ab-c+1$	SS_E	MS_E	σ^2	
Total	$n-1$	SS_T			

Adjusted sum of squares and mean of squares, and observations averages and totals are calculated under the same criteria followed to compute the equivalent functions in case of two-factor designs.

The F test on the existence of block variance is taken as an approximate procedure due to the restriction in randomization caused by introducing blocks in the experiment.

F.2.1.3. Adequacy checking

Residuals, e_{ij}, must be examined to check that errors, ε_{ij}, are normally and independently distributed with mean zero and constant but unknown variance σ^2, $\varepsilon_{ij}\sim N(0,\sigma^2)$.

$$e_{ij}=y_{ij}-\hat{y}_{ij} \tag{80}$$

where y_{ij} is the jth observation of the treatment i and $\hat{y}_{ij}$ is the value of y_{ij} fitted by them model under consideration.

Model diagnostic checking is performed by graphical analysis of residuals, which should be structureless and do not present any obvious pattern.

- Normal probability plot of residuals (normality assumption). If the underlying error distribution is normal, this plot will resemble a straight line.
- Plot of residuals in time sequence (independence assumption). It is helpful in detecting correlation between residuals that would imply that the independence assumption on the errors has been violated. Proper randomization of the experiment is an important step in obtaining independence. Runs must be conducted in a randomized order.
- Plot of residuals versus fitted values (constant variance assumption). This plot should not reveal any obvious pattern if the residuals are structureless, that is to say, variance on the observations does not depend on the magnitude of the observation.

- Plot of residuals versus variables. Patterns in such residuals plots imply that theses variables affects the response. This suggests that the variables should be either controlled more carefully in future experiments or include in the analysis.

Apart from in plot of residuals versus fitted values, non-constant variance also arises in cases where the data follow a non-normal and skewed distribution. Non-constant variance only affects slightly F-tests in case of balanced fixed-effects models; however, the problem is more serious in unbalanced designs or in large variations of variance. If the factor levels having the larger variances also have the smaller sample size, the actual type I error is larger than expected. For random-effects models, unequal error variance can significantly disturb inferences on variance components even if balance designs are used.

The variance assumption can be alternatively checked by statistical tests for equality of variance such as the Bartlett's test, which is still sensitive to the normality assumption, and the modified Levene's test, which is robust to departures from normality.

Sometimes a curvilinear shape may arise in the plot of residuals versus fitted values, negative residuals for low and high $\hat{y}_{ij}$, and positive residuals for intermediate $\hat{y}_{ij}$. This pattern is suggestive of an interaction between treatments and blocks in RBDs.

F.2.2. Factorial designs

Factorial designs are usually used in experiments in which it is necessary to study the joint effect of some factors on a response. In a factorial design, in each complete trial or replication of the experiment, all possible combinations of the levels of the factors are investigated. This factor arrangement in a factorial design corresponds to a crossed structure including main factors and their interactions. Factorial designs are based on balanced fixed-effects models with equal number of replications for each treatment.

Factorial designs present three main advantages: they are more efficient that one-factor-at-a-time experiments, it is avoided misleading conclusions when interactions are present, and they allow the effects of a factor to be estimated at several levels of the other factors, yielding conclusions that are valid over a range of experimental conditions.

As in the case of the GLMs, factorial designs can be addressed through ANOVA. A statistical model for a general fixed-effects model for three crossed factors including all multiple-factor interactions with n replicates applies to a conventional three-factor factorial design.

$$y_{ijkl} = \mu + \tau_i + \beta_j + \gamma_k + (\tau\beta)_{ij} + (\tau\gamma)_{ik} + (\beta\gamma)_{jk} + (\tau\beta\gamma)_{ijk} + \varepsilon_{ijkl} \begin{cases} i = 1,\cdots,a \\ j = 1,\cdots,b \\ k = 1,\cdots,c \\ l = 1,\cdots,n \end{cases} \quad (81)$$

where y_{ijkl} is the lth observation of the ijkth treatment, μ is the overall mean, τ_i is the ith effect level of factor A, β_j is the jth effect level of factor B, γ_k is the kth effect level of factor C, ε_{ijkl} is the random error term associated with the $ijkl$th observation, a is the quantity of different effect levels of factor A, b is the quantity of different effect levels of factor B and c is the quantity of different effect levels of factor C. Random errors are assumed to be normally and independently distributed with mean zero and constant for all treatments but unknown variance σ^2, $\varepsilon_{ijkl} \sim N(0, \sigma^2)$.

The corresponding ANOVA is shown in Table F.6. F-tests are constructed from the expected mean squares as in the various designs treated in Section F.2.1.

Table F.6 ANOVA table for the fixed-effects model for three crossed factors.

Source	df	SS	MS	Expected MS	F_0
A	$a-1$	SS_A	MS_A	$\sigma^2 + \frac{bcn\sum \tau_i^2}{a-1}$	$\frac{MS_A}{MS_E}$
B	$b-1$	SS_B	MS_B	$\sigma^2 + \frac{acn\sum \beta_i^2}{b-1}$	$\frac{MS_B}{MS_E}$
C	$c-1$	SS_C		$\sigma^2 + \frac{abn\sum \gamma_i^2}{c-1}$	$\frac{MS_C}{MS_E}$
AB	$(a-1)(b-1)$	SS_{AB}	MS_{AB}	$\sigma^2 + \frac{cn\sum\sum(\tau\beta)_{ij}^2}{(a-1)(b-1)}$	$\frac{MS_{AB}}{MS_E}$
AC	$(a-1)(c-1)$	SS_{AC}	MS_{AC}	$\sigma^2 + \frac{cn\sum\sum(\tau\beta)_{ij}^2}{(a-1)(c-1)}$	$\frac{MS_{AC}}{MS_E}$
BC	$(b-1)(c-1)$	SS_{BC}	MS_{BC}	$\sigma^2 + \frac{bn\sum\sum(\tau\gamma)_{ij}^2}{(b-1)(c-1)}$	$\frac{MS_{BC}}{MS_E}$
ABC	$(a-1)(b-1)(c-1)$	SS_{ABC}	MS_{ABC}	$\sigma^2 + \frac{n\sum\sum\sum(\tau\beta\gamma)_{ijk}^2}{(a-1)(b-1)(c-1)}$	$\frac{MS_{ABC}}{MS_E}$
Error	$abc(n-1)$	SS_E	MS_E	σ^2	
Total	$abcn-1$	SS_T			

The set of sum of squares shown in Table F.6 can be calculated from the following simplified expressions based on observations totals:

$$SS_T = \sum_{i=1}^{a}\sum_{j=1}^{b}\sum_{k=1}^{c}\sum_{l=1}^{n} y_{ijkl}^2 - \frac{y_{....}^2}{abcn}$$

$$SS_A = \frac{1}{bcn}\sum_{i=1}^{a} y_{i...}^2 - \frac{y_{....}^2}{abcn}, \qquad y_{i...} = \sum_{j=1}^{b}\sum_{k=1}^{c}\sum_{l=1}^{n} y_{ijkl}, \qquad i = 1,\cdots,a$$

$$SS_B = \frac{1}{acn}\sum_{j=1}^{b} y_{.j..}^2 - \frac{y_{....}^2}{abcn}, \qquad y_{.j..} = \sum_{i=1}^{a}\sum_{k=1}^{c}\sum_{l=1}^{n} y_{ijkl}, \qquad j = 1,\cdots,b$$

$$SS_C = \frac{1}{abn}\sum_{k=1}^{c} y_{..k.}^2 - \frac{y_{....}^2}{abcn}, \qquad y_{..k.} = \sum_{i=1}^{a}\sum_{j=1}^{b}\sum_{l=1}^{n} y_{ijkl}, \qquad k = 1\cdots,c$$

$$SS_{AB} = \frac{1}{cn}\sum_{i=1}^{a}\sum_{j=1}^{b} y_{ij..}^2 - \frac{y_{....}^2}{abcn} - SS_A - SS_B, \qquad y_{ij..} = \sum_{k=1}^{c}\sum_{l=1}^{n} y_{ijkl},$$
$$\begin{cases} i = 1,\cdots,a \\ j = 1,\cdots,b \end{cases} \tag{82}$$

$$SS_{AC} = \frac{1}{bn}\sum_{i=1}^{a}\sum_{k=1}^{c} y_{i.k.}^2 - \frac{y_{....}^2}{abcn} - SS_A - SS_C, \qquad y_{i.k.} = \sum_{j=1}^{b}\sum_{l=1}^{n} y_{ijkl},$$
$$\begin{cases} i = 1,\cdots,a \\ k = 1,\cdots,c \end{cases}$$

$$SS_{BC} = \frac{1}{an}\sum_{j=1}^{b}\sum_{k=1}^{c} y_{.jk.}^2 - \frac{y_{....}^2}{abcn} - SS_B - SS_C, \qquad y_{.jk.} = \sum_{i=1}^{a}\sum_{l=1}^{n} y_{ijkl},$$
$$\begin{cases} j = 1,\cdots,b \\ k = 1,\cdots,c \end{cases}$$

$$SS_{ABC} = \frac{1}{n}\sum_{i=1}^{a}\sum_{j=1}^{b}\sum_{k=1}^{c} y_{ijk.}^2 - \frac{y_{....}^2}{abcn} - SS_A - SS_B - SS_C - SS_{AB} - SS_{AC} - SS_{BC},$$

$$y_{ijk.} = \sum_{l=1}^{n} y_{ijkl}, \qquad \begin{cases} i = 1,\cdots,a \\ j = 1,\cdots,b \\ k = 1,\cdots,c \end{cases}$$

$$SS_E = SS_T - -SS_A - SS_B - SS_C - SS_{AB} - SS_{AC} - SS_{BC} - SS_{ABC}$$

where the grand total of all observations is computed as

$$y_{....} = \sum_{i=1}^{a}\sum_{j=1}^{b}\sum_{k=1}^{c}\sum_{l=1}^{n} y_{ijkl}$$

A set of hypothesis is stated for each main factor or multiple-factor interaction and tested by means of the corresponding F_0 ratio.

In the analysis of factorial designs, the most common case is that of k factors, each at only two levels, usually referred as high $(+)$ and low $(-)$. Both levels can describe quantitative or qualitative magnitudes. The 2^k factorial design is particularly useful in early stages of experimental work, when it is likely that too many factors are investigated. Consequently, these designs are widely used in screening experiments. A standard 2^3 factorial design is graphically presented in Figure F.1. In the design matrix, the corresponding configurations of 2^1 and 2^2 factorial designs are also framed.

(a)

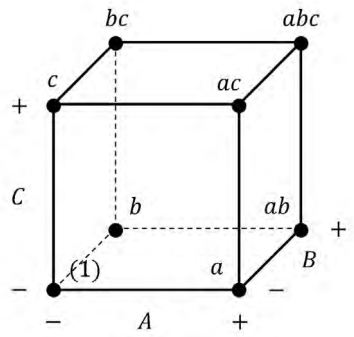

(b)

Run	Treatment combination	Factor A	Factor B	Factor C
1	(1)	−	−	−
2	a	+	−	−
3	b	−	+	−
4	ab	+	+	−
5	c	−	−	+
6	ac	+	−	+
7	bc	−	+	+
8	abc	+	+	+

..... 2^1 factorial design
– – – – 2^2 factorial design

Figure F.1 The 2^3 factorial design: (a) geometric view and (b) design matrix.

The effect of a factor (or interaction) is defined to be the change in response produced by a change in the level factor. In two-level designs, it corresponds to the difference between the average response at the high level of the factor (or interaction), $\bar{y}_{A^+}$, and the average response at the low level of the factor (or interaction), $\bar{y}_{A^-}$.

$$\text{Effect}_A = \bar{y}_{A^+} - \bar{y}_{A^-} \tag{83}$$

Factor and interaction effects are usually represented through main factors and interaction plots, Pareto plots or normal probability plots of effects. These plots allow a simple form of interpretation of the magnitude and direction of effects.

The total effect of a factor, named as contrast, is alternatively defined as

$$\text{Contrast}_A = n \cdot 2^{k-1}(\bar{y}_{A^+} - \bar{y}_{A^-}) \tag{84}$$

where k is the order of the factorial design and n the quantity of replicates. It is worth noting that the contrast of a factor is directly connected with its corresponding sum of squares via

$$SS_A = \frac{(\text{Contrast}_A)^2}{n \cdot 2^k} \tag{85}$$

In a 2^k factorial design, it is easy to express the results of an experiment in terms of a regression model, which is different from the effects model introduced in Equation (81),

$$\hat{y} = \beta_0 + \beta_1 x_1 + \beta_2 x_2 + \cdots + \epsilon$$

where $\hat{\beta}_i$ are regression coefficients and x_i are coded variables that represent significant factors in the model. In 2^k factorial designs, regression coefficients can be estimated by the factor effects such that

$$\hat{\beta}_A = \frac{\text{Effect}_A}{A^+ - A^-} \tag{86}$$

In case of using the standard codification for categorical variables ± 1, $\hat{\beta}_A$ correspond to one-half of the corresponding factor effect, $\hat{\beta}_A = \text{Effect}_A/2$.

Model adequacy is checked via the same procedure followed in the GLM: normal probability plot of the residuals, plot of residuals in time sequence, plot of the residuals versus predicted values and plot of residuals versus the variables included in the analysis.

Finally, it is important to note that replication and repeated measurements refer to different concepts. Replication of a treatment implies that the whole experimental treatment is repeated, reflecting sources of variability between runs and within runs. In repeated measurements, the experimental treatment is not repeated, only sources of variability within runs are reflected. In factorial designs, it is necessary to replicate experiments to allow the computation of SS_E and perform the analysis of variance; nevertheless, in order to deal with repeated measurements, only the average of these measurements is included in the analysis as response values.

F.2.2.1. Fractional factorial design

If the experimenter can reasonably assume that certain high-order interactions are negligible, information on the main effects and low-order interactions may be obtained by running only a fraction of the complete factorial experiment. Furthermore, the subset of significant factors can be projected in larger factorial designs if it is required in later analyses, or the factorial design can collapse into lower order factorial designs. A good practice in these types of experiments is to spread out the factor levels aggressively, because of uncertainty on error magnitude.

A major use of fractional factorials is in screening experiments. Screening experiments are usually performed in the early stages of a project when it is likely that many of the factors initially considered have little or no effect on the response. In screening experiments, it is more serious to miss important factors than to misidentify unimportant factors. The successful use of fractional factorial designs is based on three key ideas:

- The sparsity of effects principle. When there are several variables, the system or process is likely to be driven primarily by some of the main effects and low-order interactions.
- The projection property. Fractional factorial designs can be projected into stronger (larger) designs in the subset of significant factors.
- Sequential experimentation. It is possible to combine the runs of simple fractional factorials to assemble sequentially a larger design to estimate the factor effects and interactions of interest.

Fractional designs can be split in two one-half fractions: principal and alternate (or complementary). Each fraction is structured according to a chosen generator. For example, in the 2^{3-1} design, the generator ABC results in the upper one-half of treatment combinations shown in Table F.7. Notice that in the corresponding column of ABC, only a plus sign appears in the upper one-half. Consequently, the defining relation of the design is defined in terms of the identity column, I, as

$$I = ABC \tag{87}$$

Table F.7. Plus and minus signs for the 2^3 factorial design.

Treatment combination	Factorial effect							
	I	A	B	C	AB	AC	BC	ABC
a	+	+	−	−	−	−	+	+
b	+	−	+	−	−	+	−	+
c	+	−	−	+	+	−	−	+
abc	+	+	+	+	+	+	+	+
ab	+	+	+	−	+	−	−	−
ac	+	+	−	+	−	+	−	−
bc	+	−	+	+	−	−	+	−
(1)	+	−	−	−	+	+	+	−

The defining relation of Equation (87) corresponds to the principal fraction of the 2^{3-1} design; meanwhile, the alternate fraction is defined by the relation:

$$I = -ABC \tag{88}$$

The alternate fraction of the 2^{3-1} design corresponds to the lower one-half of Table F.7. Notice, that in both one-half fractions, sign columns of main factors and interactions are not independent. At estimating effects according to Equation (83), main factor and interaction effects are aliased. It is impossible to differentiate between them. For the principal fraction, the alias structure includes

$$l_A \to A + BC, \qquad l_B \to B + AC, \qquad l_C \to C + AB$$

while, for the alternate fraction,

$$l'_A \to A - BC, \qquad l'_B \to B - AC, \qquad l'_C \to C - AB$$

The 2^{3-1} design is called a resolution III design. A design is of resolution R if no p-factor effect is aliased with another effect containing less than $R - p$ factors.

- Resolution III designs. No main effects are aliased with any other main effect, but main effects are aliased with two-factor interactions and two-factor interactions may be aliased with each other, e.g. 2^{3-1}_{III}.
- Resolution IV designs. No main effect is aliased with any other main effect or with any two-factor interaction, but two-factor interactions are aliased with each other, e.g. 2^{4-1}_{IV}.
- Resolution V designs. No main effect of two-factor interaction is aliased with any other main effect or two-factor interaction, but two-factor interactions are aliased with three-factor interactions, e.g. 2^{5-1}_{V}.

Throughout this thesis, only experiments with $2_{III}^{3-1}$and 2_{IV}^{4-1} designs were conducted. Treatment combinations for both principal and alternate fractions of the 2_{IV}^{3-1} design are shown in Table F.8.

Table F.8 The 2_{IV}^{3-1} designs with defining relations $I = ABC$ (left) and $I = -ABC$ (right).

Treatment combination	Basic design		$C = AB$	Treatment combination	Basic design		$C = -AB$
	A	B			A	B	
c	−	−	+	(1)	−	−	−
b	−	+	−	bc	−	+	+
a	+	−	−	ac	+	−	+
abc	+	+	+	ab	+	+	−

Treatment combinations for both principal and alternate fractions of the 2_{IV}^{4-1} design are shown in Table F.9.

Table F.9 The 2_{IV}^{4-1} designs with defining relations $I = ABCD$ (left) and $I = -ABCD$ (right).

Treatment combination	Basic design			$D = ABC$	Treatment combination	Basic design			$D = -ABC$
	A	B	C			A	B	C	
(1)	−	−	−	−	d	−	−	−	+
ad	+	−	−	+	a	+	−	−	−
bd	−	+	−	+	b	−	+	−	−
ab	+	+	−	−	abd	+	+	−	+
cd	−	−	+	+	c	−	−	+	−
ac	+	−	+	−	acd	+	−	+	+
bc	−	+	+	−	bcd	−	+	+	+
$abcd$	+	+	+	+	abc	+	+	+	−

Alias structures of the 2_{IV}^{4-1} principal fraction design include

$$l_A \to A - BCD, \qquad l_B \to B - ACD, \qquad l_C \to C - ABD, \qquad l_D \to D - ABC$$

$$l_{AB} \to AB - CD, \qquad l_{AC} \to AC - BD, \qquad l_{AD} \to AD - BC$$

The four main effects plus the three two-factor interaction alias pairs count for the seven design degrees of freedom. The corresponding alias pairs for the alternate fraction are

$$l'_A \to A + BCD, \qquad l'_B \to B + ACD, \qquad l'_C \to C + ABD, \qquad l'_D \to D + ABC$$

$$l'_{AB} \to AB + CD, \qquad l'_{AC} \to AC + BD, \qquad l'_{AD} \to AD + BC$$

In order to identify the really significant factor or interaction into an alias structure, it is necessary to apply the acquired kwon-how about the experiment and consider specific conditions of each analysis.

For a moderately large number of factors, smaller fractions of the 2^k design are frequently used, such as the one-quarter fraction. However, these fractions are not considered in this section since they are beyond the scope of the thesis.

Fractional factorials are often saturated single-replicate experiments; hence, there is no available degrees of freedom to compute error variance in order to find F_0 ratios for each factor and interaction involved. A typical solution to this problem is to construct normal probability plots of the estimated effects and judge as significant those that departed from linearity by a substantial distance. Negligible effects are normally distributed with mean zero and variance σ^2 and tend to fall along a straight line on this plot, whereas significant effects have non-zero means and do not lie along the straight line. In experiments with only few runs, such as eight-run designs, interpretation of half-normal probability plots of effects may result easier.

After identifying the most significant effects, negligible effects can be combined to estimate experimental error; therefore, an analysis of variance should be conducted again including only significant effects as in conventional factorial design analyses. It must be pointed out that to include any interaction in the analysis, corresponding main factors must be included too.

Effect significance can also be checked by means of the pseudo standard error introduced by Lenth, PSE, which is an objective method for deciding which effects are active in the analysis of unreplicated experiments. In a unreplicated 2^k factorial design with contrast estimates $c_1, c_2, \cdots, c_m$ and $m = 2^k - 1$,

$$PSE = 1{,}5 \cdot median\{|c_j| : |c_j| \leq 2{,}5 s_0\} \tag{89}$$

where $s_0 = 1{,}5 \cdot median\{|c_j|\}$. An individual contrast can be compared to the margin error

$$ME = t_{0{,}025,d} \cdot PSE \tag{90}$$

where $d = m/3$.

Contrasts that exceed the ME in absolute value are deemed active at the 5% significance level. Alternatively, it can be computed a simultaneous margin of error

$$SME = t_{\gamma,d} \cdot PSE \tag{91}$$

where the percentage point of the t distribution is $\gamma = 1 - (1 + 0{,}95^{1/m})/2$.

The distinction between ME and SME is that there is at most a 5% chance that one individual inactive contrast will exceed the ME, while there is at most a 5% chance that any inactive contrast will exceed the SME.

Lenth's method is a useful procedure to supplement the usual normal probability plot of effects, but not to replace it. In the present work, effect significance of saturated factorial designs was addressed through half-normal probability plots of effects.

F.2.2.2. Factorial design with a covariate

In an experiment with a response variable, y, there is another variable, x, which is linearly related to y. Suppose that x cannot be controlled by the experiment, but can be observed along with y. The variable x is an uncontrollable nuisance factor referred from now on as covariate.

The analysis of covariance (ANCOVA) involves adjusting the observed response variable for the effect of the covariate, as well as the effects of the different treatments. ANCOVA is a technique that is occasionally useful for improving the precision of an experiment, since the covariate could inflate the error mean of squares. The procedure is a combination of ANOVA and regression analysis. Only the case with one covariate and no interaction with factors is treated in this section.

In a single-factor experiment, fixed-effect factor, with one covariate, assuming that there is a linear relationship between the response and the covariate, an appropriate linear model is

$$y_{ij} = \mu + \tau_i + \beta(x_{ij} - \bar{x}_{..}) + \varepsilon_{ij} \begin{cases} i = 1,\cdots,k \\ j = 1,\cdots,n_i \end{cases} \quad (92)$$

where y_{ij} is the jth observation of the treatment i, μ is the overall mean, τ_i is the ith treatment effect, x_{ij} is the measurement of the covariate corresponding to y_{ij}, $\bar{x}_{..}$ is the mean of x_{ij}, β is the regression coefficient indicating the dependence of y_{ij} on x_{ij}, ε_{ij} is the random error term associated with the ijth observation, k is the quantity of different treatments and n is the quantity of observations per treatment. Random errors are assumed to be normally and independently distributed with mean zero and constant for all treatments but unknown variance σ^2, $\varepsilon_{ij} \sim N(0, \sigma^2)$.

It is assumed that $\beta \neq 0$ and the true relationship between y_{ij} and x_{ij} is linear, that regression coefficients for each treatment are identical, and that the covariate x_{ij} is not affected by the treatments. Furthermore, constrains applied to fixed-effect factors are also required

$$\sum_{i=1}^{k} \tau_i = 0$$

An alternative model to Equation (92) can be rewritten as

$$y_{ij} = \mu' + \tau_i + \beta x_{ij} + \varepsilon_{ij} \begin{cases} i = 1,\cdots,k \\ j = 1,\cdots,n \end{cases} \tag{93}$$

where $\mu' = \mu - \beta \bar{x}_{..}$.

The following notation is introduced to proceed with the description of the analysis:

$$S_{yy} = \sum_{i=1}^{k}\sum_{j=1}^{n}\left(y_{ij} - \bar{y}_{..}\right)^2 = \sum_{i=1}^{k}\sum_{j=1}^{n} y_{ij}^2 - \frac{y_{..}^2}{kn}$$

$$S_{xx} = \sum_{i=1}^{k}\sum_{j=1}^{n}\left(x_{ij} - \bar{x}_{..}\right)^2 = \sum_{i=1}^{k}\sum_{j=1}^{n} x_{ij}^2 - \frac{x_{..}^2}{kn}$$

$$S_{xy} = \sum_{i=1}^{k}\sum_{j=1}^{n}\left(x_{ij} - \bar{x}_{..}\right)\left(y_{ij} - \bar{y}_{..}\right) = \sum_{i=1}^{k}\sum_{j=1}^{n} x_{ij}y_{ij} - \frac{x_{..}y_{..}}{kn}$$

$$T_{yy} = n\sum_{i=1}^{k}(\bar{y}_{i.} - \bar{y}_{..})^2 = \frac{1}{n}\sum_{i=1}^{k} y_{i.}^2 - \frac{y_{..}^2}{kn}$$

$$T_{xx} = n\sum_{i=1}^{k}(\bar{x}_{i.} - \bar{x}_{..})^2 = \frac{1}{n}\sum_{i=1}^{k} x_{i.}^2 - \frac{x_{..}^2}{kn}$$

$$T_{xy} = n\sum_{i=1}^{k}(\bar{x}_{i.} - \bar{x}_{..})(\bar{y}_{i.} - \bar{y}_{..}) = \frac{1}{n}\sum_{i=1}^{k} x_{i.}y_{i.} - \frac{x_{..}y_{..}}{kn}$$

$$E_{yy} = \sum_{i=1}^{k}\sum_{j=1}^{n}\left(y_{ij} - \bar{y}_{i.}\right)^2 = S_{yy} - T_{yy}$$

$$E_{xx} = \sum_{i=1}^{k}\sum_{j=1}^{n}\left(x_{ij} - \bar{x}_{i.}\right)^2 = S_{xx} - T_{xx}$$

$$E_{xy} = \sum_{i=1}^{k}\sum_{j=1}^{n}(x_{ij} - \bar{x}_{i.})(y_{ij} - \bar{y}_{i.}) = S_{xy} - T_{xy}$$

where S, T and E are used to denote sum of squares and cross-products for total, treatments and error, respectively.

In order to proceed with the ANOVA, the concept of adjusted sum of squares, introduced in Section F.2.1.2, must be addressed; since covariates and factors are not in general uncorrelated. The error sum of squares in the full model with $k(n-1)-1$ degrees of freedom is

$$SS_E = E_{yy} - \frac{E_{xy}^2}{E_{xx}}$$

However, if only the covariate is considered to describe the response behaviour, the following reduced model arises,

$$y_{ij} = \mu + \beta(x_{ij} - \bar{x}_{..}) + \varepsilon_{ij} \begin{cases} i = 1,\cdots,k \\ j = 1,\cdots,n \end{cases}$$

and the error sum of squares is computed by

$$SS_E(x) = S_{yy} - \frac{S_{xy}^2}{S_{xx}}$$

Whereas, if only treatments are considered, the reduced model obtained is

$$y_{ij} = \mu + \tau_i + \varepsilon_{ij} \begin{cases} i = 1,\cdots,k \\ j = 1,\cdots,n \end{cases}$$

and the error sum of squares corresponds to

$$SS_E(\tau) = E_{yy}$$

Therefore, the adjusted sums of squares of both covariate and treatments can be calculated from

$$\text{Adjusted } SS_x = SS_E(\tau) - SS_E(\tau, x) = \frac{E_{xy}^2}{E_{xx}}$$

$$\text{Adjusted } SS_{treat.} = SS_E(x) - SS_E(\tau, x) = \left(S_{yy} - \frac{S_{xy}^2}{S_{xx}}\right) - \left(E_{yy} - \frac{E_{xy}^2}{E_{xx}}\right)$$

Instead of using the previously defined sums of squares and cross-products expressions, the adjusted error sums of squares of the reduced models can be also computed via the general procedure presented in Section F.2.1.2.

Then the following set of hypotheses are tested through the ANOVA summarized in Table F.10.

- Treatments,

$$H_0: \tau_i = 0, \qquad i = 1,\cdots,k$$
$$H_A: \tau_i \neq 0 \text{ for at least one } i \tag{94}$$

- Covariate,

$$H_0: \beta = 0$$
$$H_A: \beta \neq 0 \tag{95}$$

Table F.10 ANCOVA table for the fixed-effects model for a single factor and a covariate.

Source	df	SS	MS	F_0
Covariate	1	SS_x	MS_x	$\frac{MS_x}{MS_E}$
Treatments	$k-1$	$SS_{Treat.}$	$MS_{Treat.}$	$\frac{MS_{Treat.}}{MS_E}$
Error	$k(n-1)-1$	SS_E	MS_E	
Total	$kn-1$	SS_T		

Hypothesis testing is stated according to the same criteria followed for fixed-effects models (Section F.2.1.1) and for linear regression (Section F.2.4).

The least square estimators of the full model parameters included in Equation (92) are

$$\hat{\mu} = \bar{y}_{..}$$
$$\hat{\tau}_i = \bar{y}_{i.} - \bar{y}_{..} - \hat{\beta}(\bar{x}_{i.} - \bar{x}_{..}), \qquad i = 1,\cdots,k$$
$$\hat{\beta} = \frac{E_{xy}}{E_{xx}}$$

Besides, the experimental error variance σ^2 is estimated by the error mean of squares as

$$\hat{\sigma}^2 = MS_E = \frac{SS_E}{k(n-1)-1}$$

In case of analysing the effects of more than one factor, multiple factors and interactions, after estimating the regression coefficient for the covariate, observations can be adjusted for the covariate to treat with factor and interaction effects separately. Under this approach, the initial model presented in Equation (92) becomes

$$y'_{ij} = y_{ij} - \hat{\beta}(x_{ij} - \bar{x}_{..}) = \mu + \tau_i + \varepsilon_{ij} \begin{cases} i = 1,\cdots,k \\ j = 1,\cdots,n \end{cases}$$

which can be addressed by the conventional procedures applied to factorial designs.

Usual tests of model adequacy are still appropriate and are strongly recommended as part of the ANCOVA model building process, Section F.2.1.3. If relationship is non-linear, the adjustment made in the ANCOVA will be biased. The magnitude of this bias depends on the degree of departure from linearly. The bias can be identified at plotting residuals versus covariates.

F.2.3. Multiple comparison methods

After ANOVA, if the analysis shows the existence of significant difference between treatments, it is convenient to investigate which effect levels are really different. There exist various procedures to compare simultaneously multiple means; however, in this section, only Tukey's and Dunnett's methods for multiple pairwise comparisons and comparison with a control, respectively, are treated. Both multiple comparison methods are based on contrasts between sample means.

Both tests take into account the scatter of all the groups, what results in a more precise value for scatter and gives the test more power to detect differences. This practice only makes sense when it is accepted the assumption that all the data are sampled from populations with the same standard deviation, even if means are different. Variance, σ^2, is estimated by the error mean of squares, MS_E, such that

$$\hat{\sigma}^2 = MS_E$$

In multiple comparison methods is necessary to distinguish between error rate per comparison and familywise error rate. The error rate per comparison is the probability of making a type I error on a given comparison; while, if more than one comparison between means is conducted, the probability that the set of drawn conclusions will contain at least one Type I error is called the familywise error rate. Both Tukey's and Dunnett's methods control the overall familywise error rate.

Let α' represent the error rate for any simple comparison and c represent the number of comparisons. The error rate per comparison is obviously expresses as

$$\alpha = \alpha' \tag{96}$$

and, in case of independent comparisons, the familywise error rate results in

$$\alpha = 1 - (1 - \alpha')^c \tag{97}$$

The previous expression still represents a good estimation of the familywise error rate even if comparisons are not independent. It is worth noting that the limits of the familywise error rate are $\alpha' \leq \alpha \leq c\alpha'$.

F.2.3.1. Tukey's method

Tukey's method [21] tests all pairwise mean comparisons, that is to say, treatment means are compared against each other:

$$\begin{aligned} &H_0: \mu_i = \mu_j \\ &H_A: \mu_i \neq \mu_j \text{ for all } i \neq \text{j} \end{aligned} \tag{98}$$

The overall significance level of the proposed procedure for testing hypotheses is exactly α when sample sizes are equal, and at most α when sample sizes are unequal.

Tukey's procedure makes use of the distribution of the studentized range statistic

$$q = \frac{\bar{y}_{max} - \bar{y}_{min}}{\sqrt{MS_E/n}} \tag{99}$$

where $\bar{y}_{max}$ and $\bar{y}_{min}$ are the largest and smallest sample means, respectively, out of the group of a sample means, and n is the number of observations per treatment. For equal samples sizes, Tukey's method declares two means significantly different if the absolute value of the sample difference exceeds

$$T_\alpha = q_\alpha(\alpha, df_E)\sqrt{\frac{MS_E}{n}}$$

where α is the significance level and df_E is number the degrees of freedom associated with MS_E. Then, the $100(1-\alpha)\%$ confidence intervals for a difference of means result in

$$\bar{y}_{i.} - \bar{y}_{j.} - q_\alpha(a, df_E)\sqrt{\frac{MS_E}{n}} \le \mu_i - \mu_j \le \bar{y}_{i.} - \bar{y}_{j.} + q_\alpha(a, df_E)\sqrt{\frac{MS_E}{n}}, \qquad i \ne j$$

When sample sizes are not equal,

$$T_\alpha = \frac{q_\alpha(a, df_E)}{\sqrt{2}}\sqrt{MS_E\left(\frac{1}{n_i} + \frac{1}{n_j}\right)}$$

and

$$\bar{y}_{i.} - \bar{y}_{j.} - \frac{q_\alpha(a, df_E)}{\sqrt{2}}\sqrt{MS_E\left(\frac{1}{n_i} + \frac{1}{n_j}\right)} \le \mu_i - \mu_j$$

$$\le \bar{y}_{i.} - \bar{y}_{j.} + \frac{q_\alpha(a, df_E)}{\sqrt{2}}\sqrt{MS_E\left(\frac{1}{n_i} + \frac{1}{n_j}\right)}, \qquad i \ne j$$

The unequal sample size version is sometimes called the Tukey-Kramer procedure [21].

Tukey's procedures are, in general, conservative and drawn conclusions may be inconsistent with ANOVA test results.

F.2.3.2. Dunnet's method

Dunnett's method [22,23] is useful if interest lies in comparing treatment means, μ_i, with a control, μ_a; hence, $a - 1$ comparisons are conducted:

$$\begin{aligned} &H_0: \mu_i = \mu_a \\ &H_A: \mu_i \ne \mu_a, \qquad i = 1, \cdots, a-1 \end{aligned} \tag{100}$$

The Dunnett's method is a modification of the t-test. Differences in sample means are calculated for each set of hypotheses such that

$$|\bar{y}_{i.} - \bar{y}_{a.}|, \qquad i = 1, \cdots a-1$$

If H_0 is rejected, and μ_i and μ_a are considered different, using a type I error rate α,

$$|\bar{y}_{i.} - \bar{y}_{a.}| > d_{\alpha}(a-1, df_E)\sqrt{MS_E\left(\frac{1}{n_i}+\frac{1}{n_a}\right)} \tag{101}$$

where $d_{\alpha}(a-1, df_E)$ is a modified t-statistic, α is the joint significance level associated with all $a-1$ tests. Dunnett's test can perform both single-tailed and two-tailed tests.

It is convenient to take more observations for the control treatment n_a than for the remaining tested treatments n_i. As a general rule, it should be checked that

$$\frac{n_a}{n_i} \approx \sqrt{a}$$

F.2.4. Multiple linear regression method

Regression methods are frequently used to analyse data from unplanned experiments, such as might arise from observation of uncontrolled phenomena or historical records.

In a multiple linear regression model, the dependent or response variable, y, is related to a linear function of the independent or regressor variables $x_1, x_2, \cdots, x_k$ such that

$$y = \beta_0 + \beta_1 x_1 + \beta_2 x_2 + \cdots + \beta_k x_k + \varepsilon \tag{102}$$

where $\beta_0, \beta_1, \cdots, \beta_k$ are the unknown regression coefficients. This model describes a hyper-plane in the k-dimensional space of the regressor variables $\{x_j\}$. The parameter β_0 defines the intercept of the plane, while the parameters β_j for $j = 1, \cdots, k$ represent the expected change in response per unit of change in x_j when all the remaining independent variables x_i ($i \neq j$) are held constant.

Estimation of parameters in multiple linear regression models, often called model fitting, is performed by means of the method of least squares. Suppose that $n > k$ observations on the response variable are available $y_1, y_2, \cdots, y_n$ and, along with each observed response y_i, an observation of each regressor variable x_{ij} is also obtained. The model introduced in Equation (102) can be rewritten in terms of the observations as

$$y_i = \beta_0 + \beta_1 x_{i1} + \beta_2 x_{i2} + \cdots + \beta_k x_{ik} + \varepsilon_i = \beta_0 + \sum_{j=1}^{k} \beta_j x_{ij} + \varepsilon_i, \qquad i = 1, \cdots, n \tag{103}$$

where random errors, ε_i, are assumed to be normally and independently distributed with mean zero and unknown variance σ^2, $\varepsilon_i \sim N(0, \sigma^2)$. Therefore, adequacy checking of the model is conducted under the same criteria presented in Section F.2.1.3.

The method of least squares determines $\beta_0, \beta_1, \cdots, \beta_k$ so that the sum of squares of ε_i is minimized. The least squares function is

$$L = \sum_{i=1}^{n} \varepsilon_i^2 = \sum_{i=1}^{n} \left(y_i - \beta_0 - \sum_{j=1}^{k} \beta_j x_{ij} \right)^2, \qquad i = 1, \cdots, n \tag{104}$$

and the least squares estimators $\hat{\beta}_0, \hat{\beta}_1, \cdots, \hat{\beta}_k$ must satisfy

$$\left. \frac{\partial L}{\partial \beta_0} \right|_{\hat{\beta}_0, \hat{\beta}_1, \cdots, \hat{\beta}_k} = -2 \sum_{i=1}^{n} \left(y_i - \hat{\beta}_0 - \sum_{j=1}^{k} \hat{\beta}_j x_{ij} \right) = 0$$

and

$$\left. \frac{\partial L}{\partial \beta_j} \right|_{\hat{\beta}_0, \hat{\beta}_1, \cdots, \hat{\beta}_k} = -2 \sum_{i=1}^{n} \left(y_i - \hat{\beta}_0 - \sum_{j=1}^{k} \hat{\beta}_j x_{ij} \right) x_{ij} = 0, \qquad j = 1, \cdots, k$$

These $p = k + 1$ equations are called the least squares normal equations. The model in terms of the observations, Equation (103), can be written in matrix notation as

$$\boldsymbol{y} = \boldsymbol{X}\boldsymbol{\beta} + \boldsymbol{\varepsilon}$$

where $\boldsymbol{y}$ is an ($n \times 1$) vector of the observations, $\boldsymbol{X}$ is an ($n \times p$) matrix of the levels of the independent variable, $\boldsymbol{\beta}$ is a ($p \times 1$) vector of the regression coefficients, and $\boldsymbol{\varepsilon}$ is an ($n \times 1$) vector of random errors. Hence,

$$\boldsymbol{y} = \begin{bmatrix} y_1 \\ y_2 \\ \vdots \\ y_n \end{bmatrix}, \qquad \boldsymbol{X} = \begin{bmatrix} 1 & x_{11} & x_{12} & \cdots & x_{1k} \\ 1 & x_{21} & x_{22} & \cdots & x_{2k} \\ \vdots & \vdots & \vdots & & \vdots \\ 1 & x_{n1} & x_{n2} & \cdots & x_{nk} \end{bmatrix}$$

$$\boldsymbol{\beta} = \begin{bmatrix} \beta_0 \\ \beta_1 \\ \vdots \\ \beta_k \end{bmatrix}, \qquad \boldsymbol{\varepsilon} = \begin{bmatrix} \varepsilon_1 \\ \varepsilon_2 \\ \vdots \\ \varepsilon_n \end{bmatrix}$$

In matrix notation, L can be expressed as

$$L = \sum_{j=1}^{k} \varepsilon_i^2 = \boldsymbol{\varepsilon}'\boldsymbol{\varepsilon} = (\boldsymbol{y} - \boldsymbol{X\beta})'(\boldsymbol{y} - \boldsymbol{X\beta}) = \boldsymbol{y}'\boldsymbol{y} - \boldsymbol{\beta}'\boldsymbol{X}'\boldsymbol{y} - \boldsymbol{y}'\boldsymbol{X\beta} + \boldsymbol{\beta}'\boldsymbol{X}'\boldsymbol{X\beta}$$

$$= \boldsymbol{y}'\boldsymbol{y} - 2\boldsymbol{\beta}'\boldsymbol{X}'\boldsymbol{y} + \boldsymbol{\beta}'\boldsymbol{X}'\boldsymbol{X\beta}$$

and the vector of least squares estimators $\widehat{\boldsymbol{\beta}}$ must satisfy

$$\left.\frac{\partial L}{\partial \boldsymbol{\beta}}\right|_{\widehat{\boldsymbol{\beta}}} = -2\boldsymbol{X}'\boldsymbol{y} + 2\boldsymbol{X}'\boldsymbol{X}\widehat{\boldsymbol{\beta}} = \boldsymbol{0}$$

which simplifies to

$$\widehat{\boldsymbol{\beta}} = (\boldsymbol{X}'\boldsymbol{X})^{-1}\boldsymbol{X}'\boldsymbol{y}$$

Finally, the fitted regression model results in

$$\widehat{\boldsymbol{y}} = \boldsymbol{X}\widehat{\boldsymbol{\beta}}$$

Residuals $e_i = y_i - \hat{y}_i$ can be also expressed in matrix notation as

$$\boldsymbol{e} = \boldsymbol{y} - \widehat{\boldsymbol{y}} = \boldsymbol{y} - \boldsymbol{X}\widehat{\boldsymbol{\beta}}$$

Furthermore, an unbiased estimator of σ^2 is given by

$$\hat{\sigma}^2 = \frac{SS_E}{n - p}$$

where SS_E is the sum of squares of the residuals and $n - p$ are the number of degrees of freedom associated to the random error variables ε_i.

SS_E can be calculated from the vector of residuals as

$$SS_E = \sum_{i=1}^{n} (y_i - \hat{y}_i)^2 = \sum_{i=1}^{n} e_i^2 = \boldsymbol{e}'\boldsymbol{e} = \left(\boldsymbol{y} - \boldsymbol{X}\widehat{\boldsymbol{\beta}}\right)'\left(\boldsymbol{y} - \boldsymbol{X}\widehat{\boldsymbol{\beta}}\right)$$

$$= \boldsymbol{y}'\boldsymbol{y} - \widehat{\boldsymbol{\beta}}'\boldsymbol{X}'\boldsymbol{y} - \boldsymbol{y}'\boldsymbol{X}\widehat{\boldsymbol{\beta}} + \widehat{\boldsymbol{\beta}}'\boldsymbol{X}'\boldsymbol{X}\widehat{\boldsymbol{\beta}} = \boldsymbol{y}'\boldsymbol{y} - 2\widehat{\boldsymbol{\beta}}'\boldsymbol{X}'\boldsymbol{y} + \widehat{\boldsymbol{\beta}}'\boldsymbol{X}'\boldsymbol{X}\widehat{\boldsymbol{\beta}}$$

Substituting $\boldsymbol{X}'\boldsymbol{X}\widehat{\boldsymbol{\beta}} = \boldsymbol{X}'\boldsymbol{y}$, this last equation becomes

$$SS_E = \boldsymbol{y}'\boldsymbol{y} - \widehat{\boldsymbol{\beta}}'\boldsymbol{X}'\boldsymbol{y}$$

Likewise, the total sum of squares can be also computed by

$$SS_T = \boldsymbol{y}'\boldsymbol{y} - \frac{(\sum_{i=1}^{n} y_i)^2}{n}$$

and the regression sum of squares

$$SS_R = \widehat{\boldsymbol{\beta}}'\boldsymbol{X}'\boldsymbol{y} - \frac{(\sum_{i=1}^{n} y_i)^2}{n}$$

The significance of the linear relationship between the response variable, y_i, and the regressor predictors, x_j, introduced in Equation (102) can be tested through the following hypotheses:

$$\begin{aligned} &H_0: \beta_1 = \beta_2 = \cdots = \beta_k = 0 \\ &H_A: \beta_j \neq 0 \text{ for at least one } \square \end{aligned} \tag{105}$$

Rejection of H_0 implies that at least one of the regressor variable, x_j, contributes significantly to the model. Hypothesis testing is conducted via an ANOVA, which follows an equivalent development to that applied to fixed-effects models for a single factor in Section F.2.1.1. The corresponding ANOVA table is depicted in Table F.11.

Table F.11 ANOVA table the for the multiple linear regression model.

Source	$\boldsymbol{df}$	$\boldsymbol{SS}$	$\boldsymbol{MS}$	$\boldsymbol{F_0}$
Regression	k	SS_R	MS_R	$\frac{MS_R}{MS_E}$
Error	$n-k-1$	SS_E	MS_E	
Total	$n-1$	SS_T		

How well data fit a statistical model can be explained by the coefficient of multiple determination

$$R^2 = \frac{SS_R}{SS_T} = 1 - \frac{SS_E}{SS_T} \tag{106}$$

It is a measure of the amount of reduction in the variability of y obtained by using the regressor variables $x_1, x_2, \cdots, x_k$ in the model. Since adding a variable to the model will always increase R^2, regardless of whether the additional variable is statistically significant or not, a large value of R^2 does not necessarily imply that the regression model is good. An adjusted R^2 statistic is defined such that

$$R^2_{adj} = 1 - \frac{SS_E/(n-p)}{SS_T/(n-1)} = 1 - \left(\frac{n-1}{n-p}\right)(1-R^2) \quad (107)$$

which often decreases if unnecessary terms are added to the model.

F.3. Screening of degassing procedures

Effectiveness of a total of eight vacuum degassing procedures were compared through the analysis of their effects on the porosity of the corresponding VI manufactured specimens (Chapter 4). Each degassing procedure was defined by the level adopted by a set of four factors previously introduced (Table F.12): nucleation medium (N), HS stirring (S), pressurization (P), and degassing time (T).

Table F.12. Design factors of the screening experiment of degassing procedures.

Factor	Level*1		Details	Motivation
	High (+)	Low (−)		
Nucleation medium (N)	On	Off	Scotch-Brite	Enhancing heterogeneous bubble formation
HS stirring (S)	On	Off	Magnetic stirrer at 300 rpm with a rod of 40 mm	Enhancing bubble formation due to cavitation
Pressurization (P)	On	Off	200 kPa*2 for 5 min	Collapse of micro-bubbles [24]
Degassing time (T)	40 min	20 min	-	-

*1 In regression models, high and low levels were considered $+1$ and -1, respectively.
*2 Relative pressure.

Factor levels were arranged according to the principal one-half fraction of a two-level fractional factorial design, 2^{4-1}_{IV} (Table F.13).

Table F.13. The 2^{4-1}_{IV} fractional factorial design, principal one-half fraction, applied to the screening experiment of degassing procedures.

Specimen	Run order	Basic design			T = NSP	Treatment
		N	S	P		
6	4	−	−	−	−	(1)
5	5	+	−	−	+	nt
3	2	−	+	−	+	st
7	8	+	+	−	−	ns
4	7	−	−	+	+	pt
1	1	+	−	+	−	np
8	6	−	+	+	−	sp
2	3	+	+	+	+	nspt

Only effects of main factors N, S, P and T, and two-factor interactions were considered in the analysis, neglecting the influence of higher order interactions. Besides, in 2^{4-1} factorial designs, effects of two-factor interactions are aliased with each other ($l_{NS} = l_{PT}$, $l_{NP} = l_{ST}$, $l_{NT} = l_{SP}$); therefore, interaction effects were carefully addressed to discern, according to main factor effects and experimental conditions, which was the predominant interaction.

The fractional factorial design was analysed with respect to porosity-related attributes: porous area fraction, s_0, and updated void volume fraction, v_0', (only corresponding to samples CY8).

Dependencies of response variables on a set of nuisance factors (RH, T_{deg}, T_{fill} and T_{pfill}) and allow-to-vary factors (P_{deb}, t_{deb}, P_{deg}, $t_{0\rightarrow fill_0}$, $t_{0\rightarrow fill_{end}}$ and t_{fill}.) was assessed visually through a series of scatterplots depicted in Figure F.2 and Figure F.3. Both response variables showed high coefficients of determination, R^2, for some factors showing small variability throughout the experiments, such as T_{deg}, T_{fill}, and P_{deg}. Since logics dictates that small variations on these factors could not affect response variables in the way they did, efforts were focussed on significant dependencies of v_0' on time-related factors. $t_{0\rightarrow fill_0}$ seemed to be the real cause behind these connections, since changes in resin viscosity, μ, at the onset of the filling step caused by different $t_{0\rightarrow fill_0}$, beyond inherent preform variability, seemed to be the real cause behind $t_{0\rightarrow fill_{end}}$ and t_{fill} scatter, as well as different t_{deb}.

Degassing procedures that included pressurization, factor P, implied an average increment of 10 min in $t_{0\rightarrow fill_0}$; while different degassing times, factor T, implied an average increment of 22 min between the high level (40 min) and the low level (20 min). Therefore, both factors were partially aliased with $t_{0\rightarrow fill_0}$. Effects of $t_{0\rightarrow fill_0}$ on v_0' was later analysed through ANCOVA.

Since the initial fractional factorial design was saturated (no available degree of freedom to compute error variance), effect significance was firstly qualitatively assessed through a half-normal probability plot of the effects. The largest effects which did not lie along the normal straight line were considered good candidates to include in the later ANOVA, which statistically evaluated significance of factor or interaction effects on response variables. Backward elimination was performed to sequentially remove any factor or interaction from models with a significance level $p > 0{,}10$ ($\equiv 10\%$); although, actually, effect significance was set at $p \leq 0{,}05$ ($\equiv 5\%$).

Figure F.4 shows experimental data of s_0 gathered according to all factor levels. Besides, main factors and two-factor interactions effects are depicted in Figure F.5. In Figure F.6, effects to be included in an ANOVA (Table F.14) are highlighted.

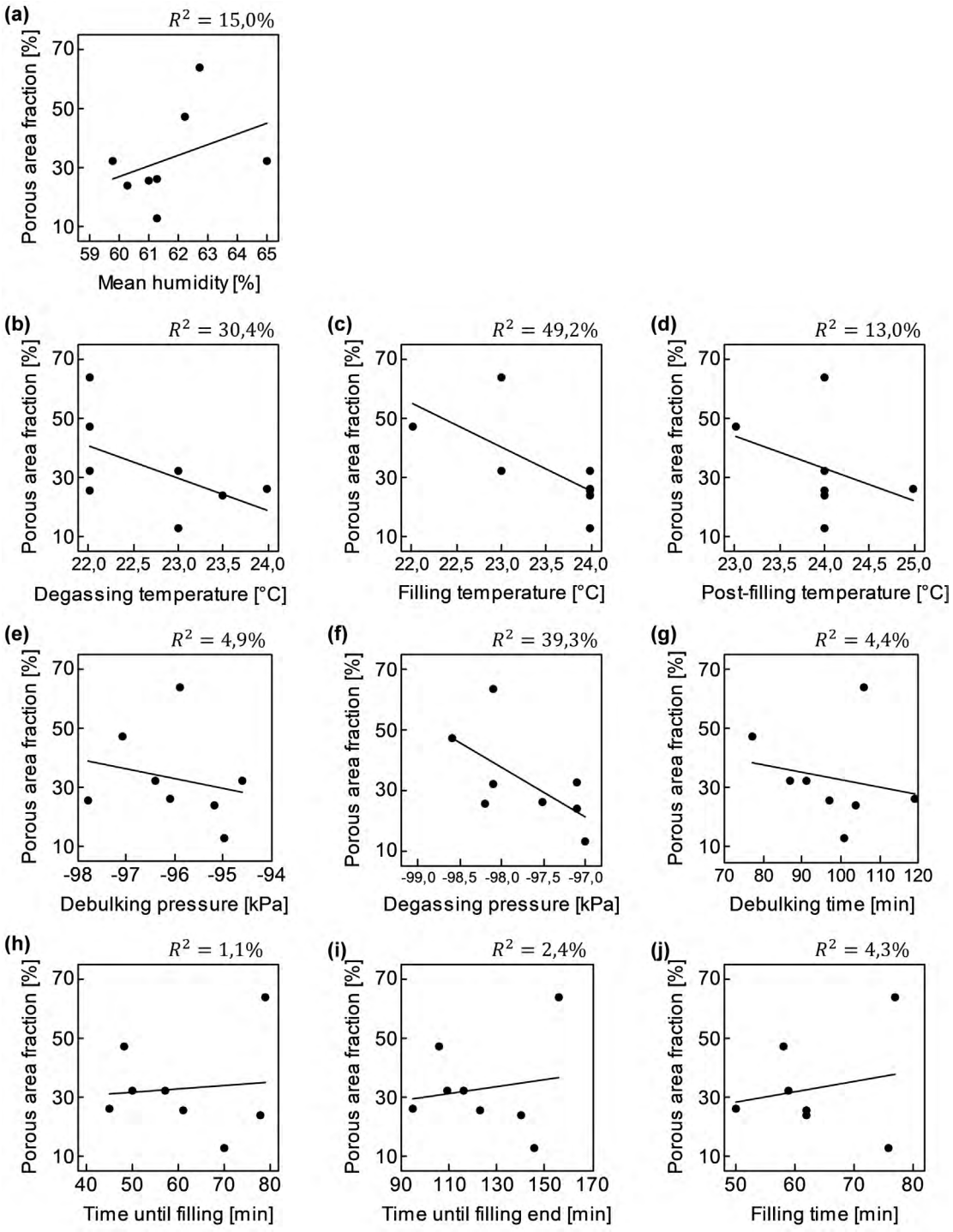

Figure F.2. Scatterplots of porous area fraction, s_0, vs. nuisance and allow-to-vary factors in the screening of degassing procedures.

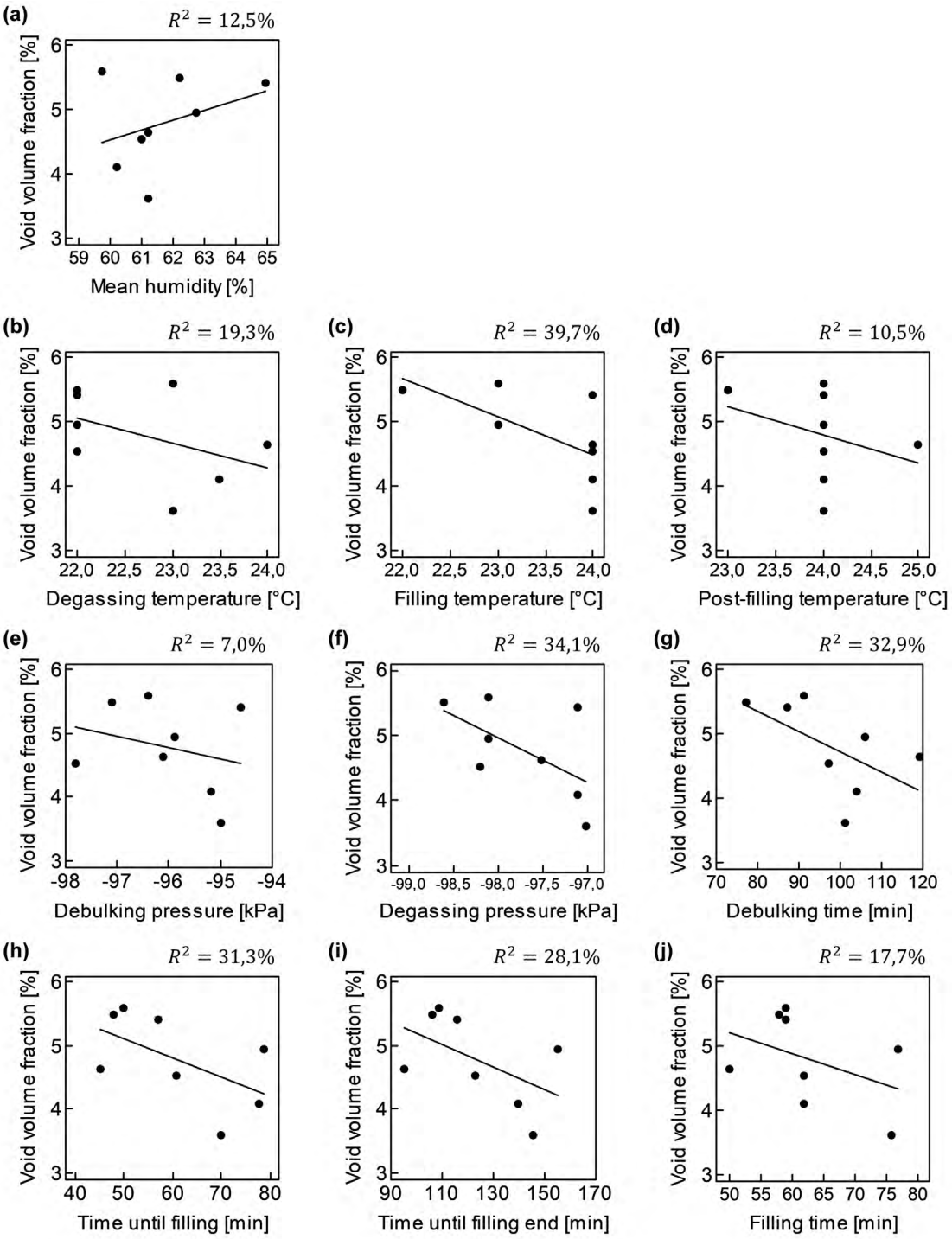

Figure F.3. Scatterplots of void volume fraction, v_0', vs. nuisance and allow-to-vary factors in the screening of degassing procedures.

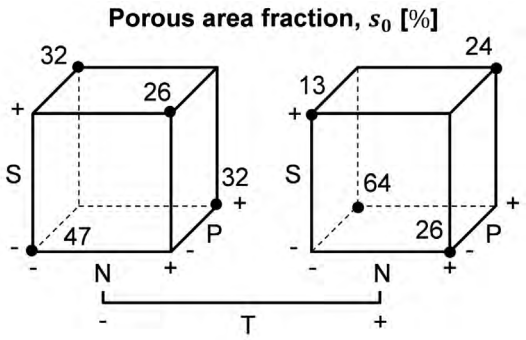

Figure F.4. Cube plot of porous area fraction, s_0, in the screening of degassing procedures.

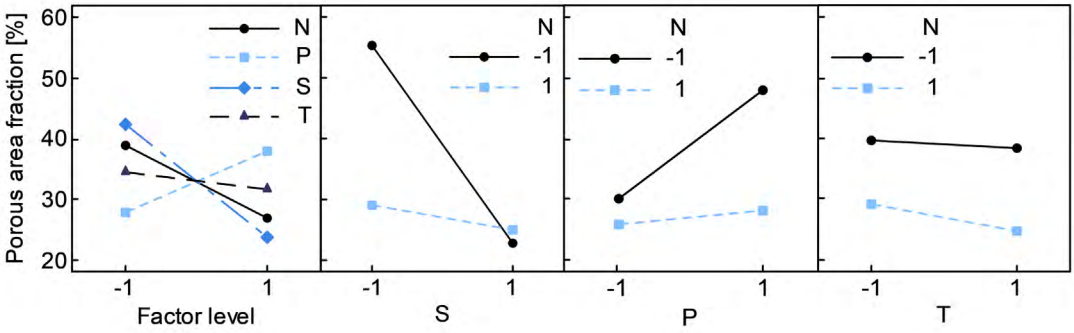

Figure F.5. Plots of main factors and two-factor interaction effects for porous area fraction, s_0, in the screening of degassing procedures.

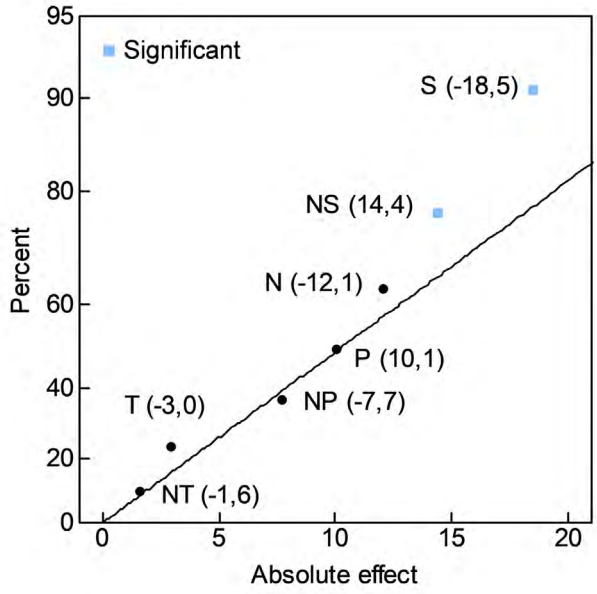

Figure F.6. Half-normal probability plot of effects of porous area fraction, s_0, in the screening of degassing procedures.

Table F.14. ANOVA table for porous area fraction, s_0, in the screening of degassing procedures considering factors N and S, and interaction NS ($R^2_{adj} = 65\%$).

Source	df	SS	MS	F_0	p
N	1	291,6	291,6	3,39	0,140
S	1	683,1	683,1	7,93	0,048
NS	1	416,2	416,2	4,83	0,093
Error	4	344,6	86,2		
Total	7	1735			

None of the factors or interaction could be eliminated from the ANOVA, since factor S resulted significant and p value of interaction NS was lower than 0,10. Besides, if an interaction is present in a model, all main factors contributing to the interaction have to be also included. Nevertheless, at analysing the residuals of the model, it was observed a considerable dependence of residuals on factor P (Figure F.7.f).

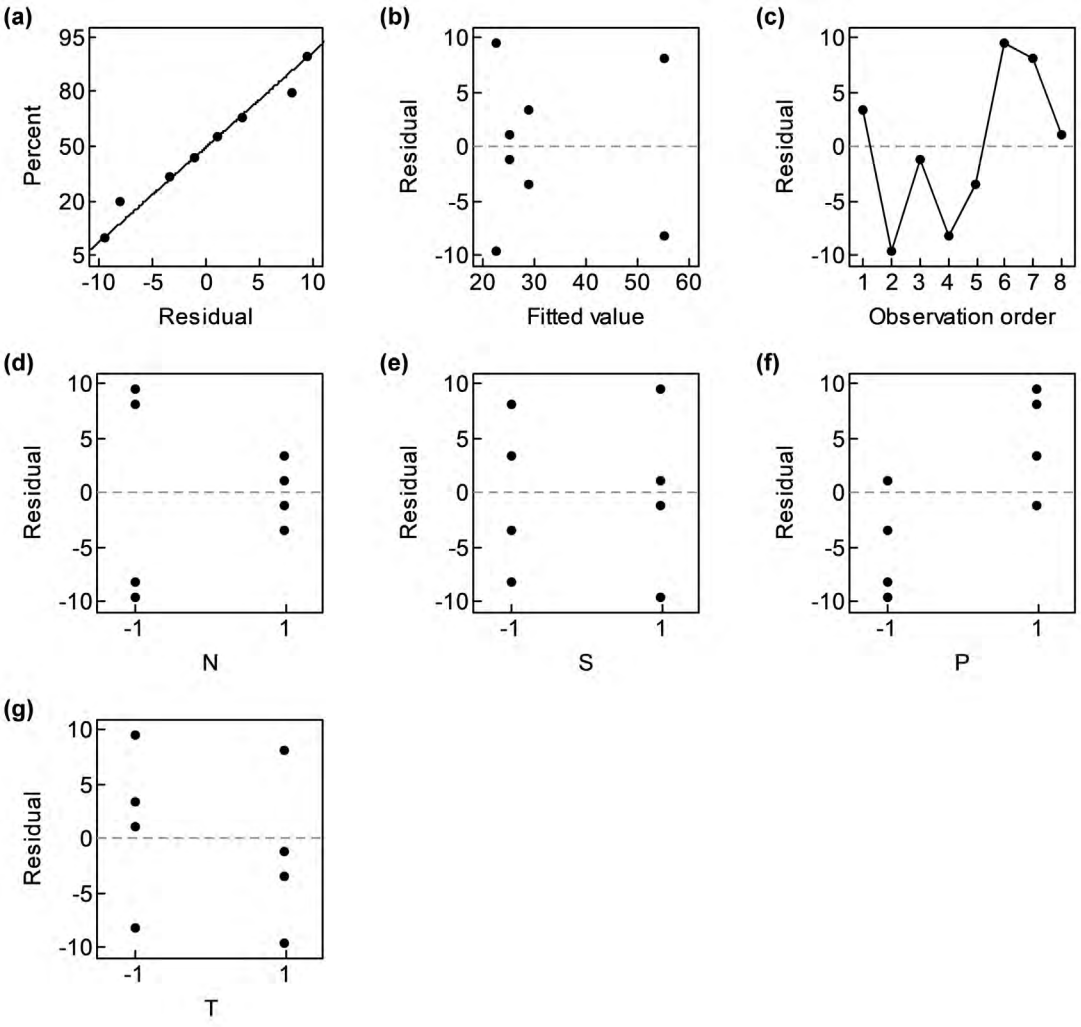

Figure F.7. Analysis of residuals of model for porous area fraction, s_0, including factors N and S, and interaction NS in the screening of degassing procedures.

Therefore, a new ANOVA was conducted adding factor P to the previous model (Table F.15). The new model including factors N, S and P, and interaction NS did not show any abnormal behaviour in the analysis of residuals (Figure F.8); hence, the model was assumed as appropriate. Finally, Figure F.9 shows the model equation and the fitted values of s_0.

Table F.15. ANOVA table for porous area fraction, s_0, in the screening of degassing procedures considering factors N, S and P, and interaction NS ($R^2_{adj} = 81\%$).

Source	df	SS	MS	F_0	p
N	1	291,6	291,6	6,19	0,089
S	1	683,1	683,1	14,5	0,032
P	1	203,2	203,2	4,31	0,129
NS	1	416,2	416,2	8,83	0,059
Error	3	141,4	47,1		
Total	7	1735			

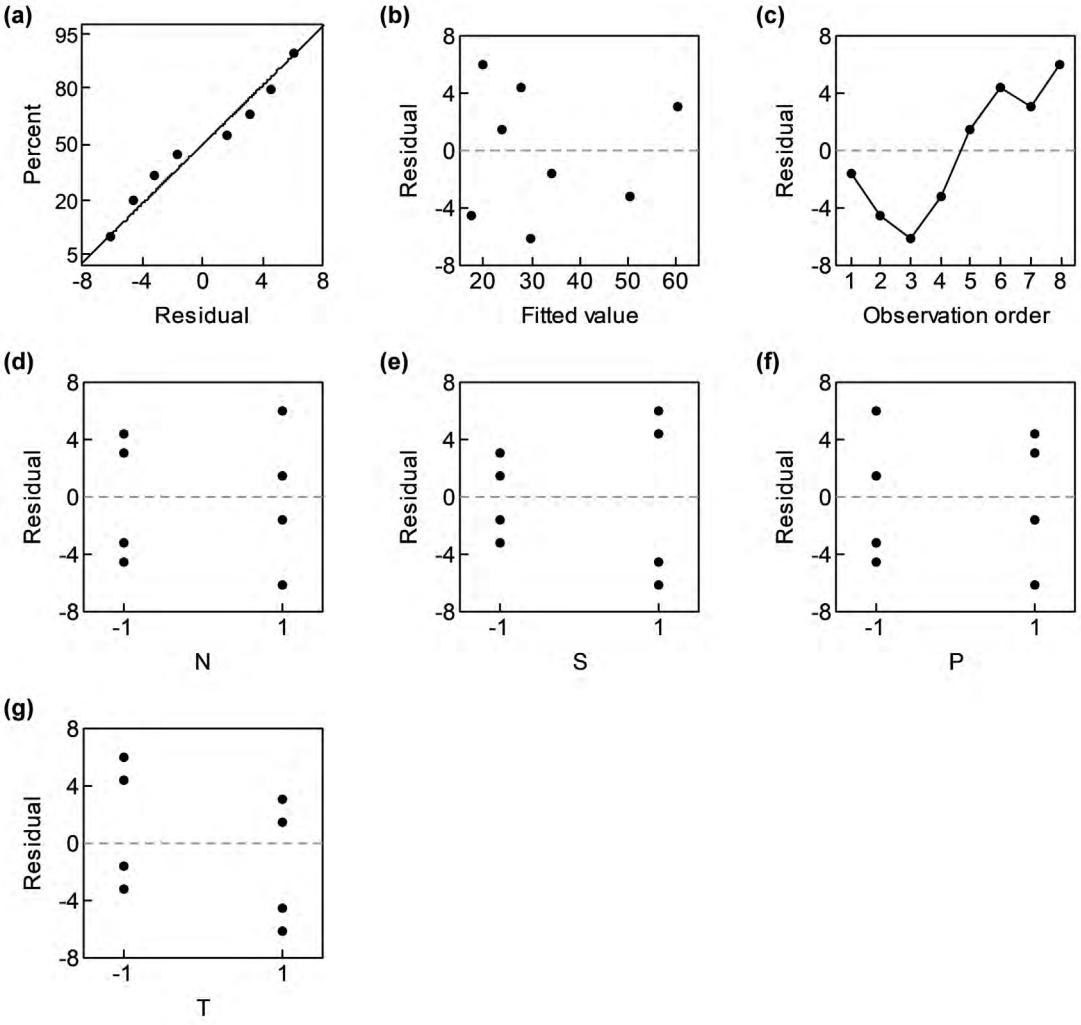

Figure F.8. Analysis of residuals of model for porous area fraction, s_0, including factors N, S and P, and interaction NS in the screening of degassing procedures.

$$\hat{s}_0[\%] = 33{,}0 - 6{,}0N$$
$$-9{,}2S + 5{,}0P + 7{,}2NS$$
$$R^2_{adj} = 81\%$$

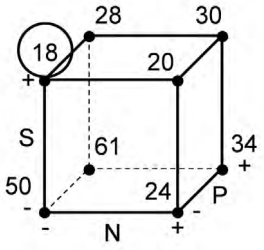

Figure F.9. Cube plot of fitted values of model for porous area fraction, s_0, including factors N, S and P, and interaction NS in the screening of degassing procedures.

Figure F.10 shows experimental data of v_0' gathered according to all factor levels. Besides, main factors and two-factor interactions effects are depicted in Figure F.11. In Figure F.12, effects to be included in an ANOVA (Table F.16) are highlighted.

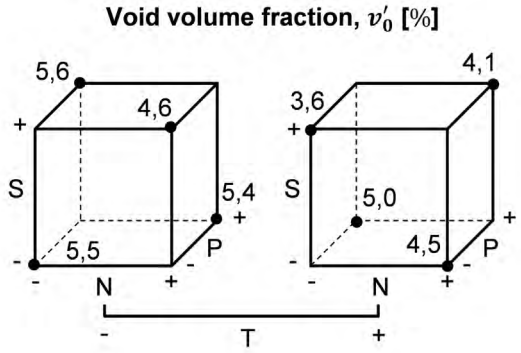

Figure F.10. Cube plot of void volume fraction, v_0', in the screening of degassing procedures.

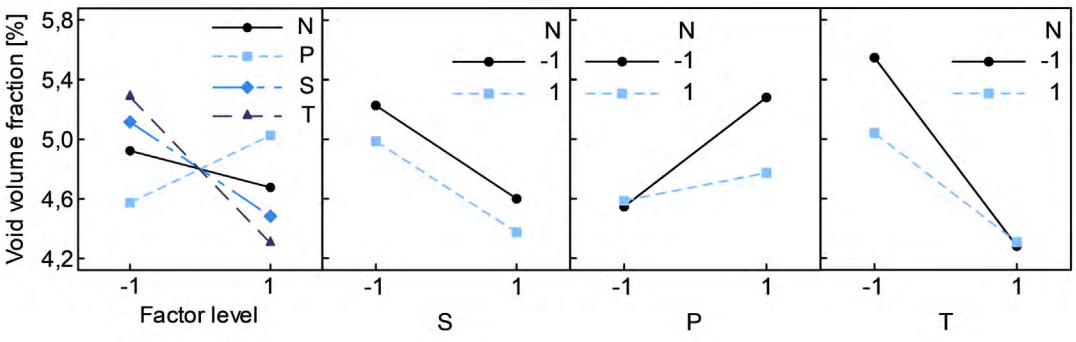

Figure F.11. Plots of main factors and two-factor interaction effects for void volume fraction, v_0', in the screening of degassing procedures.

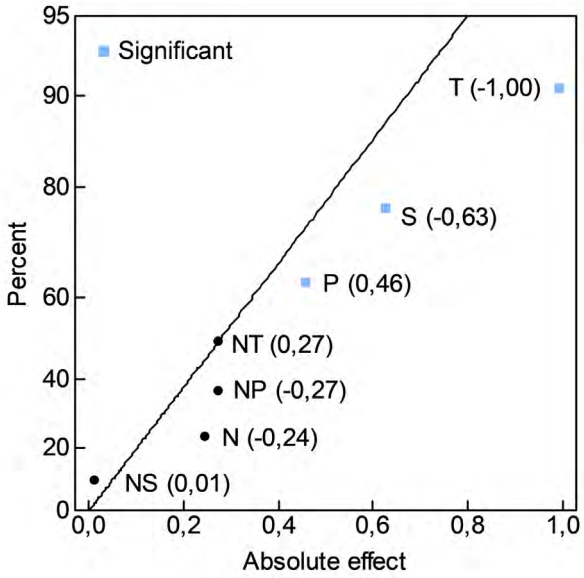

Figure F.12. Half-normal probability plot of effects of void volume fraction, v_0', in the screening of degassing procedures.

Table F.16. ANOVA for adjusted void volume fraction, v_0', in the screening of degassing procedures considering factors S, P and T ($R^2_{adj} = 80\%$).

Source	df	SS	MS	F_0	p
S	1	0,7834	0,7834	7,60	0,051
P	1	0,4164	0,4164	4,04	0,115
T	1	1,981	1,981	19,2	0,012
Error	4	0,4123	0,1031		
Total	7	3,593			

Factor P showed a p value higher than 0,10; therefore, it was eliminated from the model and a new ANOVA was conducted only including main factors S and T (Table F.17). In the ANOVA, only factor T resulted statistically significant, although p value of factor S was still lower than 0,10. Nevertheless, at analysing the residuals of the model, it was observed a considerable dependence of residuals on factor P (Figure F.13.f). Therefore, the analysis of residuals of the previous model was conducted, showing no abnormal behaviour (Figure F.14).

Table F.17. ANOVA table for adjusted void volume fraction, v_0', in the screening of degassing procedures considering factors S and T ($R^2_{adj} = 68\%$).

Source	df	SS	MS	F_0	p
S	1	0,7834	0,7834	4,73	0,082
T	1	1,98	1,981	11,9	0,018
Error	5	0,8288	0,1658		
Total	7	3,593			

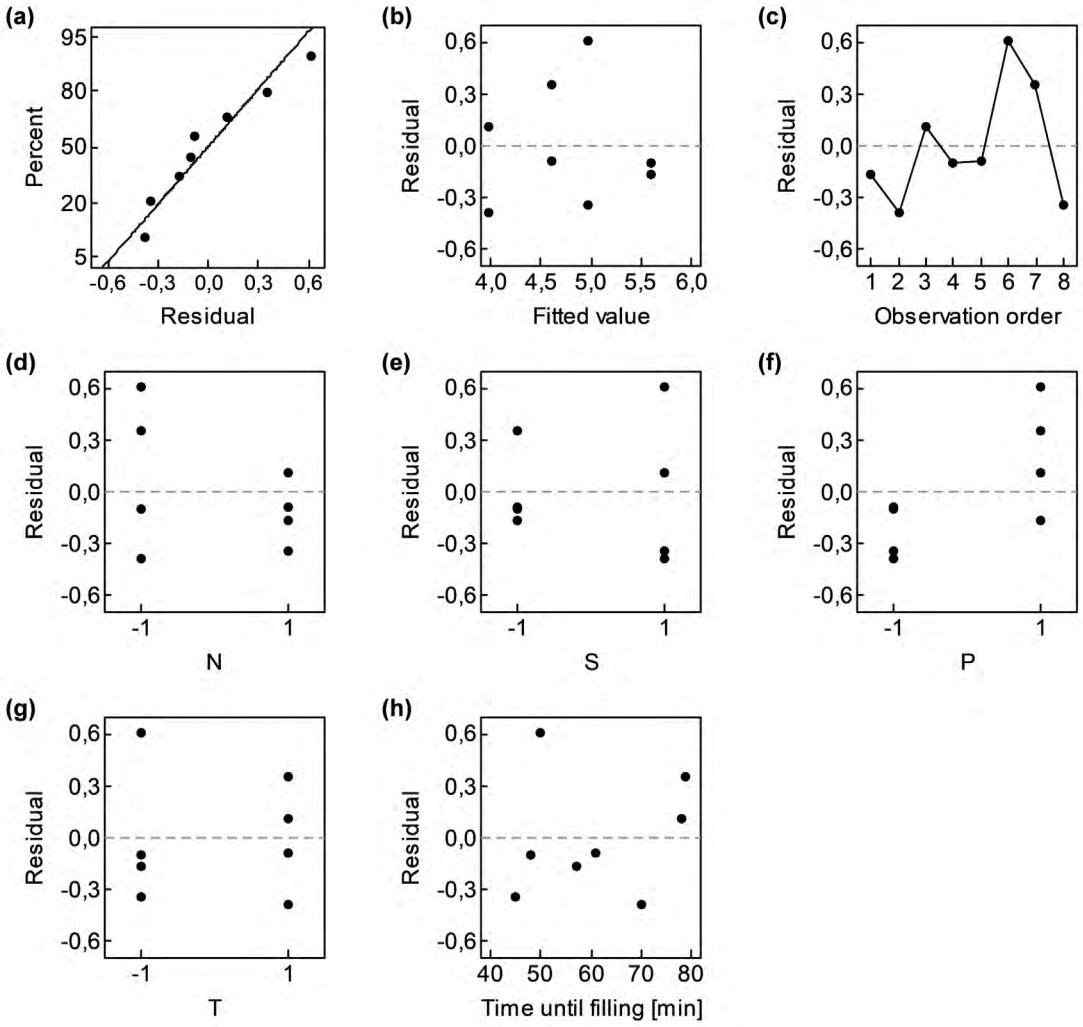

Figure F.13. Analysis of residuals of model for void volume fraction, v_0', including factors S and T in the screening of degassing procedures.

In order to address the dependence of v_0' on $t_{0\rightarrow fill_0}$ and the aliasing between T and $t_{0\rightarrow fill_0}$, an ANCOVA procedure was applied to the same model analysed in Table F.16, substituting factor T by $t_{0\rightarrow fill_0}$. Effect significance of each main factor and the covariate is provided in Table F.18. The resulting model showed even a higher adjusted coefficient of determination, $R^2_{adj} = 87\%$, than the model including main factors S, P and T ($R^2_{adj} = 80\%$); however, the analysis of residuals showed a non-constant variance across the range of fitted values (Figure F.15.b), hence it was preferred to present only the equation model and the cube plot of fitted values of the model including main factors S, P and T (Figure F.16).

The apparent relation between v_0' and $t_{0\rightarrow fill_0}$, the aliasing between T and $t_{0\rightarrow fill_0}$, the fact that T is the only main factor whose influence considerably changed between both response variables and, finally, conducted ANOVA and ANCOVA suggested that variations in $t_{0\rightarrow fill_0}$ affected

resulting v_0' more than different degassing times. However, it was not possible to isolate effects of T and $t_{0\rightarrow fill_0}$ from each other.

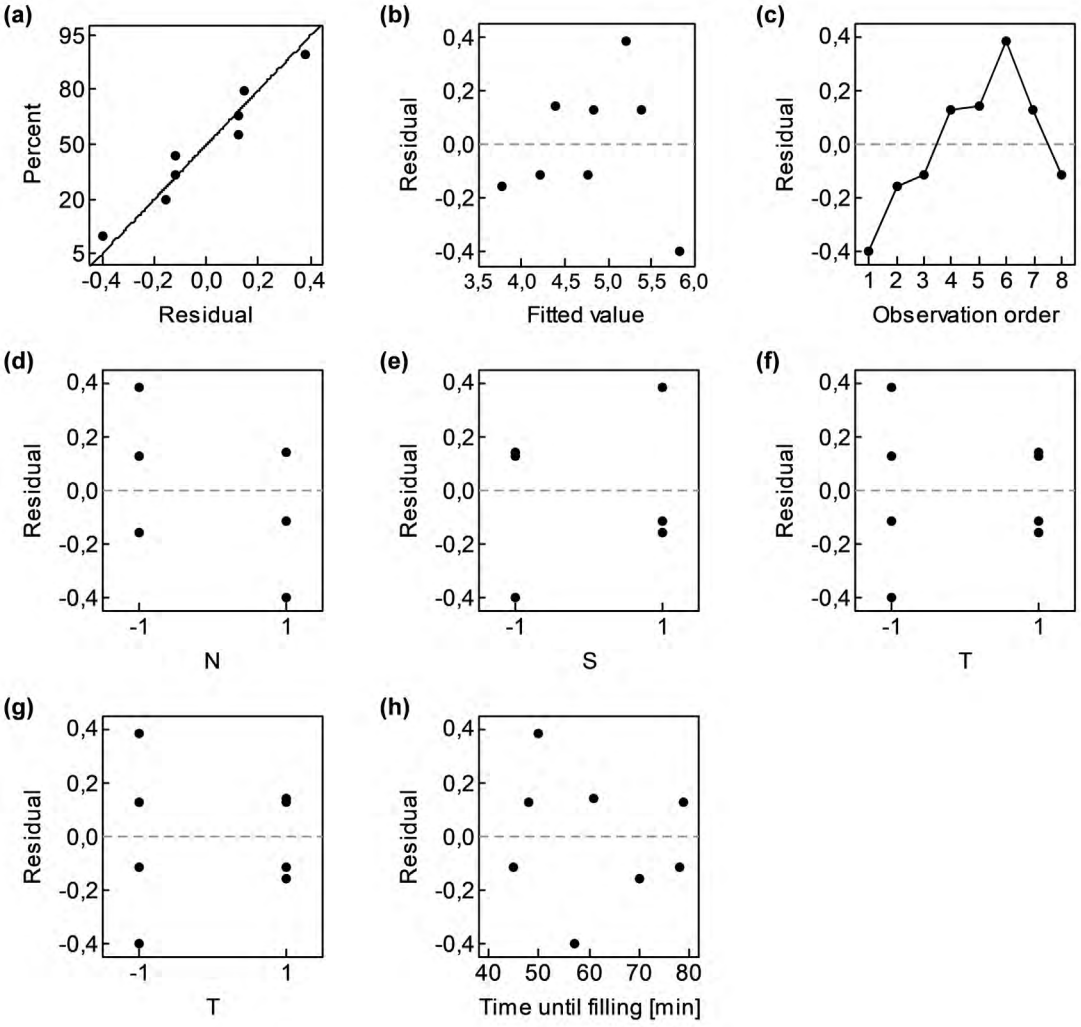

Figure F.14. Analysis of residuals of model for void volume fraction, v_0', including factors S, P and T in the screening of degassing procedures.

Table F.18. ANOVA table for adjusted void volume fraction, v_0', in the screening of degassing procedures considering factors S and T, and covariate $t_{0\rightarrow fill_0}$ ($R^2_{adj} = 87\%$).

Source	df	SS	MS	F_0	p
S	1	0,8402	0,8402	12,4	0,024
P	1	1,377	1,377	20,4	0,011
$t_{0\rightarrow fill_0}$	1	2,124	2,124	31,4	0,005
Error	4	0,2701	0,06754		
Total	7	3,593			

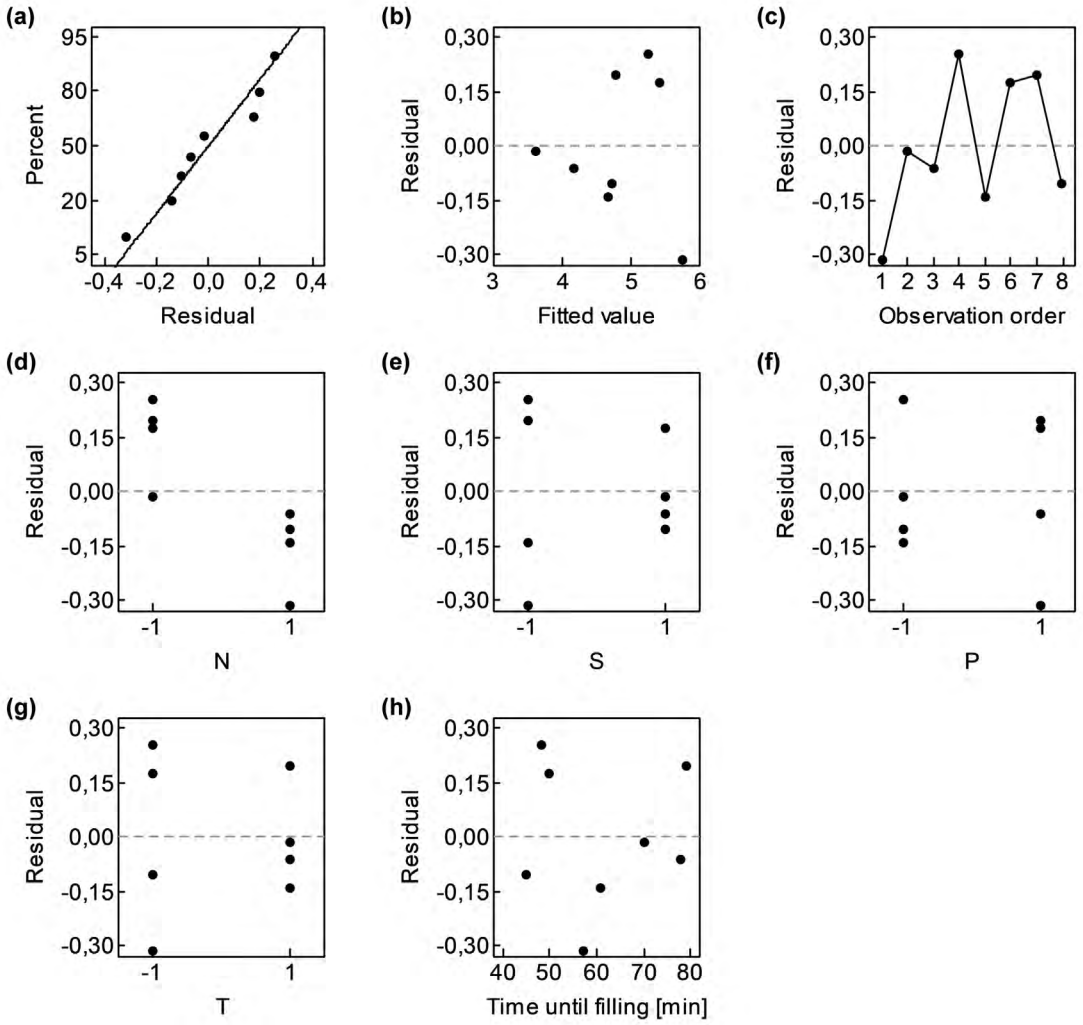

Figure F.15. Analysis of residuals of model for void volume fraction, v_0', including factors S and T, and covariate $t_{0\rightarrow fill_0}$ in the screening of degassing procedures.

$$\hat{v}_0'[\%] = 4{,}80 - 0{,}31S + 0{,}23P - 0{,}50T$$

$$R^2_{adj} = 80\%$$

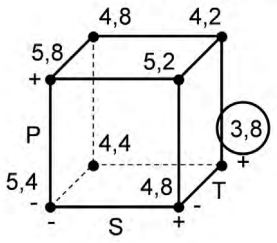

Figure F.16. Cube plot of fitted values of model for void volume fraction, v_0', including factors S, P and T in the screening of degassing procedures.

F.4. Screening of filling and post-filling conditions

Effects on specimen quality attributes of different filling and post-filling pressure conditions, and preform assemblies were addressed through two simple two-level factorial designs, 2^2. A total of four design factors were analysed (Table F.19): pressure increment (P), gradient of pressure (G), preform assembly (A) and inlet condition (I).

Table F.19. Design factors of the screening experiment of filling and post-filling conditions.

Factor	Level*1		Details	Motivation
	High (+)	Low (−)		
Pressure increment (P)	5 kPa	0 kPa	Between filling and post-filling steps	Enhancing air dissolution capacity and bubble collapse
Gradient of pressure (G)	Full	Reduced	Gradient of pressure is reduced by setting $P_{fill}^{inlet} = -40$ kPa*2	Altering void formation due to resin flow through dual-scale porous medium
Preform assembly (A)	ISFLIP	VI	Figure 5.3 on Chapter 5	Comparing conventional VI processing conditions
Inlet condition (I)	Turned into vent	Clamped	From post-filling onwards	

*1 In regression models, high and low levels were considered $+1$ and -1, respectively.
*2 Relative pressure.

In the first set of runs, four ISFLIP assembly-like specimens were manufactured in order to screen the effects of factors P and G in a manufacturing scenario in which resin inlet was turned into vent after the filling step. Factor levels were arranged in a 2^2 factorial design as mentioned (Table F.20).

Table F.20. The 2^2 factorial design applied to the first stage of the screening experiment of filling and post-filling conditions.

Specimen	Run order	P	G	Treatment
A1	3	−	−	(1)
A2	2	+	−	p
A3	4	−	+	g
A4	1	+	+	pg

A combination of factor levels (P and G) was chosen from the first screening experiment according to the best performance of the analysed response variables and used in a second round of experimentation, in which the effects of factors A and I were considered. The arrangement of factor levels in this second set of runs is depicted in Table F.21.

Table F.21. The 2^2 factorial design applied to the second stage of the screening experiment of filling and post-filling conditions.

Specimen	Run order	P	G	Treatment
B1	3	–	–	(1)
B2	1	+	–	a
B3	4	–	+	i
B4*	2	+	+	ai

* It corresponds to the chosen experiment from previous factorial design (Table F.20).

In specimens in which preform was clamped after preform filling (B1 and B2), a full gradient of pressure was applied to carry out preform impregnation, $\Delta P_{fill}^{inlet \rightarrow vent} = -90$ kPa, and no pressure increment between filling and post-filling steps was forced, $\Delta P_{fill \rightarrow pfill}^{vent} = 0$ kPa. These practices fit in with conventional VI manufacturing conditions. On the other hand, filling and post-filling pressure conditions of specimen B3 were determined according to the combination of levels chosen from the first factorial design (specimen B4). It is worth noting that the design factors of the first screening experiment became held-constant factors in the second one, and vice versa.

Proposed factorial designs were analysed with respect to the porous area fraction which negatively affected flexure performance, s_0^{II+III}. Collected data belonged to the experimentation conducted in Chapter 5.

Dependencies of the response variable s_0^{II+III} on a set of nuisance factors (RH, T_{deg}, T_{fill} and T_{pfill}) and allow-to-vary factors (P_{deb}, t_{deb}, P_{deg} and $t_{0 \rightarrow fill_0}$) was assessed visually through a series of scatterplots depicted in Figure F.17 for the first stage of the screening experiment analysed in this section. Among the factors that showed large variability throughout the experimentation campaign, only a significant dependence arose on t_{deb}.

Since factorial designs were initially saturated (no available degree of freedom to compute error variance), effect significance was firstly qualitatively evaluated through a half-normal probability plot of the effects. The largest effects which did not lie along the normal straight line were considered good candidates to include in the later ANOVA. Backward elimination was then performed to sequentially remove any factor or interaction from models with a significance level $p > 0{,}10$ ($\equiv 10\%$); although, effect significance was actually set at $p \leq 0{,}05$ ($\equiv 5\%$).

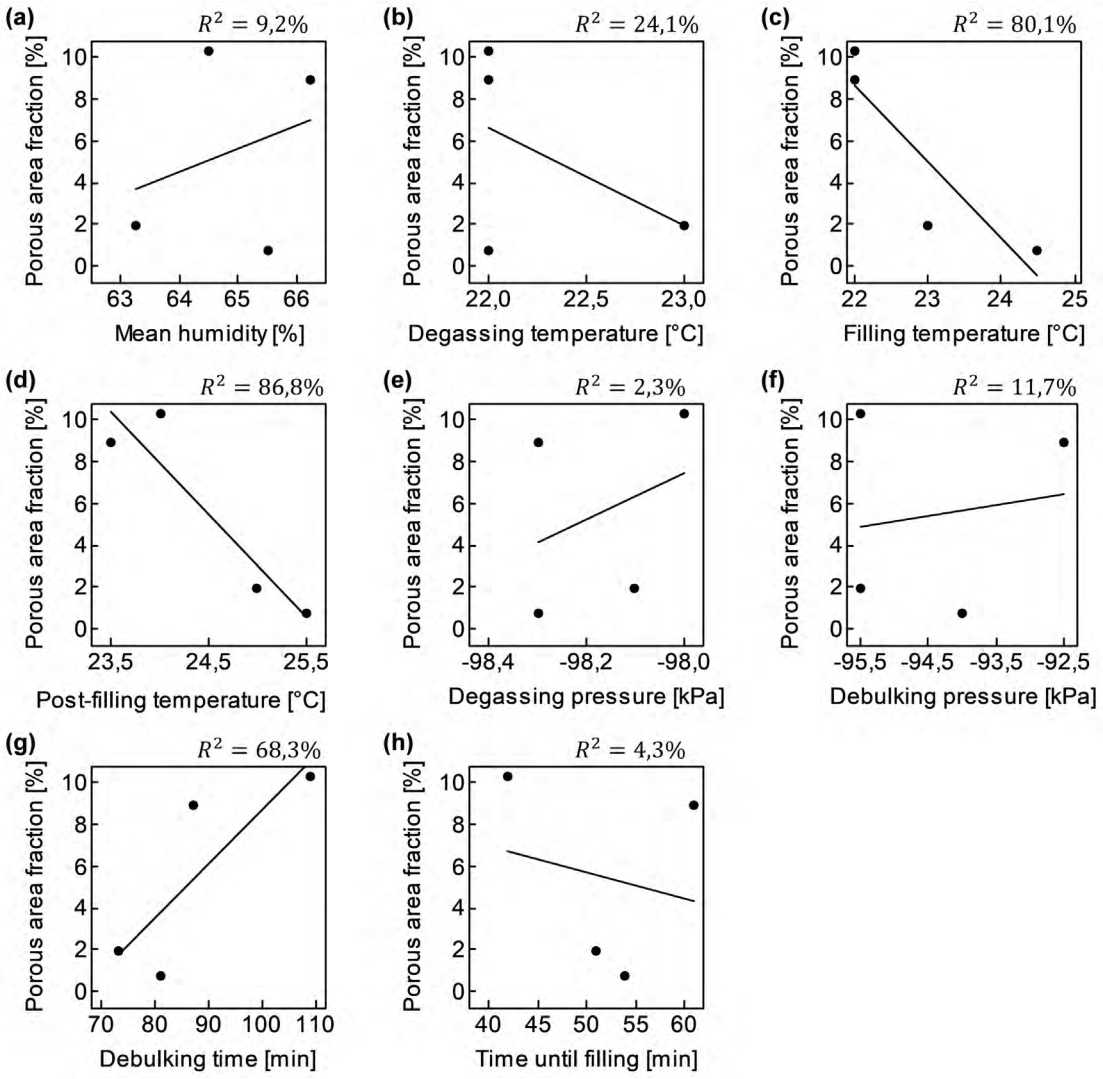

Figure F.17. Scatterplots of porous area fraction, s_0^{II+III}, vs. nuisance and allow-to-vary factors in the first stage of the screening experiment of filling and post-filling conditions.

Figure F.18 shows experimental data of s_0^{II+III} gathered according to all factor levels in the first stage of the screening experiment. Besides, main factors and two-factor interactions effects are depicted in Figure F.19. In Figure F.20, only effect of factor P is highlighted to be included in an ANOVA (Table F.22).

Factor P resulted statistically significant. At analysing the residuals of the model, the normal probability plot of effects showed and odd behaviour; however, it could be attributed to the few runs of the experiment (Figure F.21.a). Besides, no linear correlation seemed to exist between residuals and t_{deb} (Figure F.21.f). Unlike the screening of degassing procedures, no aliasing between factor P and t_{deb} existed and it seemed that the apparent dependence of s_0^{II+III} on t_{deb} was coincidental. Figure F.22 shows the model equation and the fitted values of s_0^{II+III}.

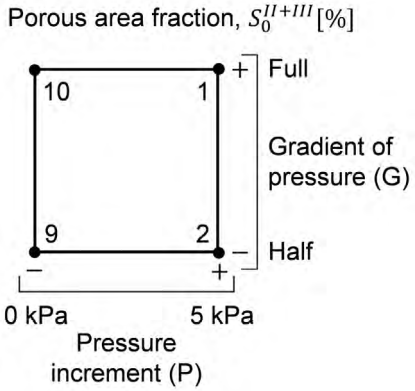

Figure F.18. Cube plot of porous area fraction, s_0^{II+III}, in the first stage of the screening experiment of filling and post-filling conditions.

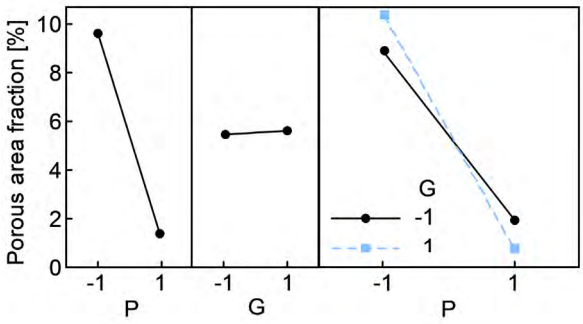

Figure F.19. Plots of main factors and two-factor interaction effects for porous area fraction, s_0^{II+III}, in the first stage of the screening experiment of filling and post-filling conditions.

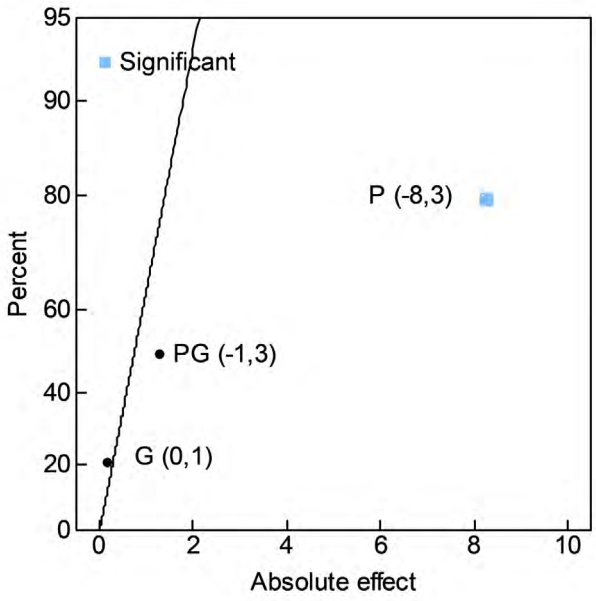

Figure F.20. Half-normal probability plot of effects of porous area fraction, s_0^{II+III}, in the first stage of the screening experiment of filling and post-filling conditions.

Table F.22. ANOVA table for porous area fraction, s_0^{II+III}, in the first stage of the screening experiment of filling and post-filling conditions considering factor P ($R^2_{adj} = 96\%$).

Source	df	SS	MS	F_0	p
P	1	68,68	68,68	80,4	0,012
Error	2	1,708	0,8539		
Total	3	70,39			

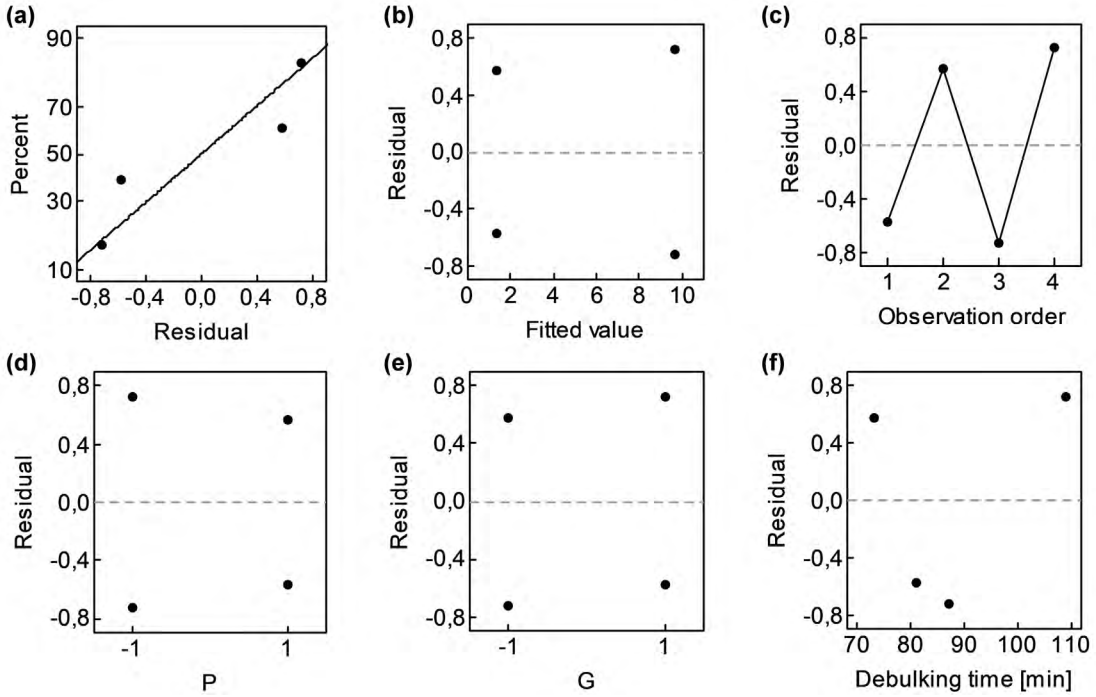

Figure F.21. Analysis of residuals of model for porous area fraction, s_0^{II+III}, including factor P in the first stage of the screening experiment of filling and post-filling conditions.

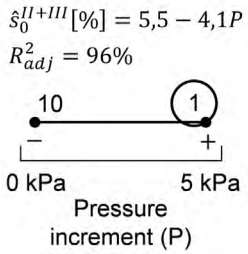

Figure F.22. Cube plot of fitted values of model for porous area fraction, s_0^{II+III}, including factor P in the first stage of the screening experiment of filling and post-filling conditions.

Since P was the only really significant factor affecting the response variable and s_0^{II+III} was minimized at high level of P; manufacturing conditions of specimen A4 were chosen for expanding the set of experiments to analyse the effects of factors A and I. It was preferred the manufacturing conditions of specimen A4 over A2 because of its shorter filling time ($t_{fill} = 114$ s in specimen A4 and $t_{fill} = 232$ s in specimen A2), which came from the application of a full gradient of pressure.

Apart from the specimens initially manufactured for this purpose B1, B2, B3 and A4 (which would correspond to B4), specimens B1' (replica of B1) and A2 (replica of A4) were also considered in the analysis to gain some degrees of freedom to compute experimental variability. Specimen A2 could be included as a replica of A4 because only factor P significantly affected s_0^{II+III} in the first stage of the screening experiment. The initially saturated factorial design became an unsaturated and unbalanced factorial design (partially replicated).

Dependencies of the response variable s_0^{II+III} on the set of nuisance factors and allow-to-vary factors was assessed visually through a series of scatterplots depicted in Figure F.23 for the second stage of the screening experiment analysed in this section. In this case, no significant dependence emerged between s_0^{II+III} and any factor which showed large variability throughout the experimentation campaign.

Figure F.24 shows experimental data of s_0^{II+III} gathered according to all factor levels in the second stage of the screening experiment. Besides, main factors and two-factor interactions effects are depicted in Figure F.25. In Figure F.26, all effects were highlighted to be included in an ANOVA (Table F.23).

All factors resulted statistically significant. Model validity was checked through the analysis of residuals (Figure F.27). Figure F.28 shows the model equation and the fitted values of s_0^{II+III}.

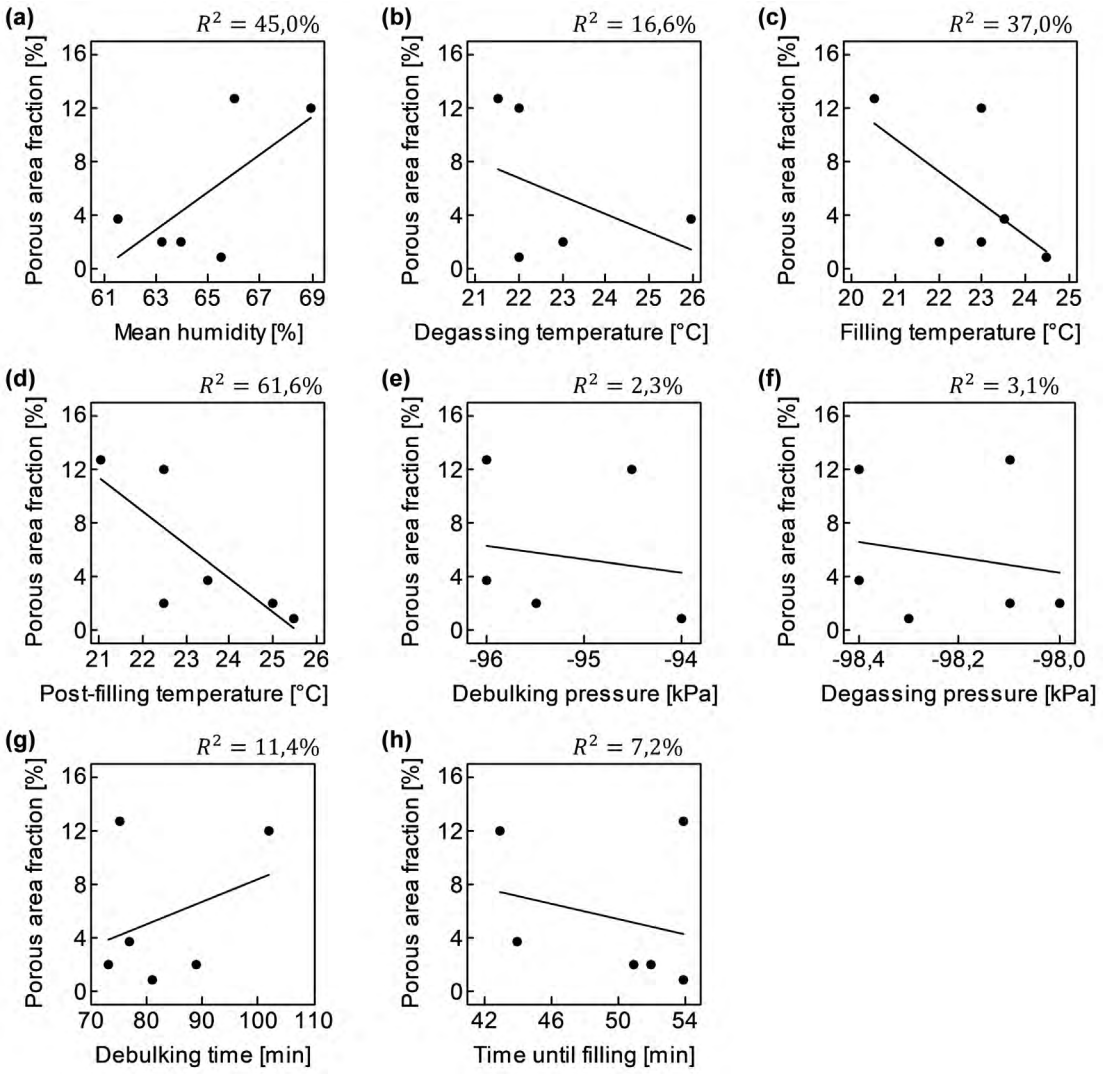

Figure F.23. Scatterplots of porous area fraction, s_0^{II+III}, vs. nuisance and allow-to-vary factors in the second stage of the screening experiment of filling and post-filling conditions.

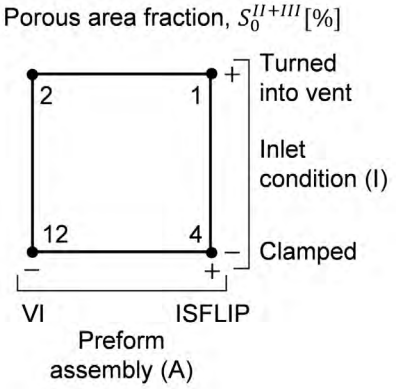

Figure F.24. Cube plot of porous area fraction, s_0^{II+III}, in the second stage of the screening experiment of filling and post-filling conditions.

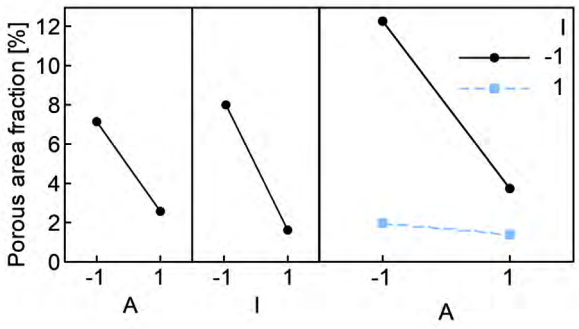

Figure F.25. Plots of main factors and two-factor interaction effects for porous area fraction, s_0^{II+III}, in the second stage of the screening experiment of filling and post-filling conditions.

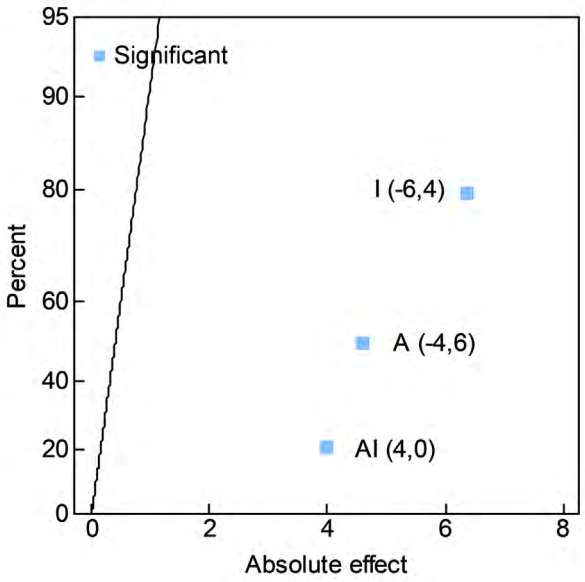

Figure F.26. Half-normal probability plot of effects of porous area fraction, s_0^{II+III}, in the second stage of the screening experiment of filling and post-filling conditions.

Table F.23. ANOVA table for porous area fraction, s_0^{II+III}, in the second stage of the screening experiment of filling and post-filling conditions considering factors A and I, and interaction AI ($R^2_{adj} = 98\%$).

Source	df	SS	MS	F_0	p
A	1	28,01	28,01	60,3	0,016
I	1	54,23	54,23	117	0,008
AI	1	21,24	21,24	45,8	0,021
Error	2	0,9290	0,4643		
Total	5	143,9			

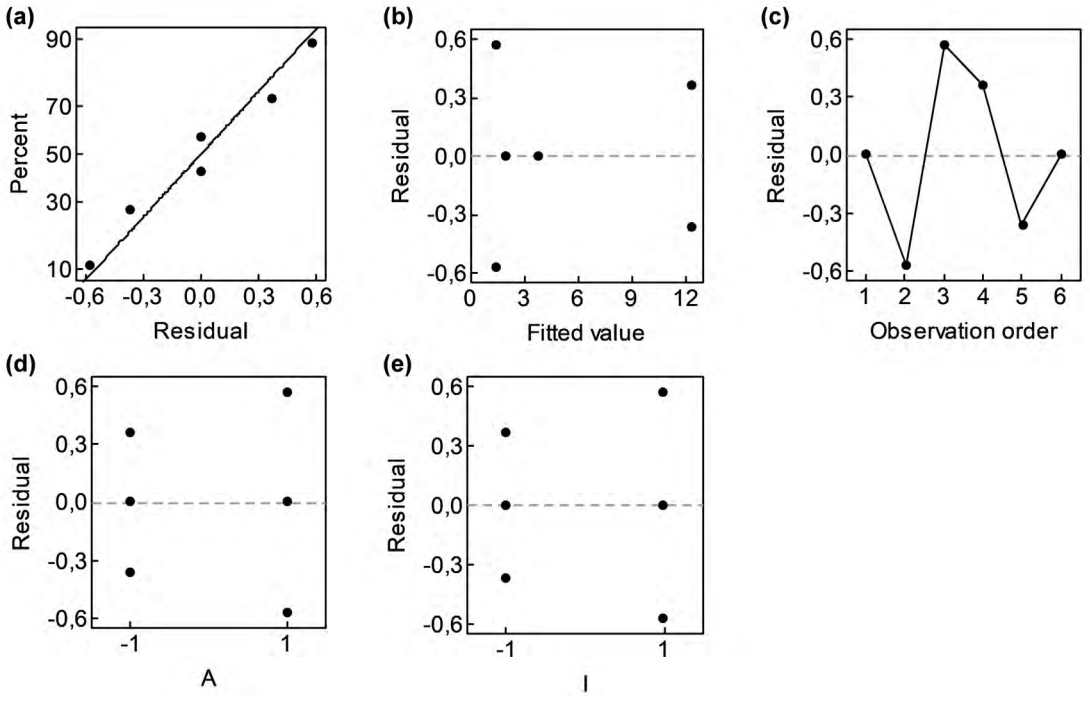

Figure F.27. Analysis of residuals of model for porous area fraction, s_0^{II+III}, including factors A and I, and interaction AI in the second stage of the screening experiment of filling and post-filling conditions.

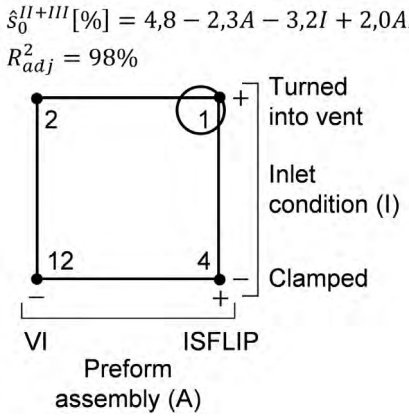

Figure F.28. Cube plot of fitted values of model for porous area fraction, s_0^{II+III}, including factors A and I, and interaction AI in the second stage of the screening experiment of filling and post-filling conditions.

F.5. Fibre volume fraction, v_f', based on thickness measures

From the results of the loss on ignition tests, a model was fitted to allow the estimation of the adjusted fibre volume fraction, v_f', from sample thickness, which was necessary to address porosity effects on flexural performance.

F.5.1. Quasi-isotropic specimens

In Figure F.29, it is depicted v_f' vs. reciprocal of sample thickness, $1/h$. It is also shown the fitted equation whose ANOVA is provided in Table F.24 and the corresponding analysis of residuals in Figure F.30. It is only worth mentioning that there were two samples, C41 and C44, both belonging to specimen 4, that showed abnormal values. This trend can be also observed in the scatterplot shown in Figure F.29.

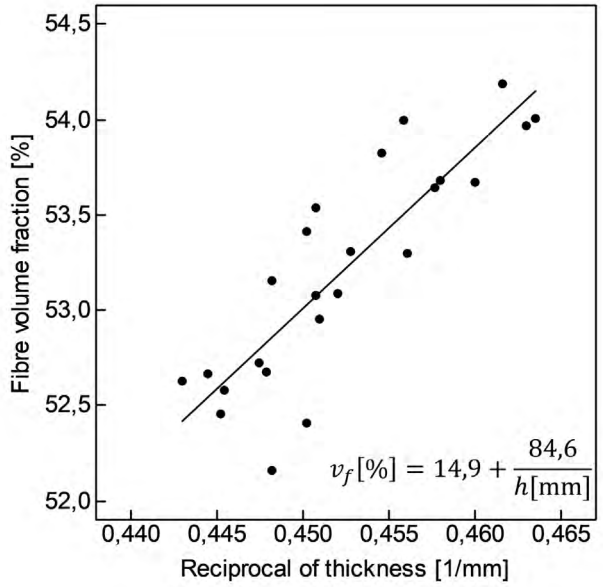

Figure F.29. Adjusted fibre volume fraction, v_f', vs. reciprocal of thickness, $1/h$, of quasi-isotropic specimens.

Table F.24. ANOVA table for adjusted fibre volume fraction, v_f', considering reciprocal of thickness, $1/h$ ($R^2 = 73{,}8\%$).

Source	df	Adjusted SS	Adjusted MS	F_0	p
$1/h$	1	5,855	5,855	62,1	0,000
Error	22	2,076	0,094		
Lack-of-fit	19	0,963	0,051	0,14	0,998
Pure error	3	1,112	0,371		
Total	23	7,931			

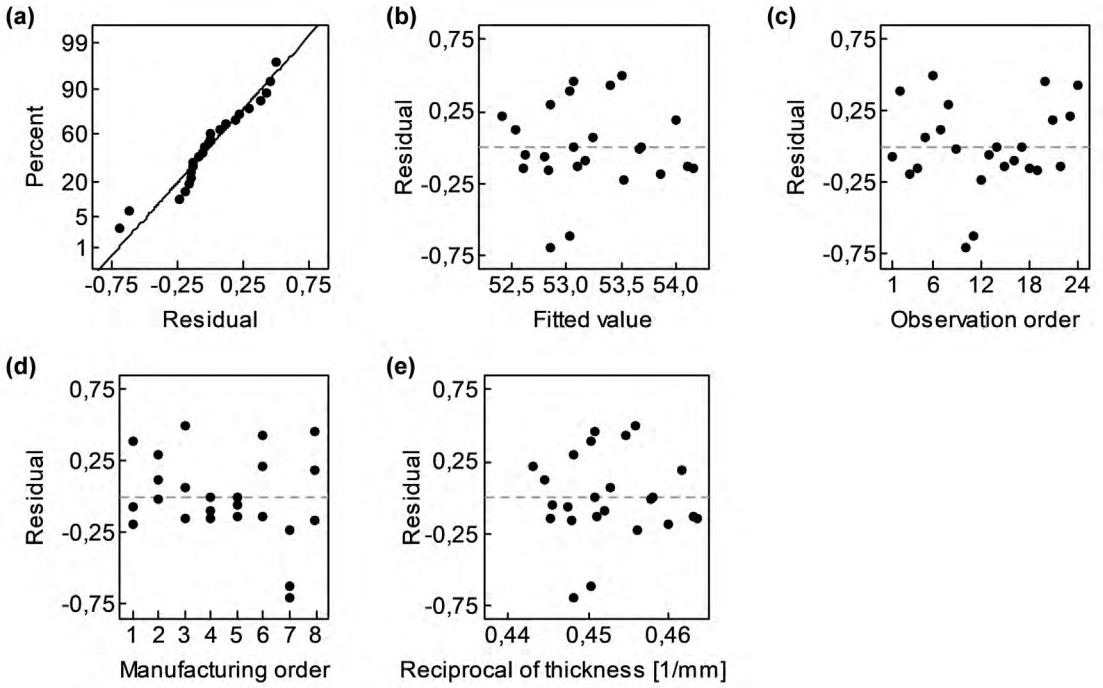

Figure F.30. Analysis of residuals of ANOVA for adjusted fibre volume fraction, v_f', of quasi-isotropic specimens considering reciprocal of thickness, $1/h$ (dimensions in %).

F.5.2. Orthotropic specimens

In Figure F.31, it is depicted v_f' vs. reciprocal of sample thickness, $1/h$. It is also shown the fitted equations whose ANOVA is provided in Table F.25 and the corresponding analysis of residuals in Figure F.32.

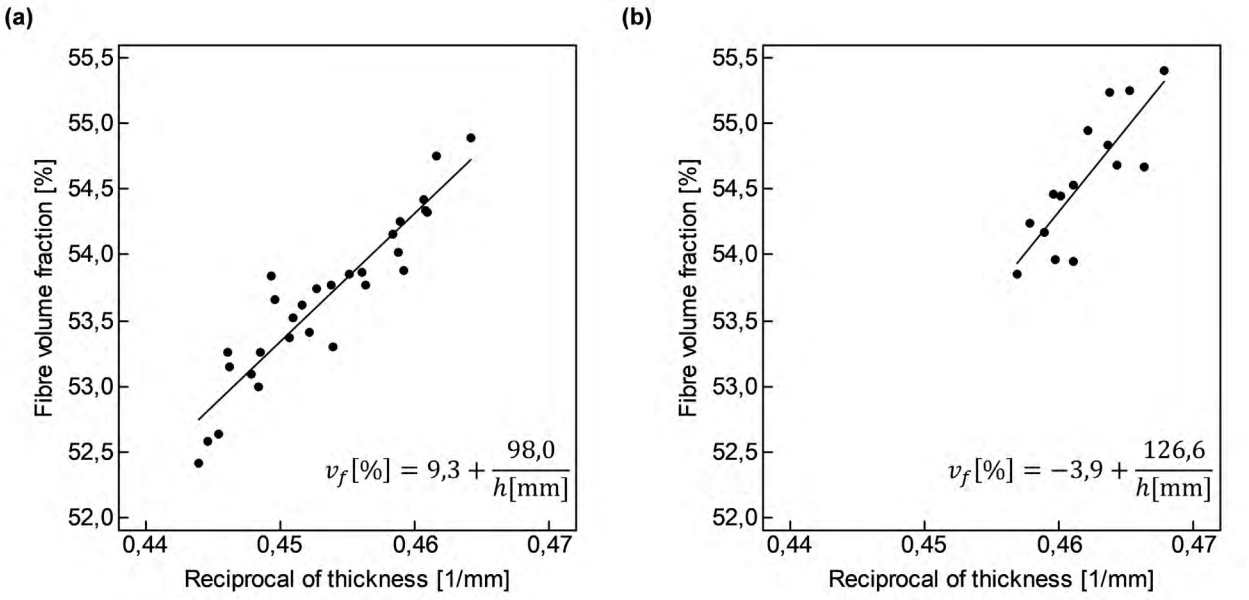

Figure F.31. Adjusted fibre volume fraction, v_f', vs. reciprocal of thickness, $1/h$, of orthotropic specimens: (a) release film surface texture and (b) peel-ply surface texture.

Table F.25. ANOVA table for adjusted fibre volume fraction, v_f', considering reciprocal of thickness, $1/h$ and factor Surface texture ($R^2 = 88{,}6\%$).

Source	df	Adjusted SS	Adjusted MS	F_0	p
$1/h$	1	6,3	6,3	99,6	0,000
Surface texture	1	0,1	0,1	1,60	0,213
$1/h$ x Surface texture	1	0,1	0,1	1,62	0,211
Error	40	2,5	0,1		
Total	43	22,3			

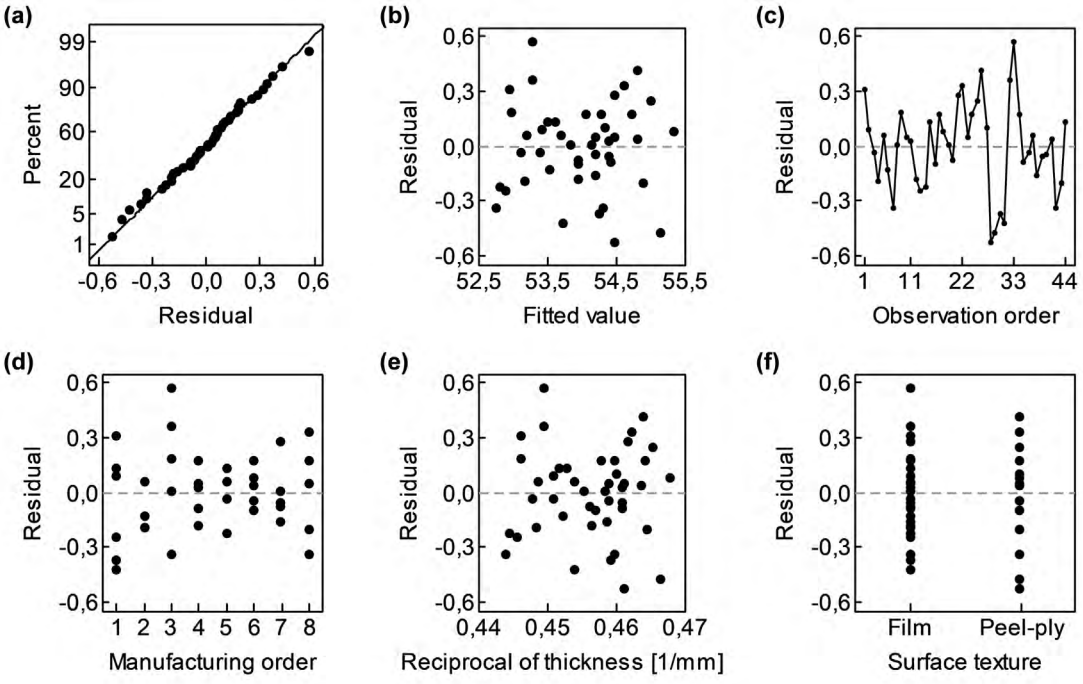

Figure F.32. Analysis of residuals of ANOVA for adjusted fibre volume fraction, v_f', of orthotropic specimens considering reciprocal of thickness, $1/h$, and factor Surface texture (dimensions in %).

Although the fixed-effect factor Surface texture (release film or peel-ply) resulted non-significant, two different equations were used to estimate v_f' for each type of preform assembly. However, if a single equation had been used, including only $1/h$ as a regressor variable, results would have been almost identical. It can be observed in the ANOVA summarized in Table F.26 that explained experimental variability in both models nearly matched, as well as the both analyses of residuals (Figure F.32 and Figure F.33).

Again, it can be also appreciated some sample whose results considerably differed from the rest of samples (C356, C436 and C436); although difference was not as severe as in the case of quasi-isotropic specimens.

Table F.26. ANOVA table for adjusted fibre volume fraction, v_f', considering reciprocal of thickness, $1/h$ ($R^2 = 88{,}2\%$).

Source	df	Adjusted SS	Adjusted MS	F_0	p
$1/h$	1	19,61	19,61	311	0,000
Error	42	2,6	0,1		
Total	43	22,3			

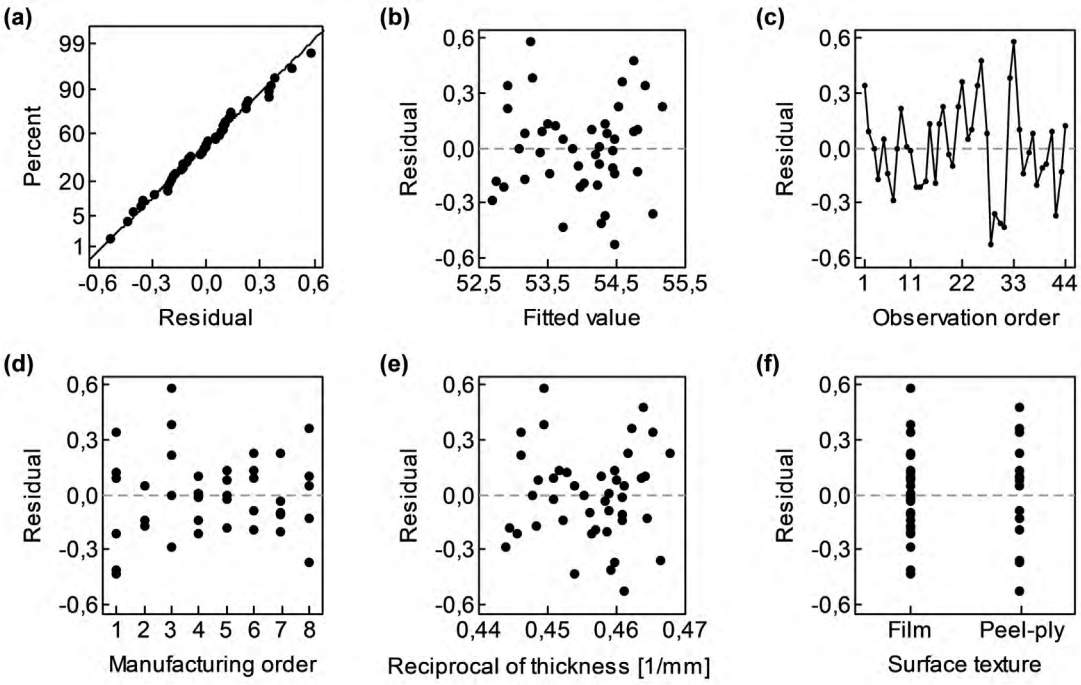

Figure F.33. Analysis of residuals of ANOVA for adjusted fibre volume fraction, v_f', of orthotropic specimens considering reciprocal of thickness, $1/h$ (dimensions in %).

F.6. Flexural properties

Effects significance on flexural properties of different continuous regressor variables and factors are analysed here below. Nevertheless, no backward elimination was carried out until reaching models of minimum order, since analyses were focused only on major significance rather than in the best models to describe response variables.

F.6.1. Quasi-isotropic specimens

In Chapter 4, flexural behaviour of quasi-isotropic E-glass-epoxy samples was analysed (coded FYZ in Figure D.1). Flexural strength, σ_{fM}, and modulus, E_f, were measured through a three-point flexure test. In Figure F.34, it is depicted σ_{fM} and E_f with respect to adjusted fibre volume fraction

estimated through Equation (108), $\hat{v}_f'$, and void volume fraction, v_0', at the corresponding sample CYZ (flexural sample FYZ and sample CYZ belonged to the same row of samples shown in Figure D.1).

$$\hat{v}_f'[\%] = 14{,}9 + \frac{84{,}6}{h[\text{mm}]}, \qquad R^2 = 73{,}8\% \tag{108}$$

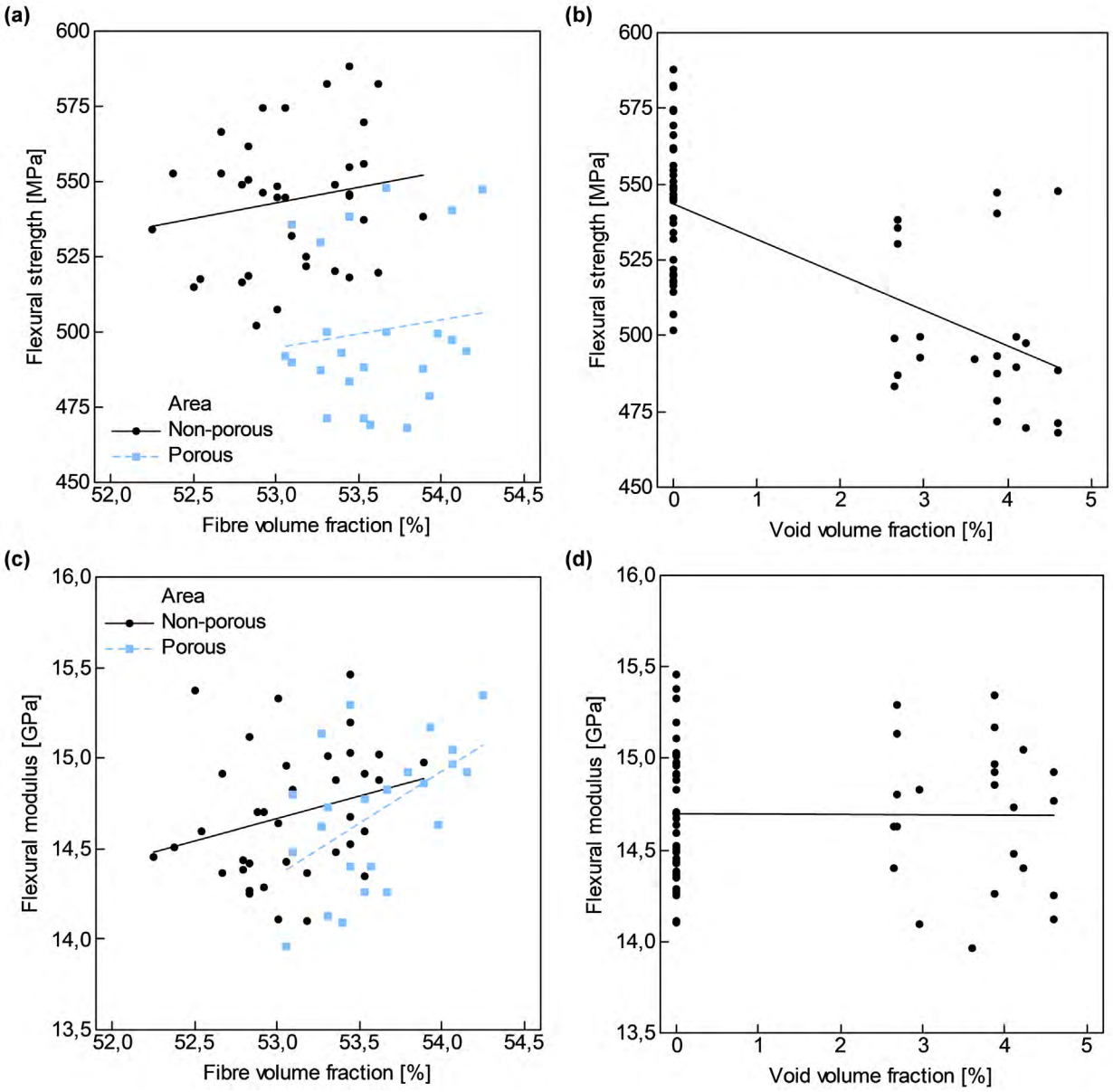

Figure F.34. Flexural strength, σ_{fM}, and modulus, E_f, vs. estimated fibre volume fraction, $\hat{v}_f'$, and void volume fraction, v_0', of quasi-isotropic specimens.

Two linear models were fitted with the experimental data to estimate σ_{fM} and E_f (response variables) from material quality attributes, $\hat{v}_f'$ and v_0' (regressor variables):

$$\hat{\sigma}_{fM}[\text{MPa}] = -83 + 11{,}8\hat{v}_f'[\%] - 13{,}4v_0'[\%], \qquad R^2 = 48{,}2\% \tag{109}$$

$$\hat{E}_f[\text{GPa}] = -5{,}55 + 0{,}381\hat{v}_f'[\%] - 0{,}0551v_0'[\%], \qquad R^2 = 14{,}5\% \tag{110}$$

Nevertheless, experimental variability explained by both models did not reach even 50%. In case of E_f, a very low coefficient of determinations, R^2, was obtained. Corresponding ANOVA tables for both models are provided in Table F.27 and Table F.28. Only v_0' showed statistical significance in case of σ_{fM} and $\hat{v}_f'$ in case of E_f. It must be noted that $\sigma_{fM} \propto 1/h^2$ and $E_f \propto 1/h^3$, hence, although variations in $\hat{v}_f'$ are small, the magnitude of their effects on E_f should be larger than on σ_{fM}, as it happened.

Table F.27. ANOVA table for flexural strength, σ_{fM}, considering estimated adjusted fibre volume fraction, $\hat{v}_f'$, and adjusted void volume fraction, v_0' ($R^2 = 48{,}2\%$).

Source	$\boldsymbol{df}$	**Adjusted** $\boldsymbol{SS}$	**Adjusted** $\boldsymbol{MS}$	$\boldsymbol{F_0}$	$\boldsymbol{p}$
$\hat{v}_f'$	1	1117	1117,5	2,06	0,157
v_0'	1	24198	24198	44,52	0,000
Error	57	30979	544		
Lack-of-fit	43	23046	536	0,95	0,580
Pure error	14	7933	567		
Total	59	59776			

At analysing the residuals of the models, in case of E_f, a slight odd behaviour emerged at representing the residuals vs. observation order and manufacturing order (according to the manufacturing order of specimen to which each sample belonged). Plots for each analysis of residuals are shown in Figure F.35 and Figure F.36. Consequently, the analysis was extended to include, apart from $\hat{v}_f'$ and v_0', the following factors:

- Specimen. A random-effect factor that accounted for the specimen to which each sample belonged.
- Testing orientation. A fixed-effect factor that accounted for sample face orientation in the test. Samples were randomly tested upwards (tensile face corresponded to the mould face) or downwards (compressive face corresponded to the mould face).

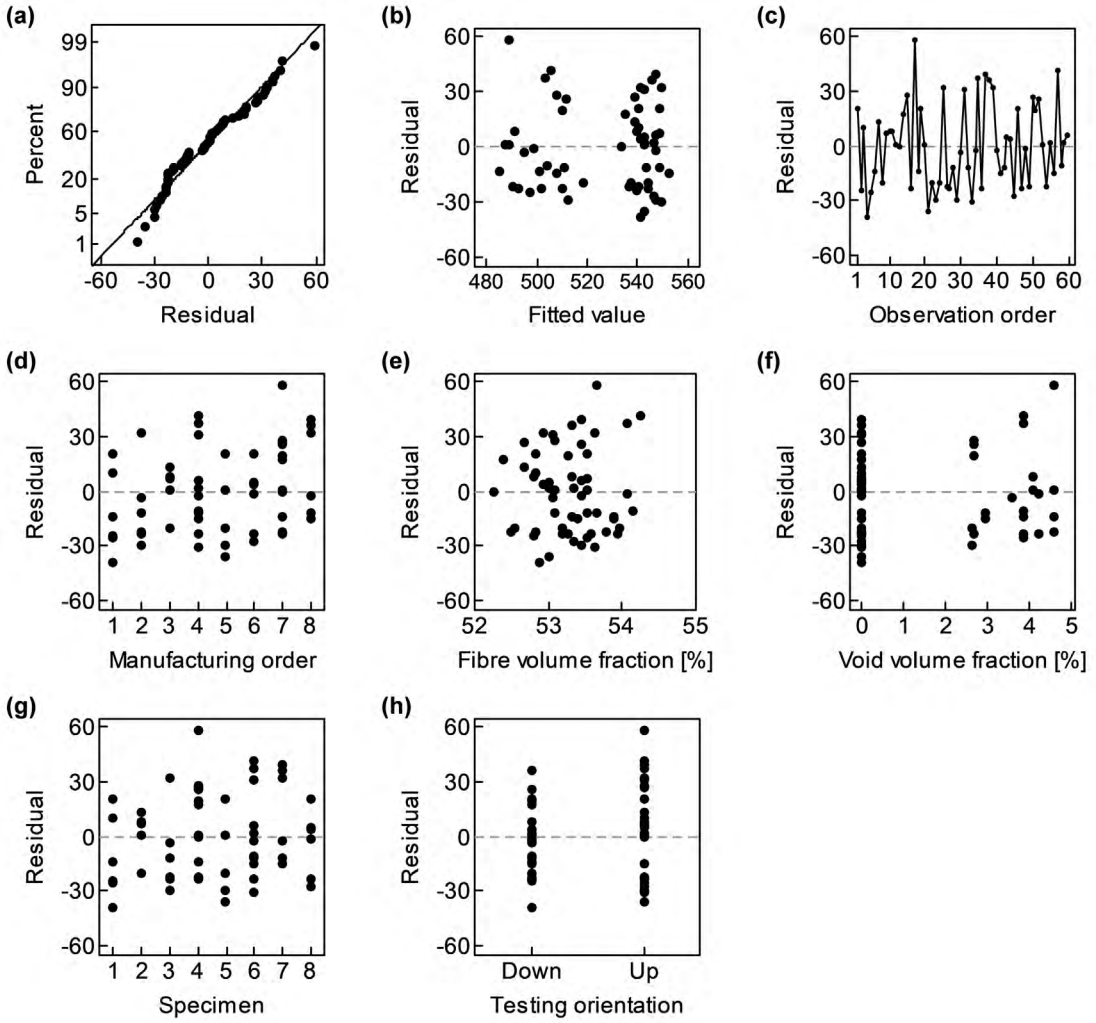

Figure F.35. Analysis of residuals of ANOVA for flexural strength, σ_{fM}, considering estimated adjusted fibre volume fraction, $\hat{v}_f'$, and adjusted void volume fraction, v_0' (dimensions in MPa).

Table F.28. ANOVA table for flexural modulus, E_f, considering estimated adjusted fibre volume fraction, $\hat{v}_f'$, and adjusted void volume fraction, v_0' ($R^2 = 14{,}5\%$).

Source	df	**Adjusted** SS	**Adjusted** MS	F_0	p
$\hat{v}_f'$	1	1,165	1,165	9,69	0,003
v_0'	1	0,408	0,408	3,40	0,070
Error	57	6,850	0,120		
Lack-of-fit	43	4,388	0,102	0,58	0,914
Pure error	14	2,462	0,176		
Total	59	8,015			

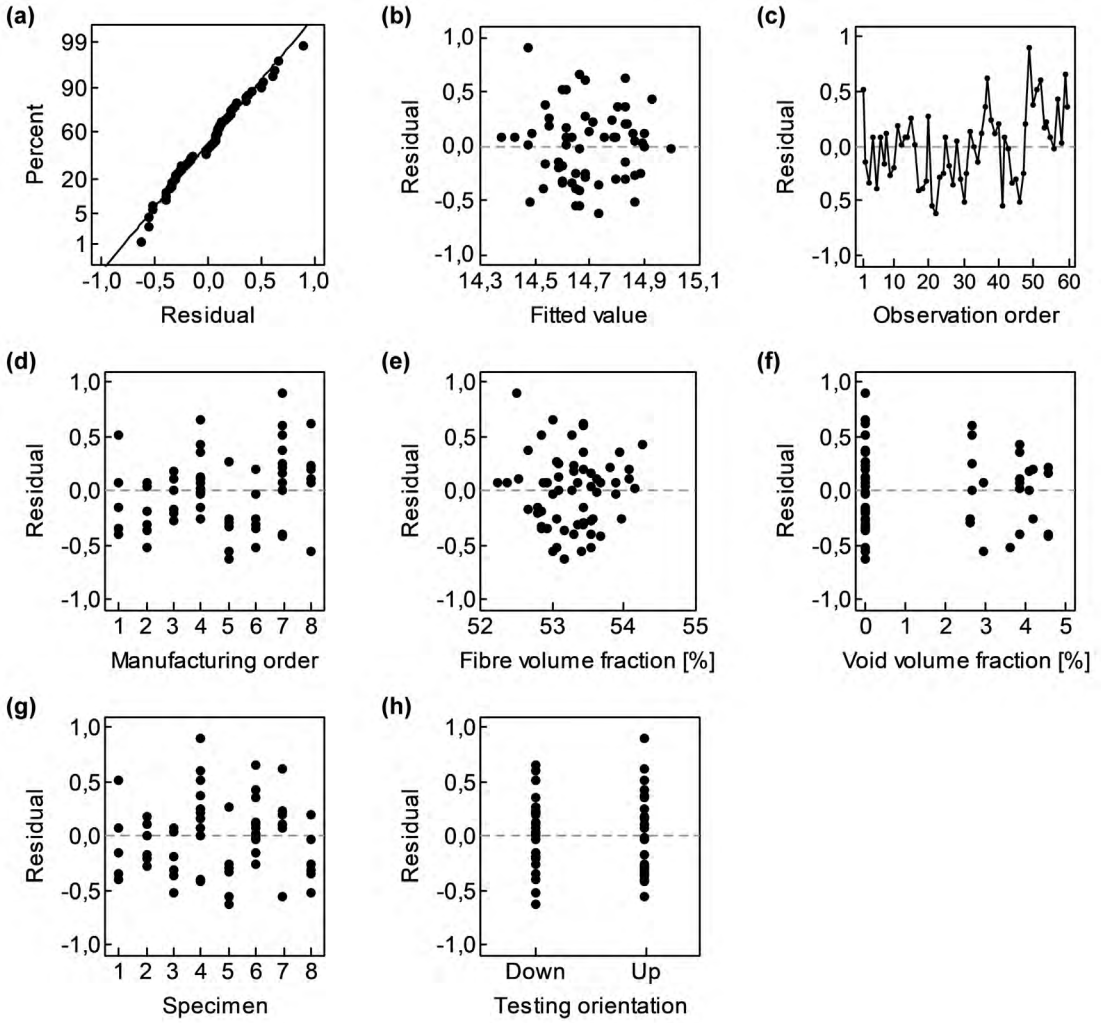

Figure F.36. Analysis of residuals of ANOVA for flexural modulus, E_f, considering estimated adjusted fibre volume fraction, $\hat{v}_f'$, and adjusted void volume fraction, v_0' (dimensions in GPa).

The factor Specimen is a blocking factor that referred to variability between specimens. It is a random-effect factor because specimens were considered a representative sample of the entire population of specimens manufactured under processing conditions specified in Chapter 4. Testing orientation helped to analyse the possible effect of a non-symmetrical trough-the-thickness distribution of voids.

This combination of factors and continuous regressor variables can be defined as a mixed-effects model with two factors (without interaction) and two covariates. Since, the quantity of samples tested per specimen differed between each other, the design was unbalanced.

A series of boxplots depicted in Figure F.37 shows variation of both flexural properties with respect to factors Specimen and Testing orientation in order to provide a first insight into data dependences.

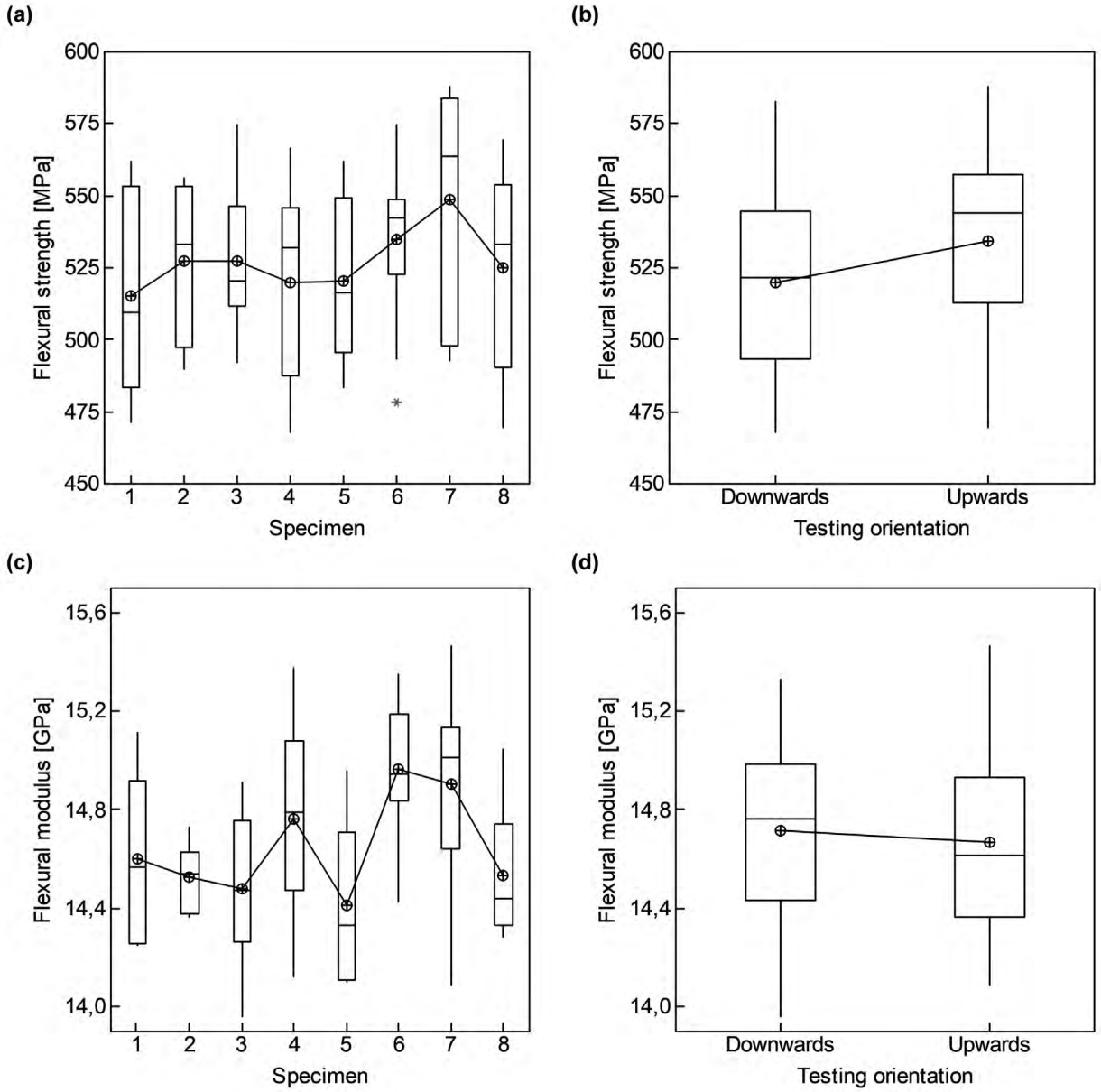

Figure F.37. Boxplots of flexural strength, σ_{fM}, and flexural modulus, E_f, of quasi-isotropic specimens (factors Specimen and Testing orientation).

ANOVA tables of models including factors Specimen and Testing orientation are provided in Table F.29 and Table F.30. In case of σ_{fM}, v_0' remained as the only significant factor; while, in case of E_f, in addition to $\hat{v}_f'$, v_0' and the factor Specimen emerged as significant. In the boxplot shown in Figure F.37.c, it can be observed as variability between specimens in terms of E_f is considerable.

Table F.29. ANOVA table for flexural strength, σ_{fM}, considering estimated adjusted fibre volume fraction, $\hat{v}_f'$; adjusted void volume fraction, v_0'; and factors Specimen and Testing orientation ($R^2 = 59{,}9\%$).

Source	df	Adjusted SS	Adjusted MS	F_0	p
$\hat{v}_f'$	1	963	963,4	1,93	0,171
v_0'	1	17168	17168	34,4	0,000
Specimen	7	4705	672	1,35	0,250
Testing orientation	1	434	434	0,90	0,356
v_0' x Testing orientation	1	464	464	0,93	0,340
Error	48	23954	499		
Lack-of-fit	46	22976	500	1,02	0,617
Pure error	2	978	489		
Total	59	59776			

* Specimen explains 5,1% of total experimental variability.

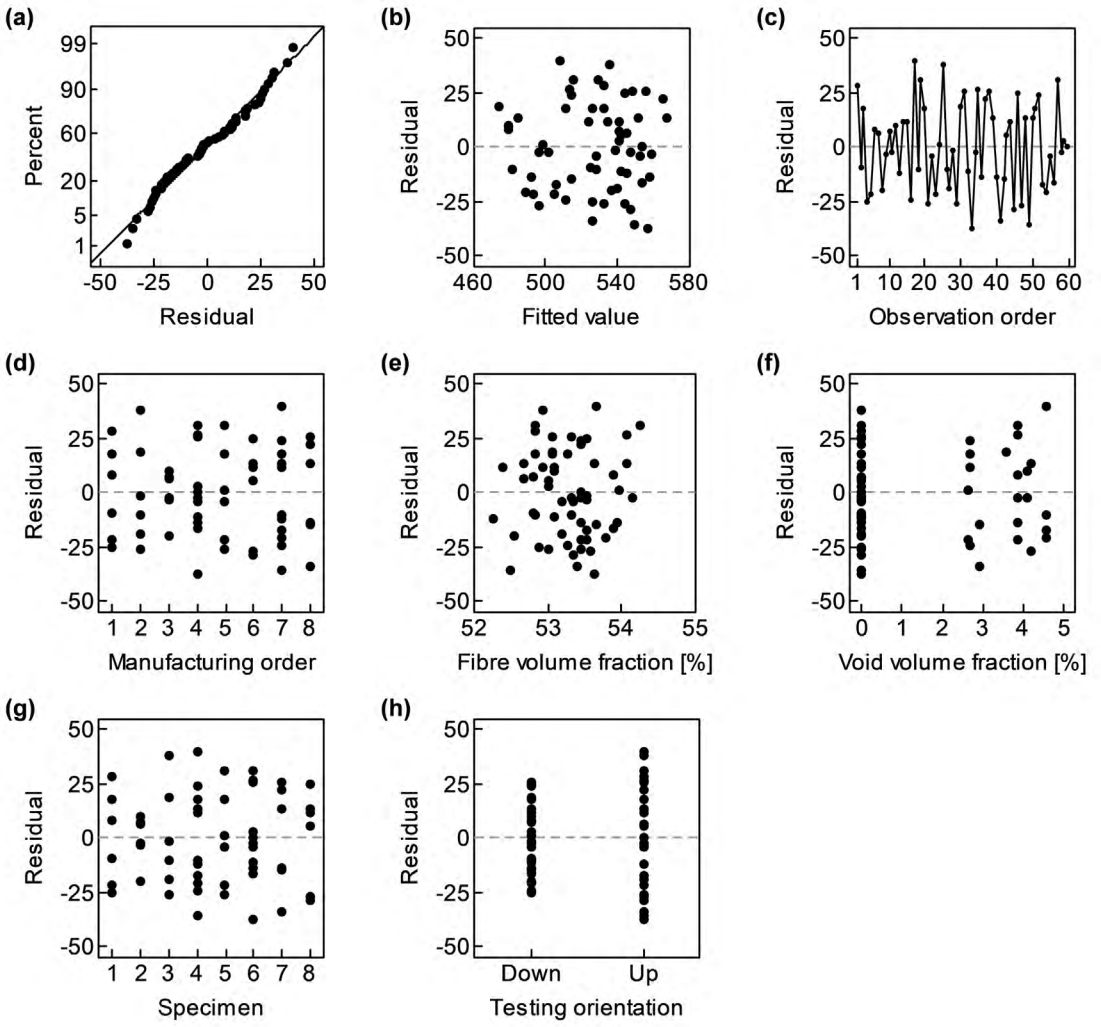

Figure F.38. Analysis of residuals of ANOVA for flexural strength, σ_{fM}, considering estimated adjusted fibre volume fraction, $\hat{v}_f'$; adjusted void volume fraction, v_0'; and factors Specimen and Testing orientation (dimensions in MPa).

Table F.30. ANOVA table for flexural modulus, E_f, considering estimated adjusted fibre volume fraction, $\hat{v}_f'$; adjusted void volume fraction, v_0'; and factors Specimen and Testing orientation ($R^2 = 40{,}3\%$).

Source	df	Adjusted SS	Adjusted MS	F_0	p
$\hat{v}_f'$	1	0,726	0,726	7,28	0,010
v_0'	1	0,580	0,580	5,82	0,020
Specimen	7	1,978	0,282	2,83	0,015
Testing orientation	1	0,000	0,000	0,0	0,978
v_0' x Testing orientation	1	0,052	0,052	0,52	0,473
Error	48	4,785	0,099		
Lack-of-fit	46	4,286	0,093	0,37	0,921
Pure error	2	0,499	0,249		
Total	59	8,015			

* Specimen explains 22,0% of total experimental variability.

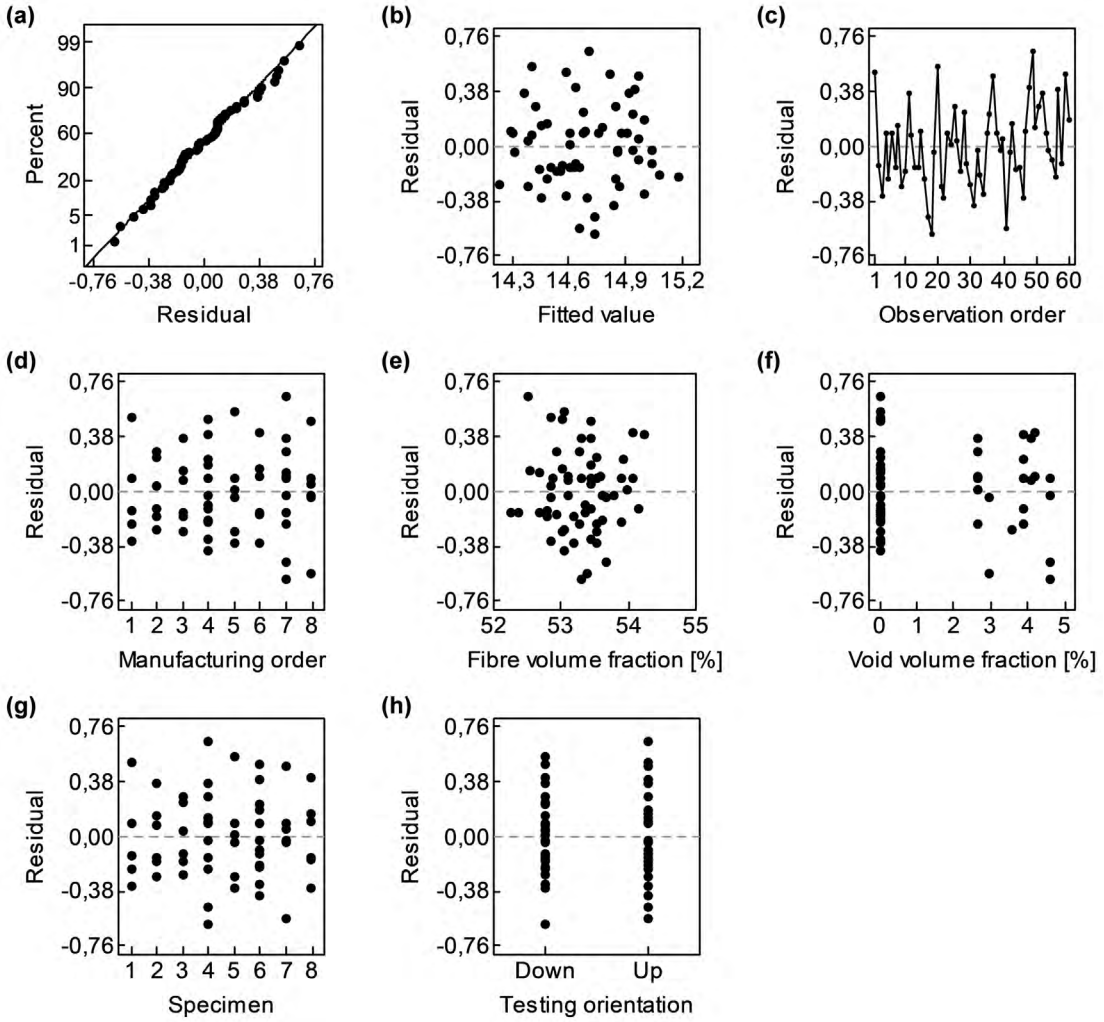

Figure F.39. Analysis of residuals of ANOVA for flexural modulus, E_f, considering estimated adjusted fibre volume fraction, $\hat{v}_f'$; adjusted void volume fraction, v_0'; and factors Specimen and Testing orientation (dimensions in GPa).

Variance associated to the blocking factor, Specimen, corresponded to 5,1% and 22,0% of the total variance of σ_{fM} and E_f, respectively, considerably helping to reduce error variability in case of the flexural modulus E_f observations and, thus, helping to unmask significance of v_0'. Analysis of residuals are shown in Figure F.38 and Figure F.39. According to Figure F.39.c, it can be suspected an increasing trend of E_f as flexural tests campaign progressed, which could have been caused by a systematic error during the test campaign. Especial attention should be kept on this respect in future experimentation.

Furthermore, it was also analysed flexural properties dependence on sample belonging to non-porous and porous areas (fixed-effect factor), instead of v_0' The boxplot presented in Figure F.40.a already points out a notable difference in σ_{fM} according to the discrete classification of areas (non-porous or porous). ANOVA tables describing response variability in this new approach are summarized in Table F.31 and Table F.32.

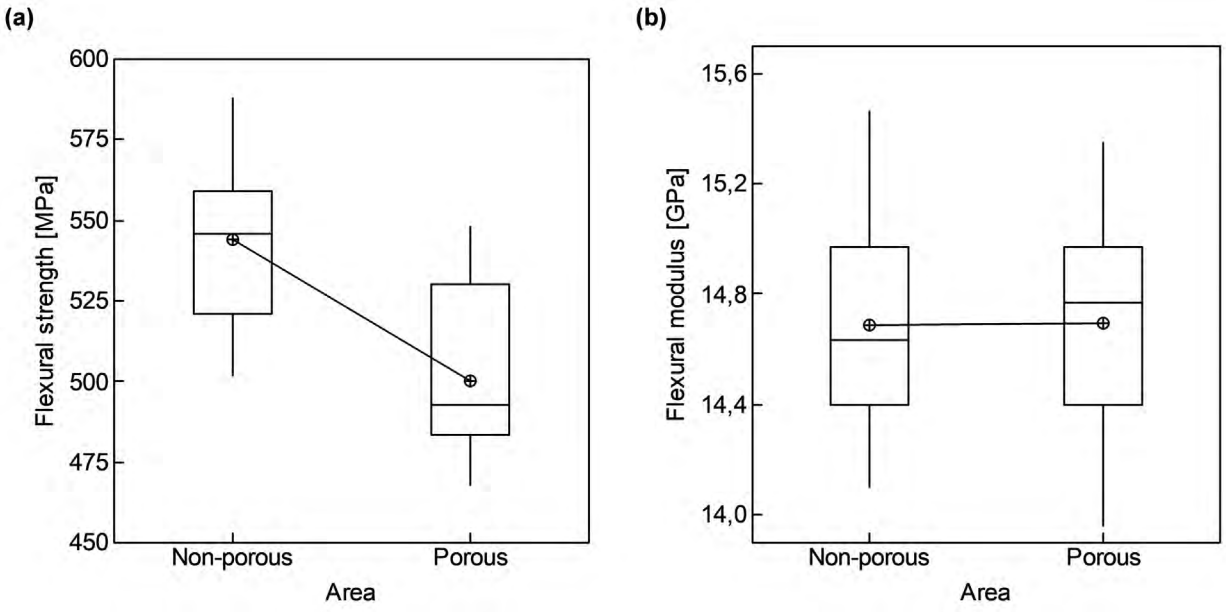

Figure F.40. Boxplots of flexural strength, σ_{fM}, and flexural modulus, E_f, of quasi-isotropic specimens (factor Area).

Model validity was checked through the corresponding analyses of residuals, which are shown in Figure F.41 and Figure F.42, without presenting any abnormal behaviour apart from the trend of residuals of E_f to increase as observation order increase.

Table F.31. ANOVA table for flexural strength, σ_{fM}, considering estimated adjusted fibre volume fraction, $\hat{v}_f'$, and factors Specimen, Testing orientation and Area ($R^2 = 57{,}0\%$).

Source	df	Adjusted SS	Adjusted MS	F_0	p
$\hat{v}_f'$	1	484	484,3	0,90	0,346
Specimen	7	4823	689	1,29	0,277
Testing orientation	1	1594	1594	2,98	0,091
Area	1	15603	15603	29,1	0,000
Testing orientation x Area	1	92,8	92,8	0,17	0,679
Error	48	25707	536		
Lack-of-fit	46	24730	538	1,10	0,590
Pure error	2	978	489		
Total	59	59776			

* Specimen explains 4,2% of total experimental variability.

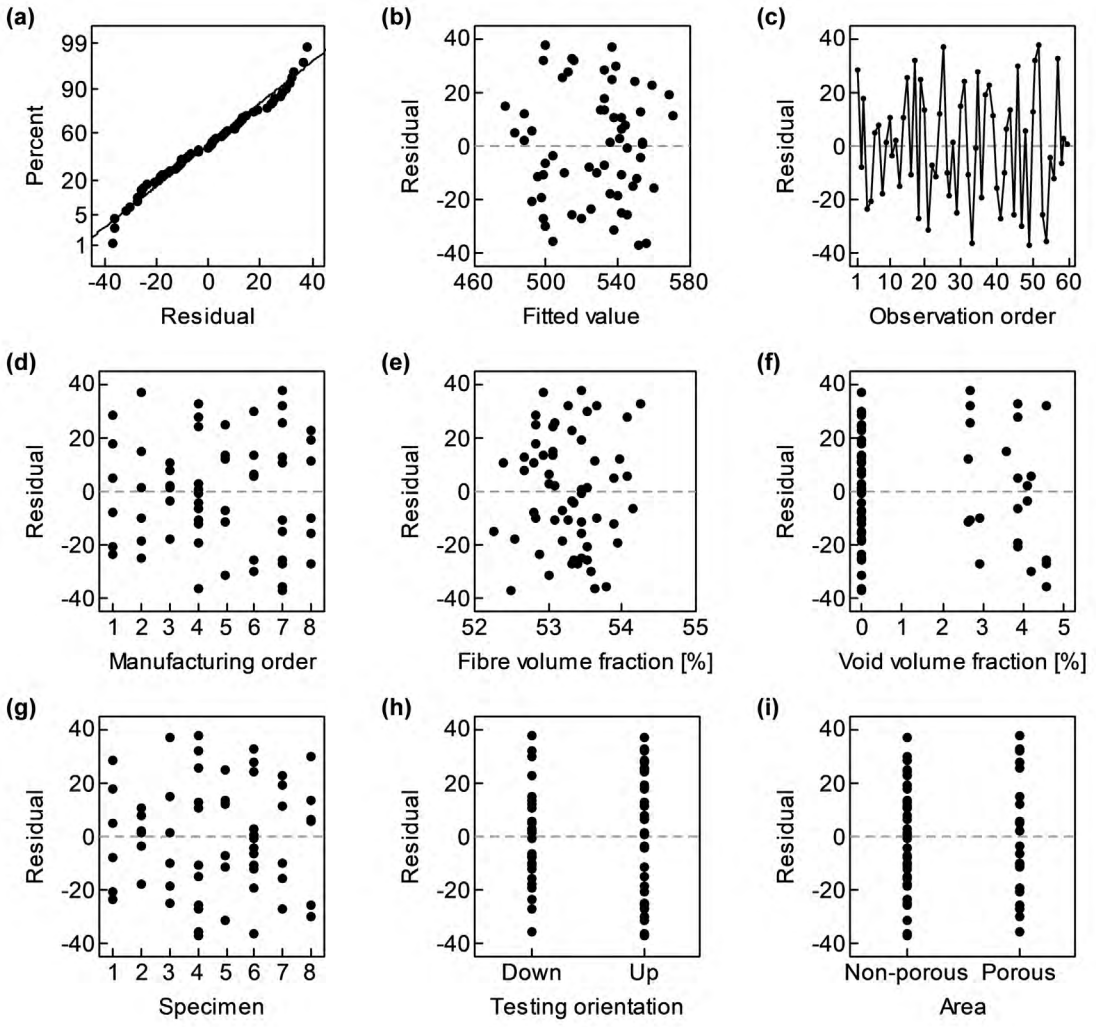

Figure F.41. Analysis of residuals of ANOVA for flexural strength, σ_{fM}, considering estimated adjusted fibre volume fraction, $\hat{v}_f'$, and factors Specimen, Testing orientation and Area (dimensions in MPa).

Table F.32. ANOVA table for flexural modulus, E_f, considering estimated adjusted fibre volume fraction, $\hat{v}_f'$, and factors Specimen, Testing orientation and Area ($R^2 = 38{,}8\%$).

Source	df	Adjusted SS	Adjusted MS	F_0	p
$\hat{v}_f'$	1	0,562	0,562	5,50	0,023
Specimen	7	1,895	0,270	2,65	0,021
Testing orientation	1	0,065	0,065	0,63	0,430
Area	1	0,414	0,414	4,05	0,050
Testing orientation x Area	1	0,100	0,100	0,98	0,327
Error	48	4,905	0,102		
Lack-of-fit	46	4,406	0,096	0,38	0,915
Pure error	2	0,499	0,250		
Total	59	8,015			

* Specimen explains 20,2% of total experimental variability.

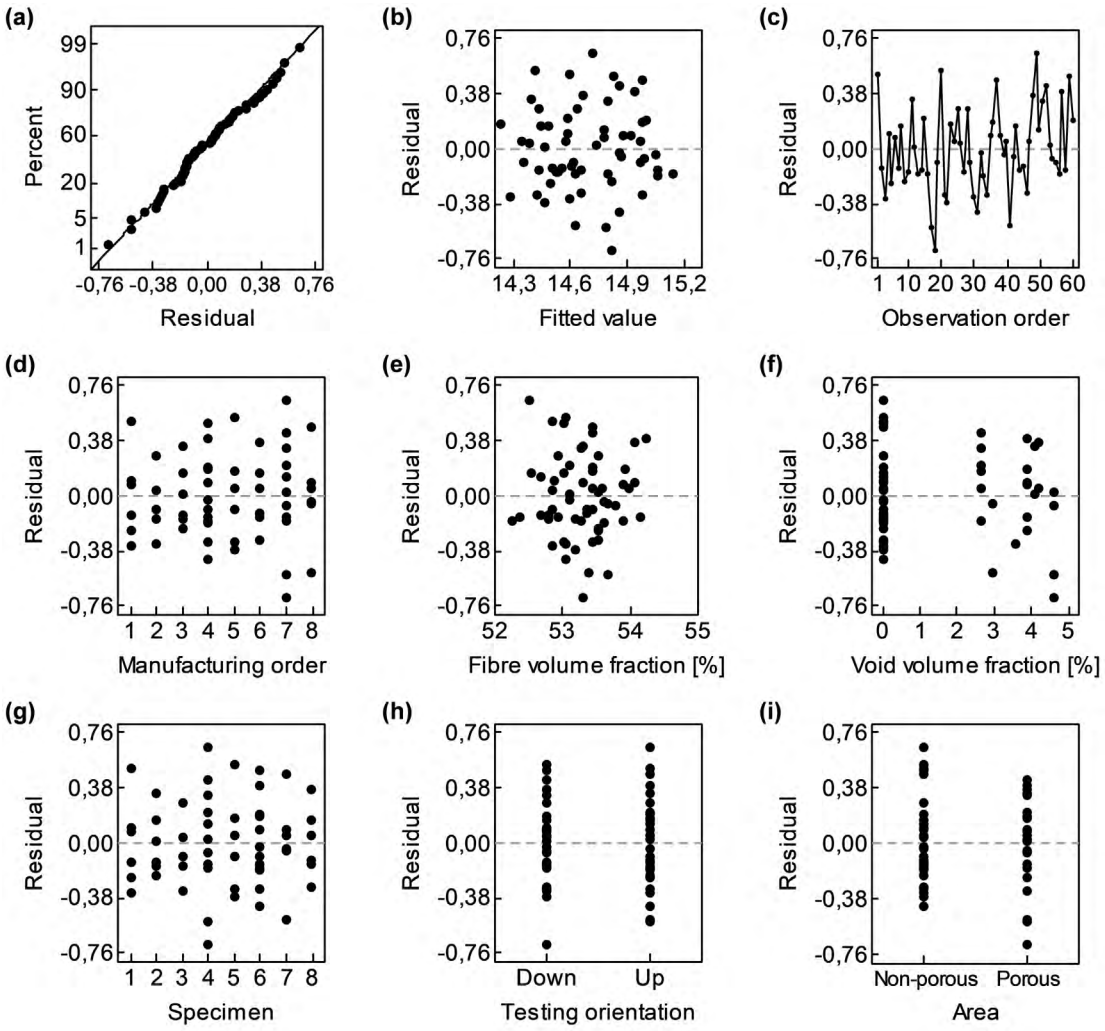

Figure F.42. Analysis of residuals of ANOVA for flexural modulus, E_f, considering estimated adjusted fibre volume fraction, $\hat{v}_f'$, and factors Specimen, Testing orientation and Area (dimensions in GPa).

F.6.2. Orthotropic specimens

In Chapter 5, flexural behaviour of quasi-isotropic E-glass-epoxy samples was analysed (coded FYZ in Figure D.2). Flexural strength, σ_{fM}, and modulus, E_f, were measured through a three-point flexure test. In Figure F.43 and Figure F.45, it is depicted σ_{fM} and E_f, respectively, with respect to adjusted fibre volume fraction estimated through Equations (111) or (112), $\hat{v}_f'$, and fixed-effect factors Porous area type and Testing orientation.

$$\hat{v}_f'[\%] = 9{,}3 + \frac{98{,}0}{h[\text{mm}]}, \qquad R^2 = 86{,}5\% \qquad \text{for ISFILP assemblies} \qquad (111)$$

$$\hat{v}_f'[\%] = -3{,}9 + \frac{126{,}6}{h[\text{mm}]}, \qquad R^2 = 67{,}6\% \qquad \text{for VI assemblies} \qquad (112)$$

Porous area type referred the Porous Area Type (PAT) to which the testing regions belonged. Porosity of specimens presented in Chapter 5 was classified according to its macroscopic aspect of pore distribution, discerning between three different Porous Area Types (PAT): scattered porosity (PAT I), isolated pore clusters (PAT II) and large pore clusters (PAT III).

Samples FYZ were randomly tested upwards (compressive face corresponded to the HPDM face) and downwards (compressive face corresponded to the mould face) and at least eight samples per specimen (four upwards and four downwards) were tested in case of void-free samples and samples PAT I. Testing orientation helped to analyse the effect of inter-tow void accumulation near the lower specimen surface (mould face). Interaction between Porous area type and Testing orientation was also considered to account for mentioned void accumulation near the lower surface according to different PAT.

ANOVA table for σ_{fM} is summarized in Table F.33. Both factors and their interaction, and the regressor variable resulted statistically significant. Besides, the analysis of residuals did not show any abnormal behaviour (Figure F.45).

ANOVA table for E_f is summarized in Table F.34. Factor Porous area type and $\hat{v}_f'$ resulted statistically significant. However, at analysing the residuals of the models, a slight odd behaviour emerged at representing the residuals vs. observation order (Figure F.46.c).

In order to discern which levels of the interaction Porous area type and Testing orientation in case of σ_{fM}, and Porous area type in case of E_f, Tukey's method for multiple pairwise comparisons was applied (Figure F.47). Analyses were focused on pairwise comparison including free-void samples to identify if flexural behaviour was damaged due to the presence of voids.

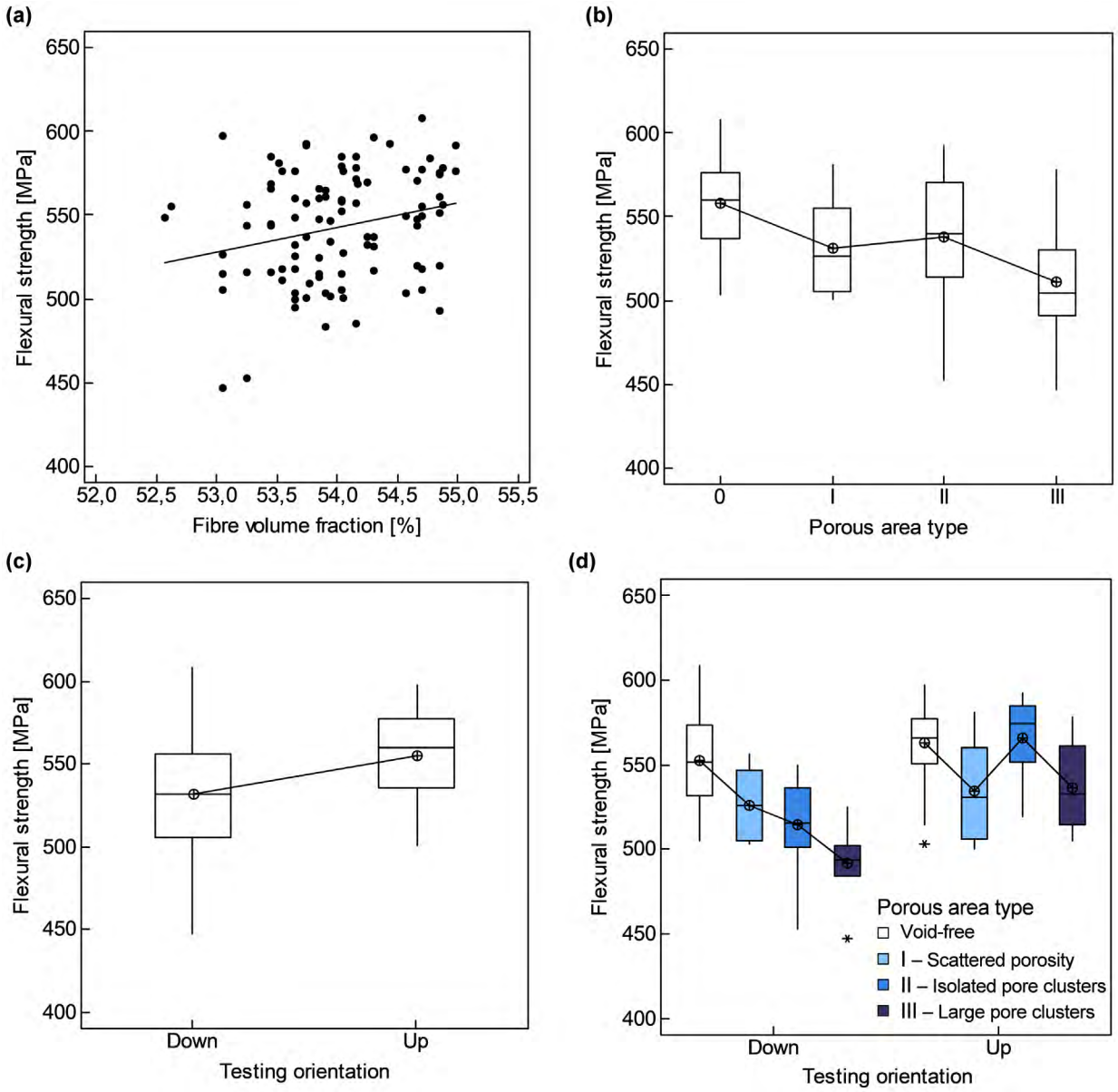

Figure F.43. (a) Flexural strength, σ_{fM}, vs. estimated fibre volume fraction, $\hat{v}_f'$, and (b-d) boxplots of flexural strength, σ_{fM}, of orthotropic specimens (factors Porous area type and Testing orientation).

In the performed Tukey's test, with a confidence level of 95% for the whole test (not for each pairwise comparison that was 99,7%), only samples of PAT II and III tested downwards showed a significant difference in σ_{fM} with both void-free samples tested upwards and downwards as can be seen in Figure F.47.a. In case of Tukey's test for E_f, samples PAT I and PAT III showed a significant difference with void-free samples; but PAT II did not showed a significant difference, that seemed incoherent (confidence level of 95% for the whole test and 99,0% for each pairwise comparison).

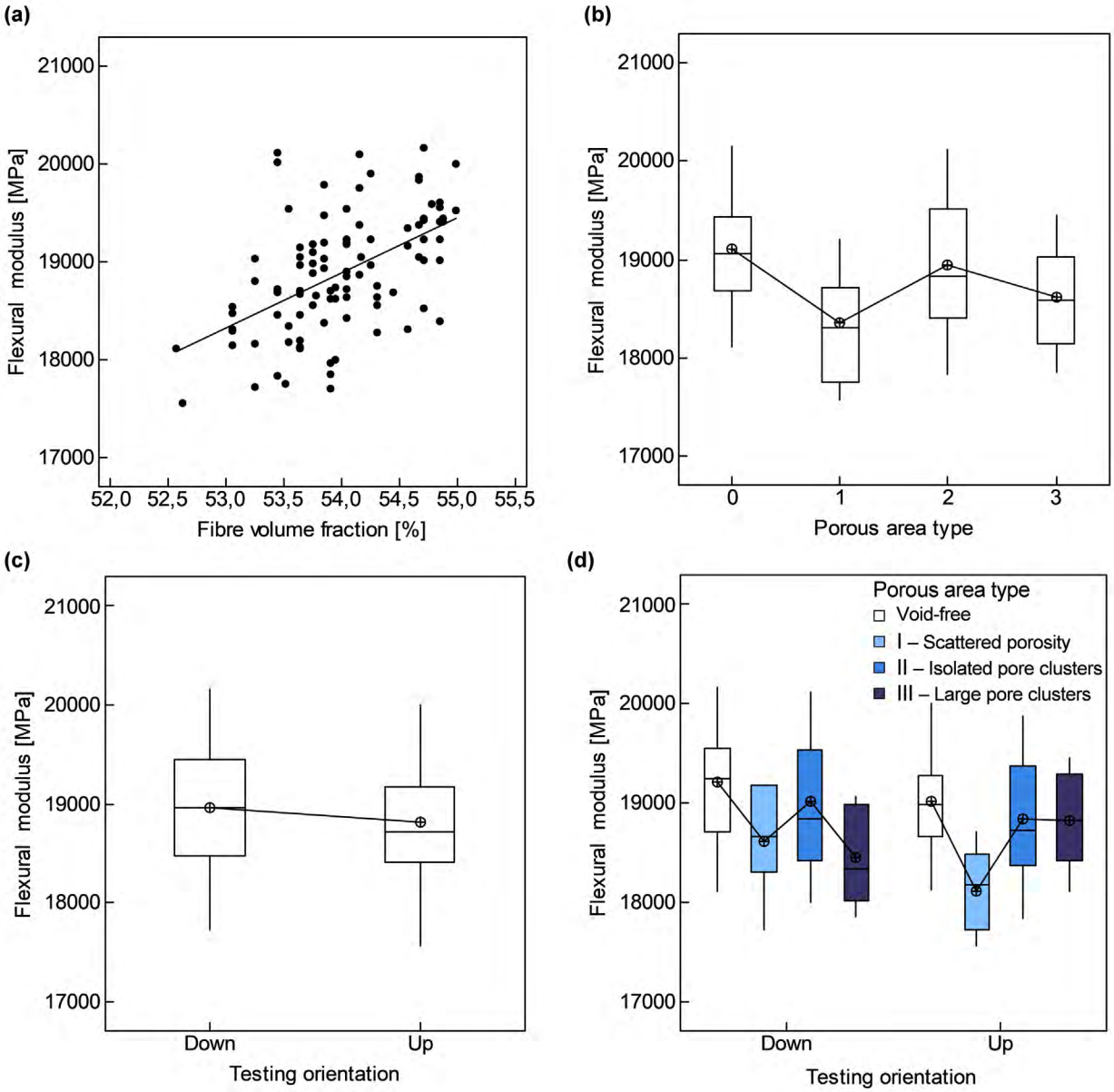

Figure F.44. (a) Flexural modulus, E_f, vs. estimated fibre volume fraction, $\hat{v}_f'$, and (b-d) boxplots of flexural strength, σ_{fM}, of orthotropic specimens (factors Porous area type and Testing orientation).

Table F.33. ANOVA table for flexural strength, σ_{fM}, considering estimated adjusted fibre volume fraction, $\hat{v}_f'$, and factors Porous area type and Testing orientation ($R^2 = 48{,}5\%$).

Source	df	Adjusted SS	Adjusted MS	F_0	p
$\hat{v}_f'$	1	2811	2811	4,51	0,036
Porous area type	3	23889	7963	12,8	0,000
Testing orientation	1	14567	14567	23,4	0,000
Porous area type x Testing orientation	3	7460	2487	3,99	0,010
Error	90	56116	623,5		
Lack-of-fit	71	46453	654,3	1,29	0,275
Pure error	19	9663	508,6		
Total	98	109021			

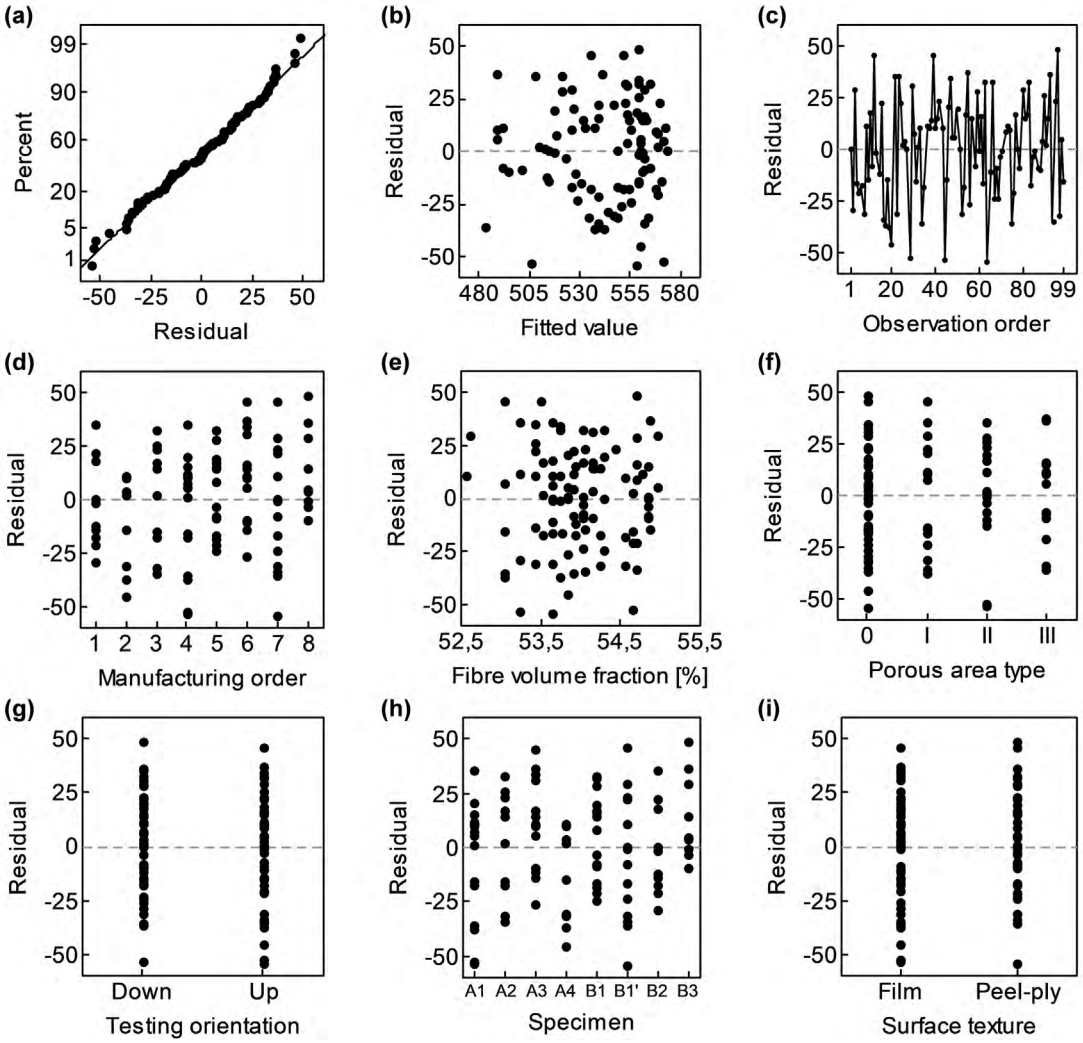

Figure F.45. Analysis of residuals of ANOVA for flexural strength, σ_{fM}, considering estimated adjusted fibre volume fraction, $\hat{v}_f'$, and factors Porous area type and Testing orientation (dimensions in MPa).

Table F.34. ANOVA table for flexural modulus, E_f, considering estimated adjusted fibre volume fraction, $\hat{v}_f'$, and factors Porous area type and Testing orientation ($R^2 = 44{,}9\%$).

Source	df	**Adjusted** SS	**Adjusted** MS	F_0	p
$\hat{v}_f'$	1	5,956	5,956	27,3	0,000
Porous area type	3	4,703	1,568	7,19	0,000
Testing orientation	1	0,556	0,556	2,55	0,114
Porous area type x Testing orientation	3	0,379	0,126	0,58	0,630
Error	90	19,610	0,217		
Lack-of-fit	71	15,435	0,217	0,99	0,54
Pure error	19	4,174	0,219		
Total	98	35,606			

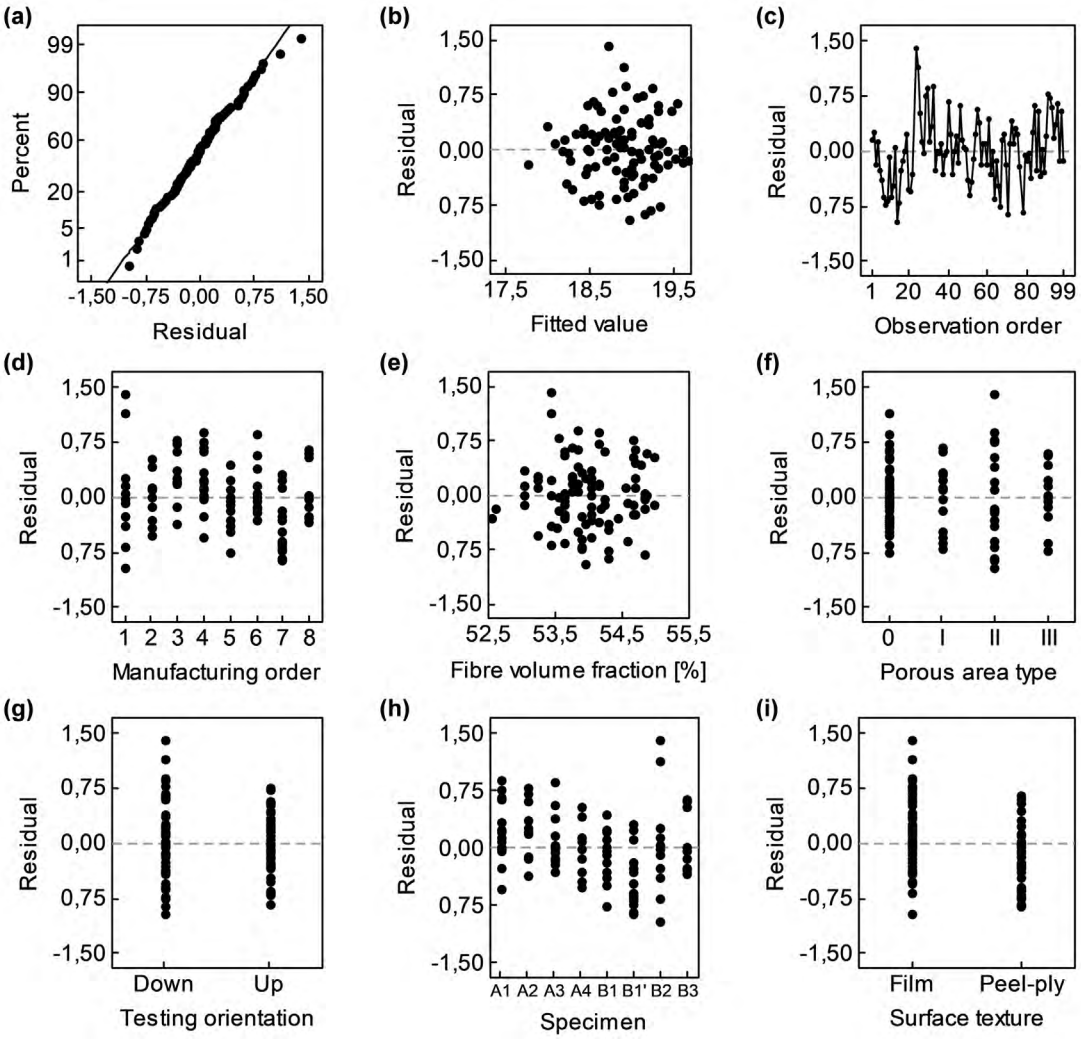

Figure F.46. Analysis of residuals of ANOVA for flexural modulus, E_f, considering estimated adjusted fibre volume fraction, $\hat{v}_f'$, and factors Porous area type and Testing orientation (dimensions in GPa).

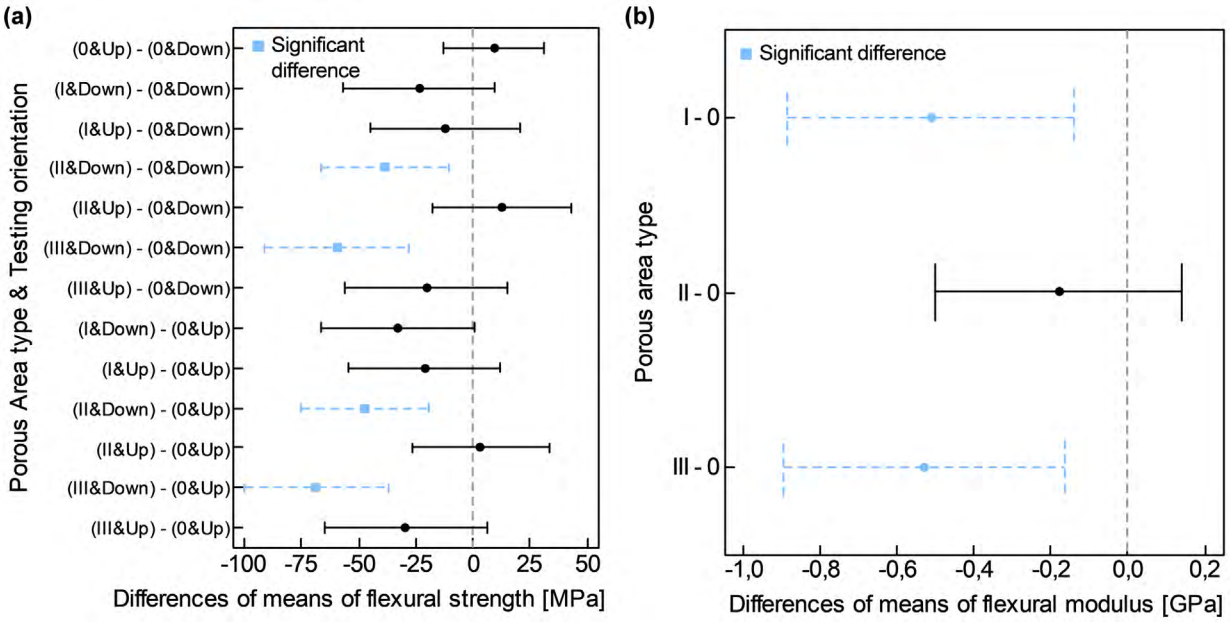

Figure F.47. Tukey's method applied to discern significant levels (a) of the interaction Porous area type and Testing orientation for flexural strength, σ_{fM}, and (b) of Porous area type for flexural modulus, E_f.

In order to address the odd distribution of residuals of E_f and the apparently incoherent significance of some levels of Porous are type, the random-effect factor Specimen was added to the analysis. It would have been also interesting to include surface texture of specimens; however, since each surface texture only exists for specific specimens, both terms cannot be included simultaneously to an ANOVA. It must be noted that surface texture was already indirectly affecting flexure response through the different range of $\hat{v}_f'$ shown for each assembly type specimen. Boxplots of both flexural properties with respect to different specimens are shown in Figure F.48.

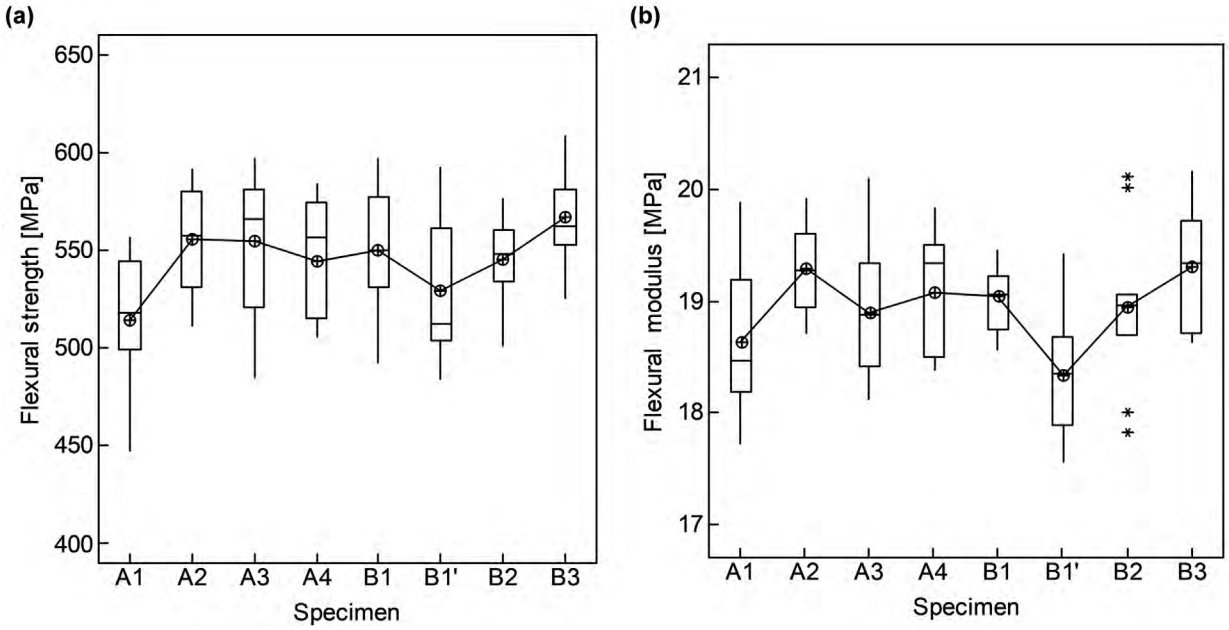

Figure F.48. Boxplots of flexural strength, σ_{fM}, and flexural modulus, E_f, of orthotropic specimens (factor Specimen).

ANOVA tables for σ_{fM} and E_f are provided in Table F.35 and Table F.36, respectively. Explained experimental variability increased from previous ANOVA, especially in case of E_f. $\hat{v}_f'$ stopped being significant for σ_{fM}, although Specimen did not result statistically significant too. On the other hand, Porous area type was not significant anymore once Specimen emerged as significant. Analyses of residuals are presented in Figure F.49 and Figure F.50. A slight odd behaviour arose again at representing the residuals of E_f vs. observation order (Figure F.50.c).

Tukey's method applied to the interaction Porous area type and Testing orientation for σ_{fM} showed similar results to those previously presented. In Chapter 5, it is presented the results of Tukey's test applied to the interaction Porous area type and Testing orientation for E_f; although, neither at considering only factors Porous area type and Testing orientation nor at adding effects of the random-effect factor Specimen, there was no evidence to conduct it. Nevertheless, it was

presented to keep coherence with the analysis of σ_{fM} without going into detail on the statistical analysis.

Table F.35. ANOVA table for flexural strength, σ_{fM}, considering estimated adjusted fibre volume fraction, $\hat{v}_f'$, and factors Specimen, Porous area type and Testing orientation ($R^2 = 55{,}4\%$).

Source	df	**Adjusted** SS	**Adjusted** MS	F_0	p
$\hat{v}_f'$	1	1700	1700	2,91	0,092
Specimen	7	7569	1081	1,85	0,089
Porous area type	3	14573	4858	8,31	0,000
Testing orientation	1	12707	12707	21,72	0,000
Porous area type x Testing orientation	3	6818	2273	3,89	0,012
Error	83	48547	585		
Lack-of-fit	78	45975	589	1,15	0,497
Pure error	5	2572	515		
Total	98	109021			

* Specimen explains 7,5% of total experimental variability.

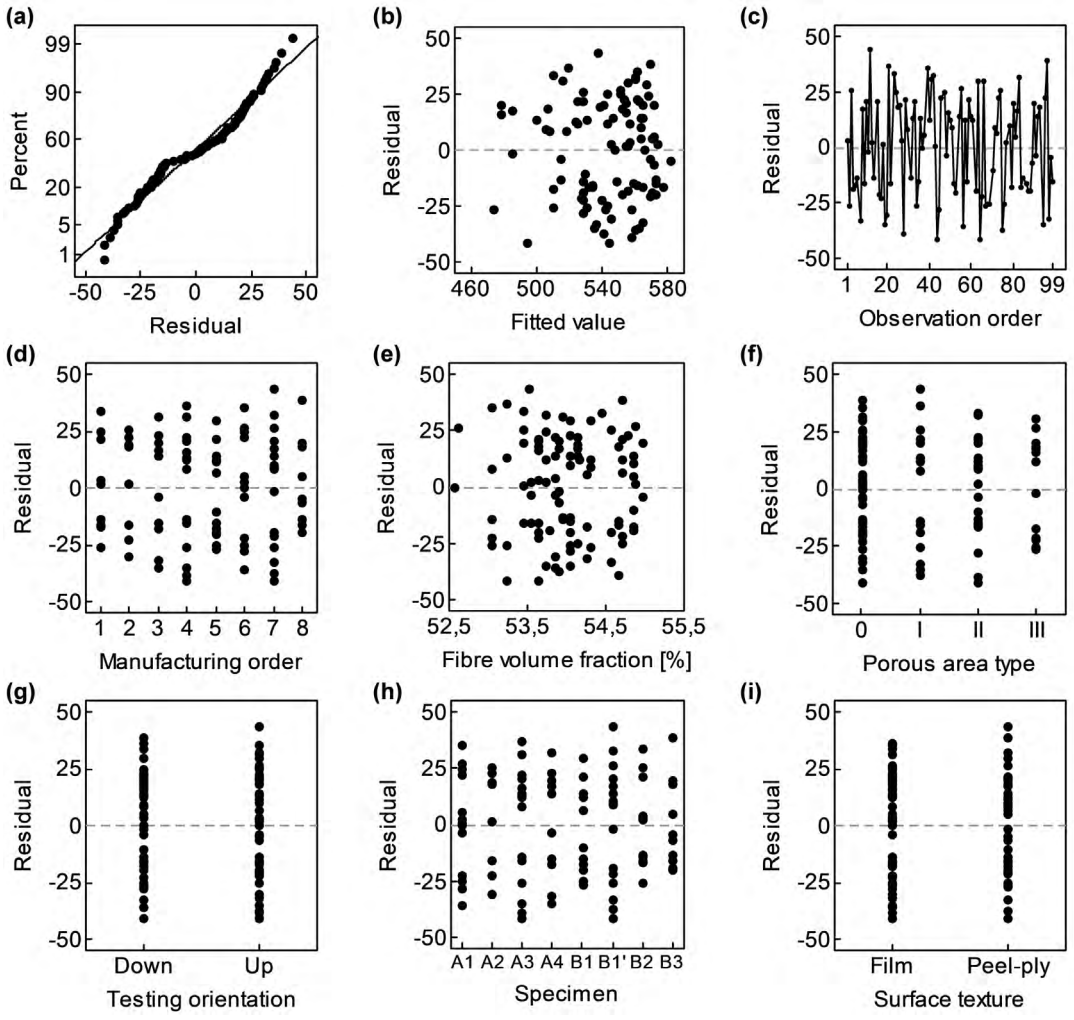

Figure F.49. Analysis of residuals of ANOVA for flexural strength, σ_{fM}, considering estimated adjusted fibre volume fraction, $\hat{v}_f'$, and factors Specimen, Porous area type and Testing orientation (dimensions in MPa).

Table F.36. ANOVA table for flexural modulus, E_f, considering estimated adjusted fibre volume fraction, $\hat{v}_f'$, and factors Specimen, Porous area type and Testing orientation ($R^2 = 58{,}7\%$).

Source	df	Adjusted SS	Adjusted MS	F_0	p
$\hat{v}_f'$	1	7,211	7,211	40,7	0,000
Specimen	7	4,907	0,701	3,96	0,001
Porous area type	3	1,213	0,404	2,28	0,085
Testing orientation	1	0,566	0,566	3,19	0,078
Porous area type x Testing orientation	3	0,187	0,062	0,35	0,788
Error	83	14,703	0,177		
Lack-of-fit	78	14,126	0,181	1,57	0,327
Pure error	5	0,576	0,115		
Total	98	35,606			

* Specimen explains 22,0% of total experimental variability.

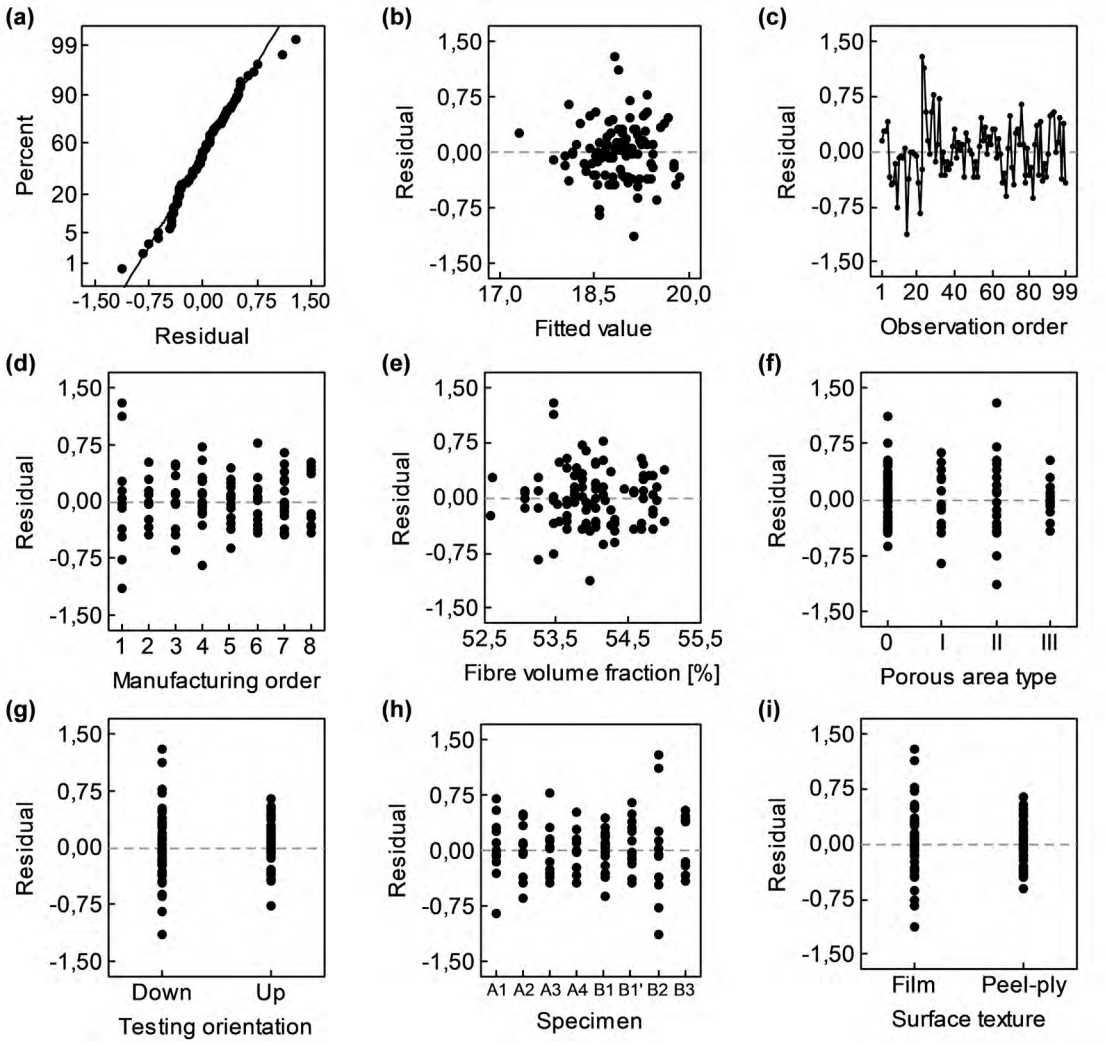

Figure F.50. Analysis of residuals of ANOVA for flexural modulus, E_f, considering estimated adjusted fibre volume fraction, $\hat{v}_f'$, and factors Specimen, Porous area type and Testing orientation (dimensions in GPa).

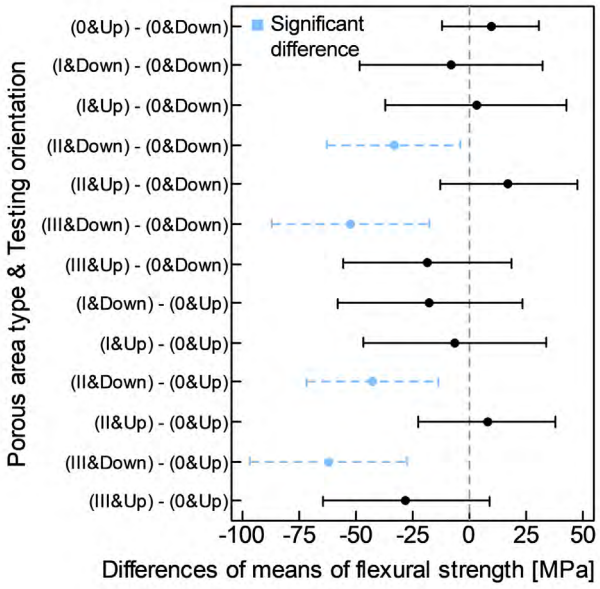

Figure F.51. Tukey's method applied to discern significant levels of the interaction Porous area type and Testing orientation for flexural strength, σ_{fM}.

Bibliography

1. Jakobsen J. *Liquid composite moulding simulation*. Masther thesis, Universitat Politècnica de Catalunya, Spain, 2014.
2. Wisnom MR, Jones MI, Hill GFJ. Interlaminar tensile strength of carbon fibre-epoxy specimen size, layup and manufacturing effects. *Advanced Composites Letters*. 2001;10(4):171–7.
3. Zhou G, Callahan J, Nash P, Ripley P, Rishton J. Investigation of interlaminar behaviour in angled laminate beams with crease. *ECCM15: 15th European Conference on Composite Materials*, Venice, Italy: 2012.
4. Makeev A, Seon G, Nikishkov Y, Lee E. Methods for assessment of interlaminar tensile strength of composite materials. *Journal of Composite Materials*. 2015;49:783–94.
5. Hao W, Ge D, Ma Y, Yao X, Shi Y. Experimental investigation on deformation and strength of carbon/epoxy laminated curved beams. *Polymer Testing*. 2012;31:520–6.
6. Shivakumar K, Allen H, Avva V. Interlaminar tension strength of graphite/epoxy composite laminates. *AIAA Journal*. 1994;32.
7. Hufenbach W, Hornig A., Zhou B, Langkamp A, Gude M. Determination of strain rate dependent through-thickness tensile properties of textile reinforced thermoplastic composites using L-shaped beam specimens. *Composites Science and Technology*. 2011;71:1110–6.
8. Lekhnit͡skiĭ SG. *Anisotropic Plates*. Translated from the Second Russian Edition by S.W. Tsai and T. Cheron. New York: Gordon and Breach; 1968.
9. Kedward K, Wilson R, McLean S. Flexure of simply curved composite shapes. *Composites*. 1989;20:527–36.
10. Hiel CC, Sumich M, Chappell DP. A curved beam test specimen for determining the interlaminar tensile strength of a laminated composite. *Journal of Composite Materials*. 1991;25:854–68.
11. Cui W, Liu T, Len J, Ruo R. Interlaminar tensile strength (ILTS) measurement of woven glass/polyester laminates using four-point curved beam specimen. *Composites Part A: Applied Science and Manufacturing*. 1996;27:1097–105.
12. Vasconcelos P, Lino FJ, Neto RJ, Teixeira A. Glass and carbon fibre reinforced hybrid composites for epoxy tooling. *Structures*. 2004.
13. Gammon LM, Hayes BS. Microscopy of composite materials. *Structures*. 2004:16–8.
14. Buehler L. *BUEHLER SUM-MET: The science behind materials preparation. A guide to materials preparation and analysis*. 2004.
15. Preibisch S, Saalfeld S, Tomancak P. Globally optimal stitching of tiled 3D microscopic image acquisitions. *Bioinformatics*. 2009;25:1463–5.
16. Montgomery DC. *Design and analysis of experiments*. Fifth Edit. New York: John Wiley & Sons; 2000.
17. Quinn GP, Keough MJ. *Experimental design and data analysis for biologists*. First Edit. New York: Cambridge University Press; 2002.
18. Fujikoshi Y. Two-way ANOVA models with unbalanced data. *Discrete Mathematics*. 1993;116:315–34.
19. Hector A, Von Felten S, Schmid B. Analysis of variance with unbalanced data: an update for ecology & evolution. *Journal of Animal Ecology*. 2010;79:308–16.
20. Shaw RG, Mitchell-Olds T. Anova for Unbalanced Data: An Overview. *Ecology*. 1993;74:1638–45.

21. Benjamini Y, Braun H. John Tukey's contributions to multiple comparisons. *ETS Research Report Series*. 2002:i-27.
22. Dunnett CW. New Tables for Multiple Comparisons with a Control. *Biometrics*. 1964;20:482–91.
23. Dunnett CW. A Multiple Comparison Procedure for Comparing Several Treatments with a Control. *Journal of the American Statistical Association*. 1955;50:1096–121.
24. Afendi M, Banks WM, Kirkwood D. Bubble free resin for infusion process. *Composites Part A: Applied Science and Manufacturing*. 2005;36:739–46.